THE UNIVERSITY OF MICHIGAN RADIATION LABORATORY

016708-1-L

31 October 1979

AFWL/ELT (W. D. Prather)

SUBJECT: R and D Status Report (Final)

PERIOD COVERED: 27 November 1978 - 26 October 1979

CONTRACT: F29601-79-C-0013
"Scale Model Measurements and Experimental Verification"

CONTRACTING OFFICER:

REPORT SUBMITTED BY: Valdis V. Liepa
Principal Investigator

Distribution

AFLW/ELT	(2)
ACFMD/PKRA	(1)
ACO	(1)
File	(1)

This is the final progress letter on Contract F29601-79-C-0013 and summarizes the work accomplished under this program which covered the period 27 November 1978 to 26 October 1979 and a total funding of $71,750.

In short, under this program measurement of surface currents and charges were made on scale model E-4B aircraft at 16 locations or test points under 7 different excitation conditions. The measured quantities were the axial surface current density component J_a, the circumferential surface current density component J_c, and the normal electric field component E_n. Of the 336 measurement situations a possible 96 were finally selected for measurement. The resulting data are presented in the Final Report, and the data in digital form have been delivered to Mitre Corporation on IBM cards in the form of amplitude and phase plots as a function of the full scale frequency.

The attached figure shows a typical plot of the data from the final report. For this particular case the right wing of the model is illuminated downward by a horizontally polarized wave. This particular measurement was made using 1/100 scale model over frequency range of 125 to 4400 MHz which for full scale frequency reduces to 1.25 to 44 MHz. The measured value is axial current on top of the fuselage at station F1560T. Because of the presence of the HF wire antennas stretching from midpoint (STA:F1365) of the fuselage to the leading edge of the vertical stabilizer, the normal resonances of the aircraft are overwhelmed by the sharp spikes in the amplitude response believed to be caused by the response fo the HF wire that were shorted at the

fuselage but open circuited at the vertical stabilizer. This spiked behavior is present in the majority of the E-4B measurements.

Attached is a table that summarizes the measurements that have been made and data delivered. This table is slightly different than that of the Contract Work Statement--the reason being that during the execution of this program some of the measurement stations and excitations were changed to match those of the full scale E-4B HPD and VPD simulator measurements. These changes did not appreciably alter the measurement effort; originally the program called for 89 measurements and by the end of the contract we had made 96 measurements.

To our present knowledge, as of 31 October 1979, all the funds allotted to this program have been expended.

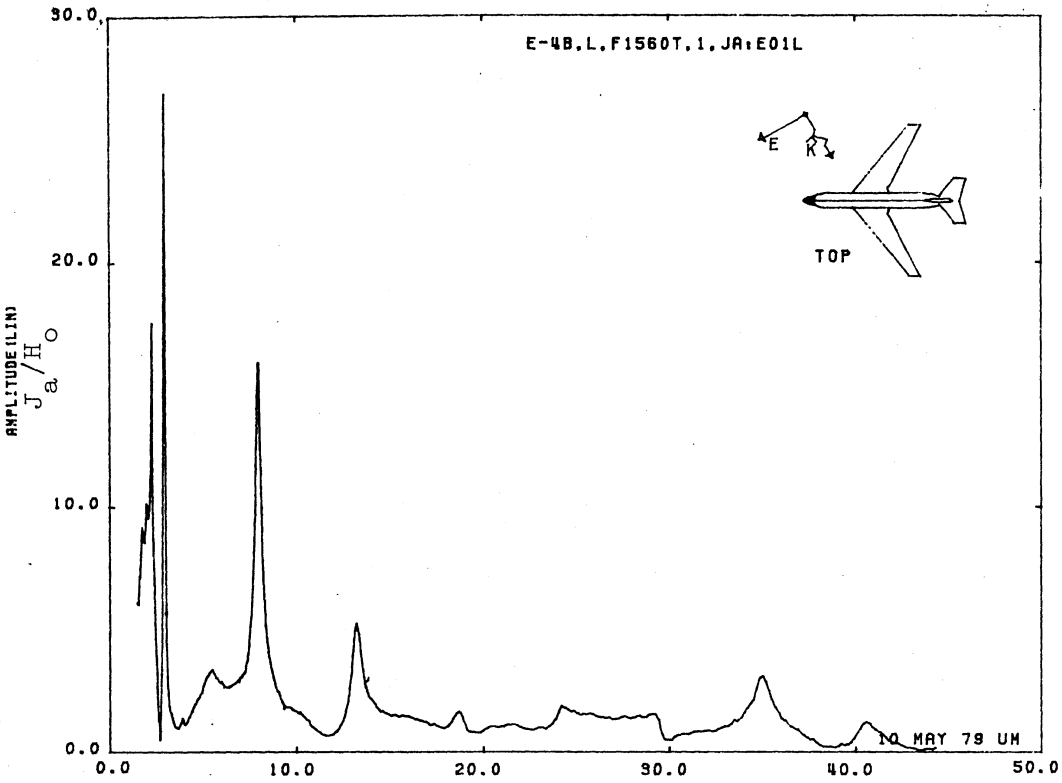

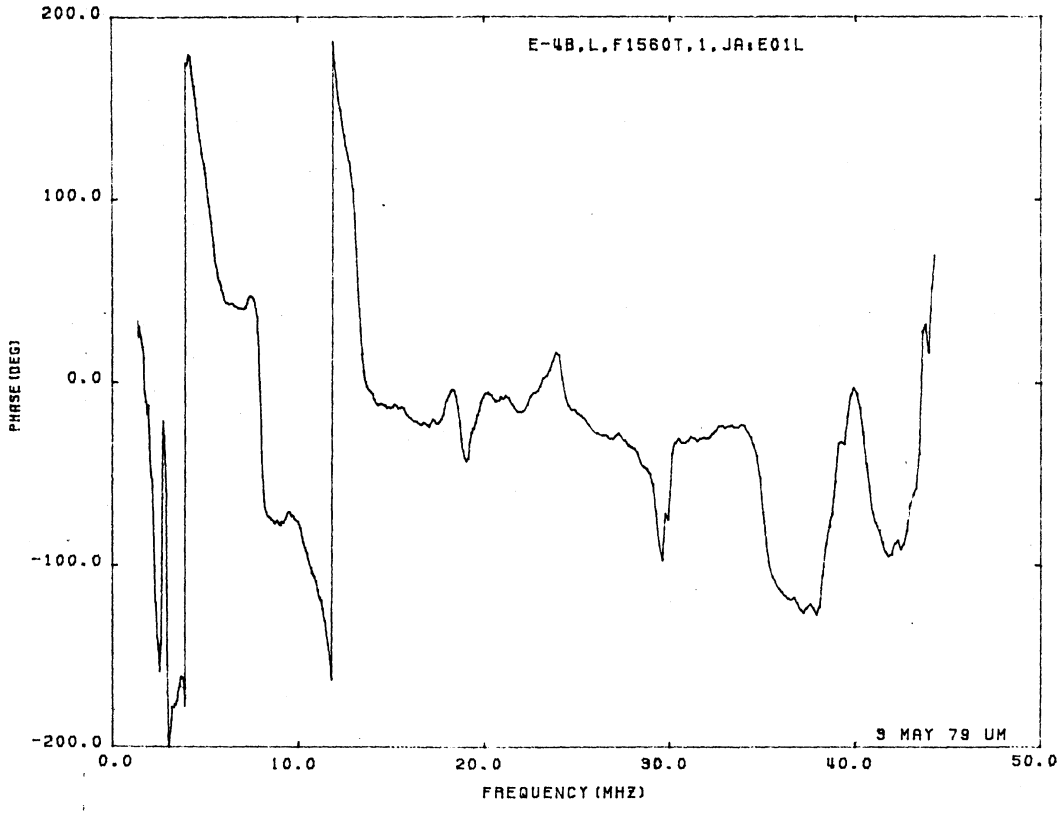

Axial Current at STA:1560T, Excitation 1, 1/100 Model.

E-4B SCALE MODEL DATA MATRIX

Test Points	EXCITATION 1 ϕ =-60° θ = 50° E-horizontal			EXCITATION 2 Nose-on E-vertical			EXCITATION 3 ϕ =-90° θ = 38° E-horizontal			EXCITATION 4 ϕ = 0° θ = 38° E-horizontal		
	J_a	J_c	E_n	J_a	J_c	E_n	J_a	J_c	E_n	J_a	J_c	E_n
1 F1560T XU03	01RS,L*	02RS,L*		04S,L			06S,L	06AS,L				
2 FIN345 XE02	12S,L	13S,L										
3 F1220T XU02	25RS,L*	26RS,L*	27S,L	28S,L		29S,L	30S,L	30AS,L	31S,L	31AS,L	32S,L	
4 RWS917T XW02	36S,L	37S,L		38S,L	39S,L		40S,L	41S,L		42S,L	43S,L	
5 F130 XC02			46S,L									
6 F460T XU01			55S,L			56S,L			57S,L			
7 F590B XL01	61S,L	62S,L		63S,L			64S,L	65S,L				
8 F1560B XL02	69S,L	70S,L										
9 F2200B XL03	73S,L	74S,L	75S,L	76S,L		77S,L			78S,L			
10 F2594B XE04	79S,L		80S,L	81S,L		82S,L			83S,L			
11 RWS917B XW03	86S,L	87S,L										
12 RWS1548T XW05	91S,L		92S,L			93S,L	94S,L		95S,L			
13 RSTAB335 XE03	98S,L		99S,L									
14 FIN595 XE01			101S,L									
15 BM1/8												
16 BM1/2												

*Data identified without R are for ϕ = -30°, θ = 50°.

E-4B SCALE MODEL DATA MATRIX (CONT.)

Test Points	EXCITATION 5 Refueling Top Incidence E-par fuselage			EXCITATION 6 Top Incidence E-par fuselage			EXCITATION 7 Top Incidence E-perp fuselage		
	J_a	J_c	E_n	J_a	J_c	E_n	J_a	J_c	E_n
1 F1560T XU03				09S,L		10S,L		11S,L	
2 FIN345 XE02				21S,L		22S,L			
3 F1220T XU02				33S,L		34S,L		35S,L	
4 RWS917T XW02				44S,L			45S,L	45AS,L	
5 F130 XC02	47L,S		48L			49S,L			
6 F460T XU01	58L,S		59L			60S,L			
7 F590B XL01	66L,S			67S,L				68S,L	
8 F1560B XL02				71S,L				72S,L	
9 F2200B XL03				78AS,L		78BS,L			
10 F2594B XE04				84S,L		85S,L			
11 RWS917B XW03	88L		89L	90S,L					
12 RWS1548T XW05				96S,L		97S,L			
13RSTAB335 XE03				100S,L					
14 FIN595 XE01									
15 BM1/8	102S,L;S.CR,L.CR								
16 BM1/2	103S,L;S.CR,L.CR								

V. V. Liepa
D. M. Brown
F. E. Lenning
R. L. Turcotte

October 1979

Interaction Application Memos

Memo

Measurements of Surface Fields on Scale Model E-4B Aircraft

ABSTRACT

Measured frequency domain data are presented for the surface current and charges induced on E-4B aircraft when illuminated by a plane electromagnetic wave in a simulated free space environment. The measurements were made on 1/200 and 1/100 scale models over frequency range 125 to 4400 MHz, simulating 0.6 to 44.0 MHz full scale coverage. The data are given for 16 test points, including the boom current for the refueling mode simulation, and seven different excitations. Excitations were chosen to complement the ATHAMAS I (HPD) and ACHILLES I (VPD) full scale measurements, and to provide data for comparison with theoretical studies.

Authors are with the Radiation Laboratory, Department of Electrical and Computer Engineering, The University of Michigan, Ann Arbor, MI 48109.

PREFACE

Generation of the data involved many contributors. In addition to the authors, M. Tomorski, I. LaHaie, C. Bickley, and M. Liepa were involved in the program. Ms. Wanita Rasey typed the manuscript. Their help is greatly appreciated. We are also grateful to Mr. W. Prather of AFWL/ELTI for the help provided from start to finish of this program.

CONTENTS

SECTION I

INTRODUCTION

The data presented here were obtained for the Mitre Corporation and the Air Force Weapons Laboratory to be used along with analytical calculations in the EMP analysis and also in determining the surface response extrapolation function [1] for the E-4B aircraft. The test points and excitation conditions in the scale model measurements were therefore chosen to conform to those of the full scale measurements made in the ATHAMAS I (Horizontally Polarized Dipole) and ACHILLES I (Vertically Polarized Dipole) simulators at Kirtland AFB, plus those appropriate for the in-flight refueling mode situation.

The measurements are presented for 16 locations or test points on the aircraft under 7 different excitation conditions. The measured quantities are the axial surface current density component J_a, the circumferential surface current density component J_c, and the normal electric field component E_n. Of the 336 measurement situations possible, 92 were finally selected for measurement. The resulting data are presented in the form of amplitude and phase plots as a function of the full scale frequency, and have been furnished to the Mitre Corporation in digital form on punched cards for further processing.

1. Carl E. Baum, "Extrapolation Techniques for Interpreting the Results of Tests in EMP Simulators in Terms of EMP Criteria," AFWL Sensor and Simulation Note 222, 1977.

SECTION II

MODELS

2.1 E-4B Models for Free Space Measurements

For these measurements two scale models of E-4B aircraft were selected, one a 1/100 scale originally in the form of a plastic kit and the other a 1/200 scale model molded of plastic with wood filler. Both models were good replicas of 747 but some modifications were required to make them electrically equivalent to E-4B aircraft. These modifications included cutting back the nose to STA:F130 to simulate the nonmetallic radome (nose of the radome at STA:F90), adding the HF probe antennas to both wingtips on both scale models, and installing an HF wire antenna from the top of the fuselage to the leading edge of the vertical stabilizer. The two wires were shorted (see Figure 1) at the fuselage but open circuited at the vertical stabilizer. Having experienced a questionable short circuit condition in some of the previous measurements [2], we attached flush with the surface a small metal plate to which a small pin was soldered. The antenna wire was then wrapped around this pin. At the vertical stabilizer the open circuit condition was simulated by using a short nylon string section as a bridge between the wire and the model; the nylon section was 1/8 inch long for the 1/100 model and 1/16 inch long for the 1/200 model.

---

2. Valdis V. Liepa, "Current and Charge Measurements on Scale Model EC-130 Aircraft," The University of Michigan, Radiation Laboratory Report No. 016104-1-F; AFWL Interaction Application Memo 25, 1978.

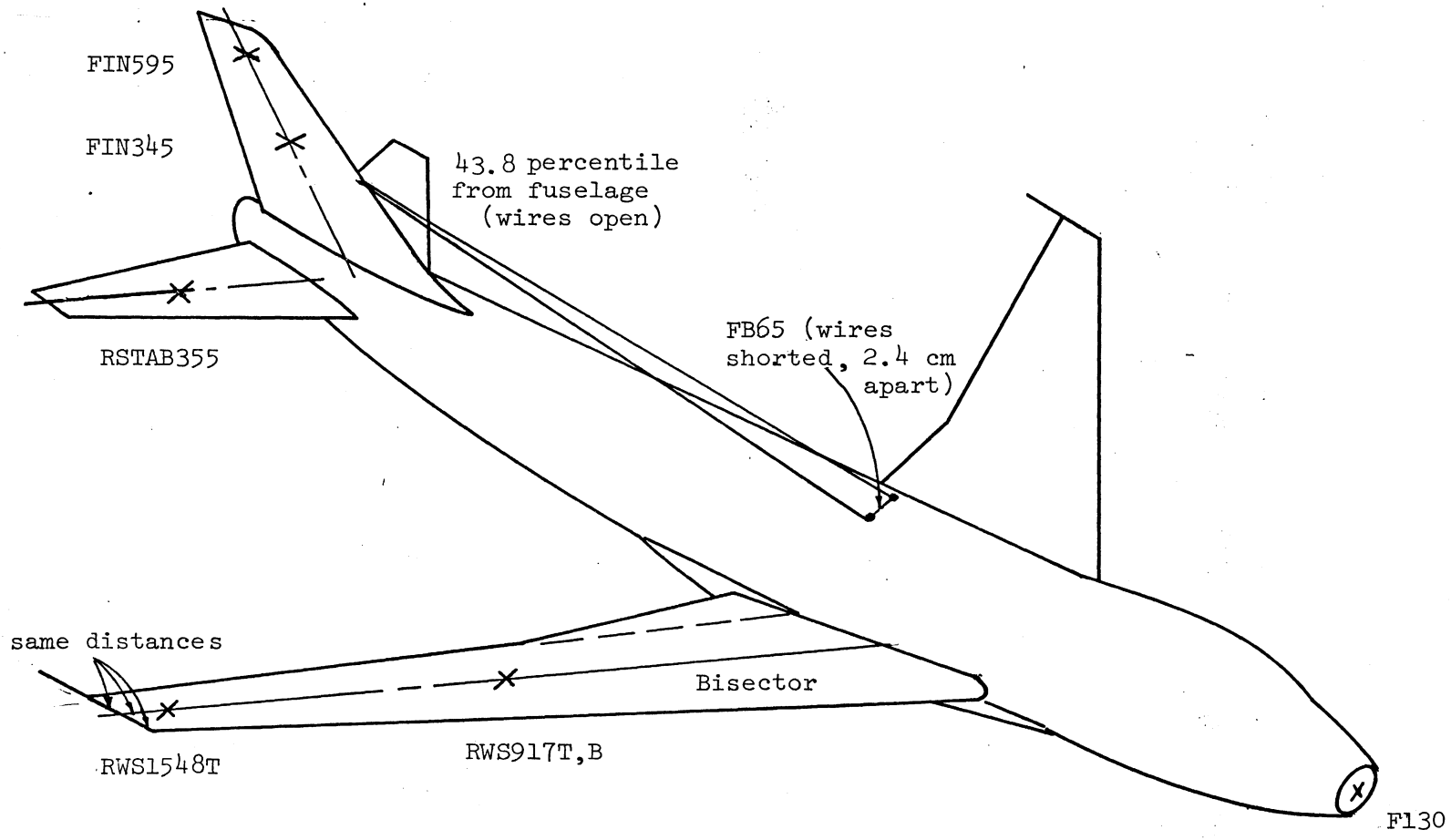

Figure 1. Location of the Wing Station and Placement of the HF Antenna. The Fuselage Stations Are Measured Along the Fuselage, as Usual.

After these modifications and smoothing the surfaces, the models were given several coats of silver paint (Dupont No. 4817) to make them conductive. To protect the "insulators" on the HF wires, the strings were masked with tape during painting. Finally, the models were very carefully measured for length and wing span to determine the scale factors to be used in translating the data from laboratory to full scale frequencies. The table below presents the scale factors.

TABLE 1. MODEL SCALE FACTORS

Model	Fuselage Length w/o Radome	Fuselage Scale*	Wingspan	Wingspan Scale*
1/100	68.10 cm	1/99.28	61.10 cm	1/97.61
1/200	31.10 cm	1/204.26	30.00 cm	1/198.80

*The above scale factors were obtained based on the following E-4B aircraft full scale dimensions.

Fuselage length	68.63 m
Fuselage w/o radome	67.61 m
Maximum length (to vertical fin)	70.51 m
Wingspan	59.64 m

Because no model is an exact replica of the full scale aircraft, both the fuselage and the wingspan scale factors were used in reducing the data. One could take the average of the two and use it to reduce the data, but better results are obtained by using the scale factor corresponding to the structure that supports the mode which produces the measured field. For example, for the case of the axial current measured on the top of the fuselage (top incidence,

E-parallel to fuselage) the fuselage scale factor was used when reducing the data, whereas for the case of the circumferential current measured on top of the fuselage (top incidence, E-perpendicular to fuselage) the wingspan scale factor was used. For most situations it was clear which scale factor to use, but when it appeared that both the fuselage and the wings were instrumental in supporting the measured field, the fuselage scale factor was used. Figure 1 shows a sketch of the E-4B model giving locations of wing stations and attachment of HF wire antennas.

2.2 E-4B and KC-135 Models for In-Flight Refueling Measurements

A new dimension added to the E-4B scale model measurements was the measuring of surface currents and charges on and near the refueling boom of an E-4B when refueled in flight from a KC-135. To simulate such conditions required a "matched pair" of models, i.e., models having the same scale. By searching through those in hobby shops and in our possession we found 1/125 scale models of both the 747 (Heller No. 856) and 707 (Heller No. 700) aircraft, and after appropriate preparation we made the first measurement of the current on the boom using a free space or external loop probe. It was expected at the onset that the combined length of the two models would determine the first resonant frequency in this case, and we hoped that it would fall within our measurement range. However, even at our lowest measurement frequency (125 MHz) we just missed the resonant peak. A pair of smaller models was therefore needed, and because we were not as lucky in finding a matched pair, we had to settle for 1/226.2 for the KC-135 and 1/204.26 for the E-4B. Since it is the combined

length of the two models that determines the resonant characteristics (at least for the lower modes), the average scale factor, 1/215.3, was used in reduction of the data. Table 2 gives pertinent numbers for refueling mode models.

TABLE 2. MODEL SCALE FACTORS FOR REFUELING SIMULATION

Model	Individual Models	Fuselage Length w/o Radome	Indiv. Scale Factor*	Boom Diameter	Scale Used
Large 1/125	E-4B (1/125) KC-135 (1/125)	54.93 cm	1/123.09 1/123.50	0.24 cm (3/32")	1/123.1
Small 1/215	E-4B (1/200) KC-135 (1/225)	31.10 cm	1/204.26 1/226.20	0.19 cm (1/8")	1/215.2

*Based on fuselage length
KC-135: 41.17 m
E-4B : 67.61 m

Figure 2 shows the dimensions of the models used for the in-flight simulation. The E-4B models were prepared the same way as before, that is, radomes removed, wing tip probes and HF wire antenna added. In fact, the small model, 1/204.26 scale, was the same as used before. The refueling booms were made of available brass stock and hence the boom diameter is only approximately to scale.* However, once the actual diameter of the beam is known, the data can easily be corrected. This technique along with the procedure used for correcting the data for probe integration is presented in Section 3.3.

*At time of preparation of this report we still do not know the actual diameter of the boom.

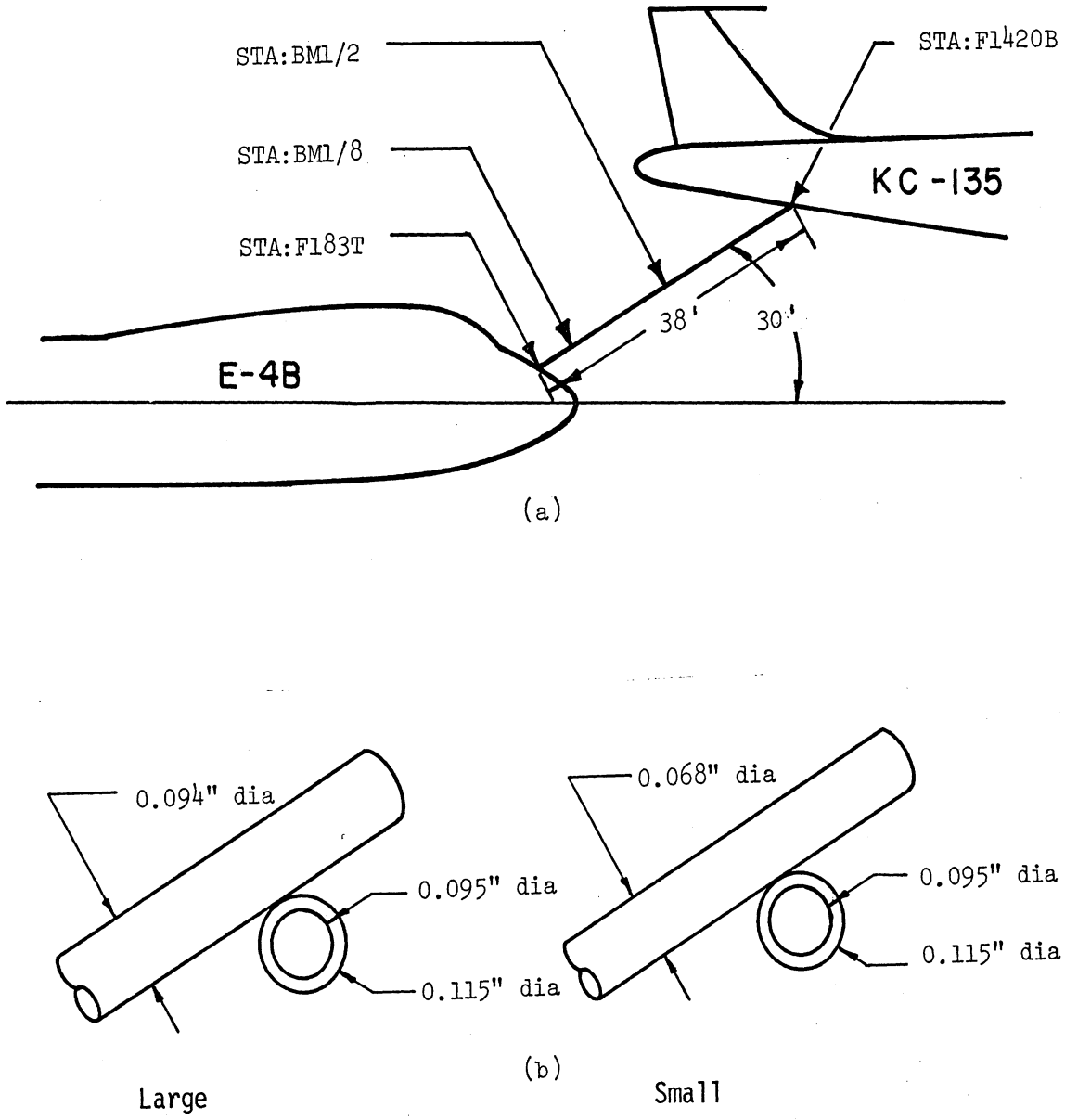

Figure 2. Modeling Used for In-Flight Refueling Simulation: (a) Geometry and Measurement Locations, (b) Size of the Current Loop (Sensor) Relative to the Refueling Boom.

SECTION III

Measurements and Data

3.1 Facility and Instrumentation

The measurements were made in the Radiation Laboratory's anechoic chamber, a facility especially designed, constructed and instrumented for surface field measurements. The measurement procedures were similar to those used in previous programs [2 through 7] apart from changes resulting from the continued upgrading of the facility and the measurement techniques. For these measurements, we extended the low frequency end of operation from 225 MHz to 125 MHz and added a phase-lock system to stabilize the frequencies at each incremental step in frequency.

---

3. Valdis V. Liepa, "Sweep Frequency Surface Field Measurements," University of Michigan Radiation Laboratory Report No. 013378-1-F; Sensor and Simulation Note 210, 1975.

4. Valdis V. Liepa, "Surface Field Measurements on Scale Model EC-135 Aircraft," University of Michigan Radiation Laboratory Report No. 014182-1-F; Interaction Application Memo 15, 1978.

5. Valdis V. Liepa, "Surface Field Measurements on Scale Model E-4 Aircraft," University of Michigan Radiation Laboratory Report No. 014182-2-F; Interaction Application Memo 17, 1978.

6. Valdis V. Liepa, "Surface Field Measurements on Scale Model F-111 Aircraft," University of Michigan Radiation Laboratory Report No. 014449-1-T; Interaction Application Memo 13, 1977.

7. Valdis V. Liepa, "Current and Charge Measurements on Scale Model E-3A Aircraft," University of Michigan Radiation Laboratory Report No. 015814-1-F; Interaction Application Memo 29, 1978.

Figure 3 shows the block diagram of the facility. Note that the setup is similar to that used in the E-3A scale model measurements [7] except that now an EIP 371/17 Source Locking Counter has been incorporated into the instrumentation. In essence, after a frequency command (from the calculator) is given to the frequency generator, a command is sent to the counter to measure the frequency and then output a correction signal to the FM input of the frequency generator to adjust the frequency. Addition of this instrumentation definitely did improve our frequency stability and frequency accuracy, but had little or no effect in decreasing the spectral spread of the signal, which still is of the order of $\pm$50 kHz.

The lower frequency capability was obtained by adding a 100 MHz to 500 MHz power amplifier. We also added a series of low-pass filters to remove harmonics that were generated by the power amplifiers because both the counter and the network analyzer seemed to prefer to lock onto the second harmonic (-20 dB down) rather than the fundamental, especially below 500 MHz.

3.2 Measurements

In all, charge and current measurements were made at 16 locations, including two on the refueling boom for the in-flight refueling simulation. Table 3 summarizes these stations. The top and bottom fuselage stations are located by measuring in (full scale) inches from the bulkhead (STA:F130) to the point indicated by the station number, such as F1220T. This station would then be 1090 inches from the bulkhead. The procedure for locating the wing and tail fin stations is shown in

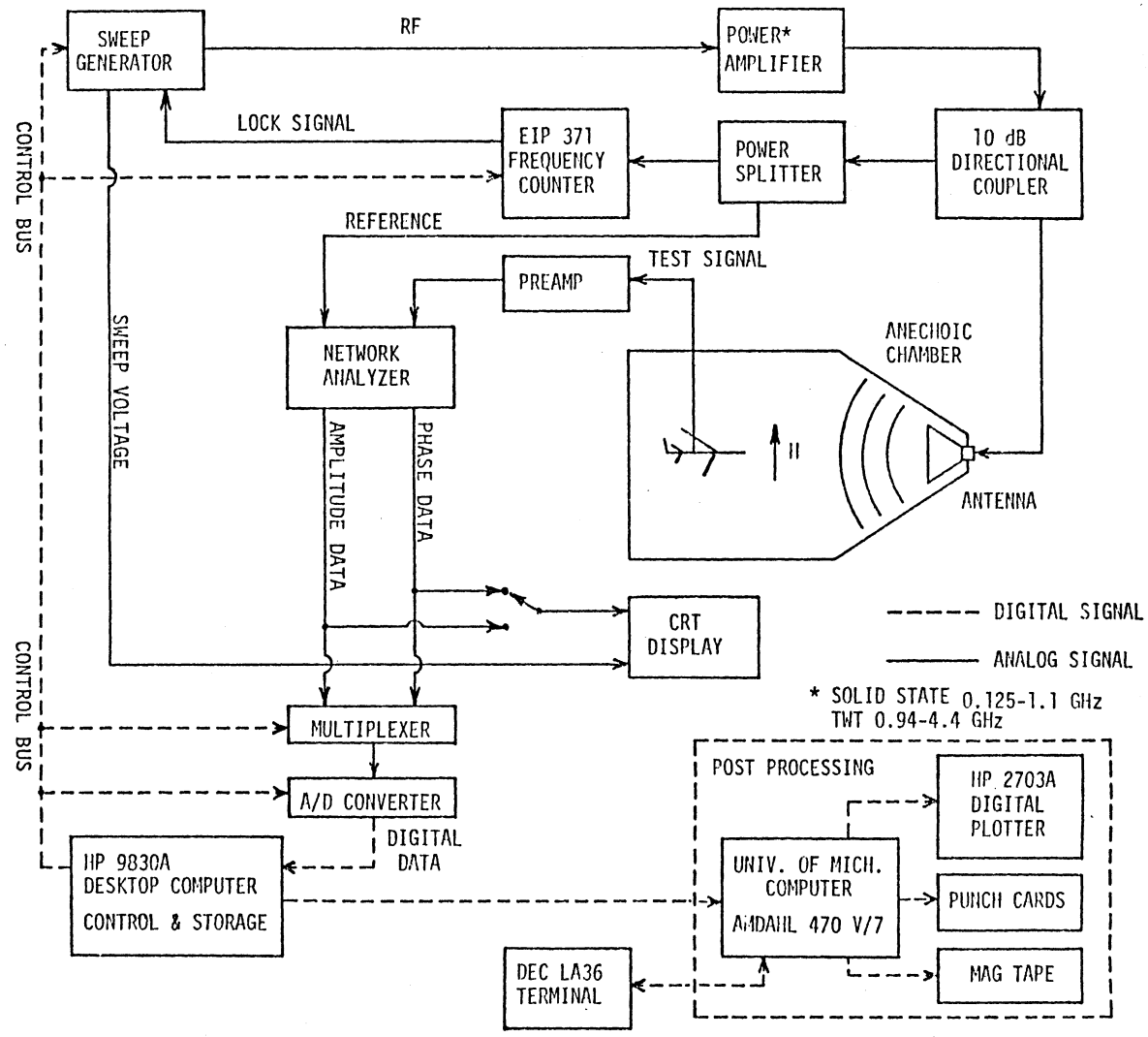

Figure 3. Block Diagram of the Measurement Facility.

TABLE 3. MEASUREMENTS LOCATIONS ON THE TEST MODELS

No.	Test Point	Station Number	Location
1	XU03	F156OT	Rear Fus Top
2	XE02	FIN345	Vert Stab, Rt Side, Mid
3	XU02	F122OT	Mid Fus Top
4	XW02	RWS917T	Rt Wing Top, Mid
5	XC02	F130	Fwd Bulkhead (nose)
6	XU01	F46OT	Fwd Fus Top
7	XL01	F590B	Fwd Fus Bottom
8	XL02	F156OB	Rear Fus Bottom
9	XL03	F220OB	Rear Fus Bottom
10	XE04	F2594B	Rear Fus Bottom
11	XW03	RWS917B	Rt Wing Bottom, Mid
12	XW05	RWS154BT	Rt Wing Tip, Top
13	XE03	RSTAB335	Rt Horiz Stab, Mid
14	XE01	FIN595	Vert Stab, Rt Side Tip
15		BM1/8	Refueling Boom, 1/8th from E-4B
16		BM1/2	Refueling Boom, Midpoint

Figure 1. To locate a station on a wing a bisector was drawn on the scale model as shown in the figure. The mid-wing stations are located at the midpoint of this bisector as measured from the fuselage to the wingtip. The wing-tip stations are also located on the bisector at a distance of one half the wing-tip width in from the wingtip edge. See the right wing in Figure 1 for details.

The measurements on the models were made for 7 different illuminations each having a prescribed polarization usually referenced to the fuselage of the aircraft. In our measurements these are often referred to as orientations since in the chamber the direction of illumination and polarization is fixed and the model is oriented to obtain appropriate excitation. Figure 4 shows the various directions of illumination and describes each one in the legend. For more details, see Figures 5 and 6 which show the aircraft orientations at the HPD and VPD simulators, respectively.

With the exception of the boom current and some of the axial current measurements at stations F130, F460T, and F590B, where the external loop probe was used, the current and charge measurements were made using miniature surface-mounted probes [8]. To mount these, holes were drilled in the model through which to pass the sensor lead. When a particular hole was not in use, it was taped over with copper tape which, as far as we can ascertain, introduced no noticeable effects on the measurements.

---

8. Valdis V. Liepa, D. L. Sengupta, J. E. Ferris, and T.B.A. Senior, "Surface Field Measurements with Image and Ground Planes," University of Michigan Radiation Laboratory Report No. 014449-1-F; Sensor and Simulation Notes, Note 224, 1977.

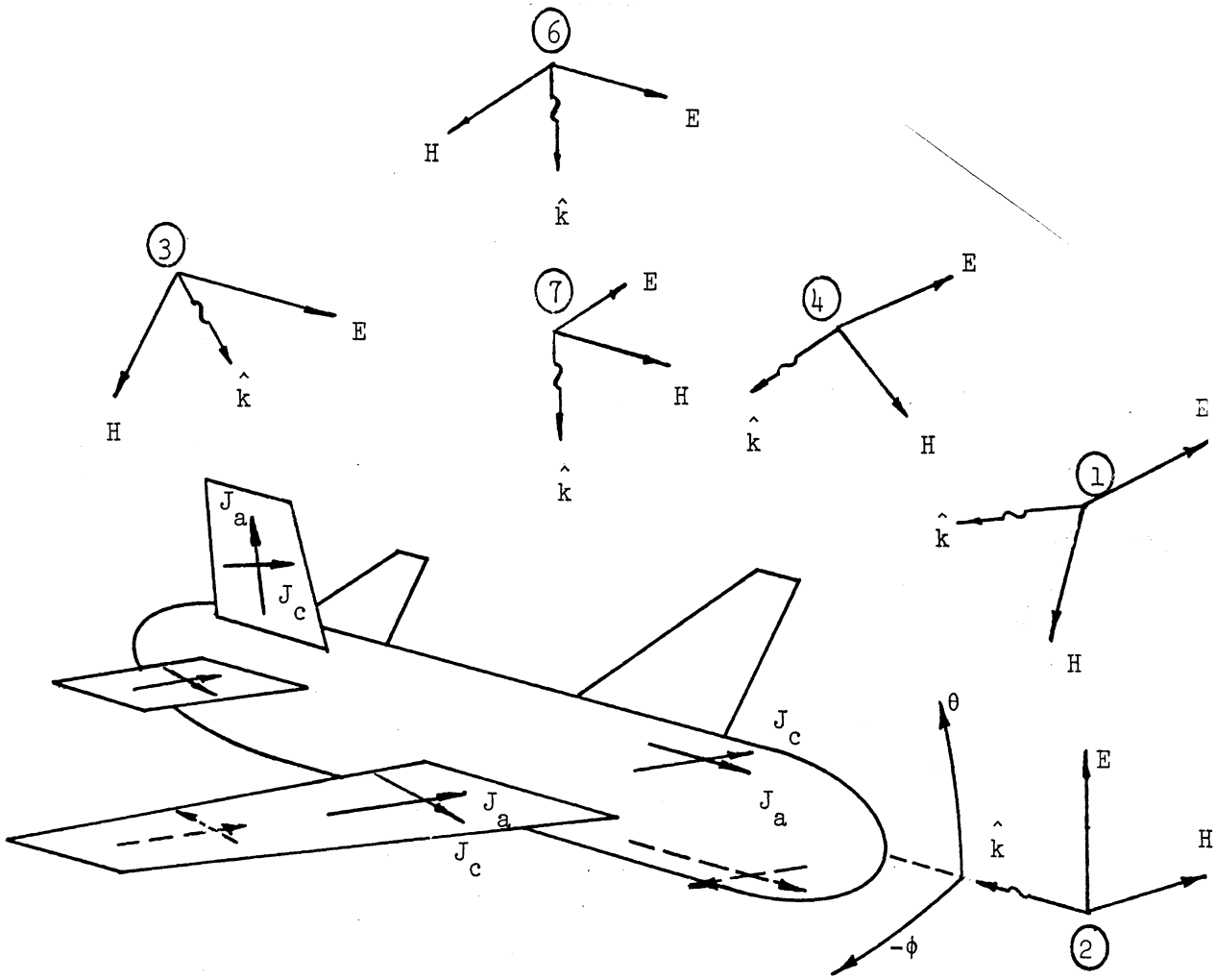

(1) E-horizontal, $\phi = -60°$, $\theta = 50°$ (HPD, Figure 4)
(2) E-vertical, Nose-on (VPD, Figure 5)
(3) E-horizontal, $\phi = -90°$, $\theta = 38°$ (HPD, Figure 4)
(4) E-horizontal, $\phi = 0°$, $\theta = 38°$ (HPD, Figure 4)
(5) E-parallel to fuselage, Refueling Mode, Top Incidence
(6) E-parallel to fuselage, Top Incidence
(7) E-perpendicular to fuselage, Top Incidence

Figure 4. Illumination Directions (Orientations) and the Measured Current Components.

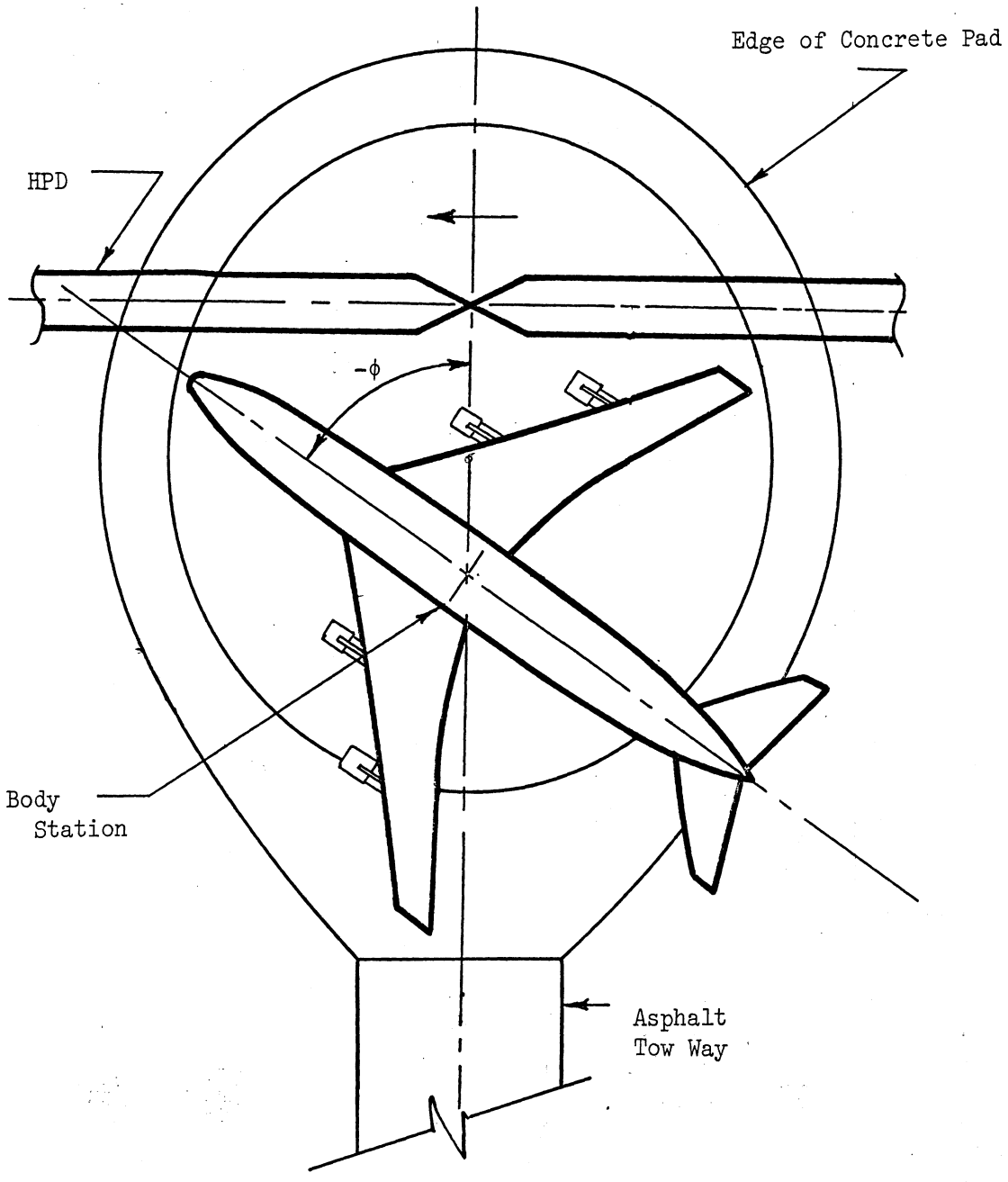

Figure 5. Notation for Aircraft Orientation at the HPD. (Elevation angle of the source with respect to the center axis of the fuselage is θ)

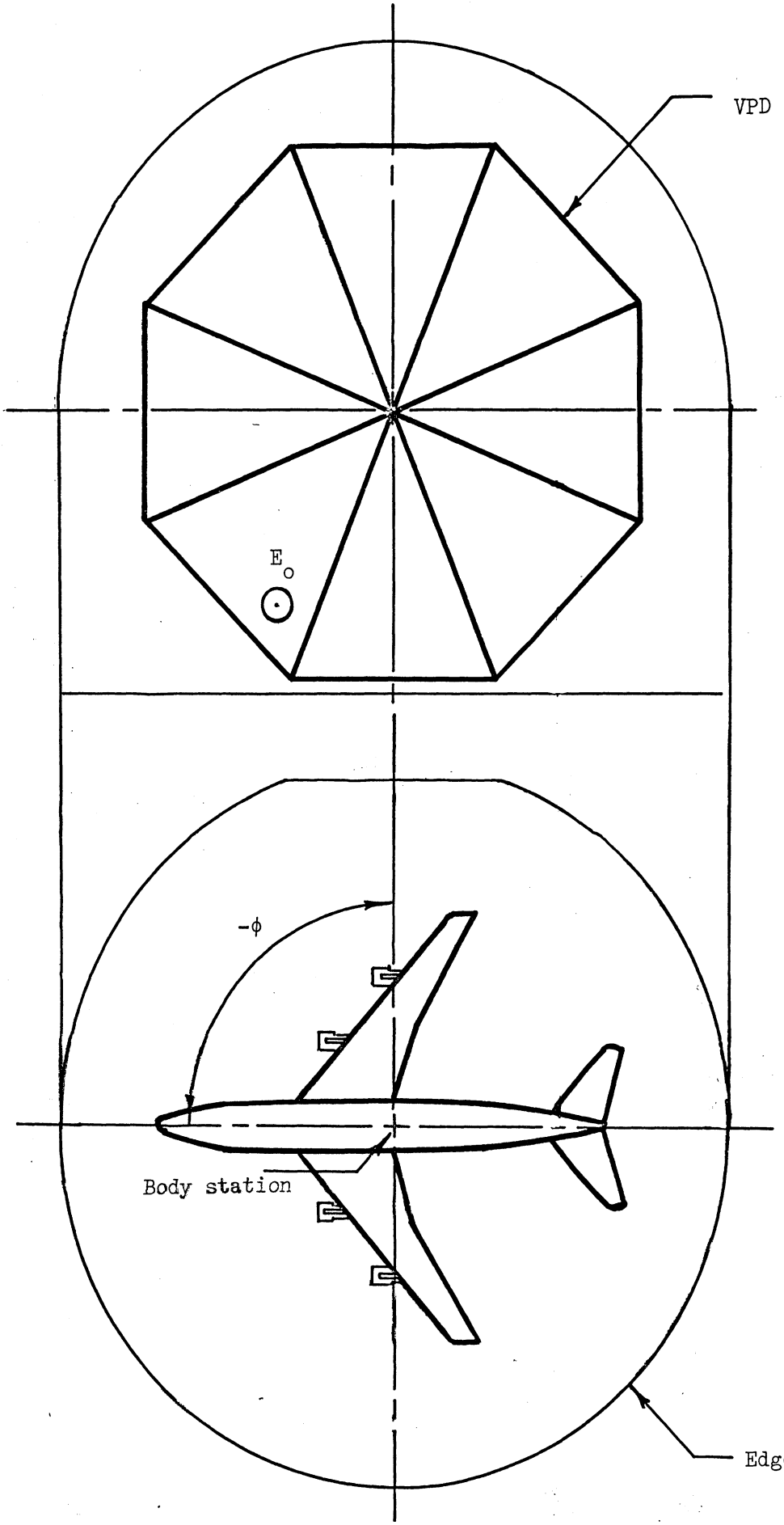

Figure 6. Notation of Aircraft Orientation at the VPD. (Elevation angle of the source with respect to the center axis of the fuselage is θ)

3.3 Data

The data presented were measured in an anechoic chamber with the model supported by a styrofoam pedestal plus especially prepared styrofoam supports to orient the model appropriately in relation to the incident field.

For each measurement situation the data were obtained for the two models over three frequency bands; the bands were then combined to provide a transfer function, as measured on the large (L) and on the small (S) scale models. Due to the different number of sampling points used in each frequency band, plus the fact that the measurement frequencies were divided by the model scale factors to obtain the full-scale data, the sampling rate is not uniform throughout the data. In addition, much of the data was resampled when the bands were combined. When the data was originally recorded, 185 points were used in Band 1 (125 - 1100 MHz), 122 in Band 2 (950 - 2200 MHz), and 144 in Band 3 (2000 - 4400 MHz). However, due to an occasional failure of the network analyzer to properly lock onto the signal at the start of a measurement, a few (perhaps a half dozen) points were sometimes omitted from a data set. In the data presented there are typically 416 data points for the transfer functions measured on large models and 347 data points for those measured on the small models. The exact number of points and the frequency range covered in the processed data are given (amongst other information) in line 5 of a data file (see Table 4). Typically, for the E-4B measurements the full scale frequency coverage obtained from the small model (1/200) is 0.63 - 20.0 MHz, and that for the large model (1/100) is 1.25 - 44 MHz.

TABLE 4. TYPICAL DATA FILE

```
LIST E-4B

>      1     E-4B
>      2     E4B,RF,RWS917T,5,0,010,B3,7/12/79,RT
>      3     SCALE FACTOR=123.10
>      4     SAMPLE DATA FOR REFUELING MODE
>      5        0.959  35.557   0.071  13.230 -227.16  197.80  347
>      6        0.959  13.230  30.64    1.059   4.076  22.00    1.159   7.973  -24.98
>      7        1.259   5.299  -9.56    1.359   5.150  34.89    1.459   6.991   16.27
>      8        1.559   4.082 -12.32    1.659   2.490 -13.06    1.759   3.502   25.95
>      9        1.859   5.544 -35.11    1.959   2.004 -138.44   2.059   0.432   77.83
>     10        2.159   0.757 -47.97    2.259   1.287  178.47   2.359   1.790  130.91
>     11        2.459   1.724  70.27    2.559   0.516  60.75    2.659   0.753   78.78
>     12        2.759   0.685  93.22    2.859   0.852  -1.10    2.959   0.499 -115.85
>     13        3.059   0.646 197.80    3.159   0.618 166.92    3.259   0.735  137.43
>     14        3.359   0.838 109.68    3.459   0.882  85.20    3.559   0.847   71.65
>     15        3.659   0.893  68.23    3.759   0.866  56.10    3.859   0.761   47.09
>     16        3.959   0.649  41.14    4.059   0.527  43.86    4.159   0.598   58.17
>     17        4.259   0.574  61.08    4.359   0.807  70.50    4.459   1.028   62.00
>     18        4.559   1.132  49.83    4.659   0.989  50.02    4.759   1.142   43.80
>     19        4.859   1.021  20.19    4.959   0.589  -9.12    5.059   0.213  -11.85
>     20        5.159   0.258  10.83    5.259   0.394 -42.45    5.359   0.390  -83.66
>     21        5.459   0.170 -97.58    5.559   0.282 -32.09    5.659   0.443  -41.89
>     22        5.759   0.417 -57.32    5.859   0.309 -35.42    5.959   0.508  -19.89
>     23        6.059   0.639 -22.81    6.159   0.623 -10.59    6.259   0.734   -2.36
>     24        6.359   1.042   6.35    6.459   1.275  -2.40    6.559   1.218   -9.76
>     25        6.659   1.192  -8.54    6.759   1.379 -14.55    6.859   1.493  -38.14
>     26        6.959   1.307 -58.19    7.059   1.236 -66.92    7.159   1.530  -71.62
>     27        7.259   1.736 -85.98    7.359   1.725 -94.57    7.459   1.839 -101.35
>     28        7.559   2.169 -111.22   7.659   2.350 -130.41   7.759   2.141 -143.65
>     29        7.859   1.797 -148.47   7.959   1.785 -137.07   8.059   2.119 -142.84
>     30        8.159   1.988 -147.89   8.259   1.762 -146.67   8.359   1.949 -148.17
>

     96       27.958   0.643 -127.03   28.058   0.639 -119.63   28.158   0.655 -116.88
>    97       28.258   0.623 -115.10   28.358   0.578 -112.21   28.458   0.552 -106.37
>    98       28.558   0.555 -114.83   28.658   0.496 -123.61   28.758   0.420 -132.63
>    99       28.858   0.394 -133.70   28.958   0.451 -147.68   29.058   0.462 -157.29
>   100       29.158   0.432 -163.65   29.258   0.502 -160.30   29.358   0.596 -164.06
>   101       29.458   0.642 -165.40   29.558   0.631 -162.15   29.658   0.779 -151.65
>   102       29.758   0.895 -150.53   29.858   0.957 -149.30   29.958   0.958 -143.40
>   103       30.058   1.025 -141.04   30.158   1.010 -138.05   30.258   0.958 -134.30
>   104       30.358   0.926 -130.42   30.458   0.896 -131.25   30.558   0.818 -133.58
>   105       30.658   0.701 -135.90   30.758   0.579 -130.65   30.858   0.593 -129.58
>   106       30.958   0.537 -134.81   31.058   0.403 -149.99   31.158   0.359 -150.64
>   107       31.258   0.382 -165.14   31.358   0.409 -180.93   31.458   0.395 -198.01
>   108       31.558   0.475 -195.30   31.658   0.504 -199.11   31.758   0.508 -202.00
>   109       31.858   0.511 -195.49   31.958   0.569 -186.96   32.058   0.602 -185.33
>   110       32.158   0.590 -185.50   32.258   0.513 -175.21   32.358   0.541 -166.14
>   111       32.458   0.519 -164.00   32.558   0.420 -167.00   32.658   0.300 -156.55
>   112       32.757   0.235 -130.25   32.857   0.209 -107.32   32.957   0.145  -94.67
>   113       33.057   0.172  -37.88   33.157   0.207  -26.27   33.257   0.204   -6.90
>   114       33.357   0.301   35.99   33.457   0.304   29.99   33.557   0.258    1.73
>   115       33.657   0.327  -26.27   33.757   0.519   -8.56   33.857   0.371  -34.93
>   116       33.957   0.071 -116.39   34.057   0.488 -221.31   34.157   0.531 -227.16
>   117       34.257   0.490 -215.87   34.357   0.499 -203.83   34.457   0.552 -199.38
>   118       34.557   0.455 -181.44   34.657   0.452 -162.78   34.757   0.474 -147.70
>   119       34.857   0.470 -132.79   34.957   0.468 -113.70   35.057   0.504 -100.24
>   120       35.157   0.519  -92.44   35.257   0.441  -88.16   35.357   0.472  -63.47
>   121       35.457   0.507  -60.12   35.557   0.479  -66.68
#END OF FILE
```

For the refueling mode measurements the frequency coverage obtained from the small model (1/215) is 0.6 - 20.5 MHz and that from the large model (1/125) is 1.0 - 35.2 MHz.

Figure 4 gives the directions of excitation, the polarization relative to the aircraft, and the convention adopted in specifying the circumferential and axial surface current components, J_c and J_a, respectively. In all cases the component J_c is perpendicular to J_a. The data presented are normalized relative to the incident field: J/H_o for the surface current data and E_n/E_o for the charge data. The phase is referenced to that of the incident field at the station where the measurement was made, based on the $e^{i\omega t}$ time convention.

For the measurements of surface currents and charges on fuselage and wing stations, the condition that the size of the sensor is small compared to the wavelength and the local radii of curvature of the surface where the measurement is made is satisfied. However, this is not the case with the axial boom current measurements in the refueling mode configuration. As shown in Figure 2, the diameter of the loop sensor is of the same order as that of the boom, and because of integration of the field over the (equivalent) area of the loop, it is to be expected that the true (magnetic) field at the surface of the boom will exceed that which was measured. We have studied the effect of loop integration previously [9] and have developed a method for correcting surface current data. The corrections have been applied to the boom current measurements and both the measured (uncorrected) and corrected

---

9. V. V. Liepa, G. A. Heyboer, and F. P. Rhine, "Response of Small Loops in Non-Uniform Magnetic Field—Experimental Results and their Implication," Presented at APS International Symposium, University of Massachusetts, Amherst, Mass. 1976.

data are presented. When using the boom current data, further correction may need to be applied to the data. As mentioned in Section 2.2, the boom diameters on the models were not precisely scaled, mainly because the actual diameter was not known, and even if it was known the mere process of silver painting would change the diameter enough to warrant correction of the data. Since the <u>total</u> bulk current on the boom is mainly determined by the combined geometry of the E-4B and KC-135 models, and the measured $|J_a| \gg 1$, i.e., the surface (magnetic) field is much greater than the incident field, the corrected surface current J'_c is

$$J'_c = J_c \frac{D_m}{D} ,$$

where D is the actual (full scale) diameter of the boom and D_m is the diameter of the boom used on the model, multiplied by its scaling factor.

Table 5 summarizes the situations for which data have been obtained and gives the figure numbers where the plots for each case can be found. The figure numbers are the same as those of the data files with the letter S (small model) or L (large model) specifying the particular model used in the measurement. The (digital) data files are also identified with the same filename given in the upper right-hand corner of the plots. Plots of the data are given in the data section.

In addition to the plots the data has also been furnished to AFWL and Mitre Corporation in digital form on punched cards. At the Radiation Laboratory the data is stored on (IBM compatible) magnetic tape in format:

Line 1 FILENAME (4A4)

2 Comments (18A4)

3 Comments (18A4)

4 TITLE used in plotting (18A4)

5 FMIN, FMAX, AMPMIN, AMPMAX, PHASEMIN, PHASEMAX, NN

(4F8.3, 2F8.2, I5)

6 F(1) AMP(1) PHASE(1) F(2) AMP(2) PHASE(2) F(3) AMP(3) PHASE(3) 3(2F8.3, F8.2)

data

..... F(NN) AMP(NN) PHASE(NN)

where NN is the number of data points in the set. Table 4 is an example of a typical data file named E-4B.

TABLE 5. E-4B SCALE MODEL DATA MATRIX

Test Points		EXCITATION 1 ϕ =-60° θ = 50° E-horizontal			EXCITATION 2 Nose-on E-vertical			EXCITATION 3 ϕ =-90° θ = 38° E-horizontal			EXCITATION 4 ϕ = 0° θ = 38° E-horizontal		
		J_a	J_c	E_n	J_a	J_c	E_n	J_a	J_c	E_n	J_a	J_c	E_n
1 F156OT	XU03	01RS,L*	02RS,L*		04S,L			06S,L	06AS,L				
2 FIN345	XE02	12S,L	13S,L										
3 F122OT	XU02	25RS,L*	26RS,L*	27S,L	28S,L		29S,L	30S,L	30AS,L	31S,L	31AS,L	32S,L	
4 RWS917T	XW02	36S,L	37S,L		38S,L	39S,L		40S,L	41S,L		42S,L	43S,L	
5 F130	XC02			46S,L									
6 F460T	XU01			55S,L			56S,L			57S,L			
7 F590B	XL01	61S,L	62S,L		63S,L			64S,L	65S,L				
8 F156OB	XL02	69S,L	70S,L										
9 F2200B	XL03	73S,L	74S,L	75S,L	76S,L		77S,L			78S,L			
10 F2594B	XE04	79S,L		80S,L	81S,L		82S,L			83S,L			
11 RWS917B	XW03	86S,L	87S,L										
12 RWS1548T	XW05	91S,L		92S,L			93S,L	94S,L		95S,L			
13 RSTAB335	XE03	98S,L		99S,L									
14 FIN595	XE01			101S,L									
15 BM1/8													
16 BM1/2													

*Data identified without R are for ϕ = -30°, θ = 50°.

TABLE 5 (CONT.). E-4B SCALE MODEL DATA MATRIX

Test Points	EXCITATION 5 Refueling Top Incidence E-par fuselage			EXCITATION 6 Top Incidence E-par fuselage			EXCITATION 7 Top Incidence E-perp fuselage		
	J_a	J_c	E_n	J_a	J_c	E_n	J_a	J_c	E_n
1 F1560T XU03				09S,L		10S,L		11S,L	
2 FIN345 XE02				21S,L		22S,L			
3 F1220T XU02				33S,L		34S,L		35S,L	
4 RWS917T XW02				44S,L			45S,L	45AS,L	
5 F130 XC02	47L,S		48L			49S,L			
6 F460T XU01	58L,S		59L			60S,L			
7 F590B XL01	66L,S			67S,L				68S,L	
8 F1560B XL02				71S,L				72S,L	
9 F2200B XL03				78AS,L		78BS,L			
10 F2594B XE04				84S,L		85S,L			
11 RWS917B XW03	88L		89L	90S,L					
12 RWS1548T XW05				96S,L		97S,L			
13RSTAB335 XE03				100S,L					
14 FIN595 XE01									
15 BM1/8	102S,L;S.CR,L.CR								
16 BM1/2	103S,L;S.CR,L.CR								

- - - DATA - - -

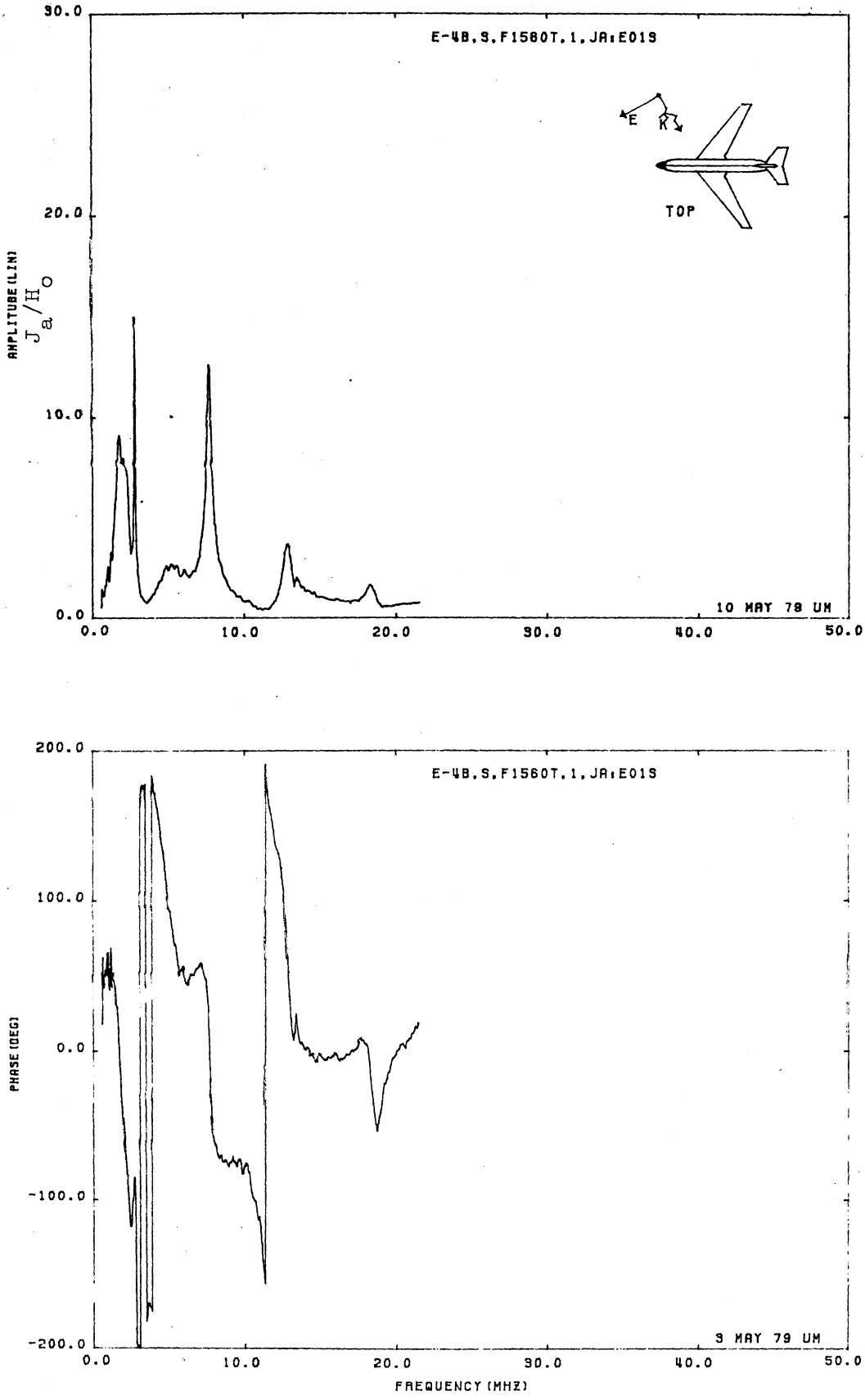

Figure 01S. Axial Current at STA:F1560T, Excitation 1*, 1/200 Model. (1* done for $\phi = -30°$, $\theta = 50°$)

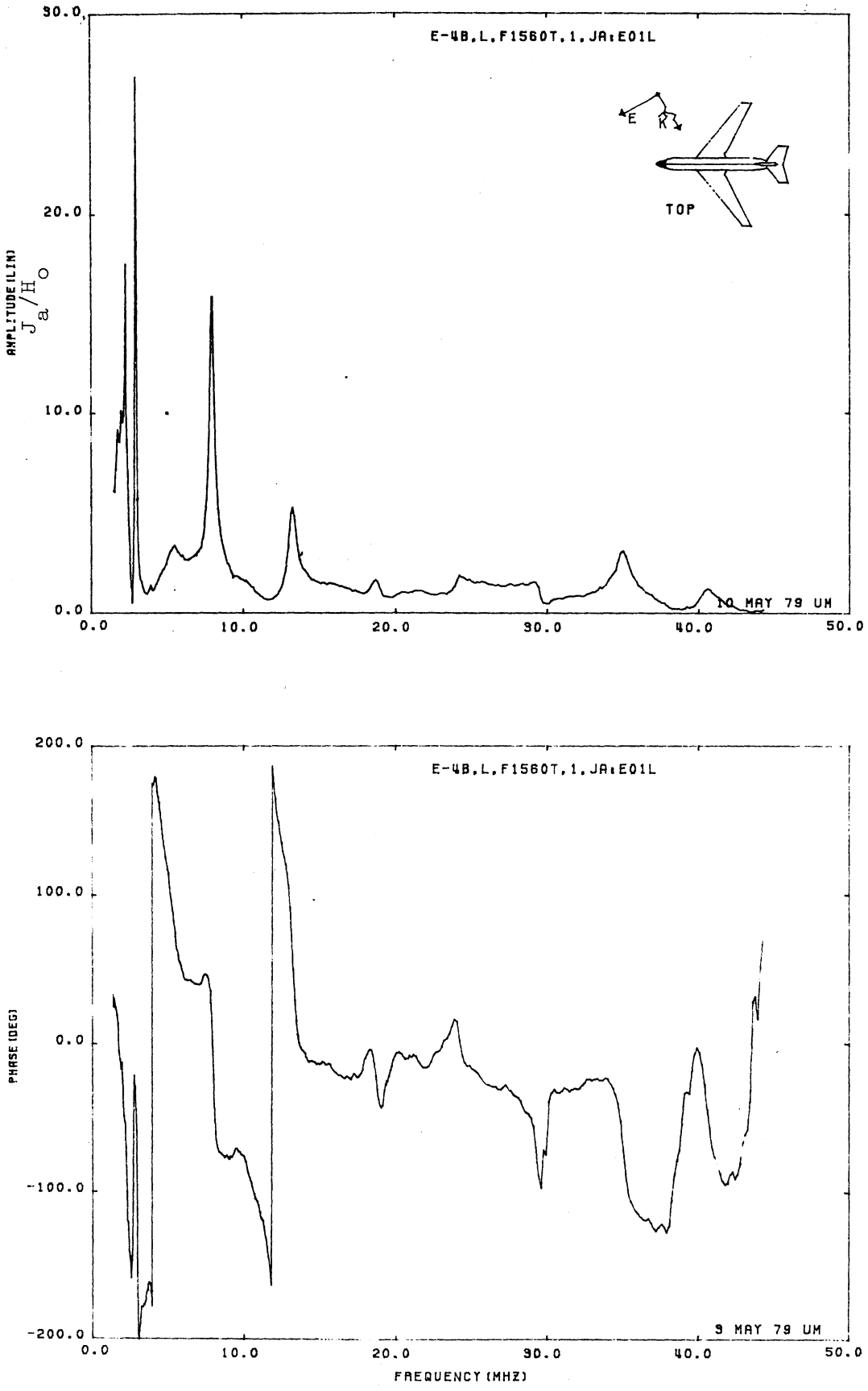

Figure 01L. Axial Current at STA:1560T, Excitation 1*, 1/100 Model. (1* done for $\phi = -30°$, $\theta = 50°$)

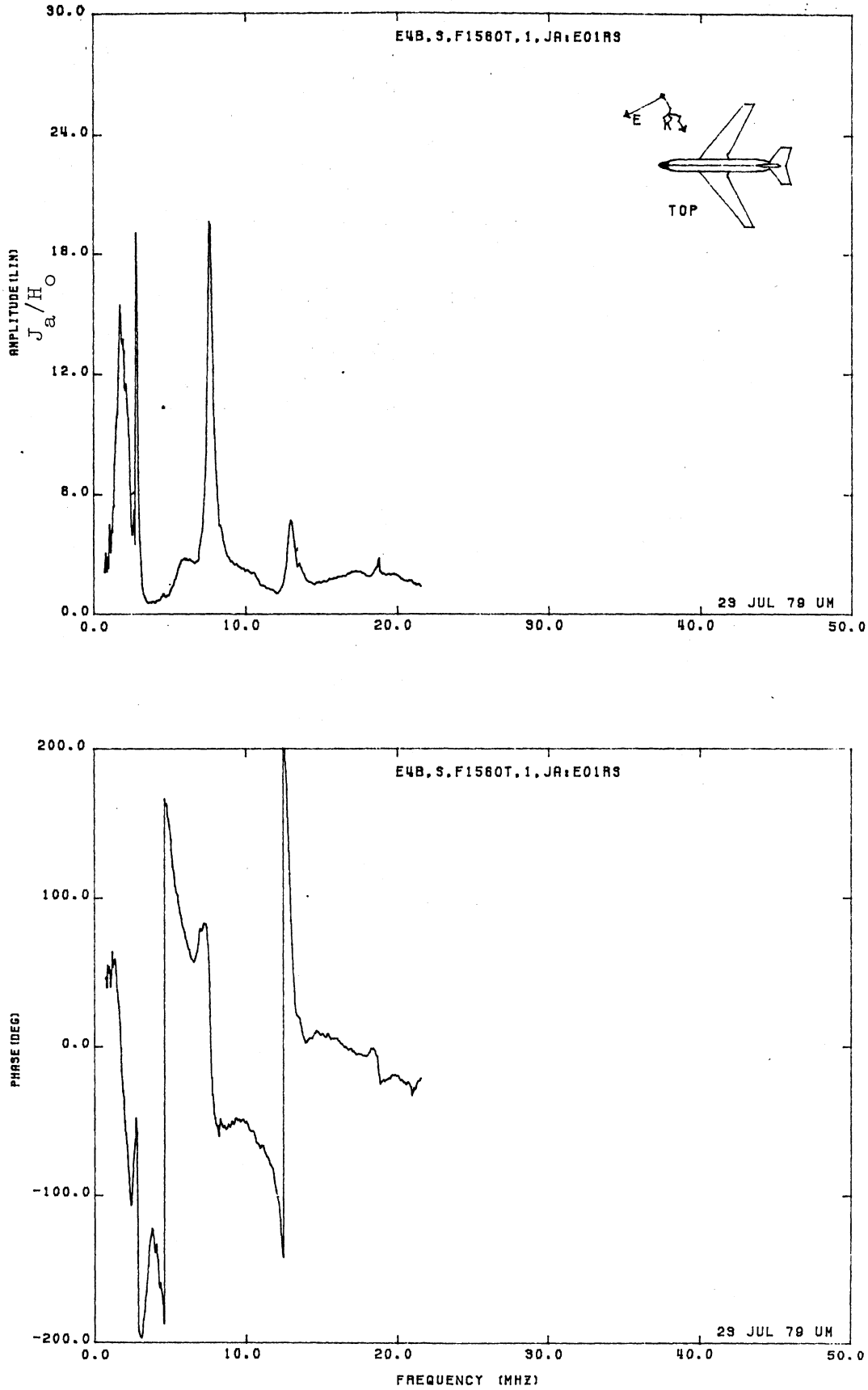

Figure 01RS. Axial Current at STA:F1560T, Excitation 1, 1/200 Model.

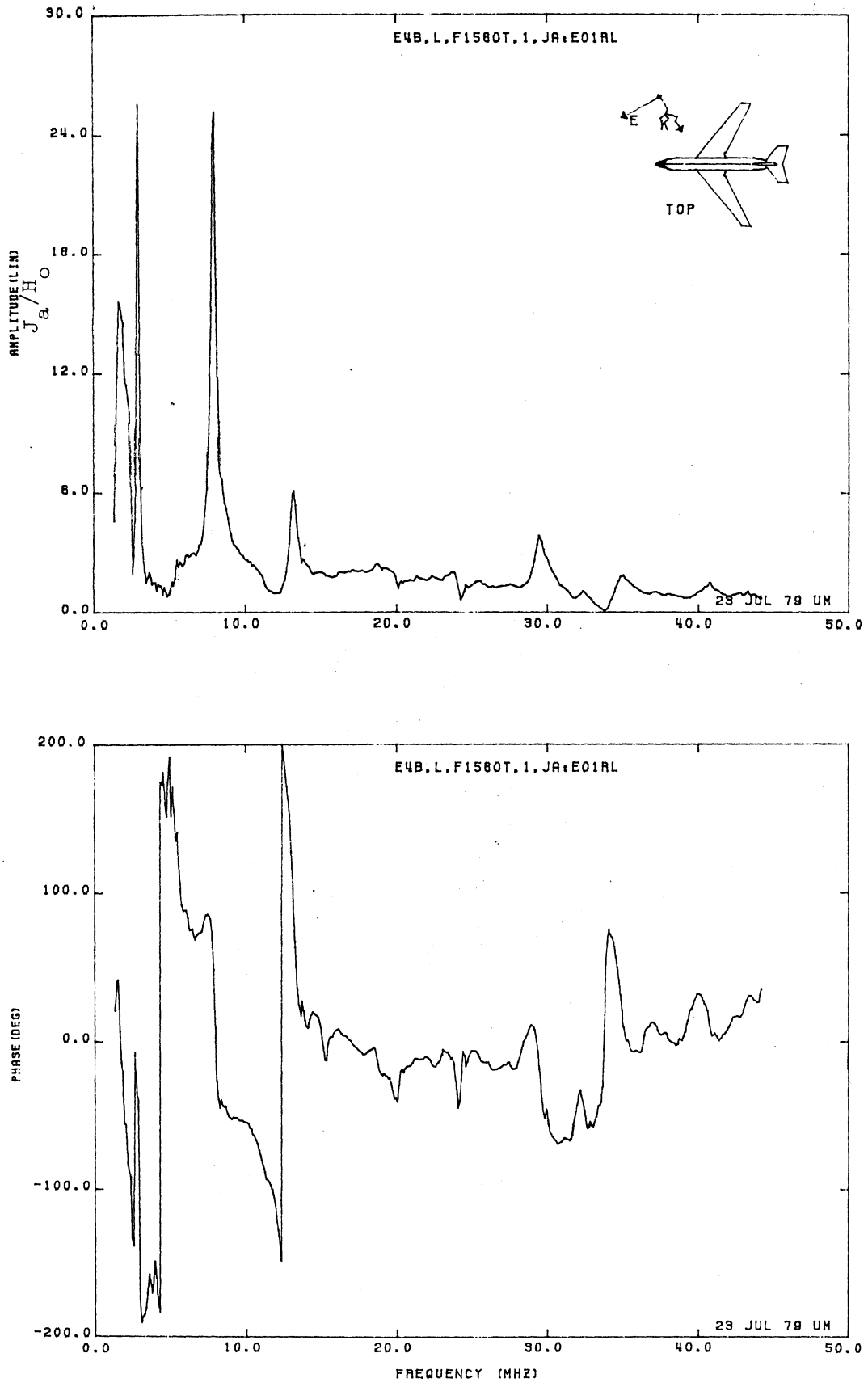

Figure 01RL. Axial Current at STA:F1560T, Excitation 1, 1/100 Model.

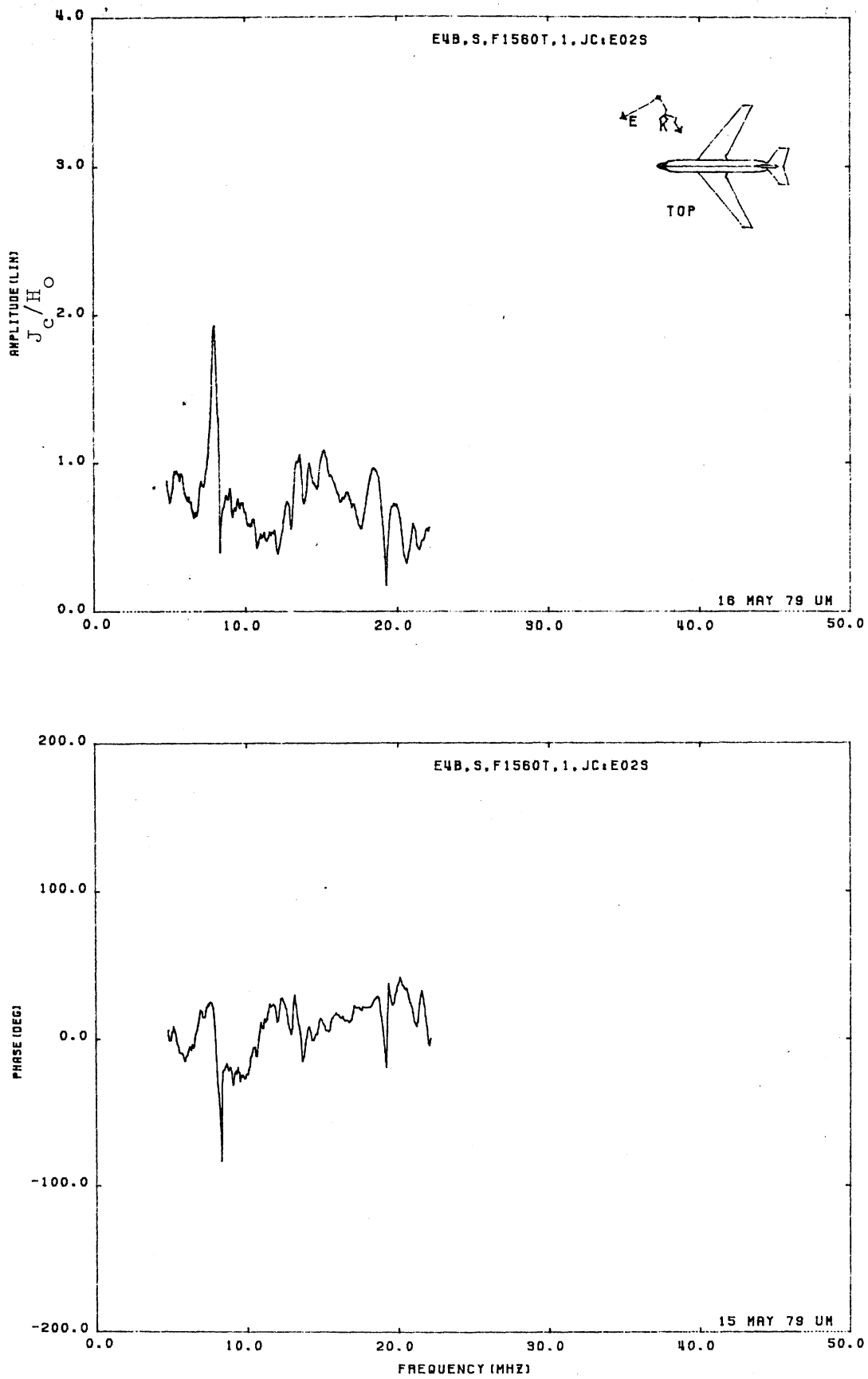

Figure 02S. Circumferential Current at STA:F1560T, Excitation 1*, 1/200 Model. (1* done for $\phi = -30°$, $\theta = 50°$)

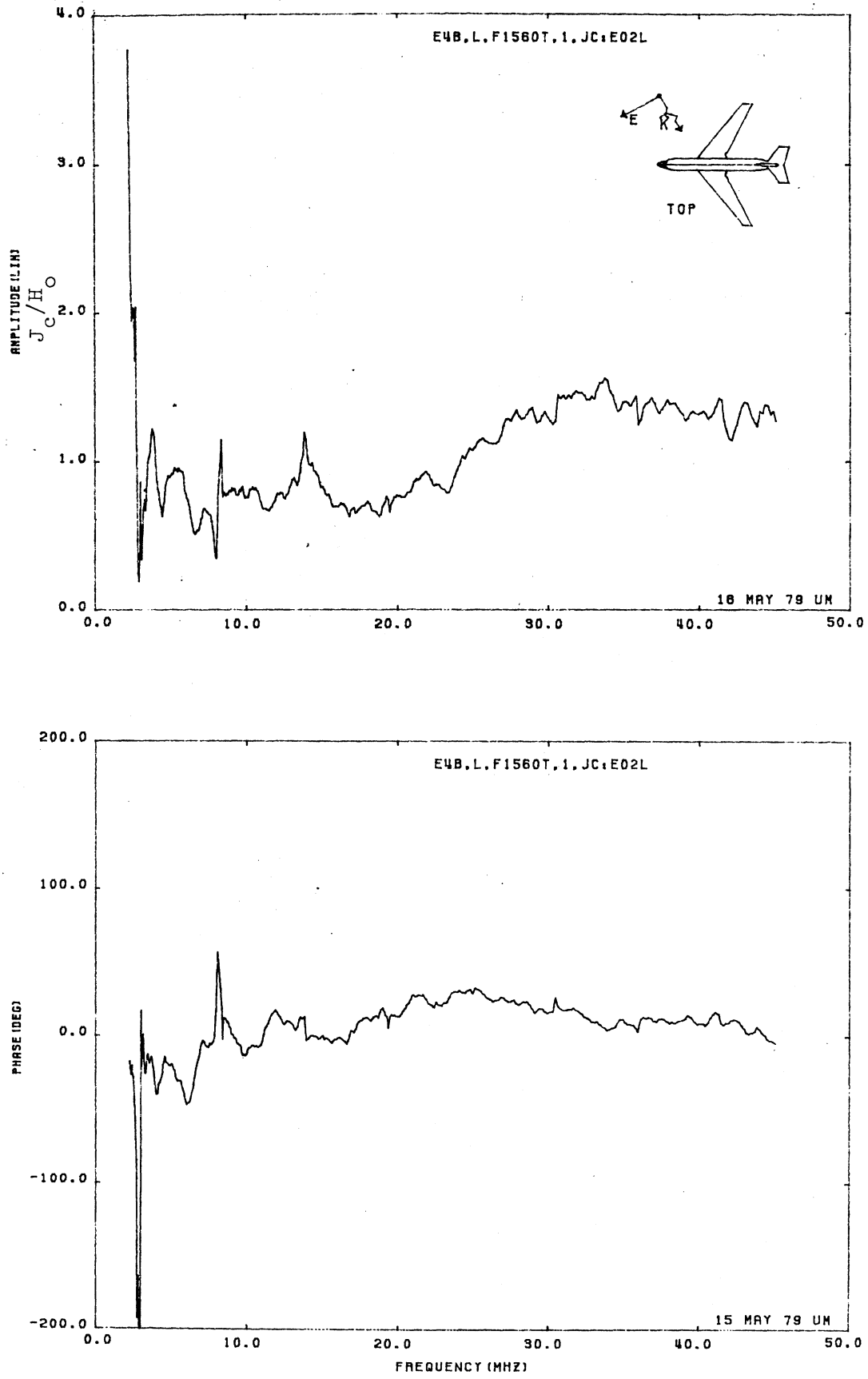

Figure 02L. Circumferential Current at STA:F1560T, Excitation 1*, 1/100 Model. (1* done for $\phi = -30°$, $\theta = 50°$)

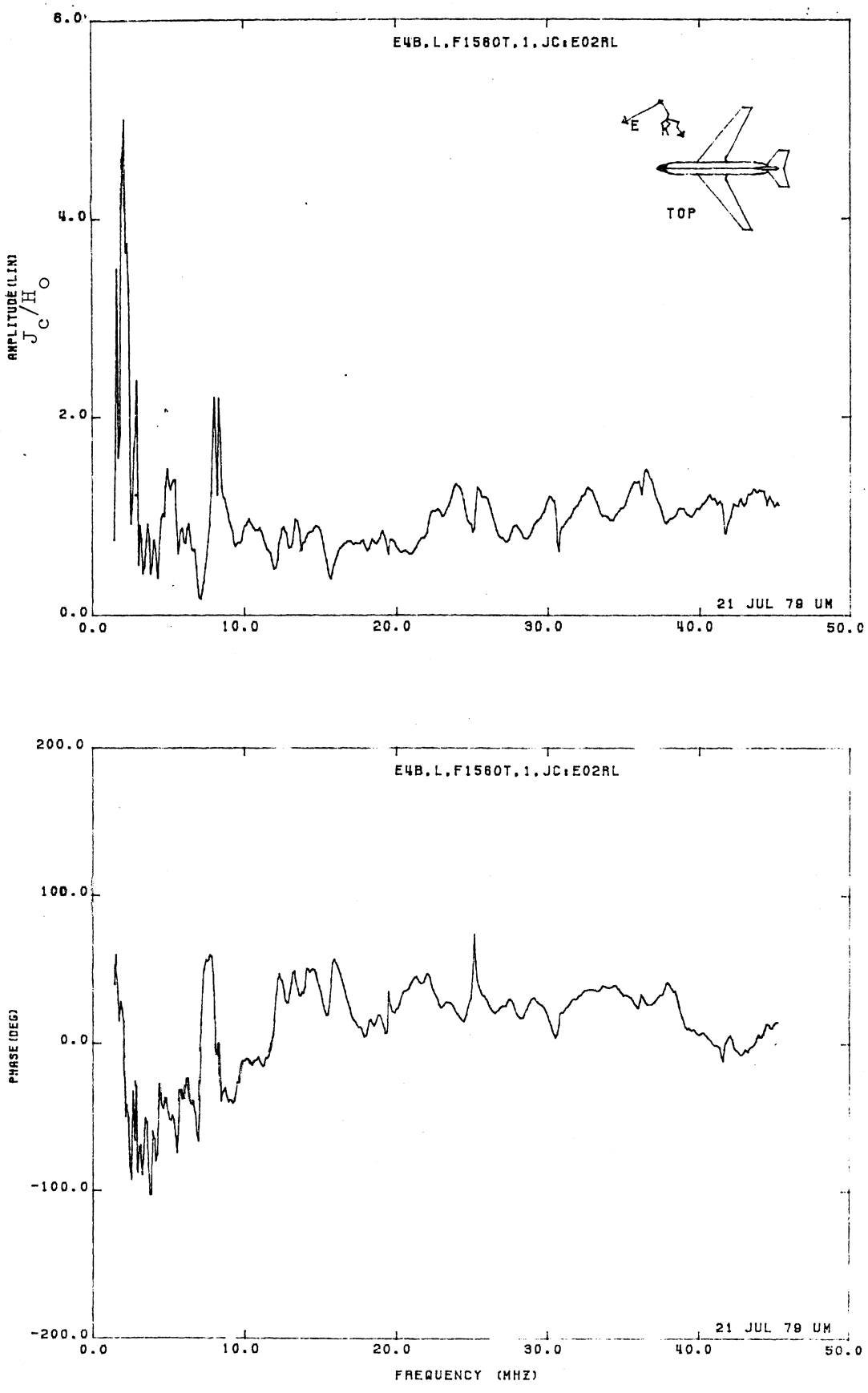

Figure 02RL. Circumferential Current at STA:F1560T, Excitation 1, 1/100 Model.

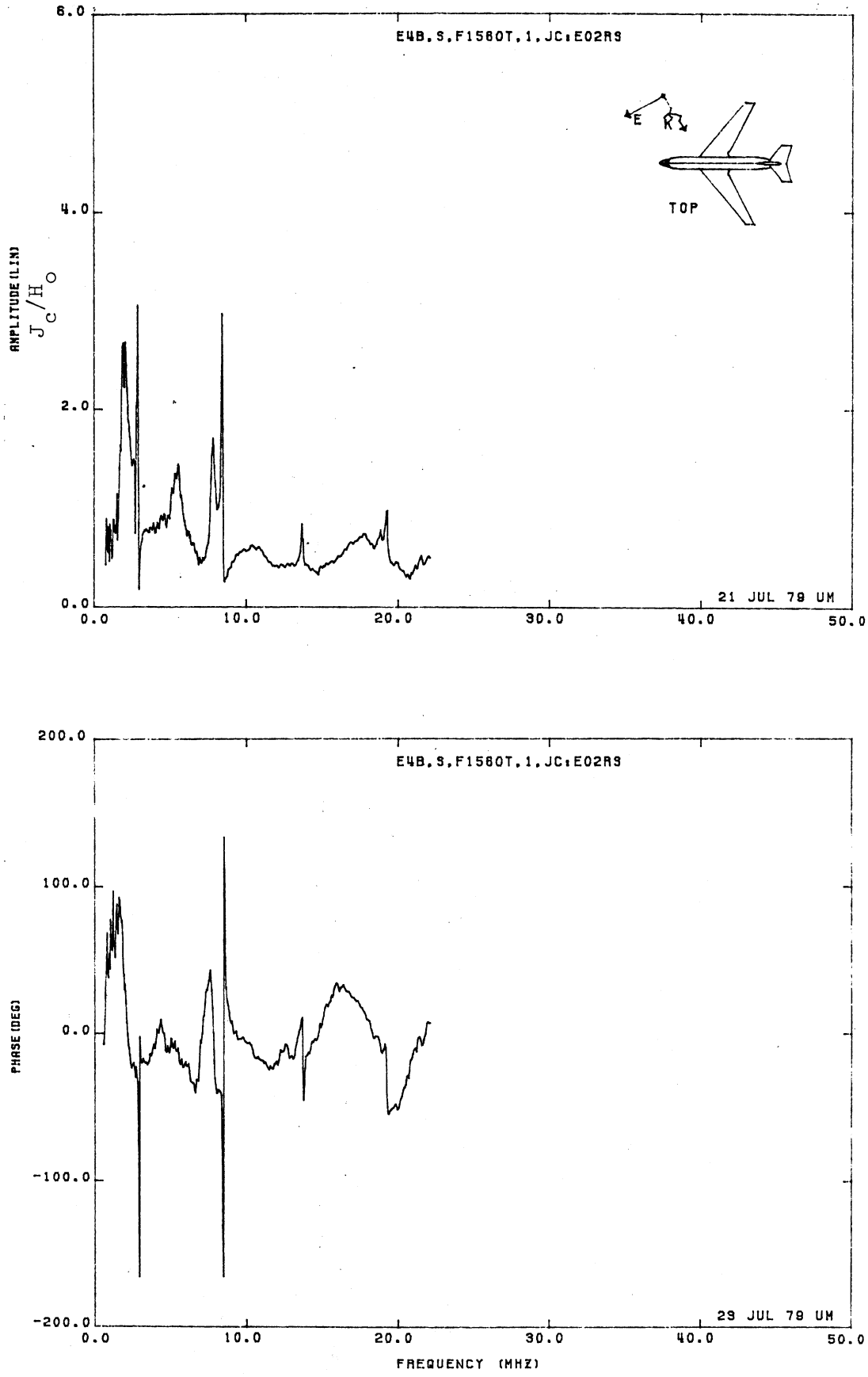

Figure 02RS. Circumferential Current at STA:F1560T, Excitation 1, 1/200 Model.

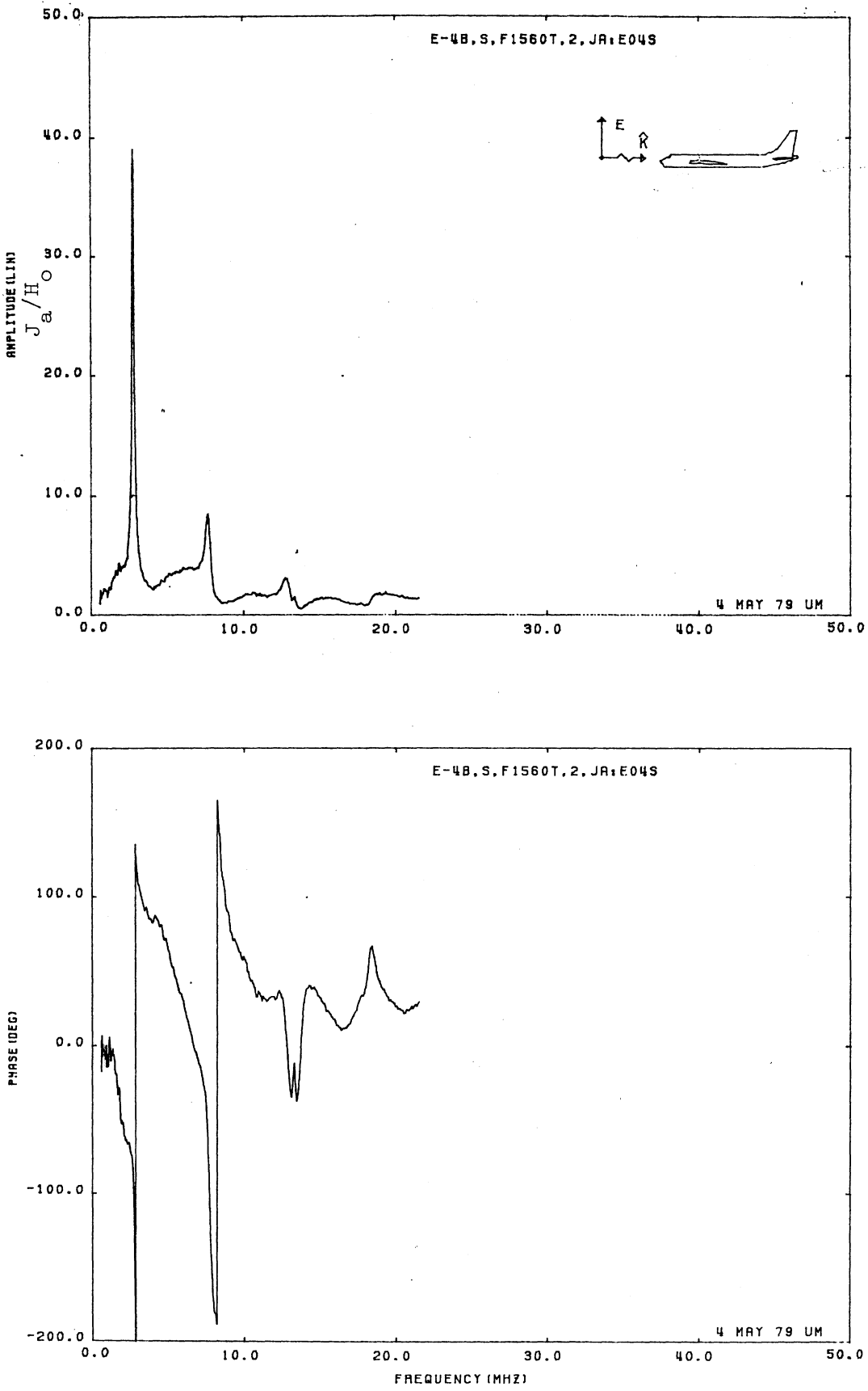

Figure 04S. Axial Current at STA:F1560T, Excitation 2, 1/200 Model.

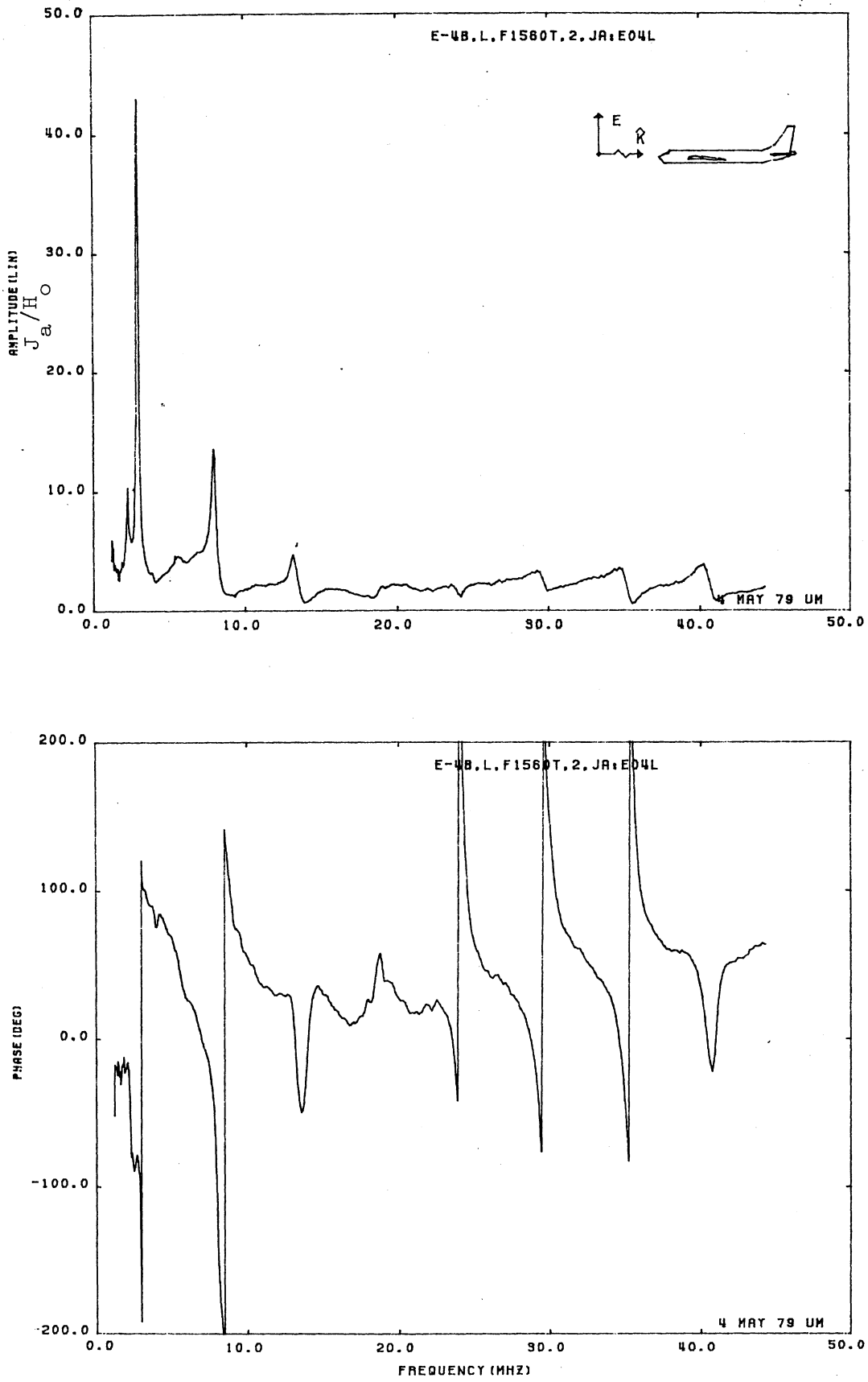

Figure 04L. Axial Current at STA:F1560T, Excitation 2, 1/100 Model.

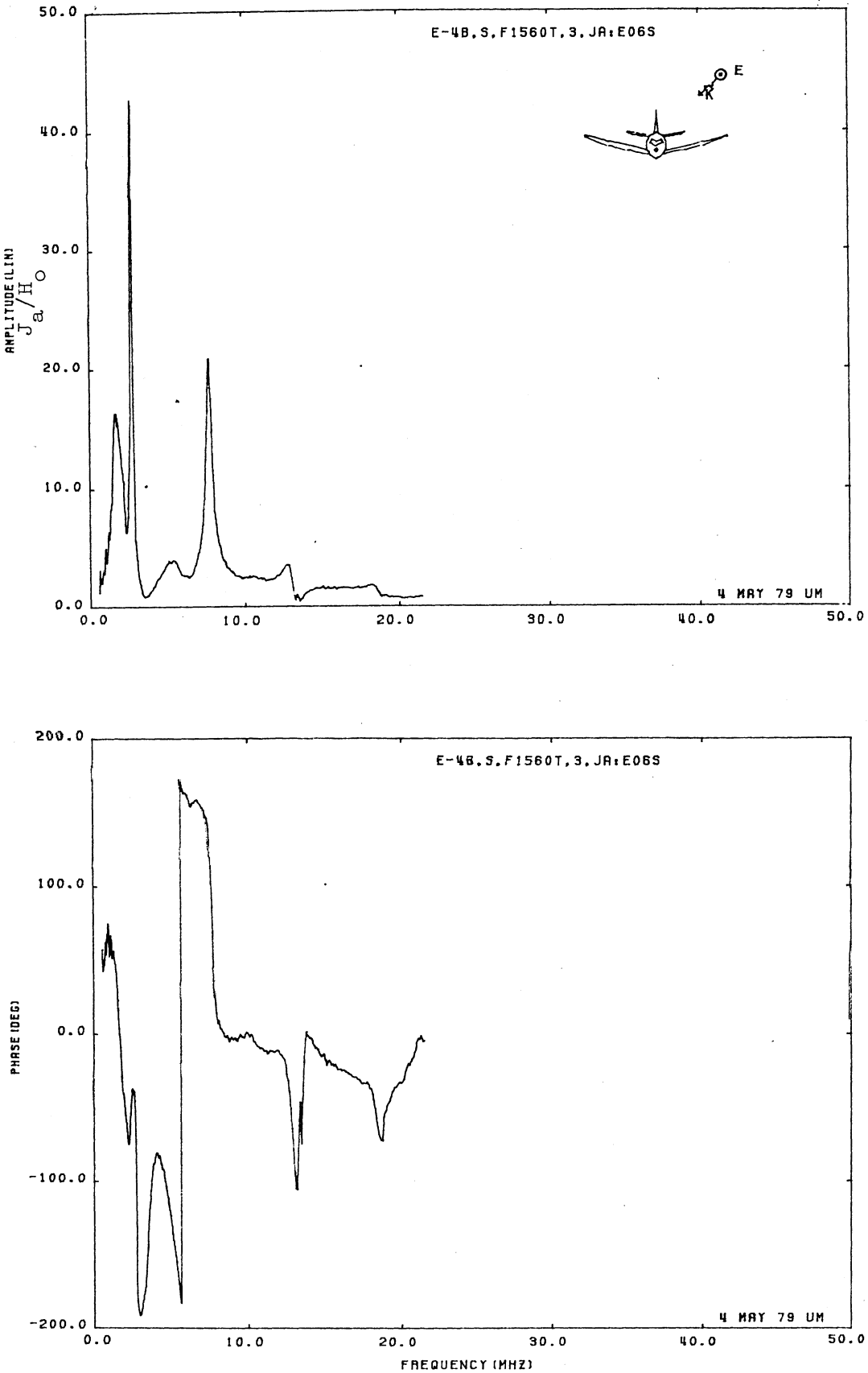

Figure 06S. Axial Current at STA:F1560T, Excitation 3, 1/200 Model.

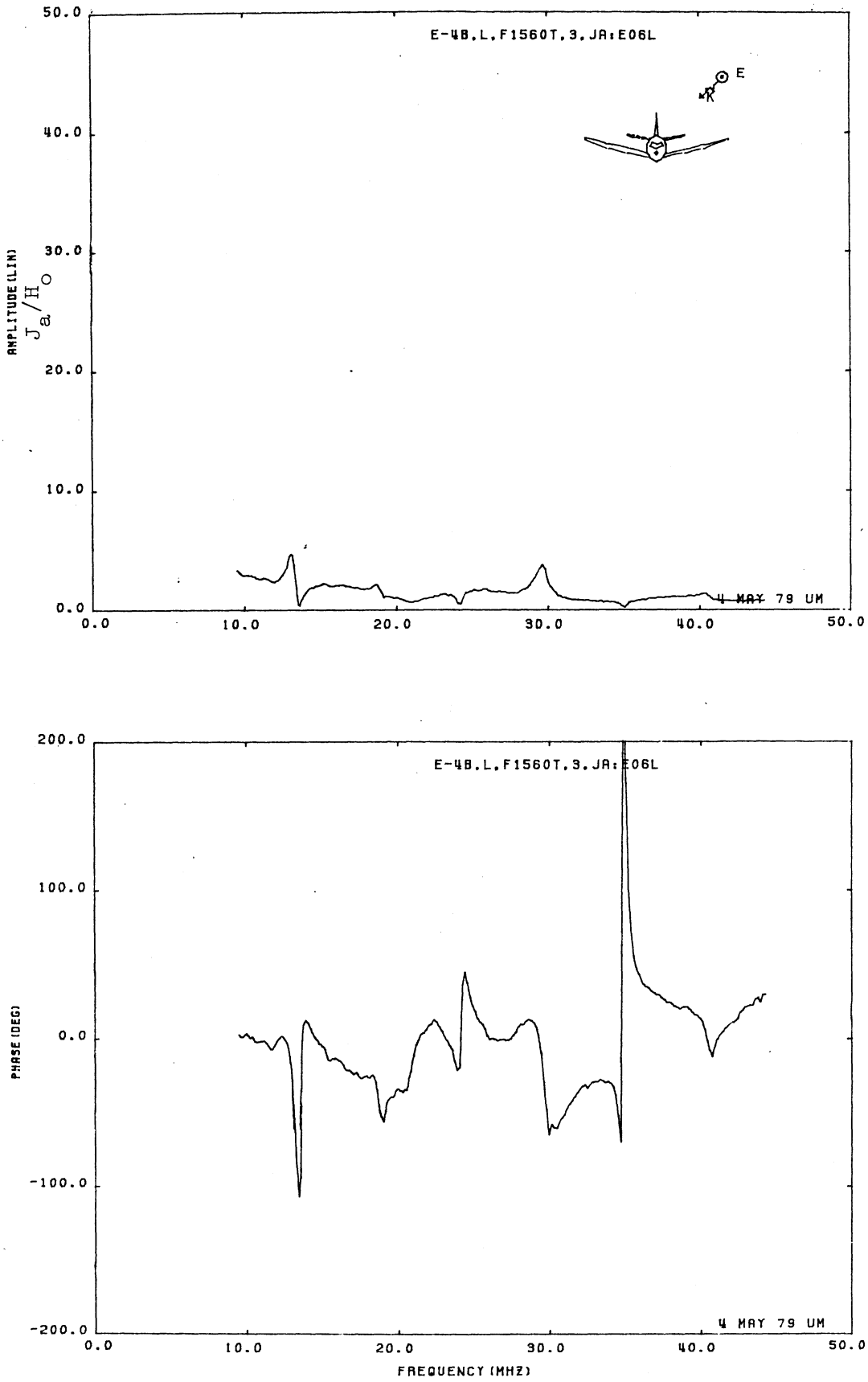

Figure 06L. Axial Current at STA:F1560T, Excitation 3, 1/100 Model.

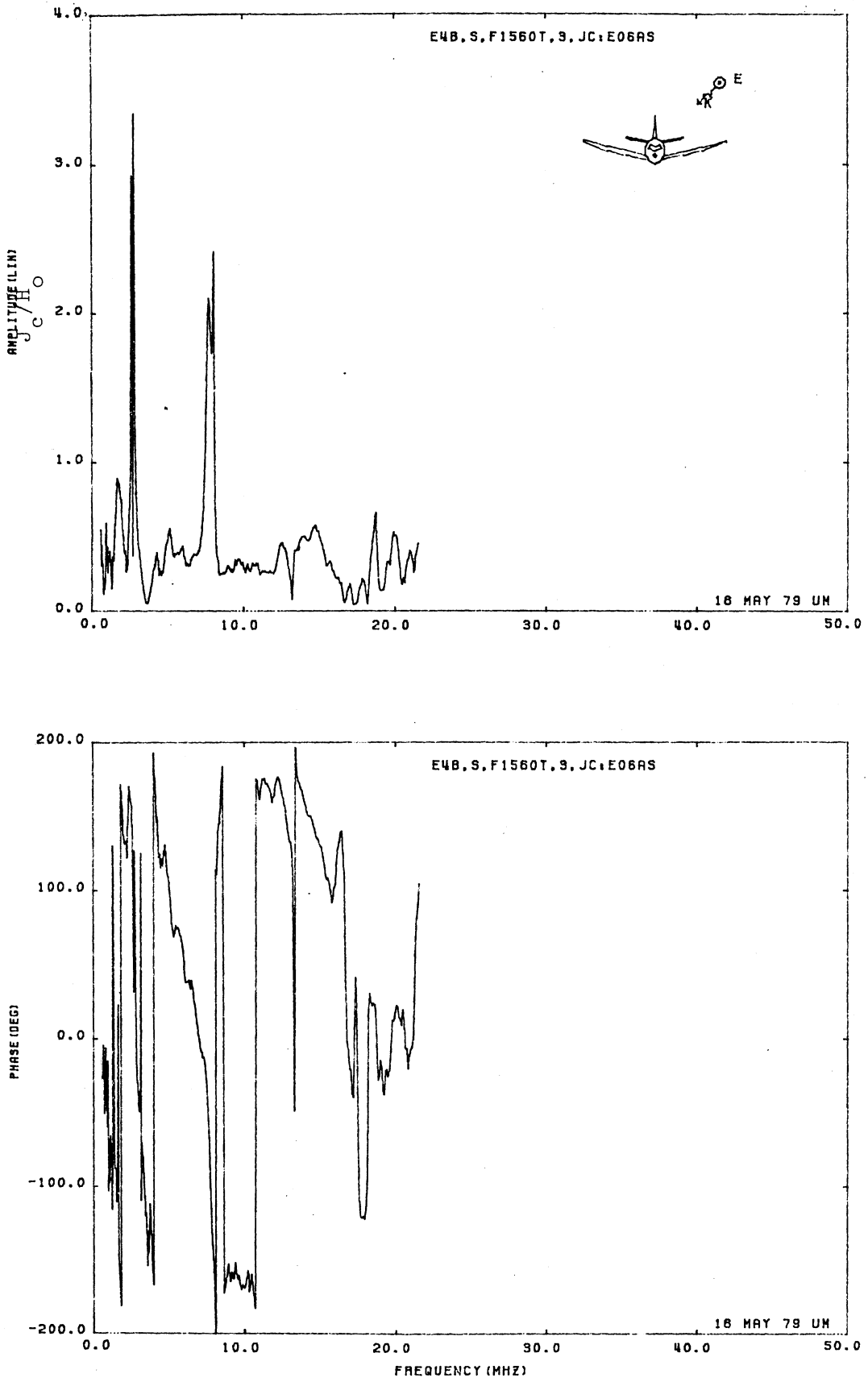

Figure 06AS. Circumferential Current at STA:F1560T, Excitation 3, 1/200 Model.

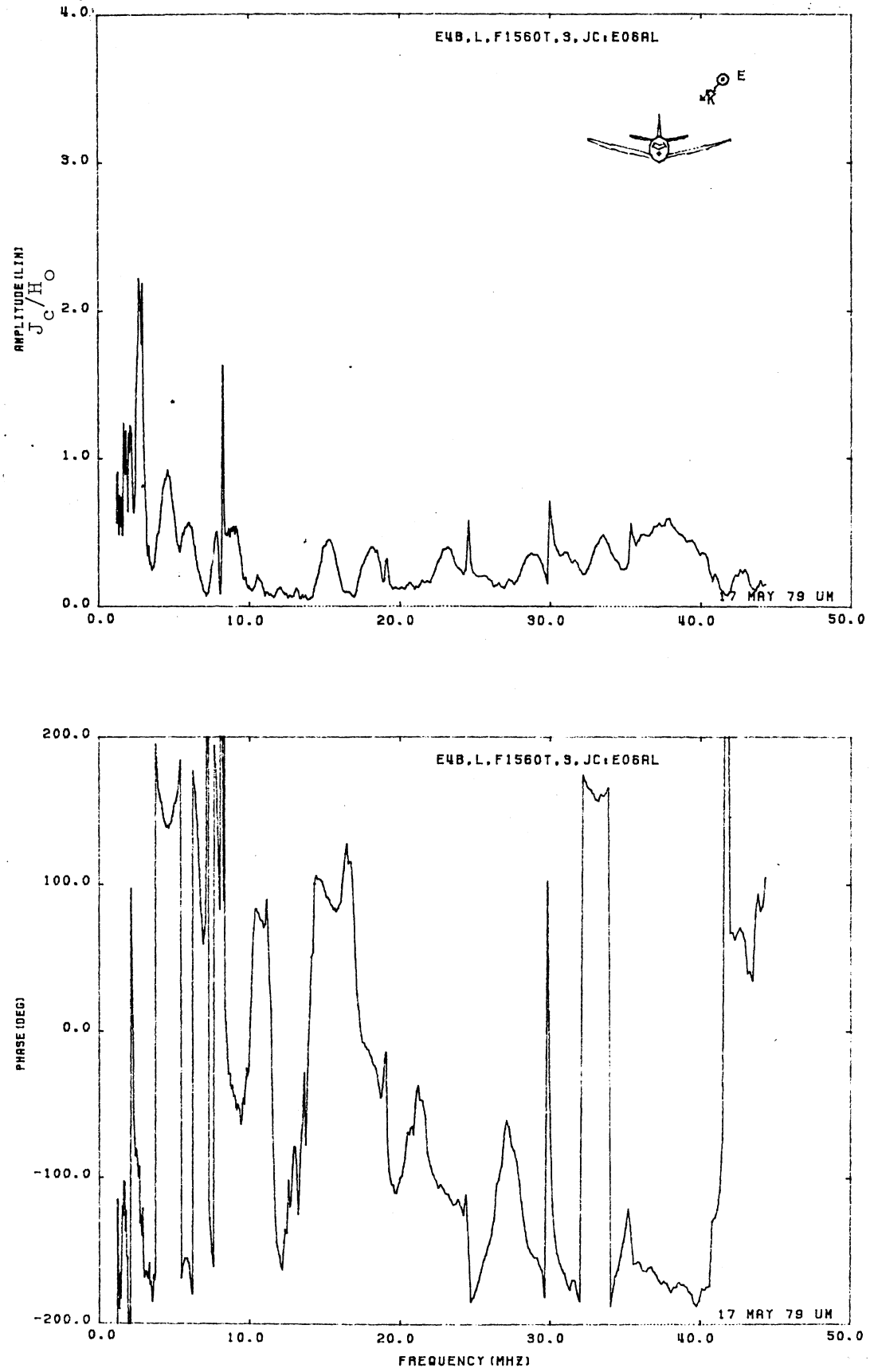

Figure 06AL. Circumferential Current at STA:F1560T, Excitation 3, 1/100 Model.

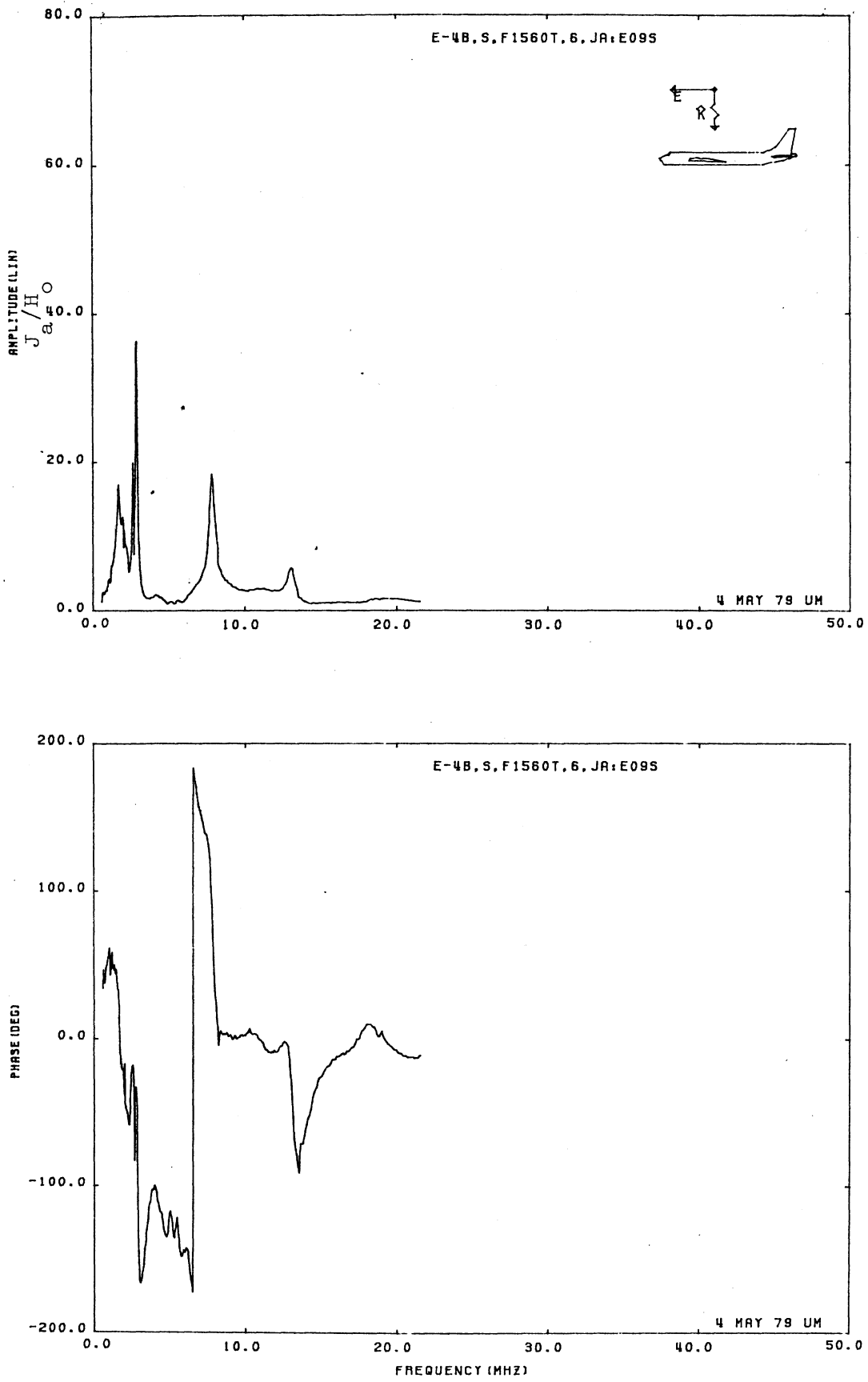

Figure 09S. Axial Current at STA:F1560T, Excitation 6, 1/200 Model.

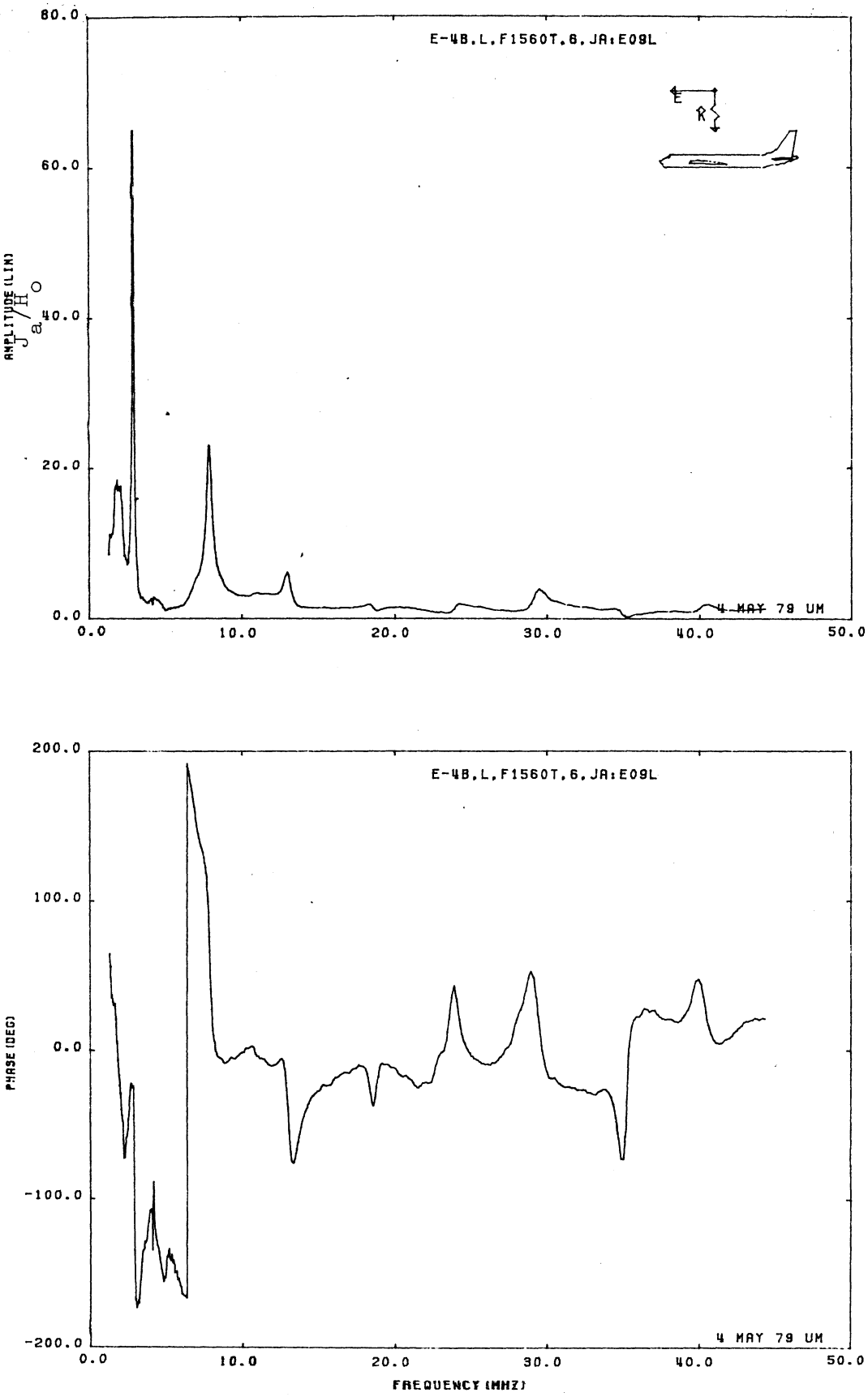

Figure 09L. Axial Current at STA:F1560T, Excitation 6, 1/100 Model.

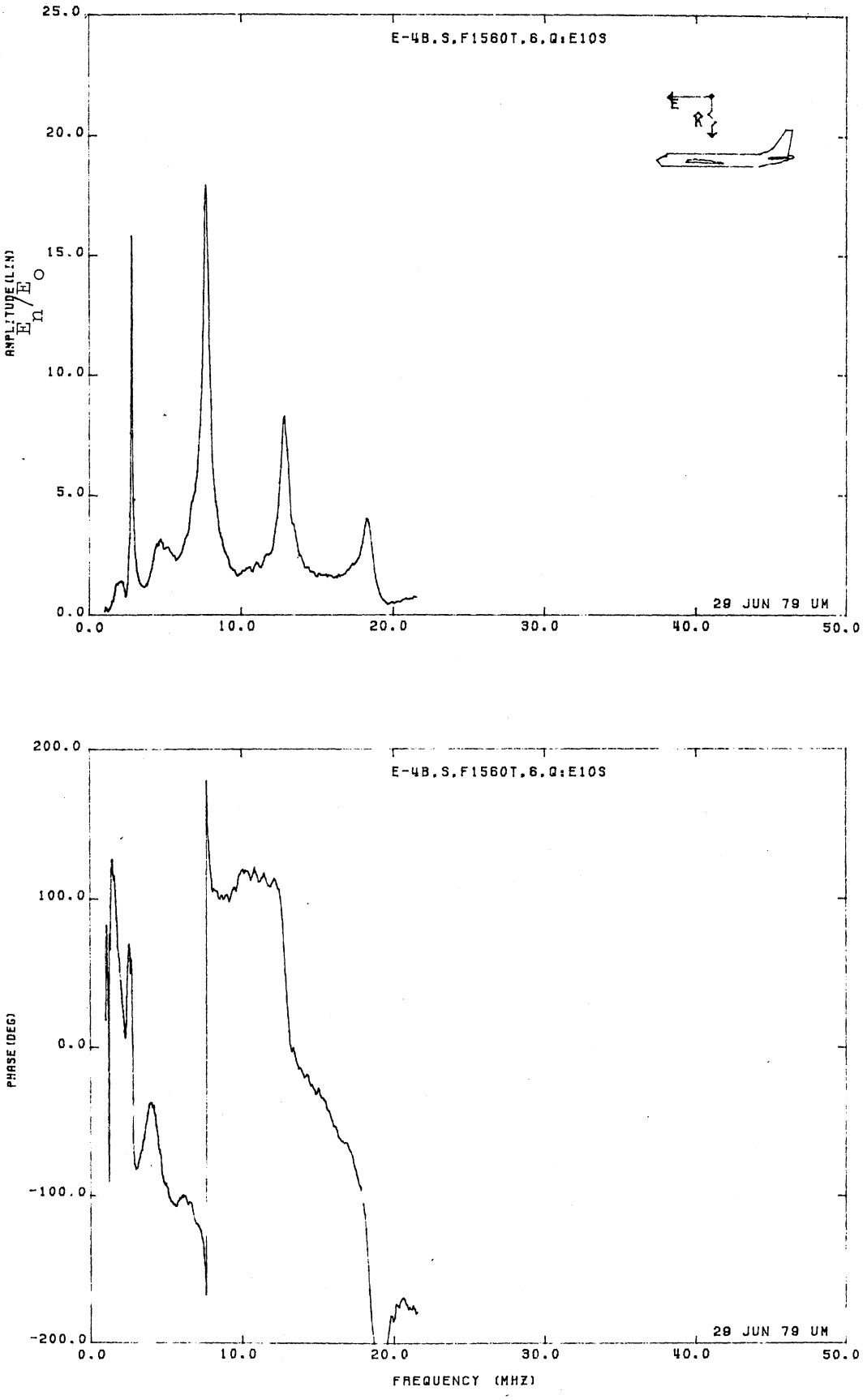

Figure 10S. Normal Electric Field at STA:F1560T, Excitation 6, 1/200 Model.

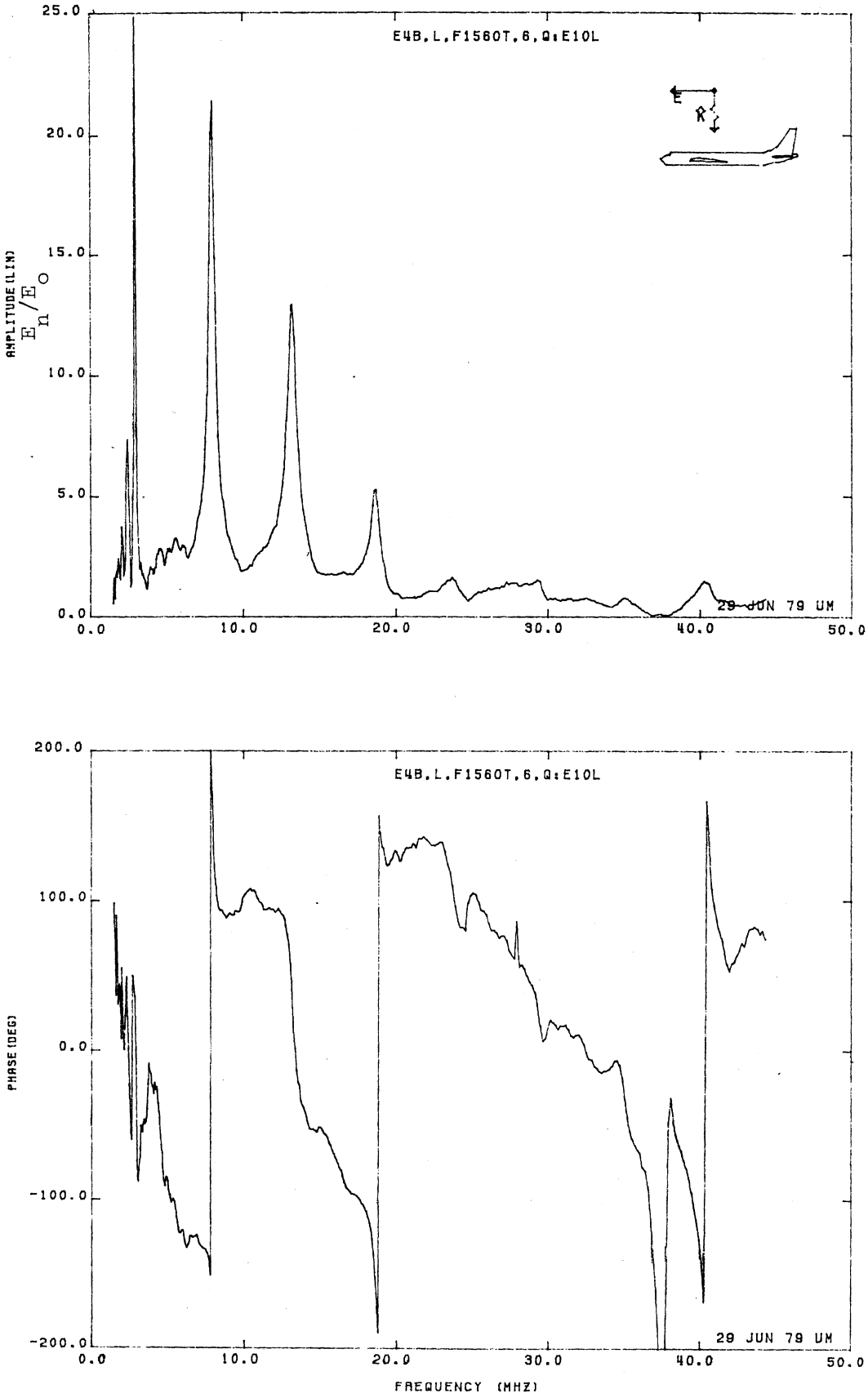

Figure 10L. Normal Electric Field at STA:F1560T, Excitation 6, 1/100 Model.

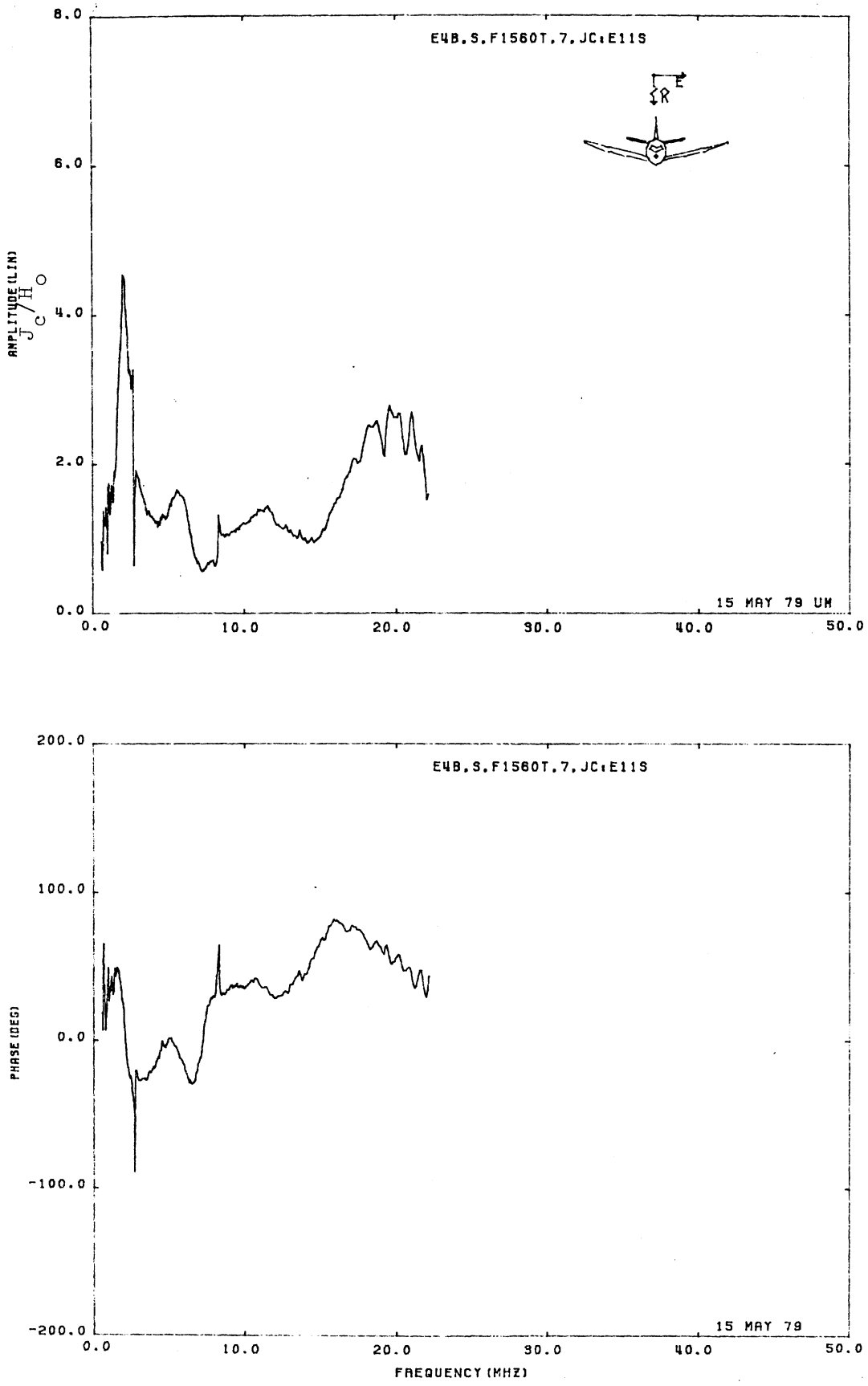

Figure 11S. Circumferential Current at STA:F1560T, Excitation 7, 1/200 Model.

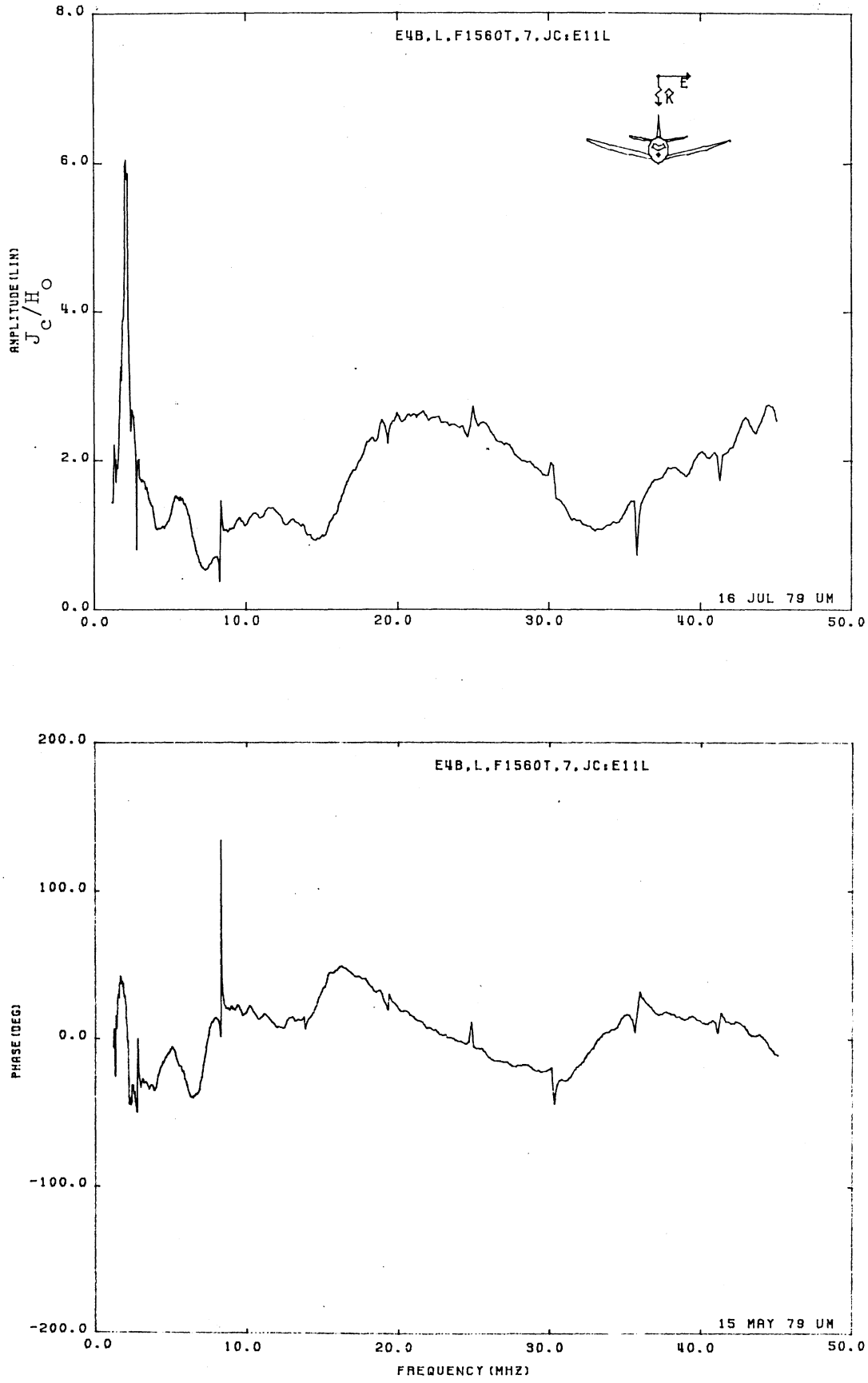

Figure 11L. Circumferential Current at STA:F1560T, Excitation 7, 1/100 Model.

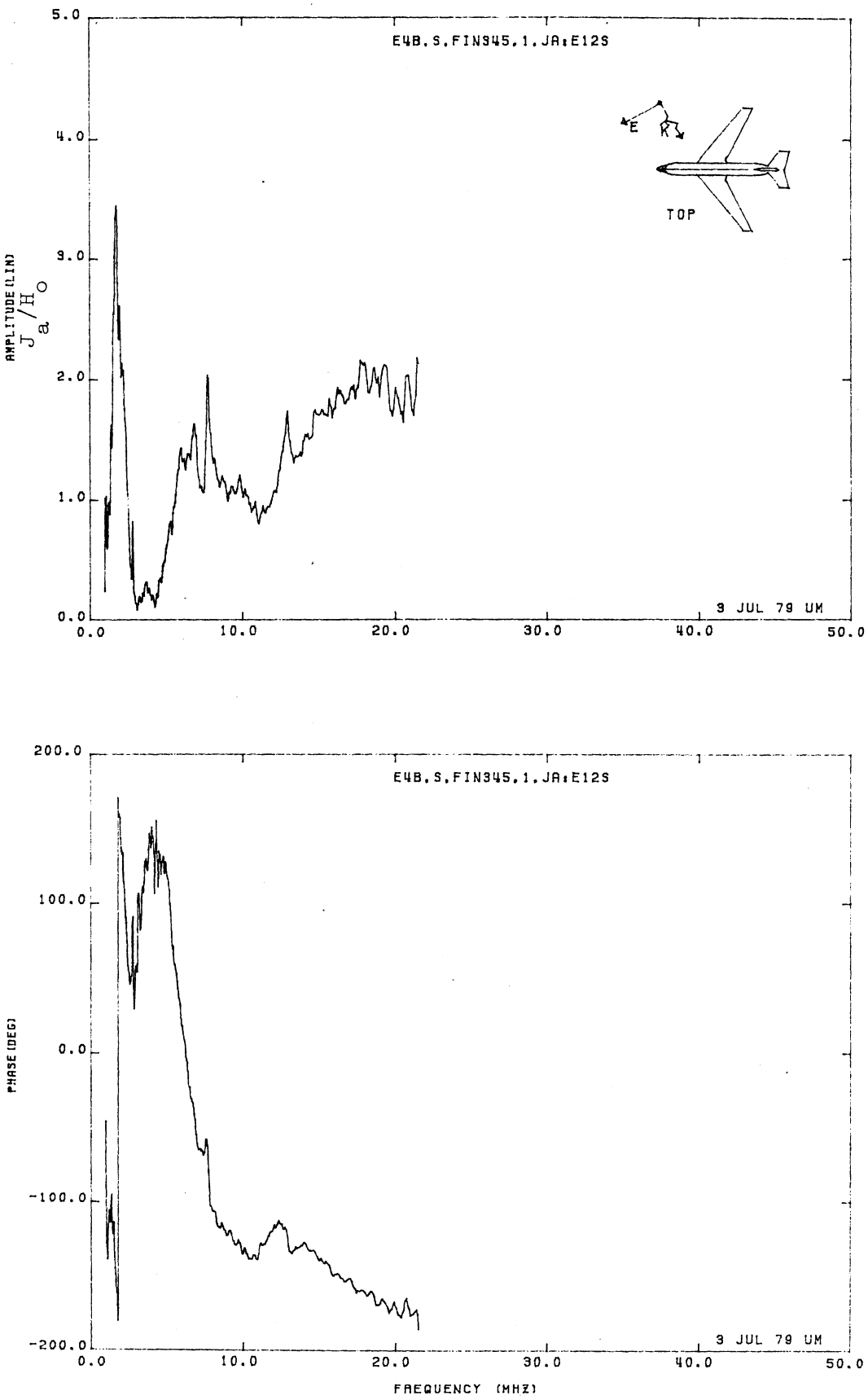

Figure 12S. Axial Current at STA:FIN345, Excitation 1, 1/200 Model.

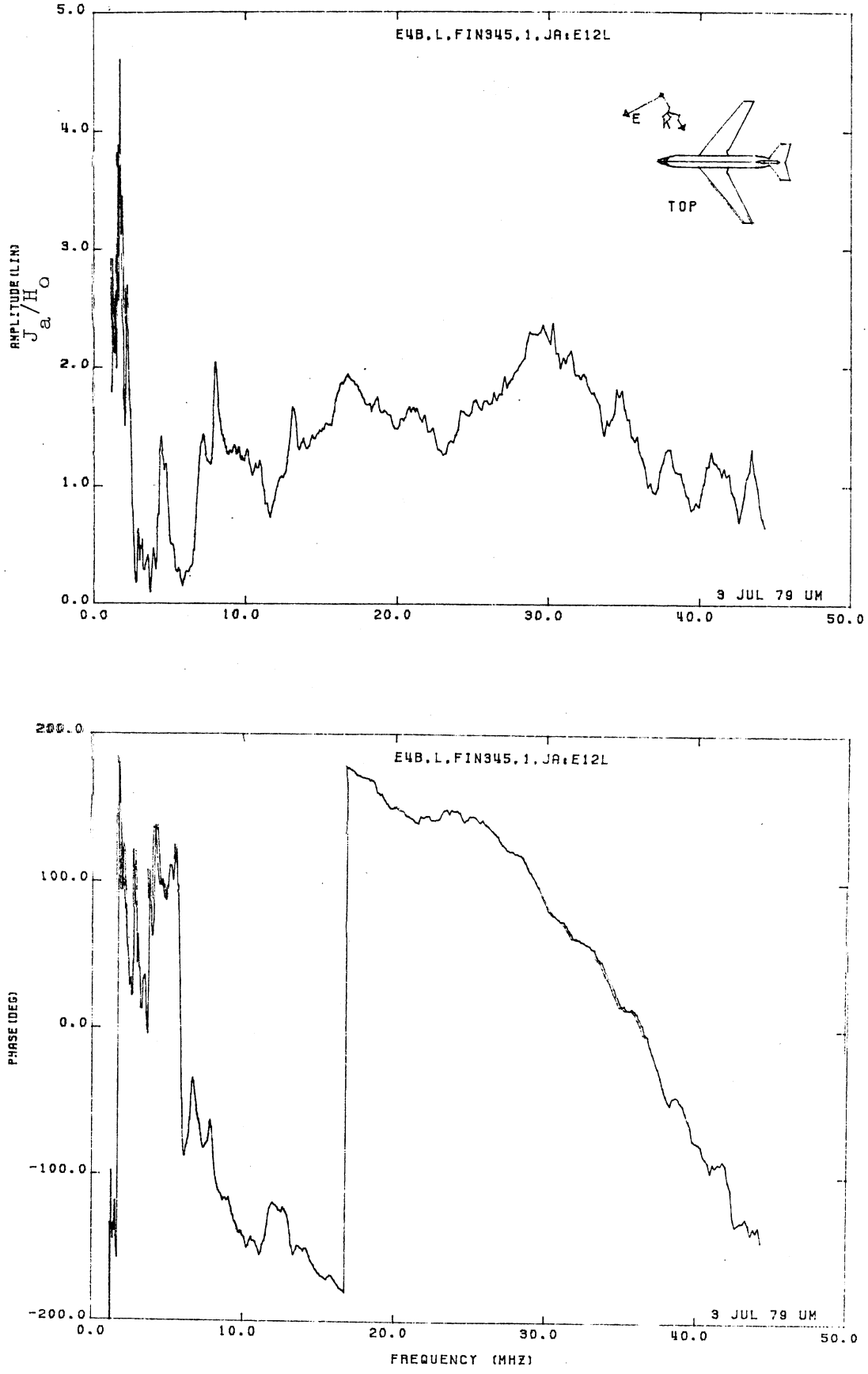

Figure 12L. Axial Current at STA:FIN345, Excitation 1, 1/100 Model.

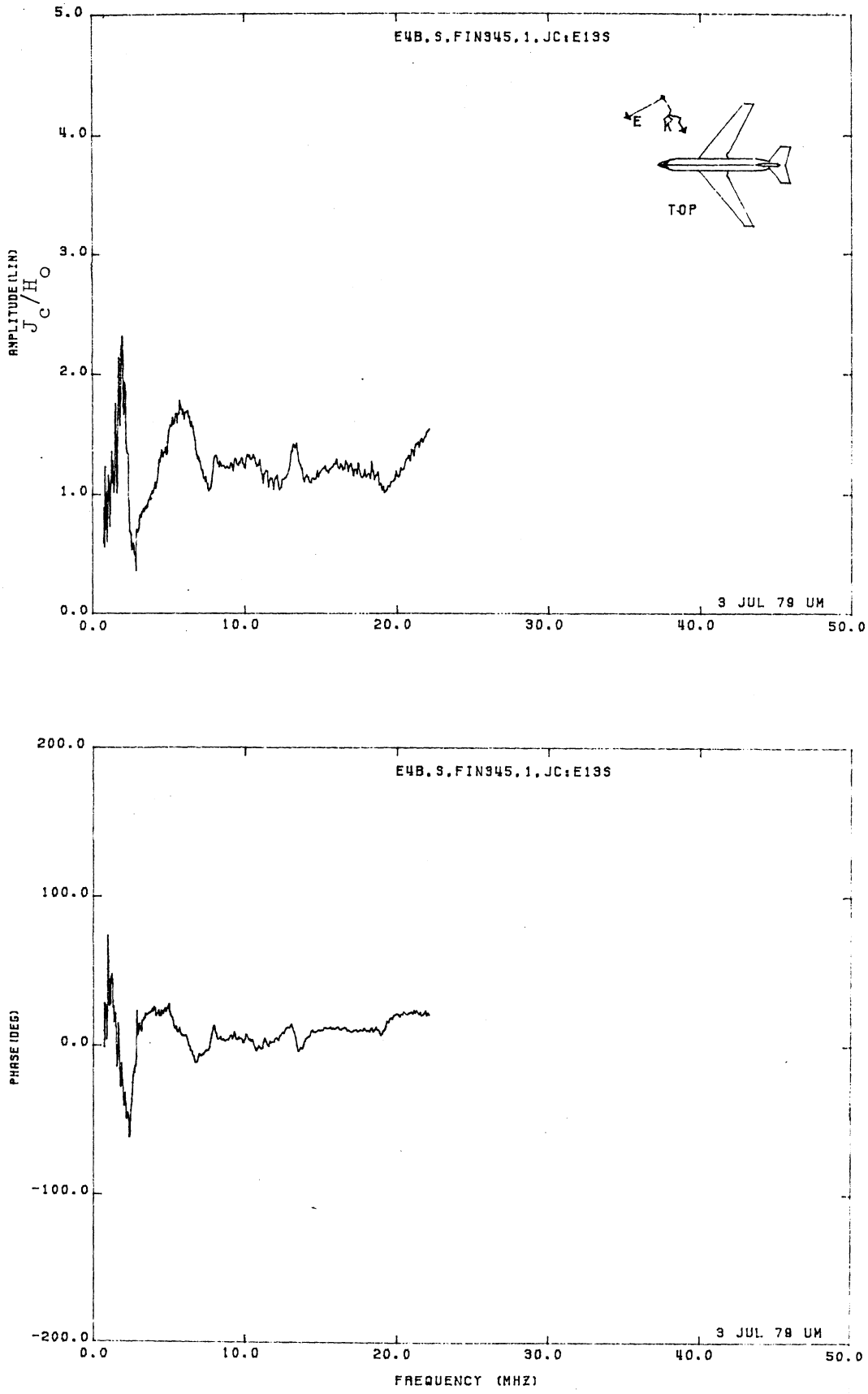

Figure 13S. Circumferential Current at STA:FIN345, Excitation 1 1/200 Model.

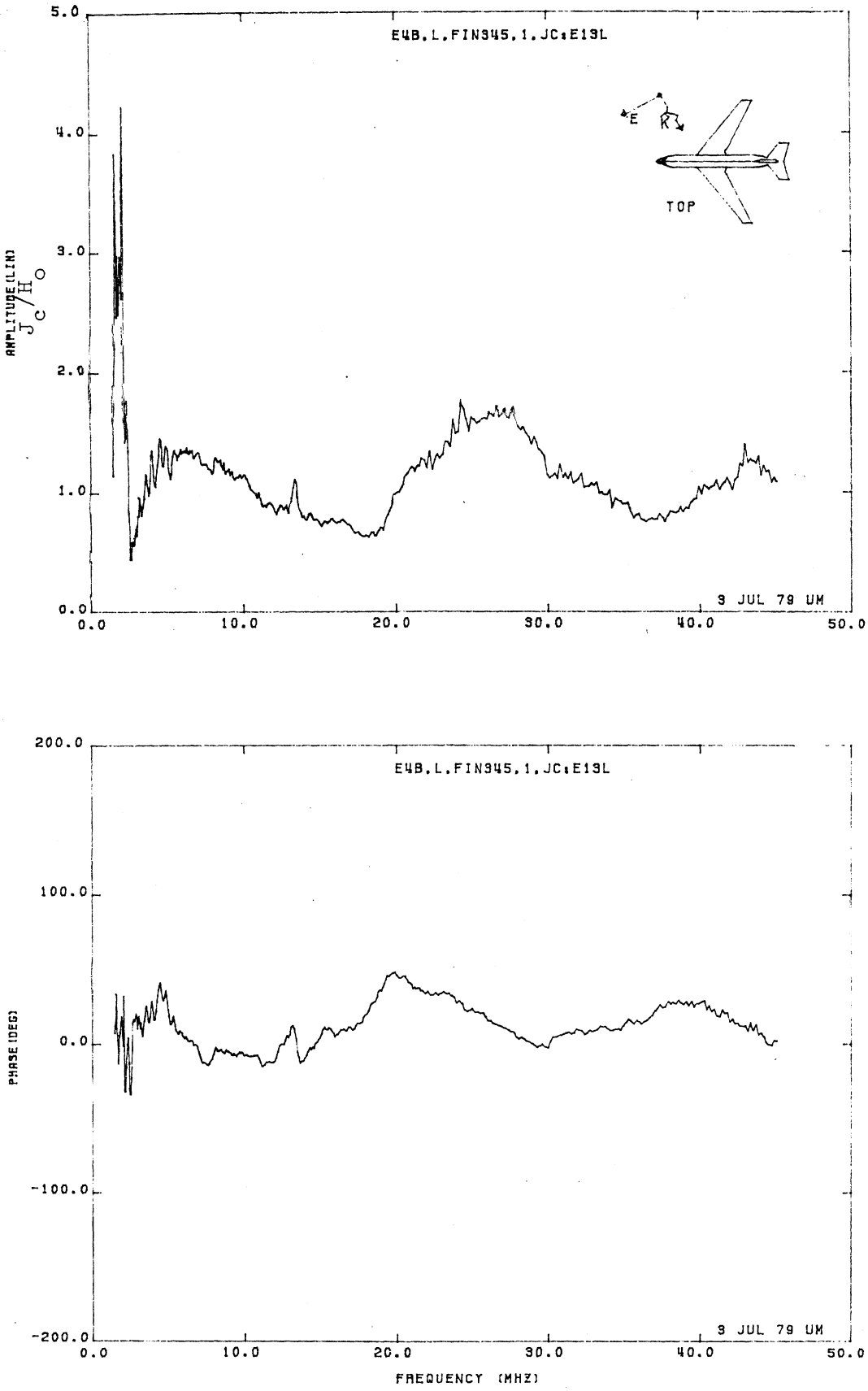

Figure 13L. Circumferential Current at STA:FIN345, Excitation 1, 1/100 Model.

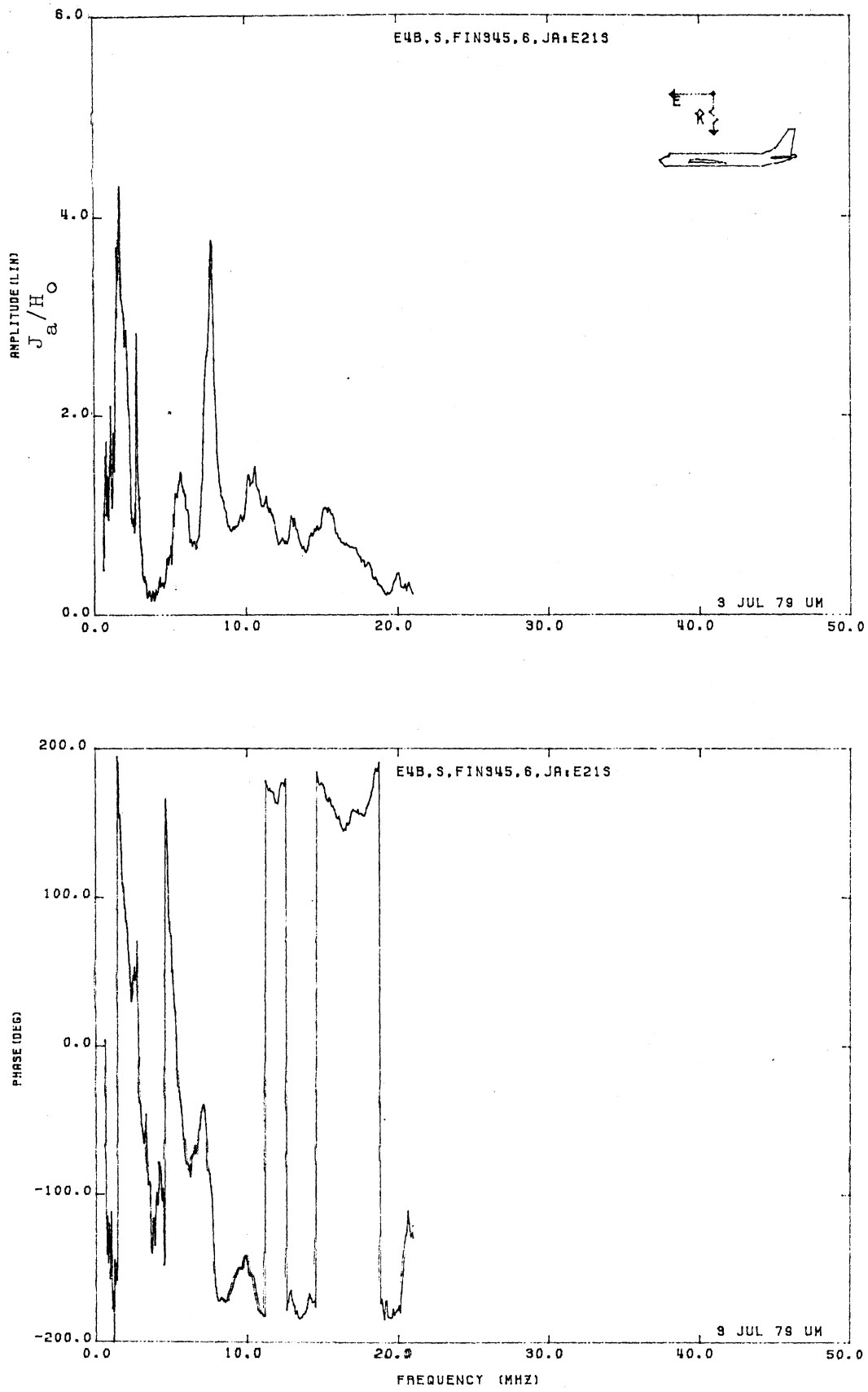

Figure 21S. Axial Current at STA:FIN345, Excitation 6, 1/200 Model.

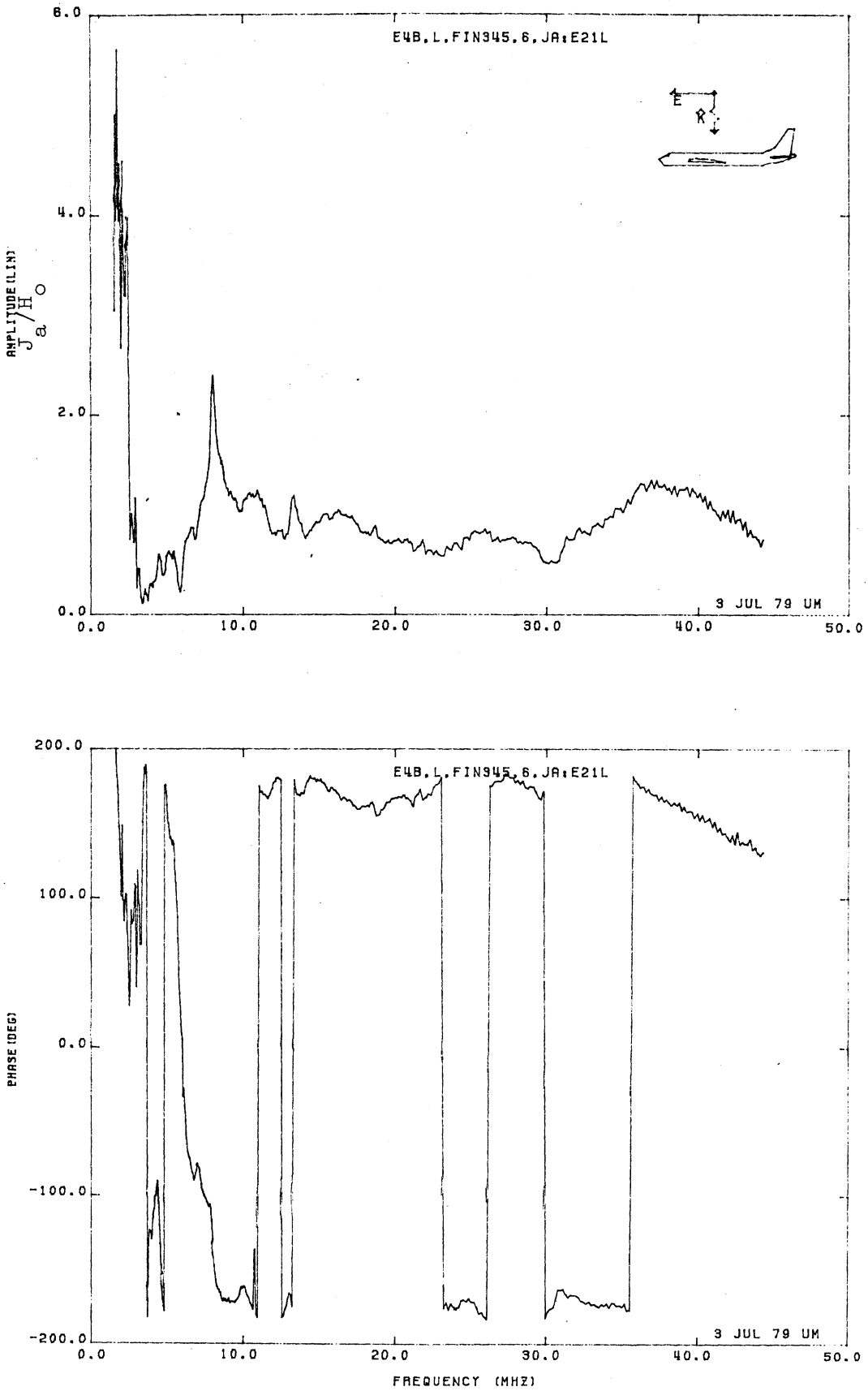

Figure 21L. Axial Current at STA:FIN345, Excitation 6, 1/100 Model.

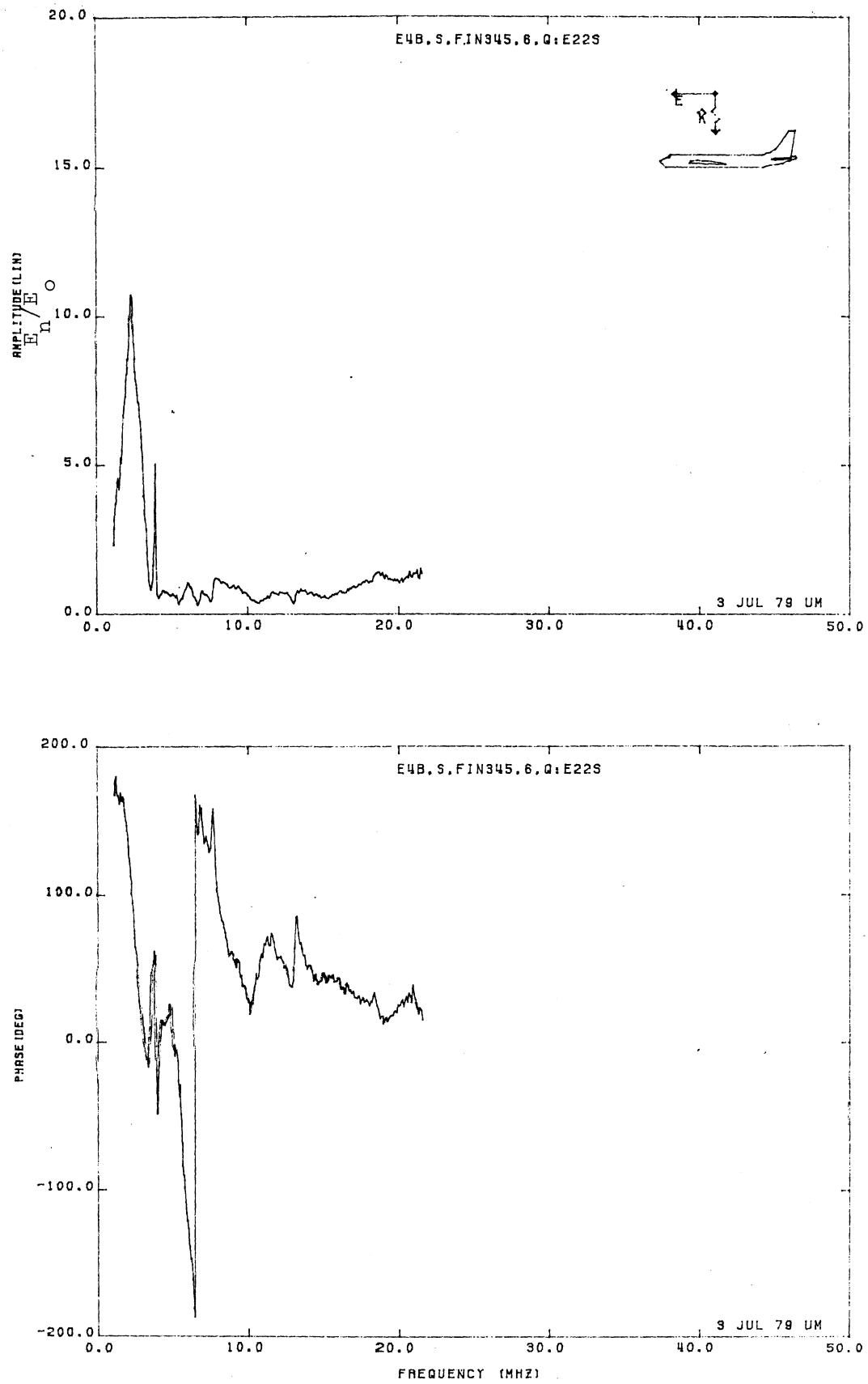

Figure 22S. Normal Electric Field at STA:FIN345, Excitation 6, 1/200 Model.

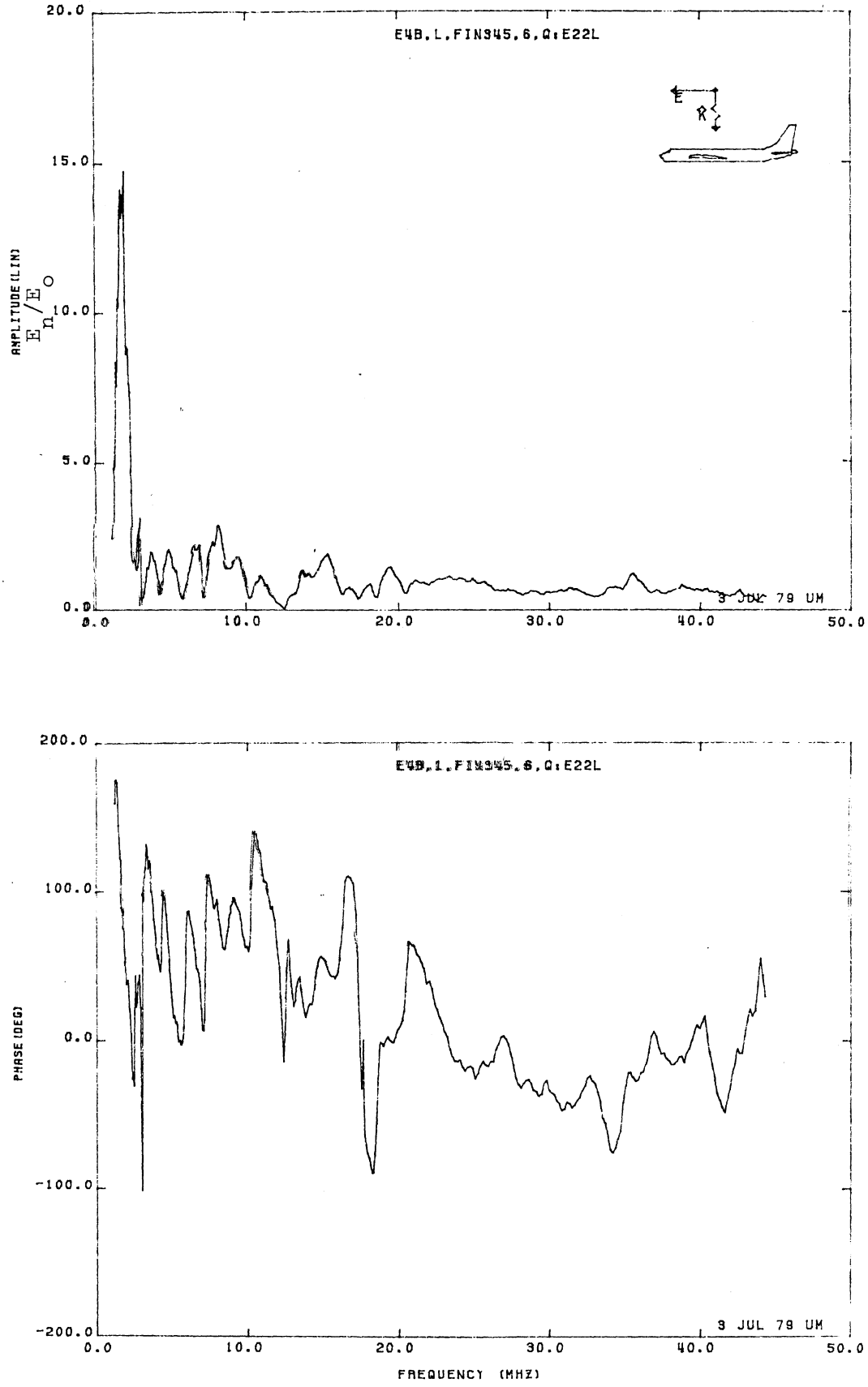

Figure 22L. Normal Electric Field at STA:FIN345, Excitation 6, 1/100 Model.

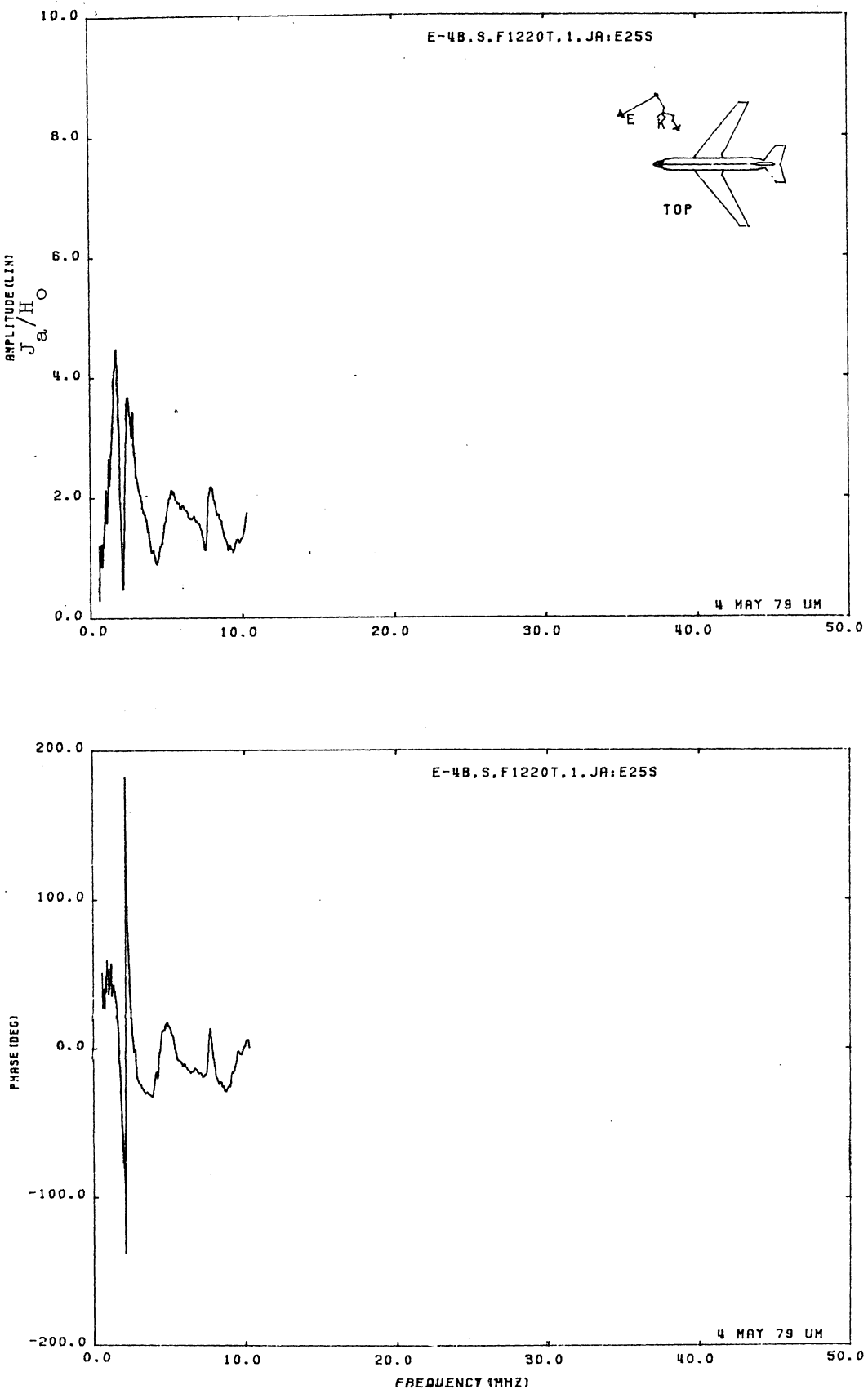

Figure 25S. Axial Current at STA:F1220T, Excitation 1*, 1/200 Model. (1* done for $\phi = -30°$, $\theta = 50°$)

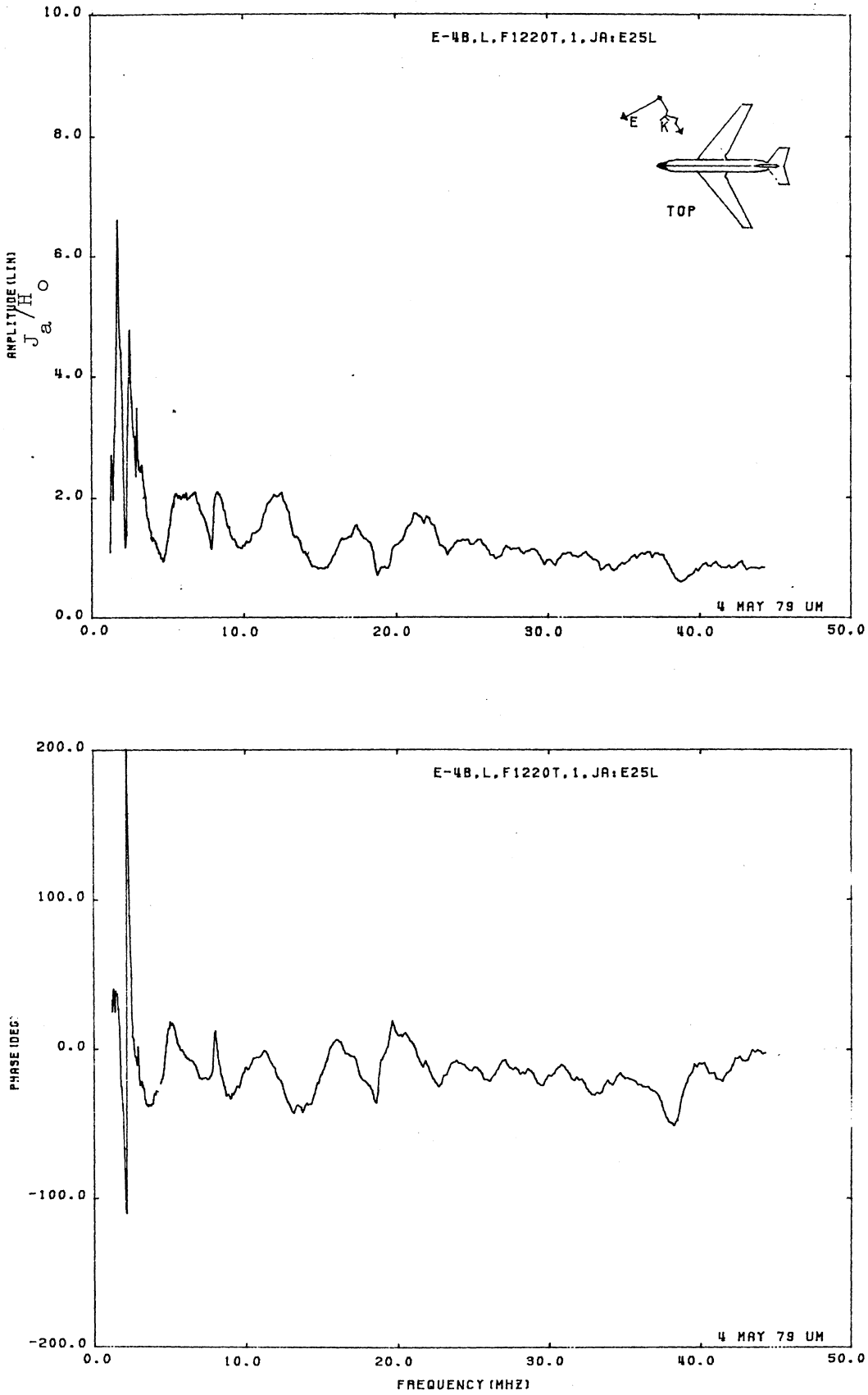

Figure 25L. Axial Current at STA:1220T, Excitation 1*, 1/100 Model. (1* done for $\phi = -30°$, $\theta = 50°$)

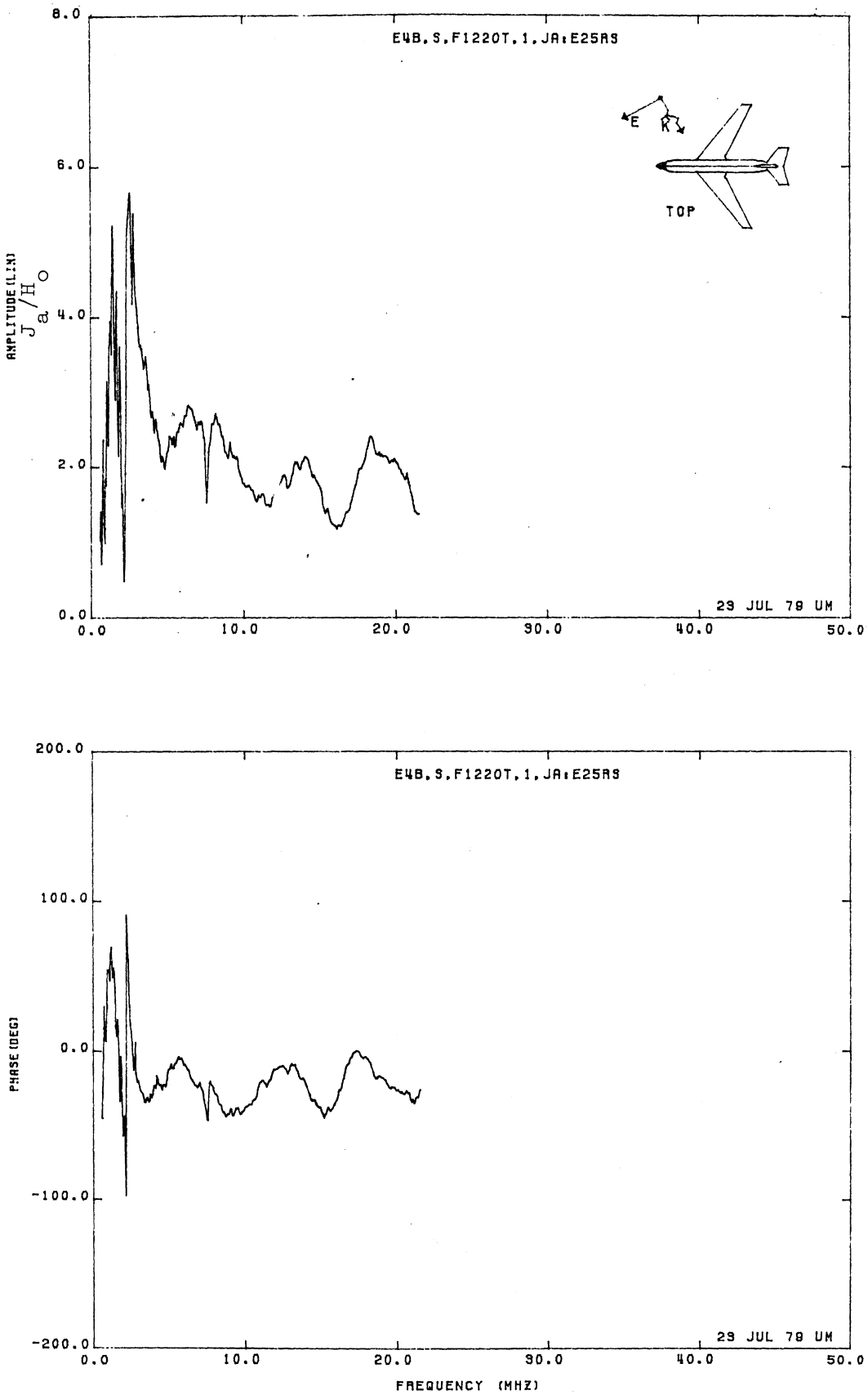

Figure 25RS. Axial Current at STA:F1220T, Excitation 1, 1/200 Model.

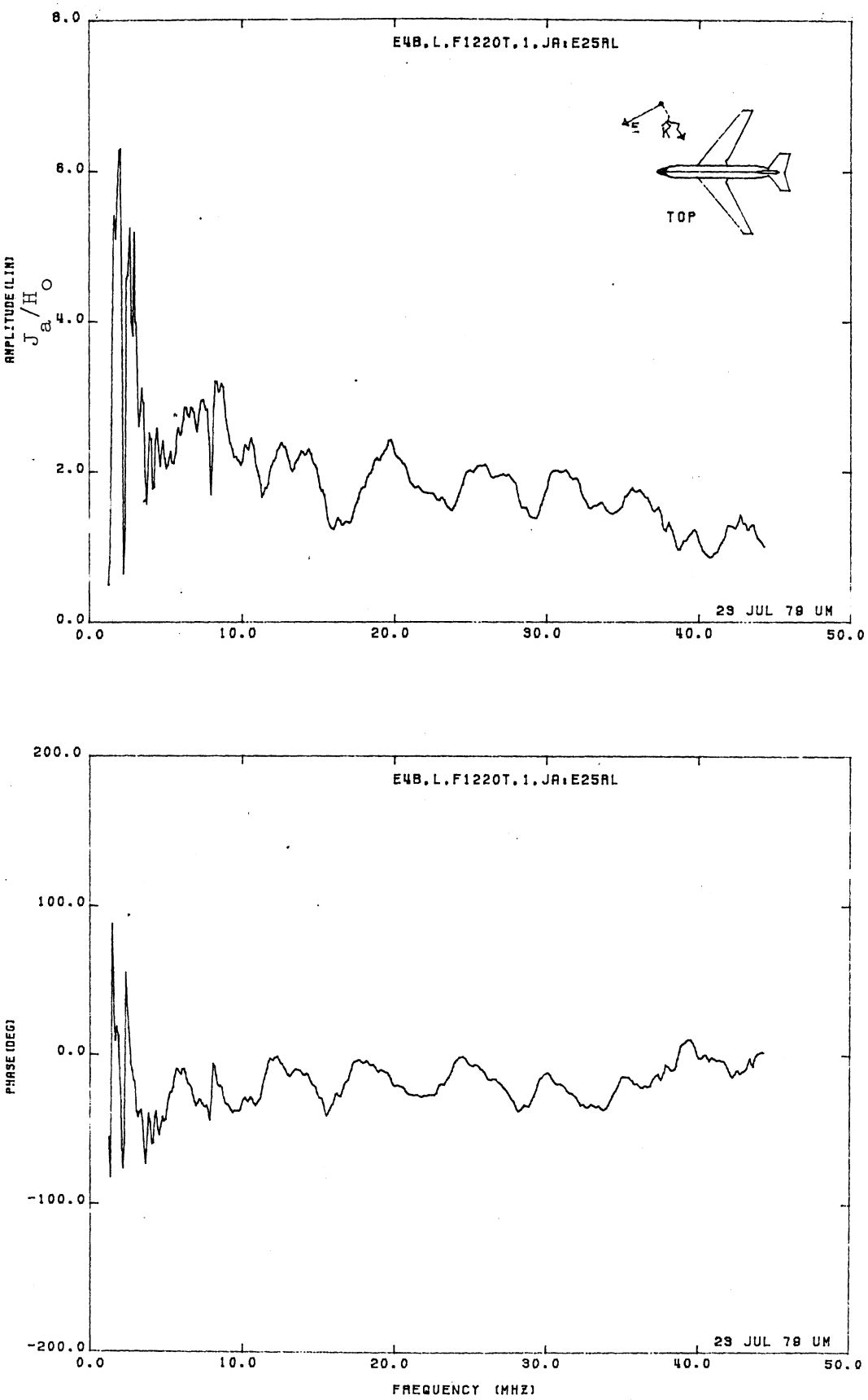

Figure 25RL. Axial Current at STA:F1220T, Excitation 1, 1/100 Model.

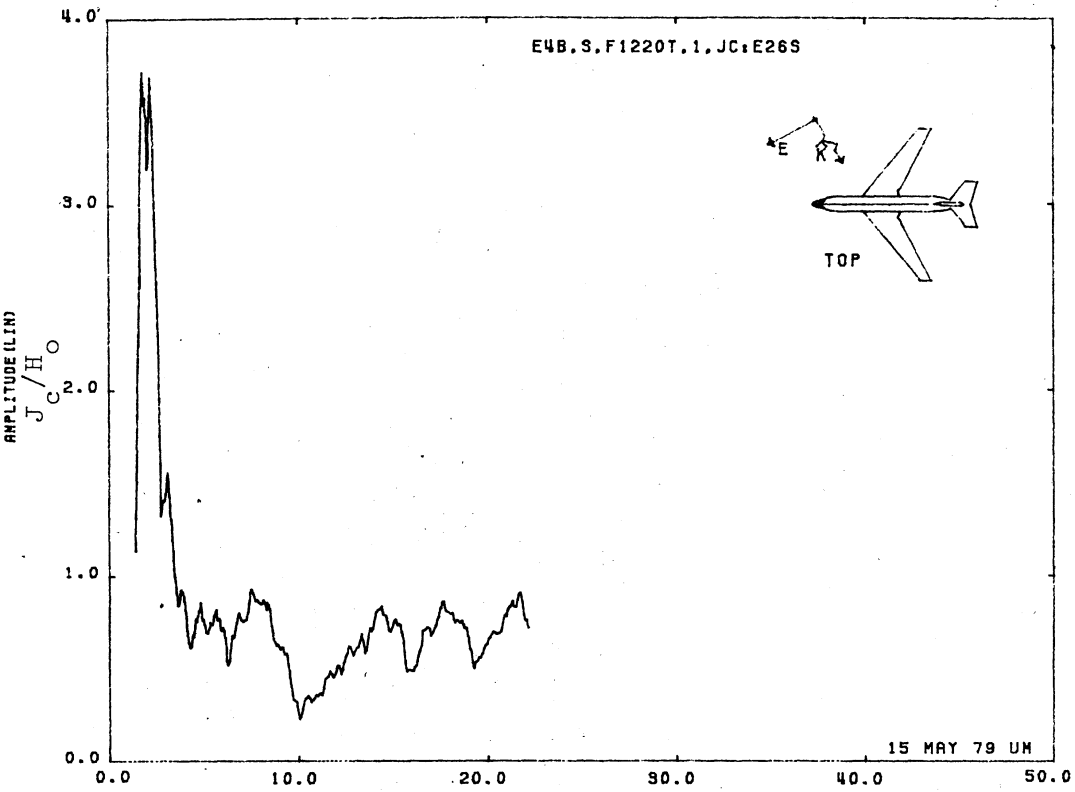

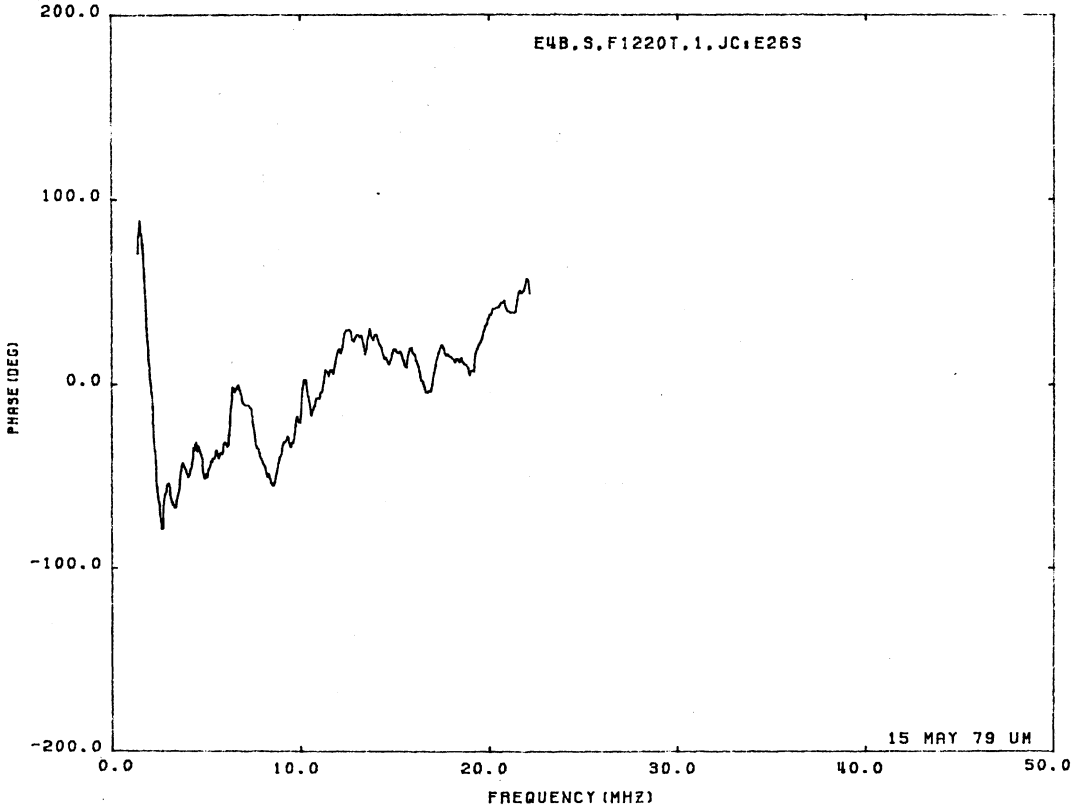

Figure 26S. Circumferential Current at STA:F1220T, Excitation 1*, 1/200 Model. (1* done for $\phi = -30°$, $\theta = 50°$)

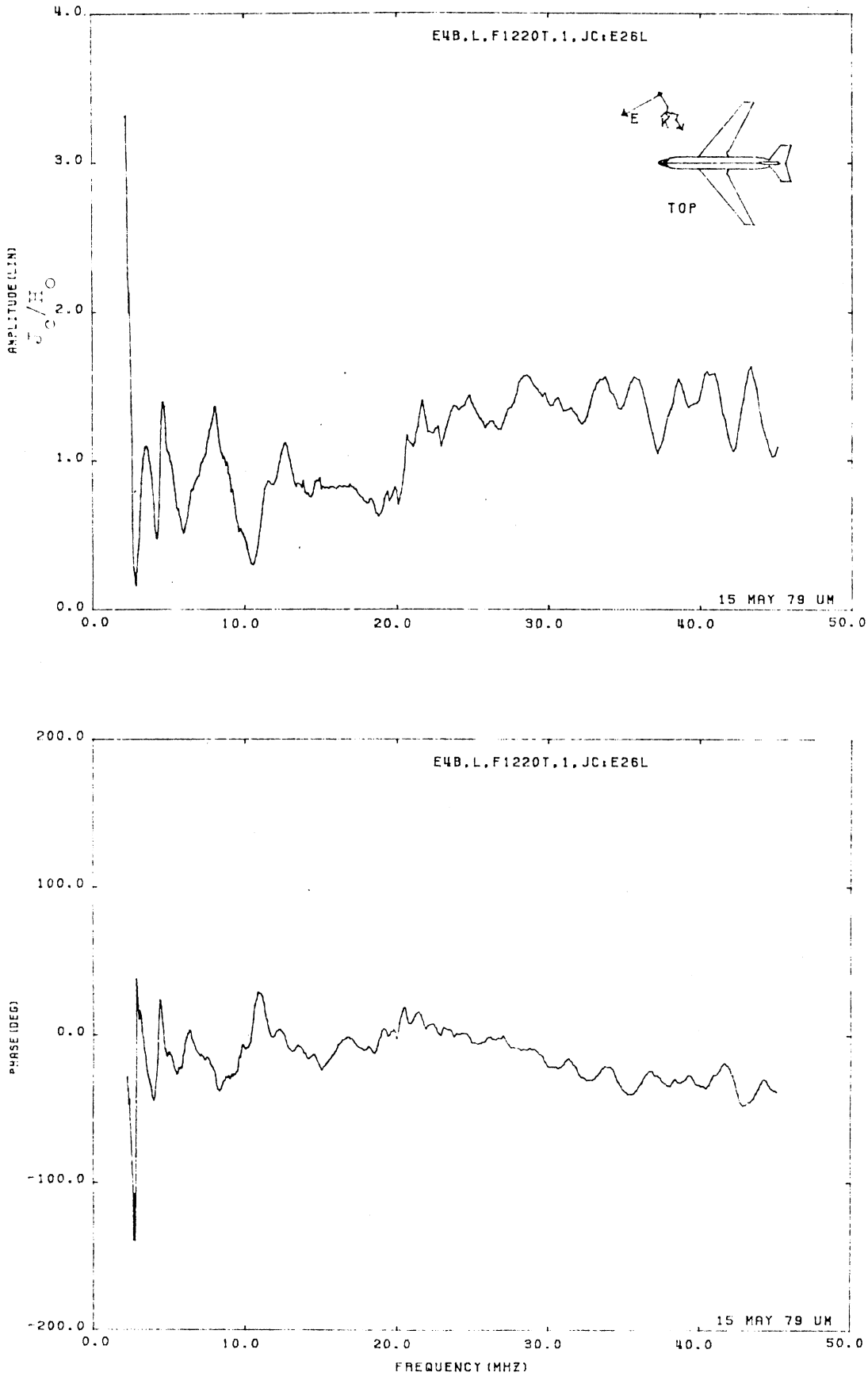

Figure 26L. Circumferential Current atSTA:F1220T, Excitation 1*, 1/100 Model. (1* done for $\phi = -30°$, $\theta = 50°$)

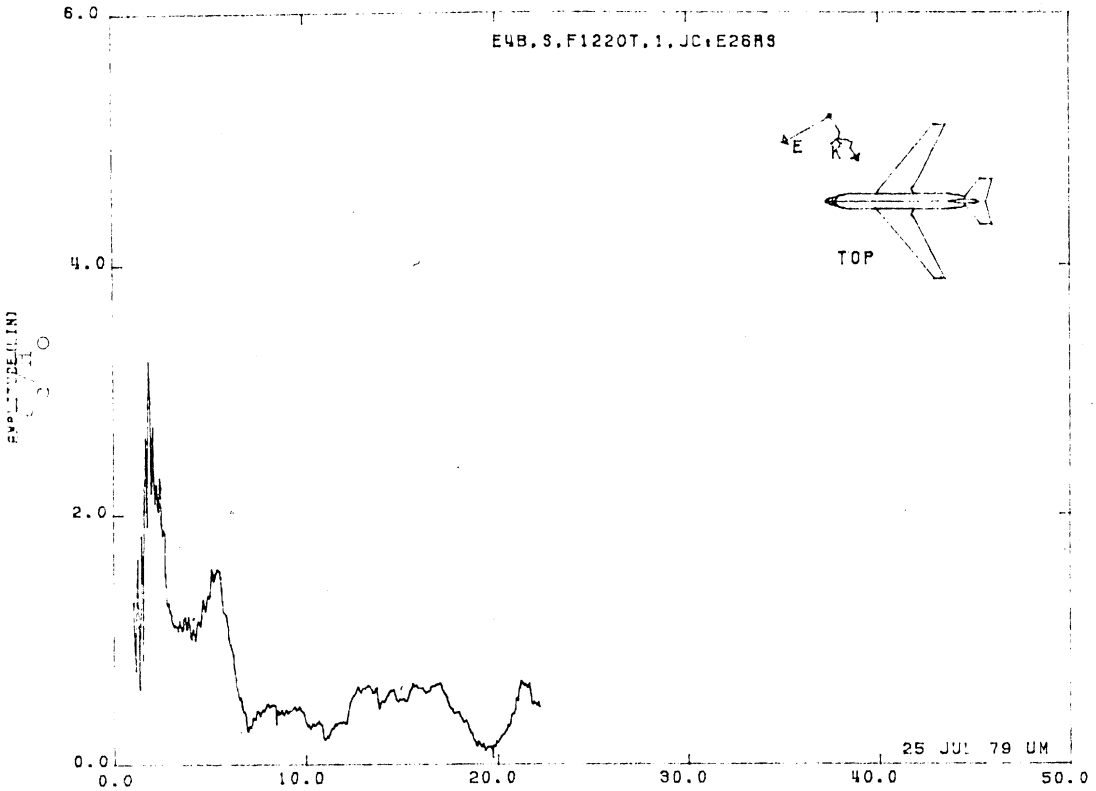

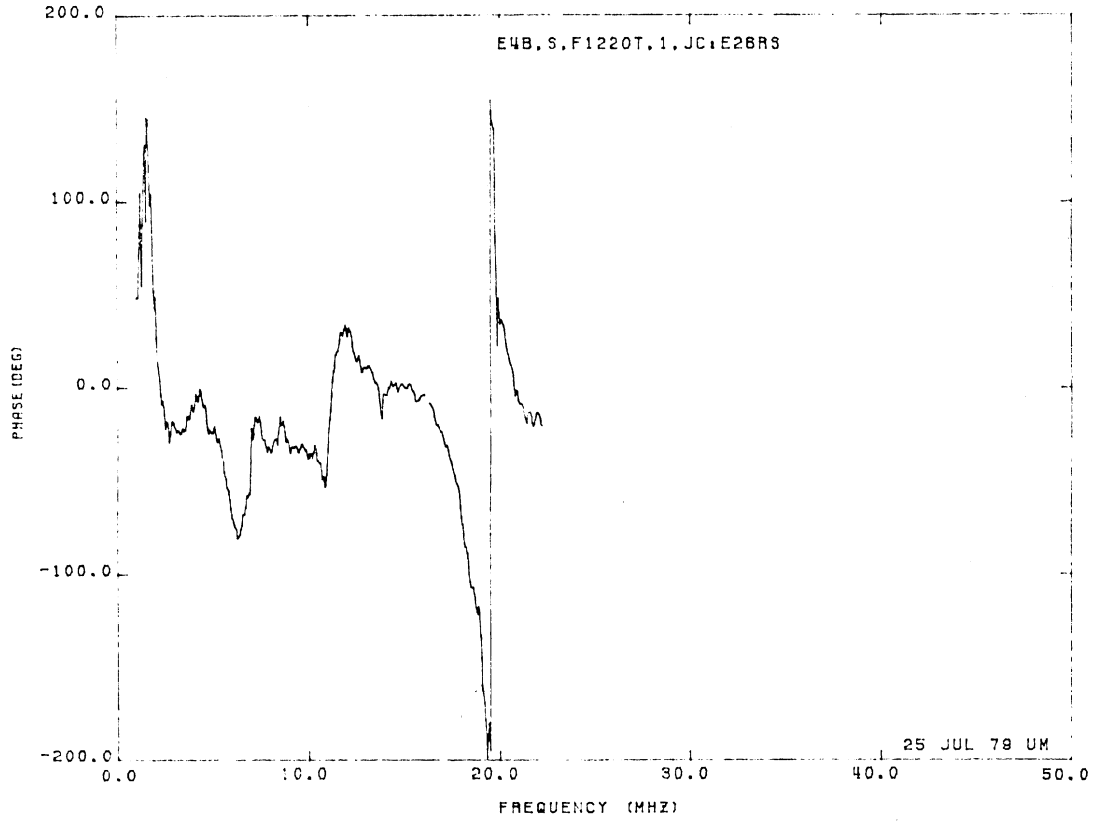

Figure 26RS. Circumferential Current at STA:F1220T, Excitation 1, 1/200 Model.

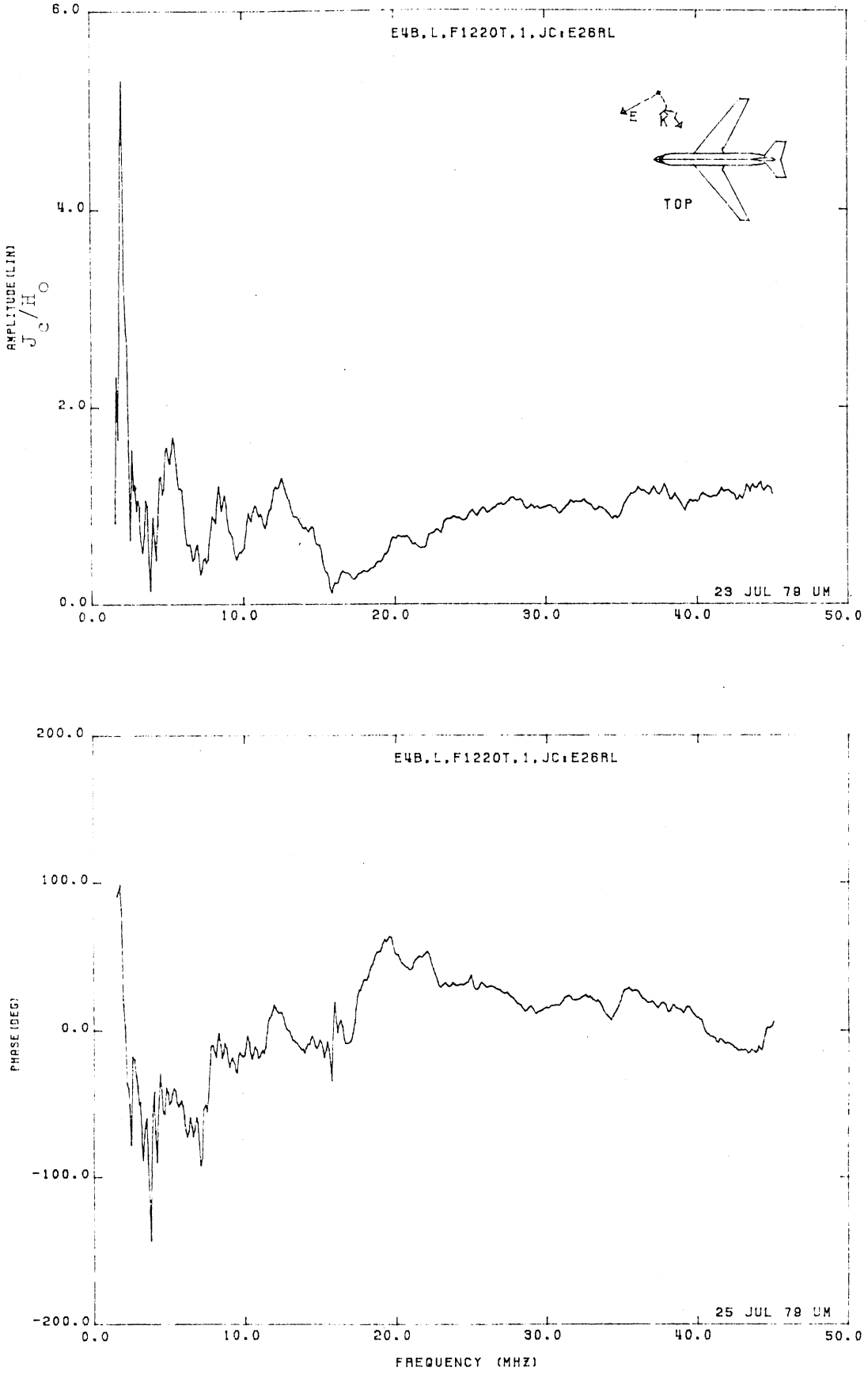

Figure 26RL. Circumferential Current at STA:1220T, Excitation 1, 1/100 Model.

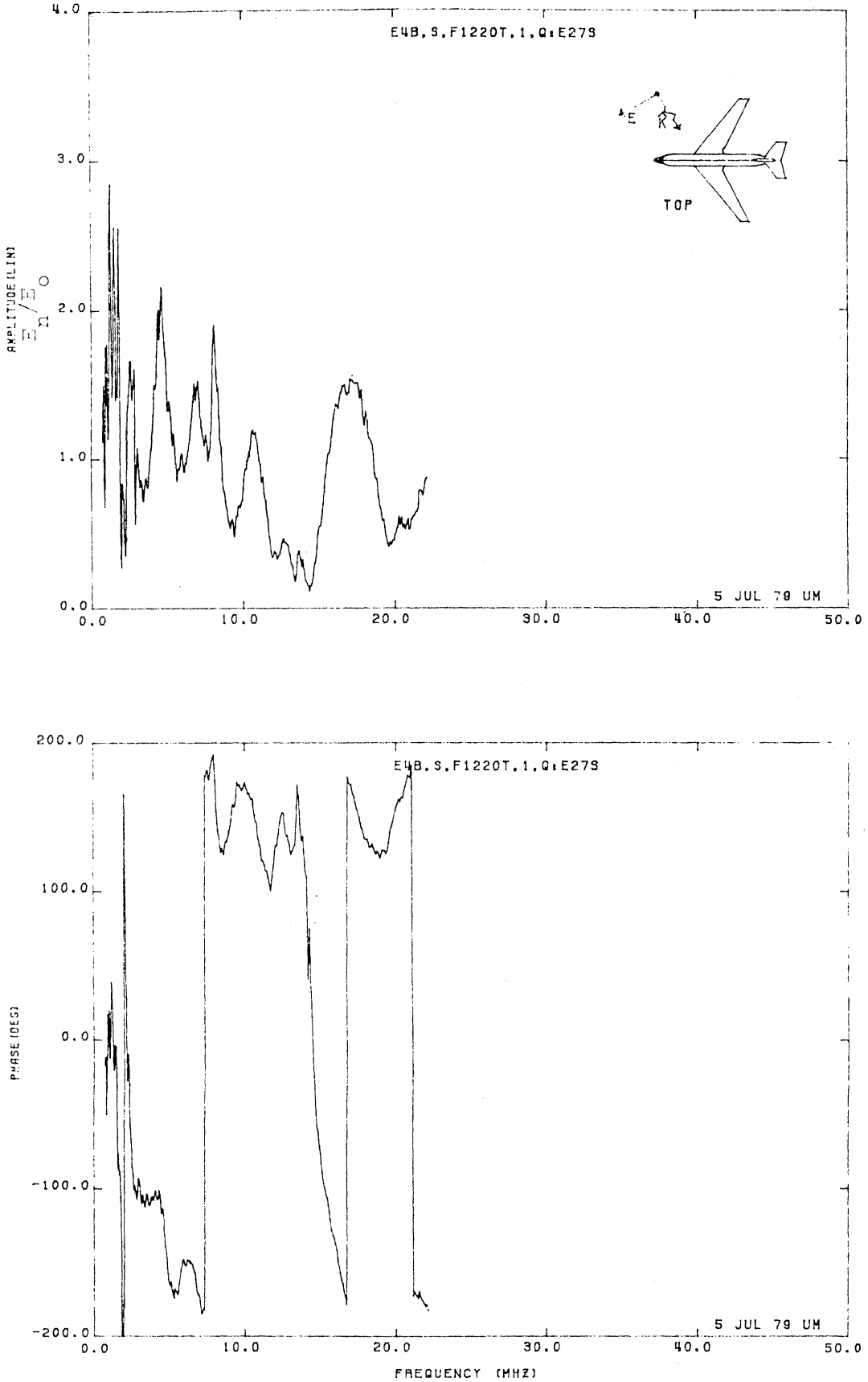

Figure 27S. Normal Electric Field at STA:F1220T, Excitation 1, 1/200 Model.

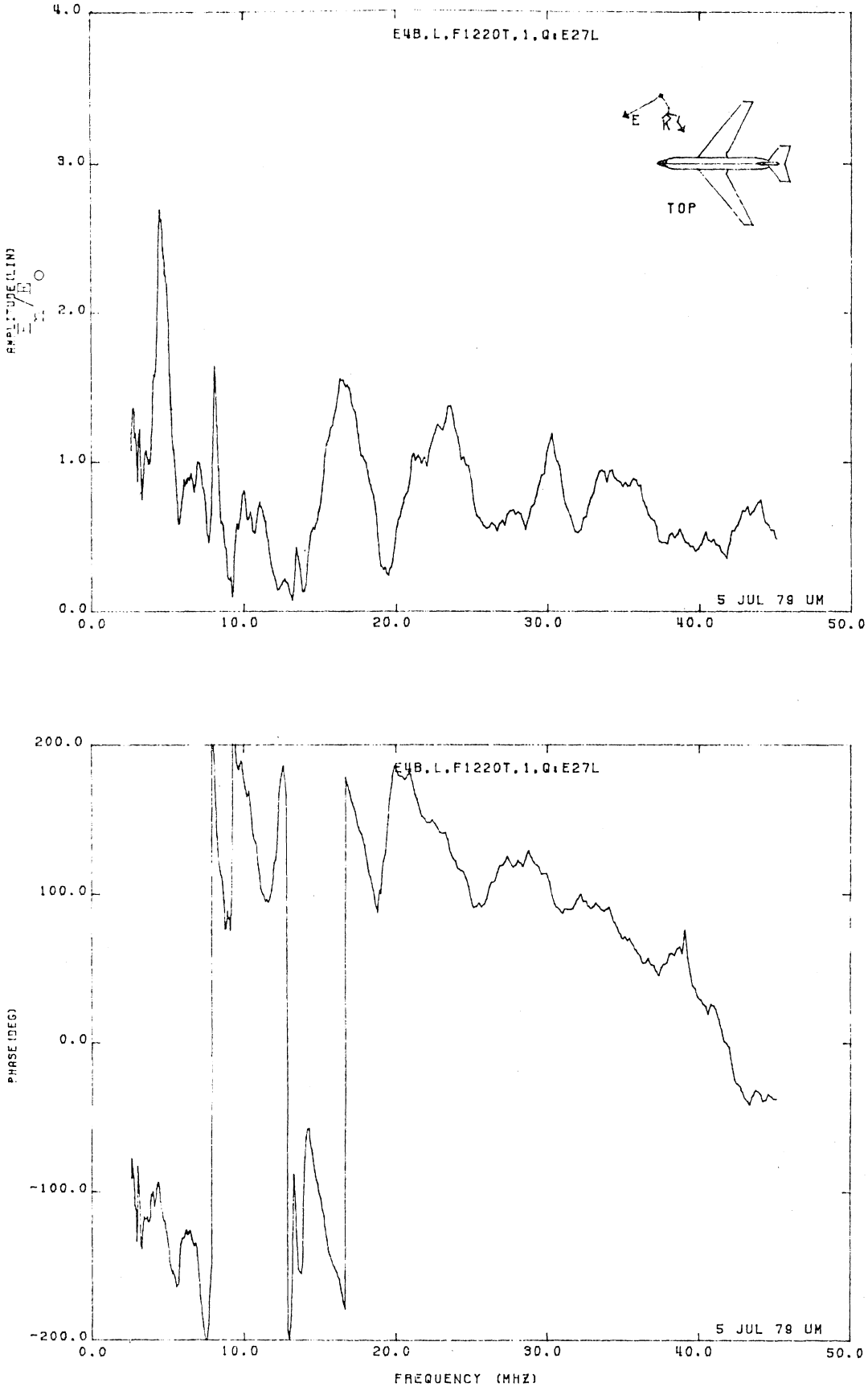

Figure 27L, Normal Electric Field at STA:F1220T, Excitation 1, 1/100 Model.

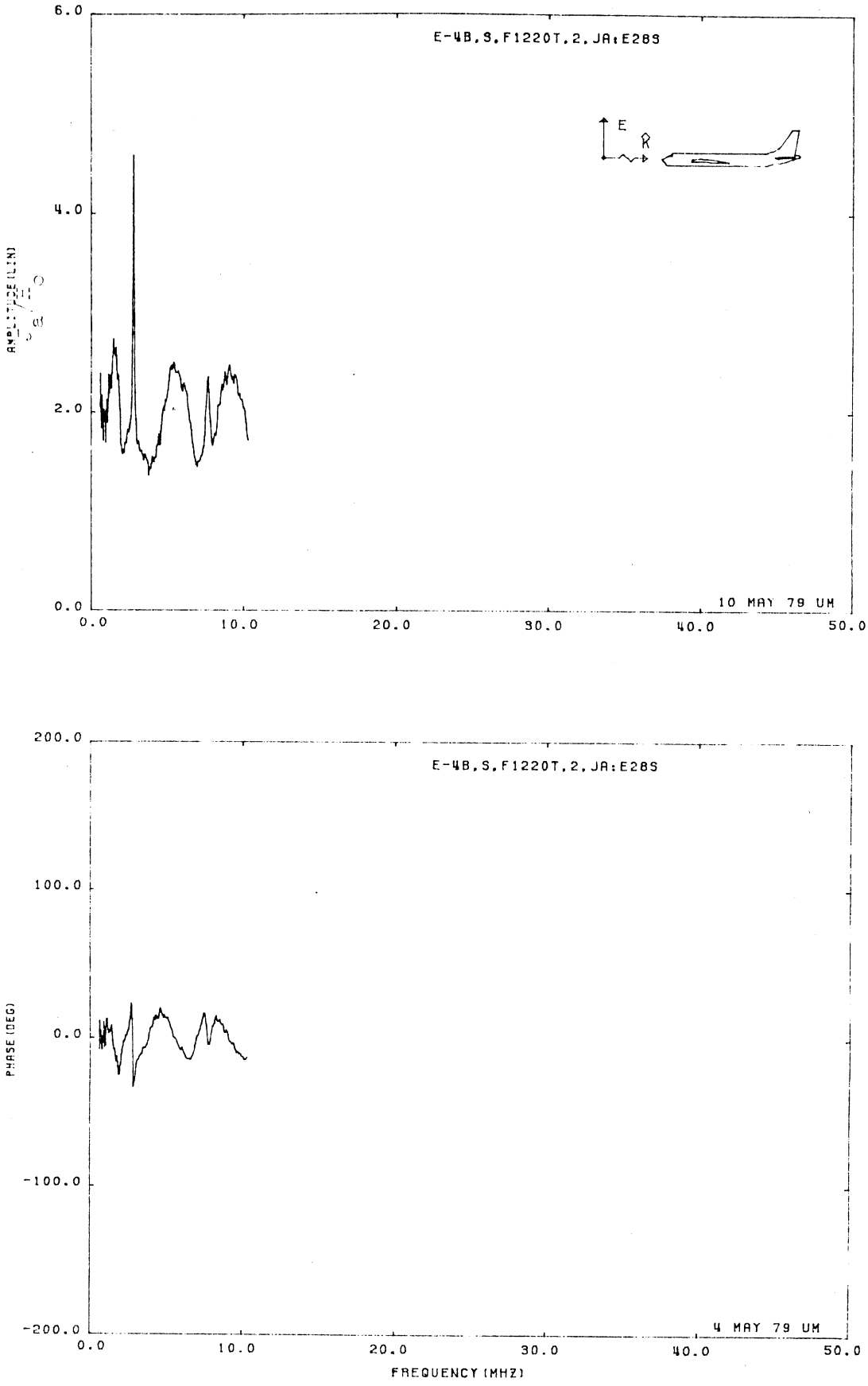

Figure 28S. Axial Current at STA:F1220T, Excitation 2, 1/200 Model.

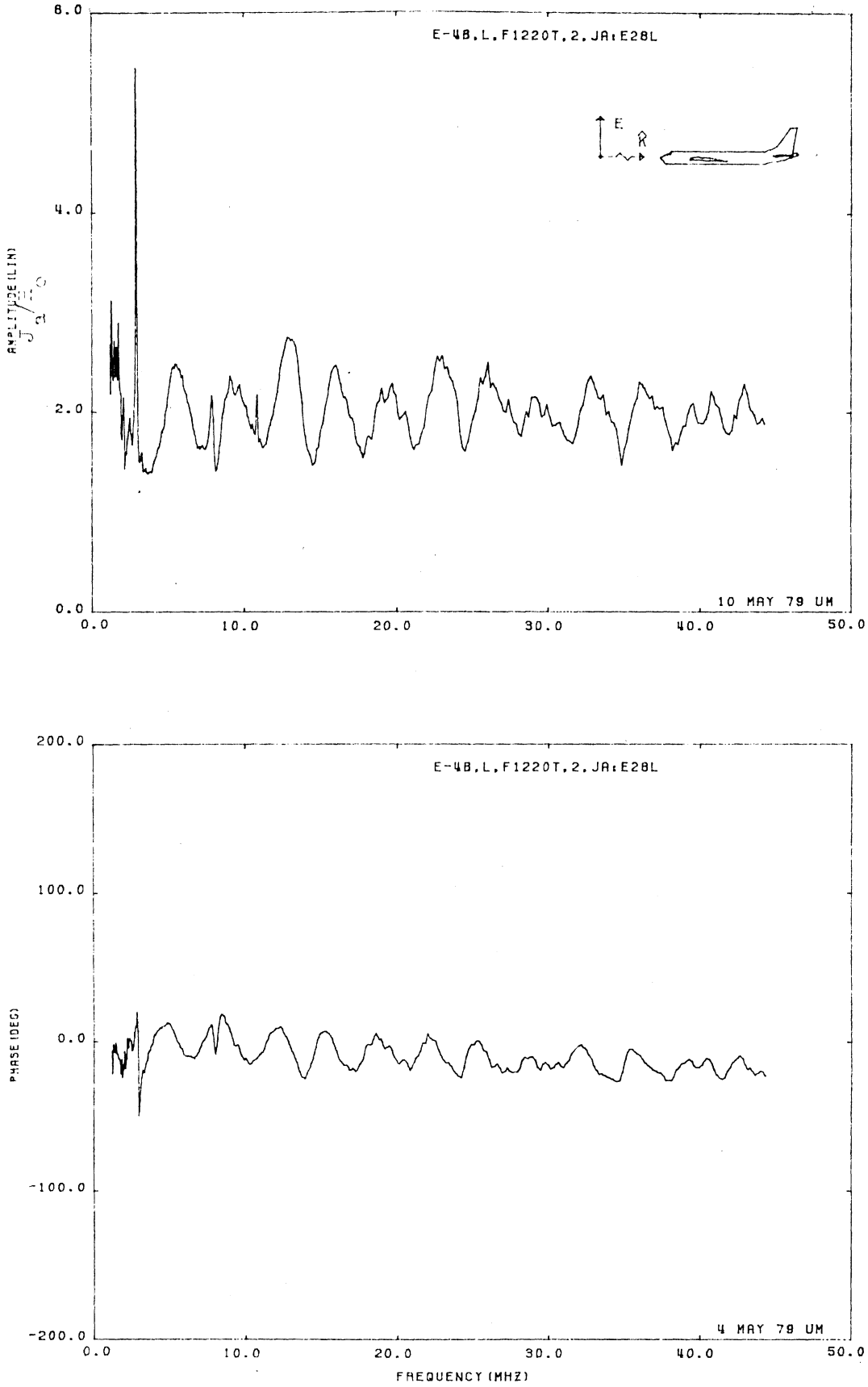

Figure 28L. Axial Current at STA:F1220T, Excitation 2, 1/100 Model.

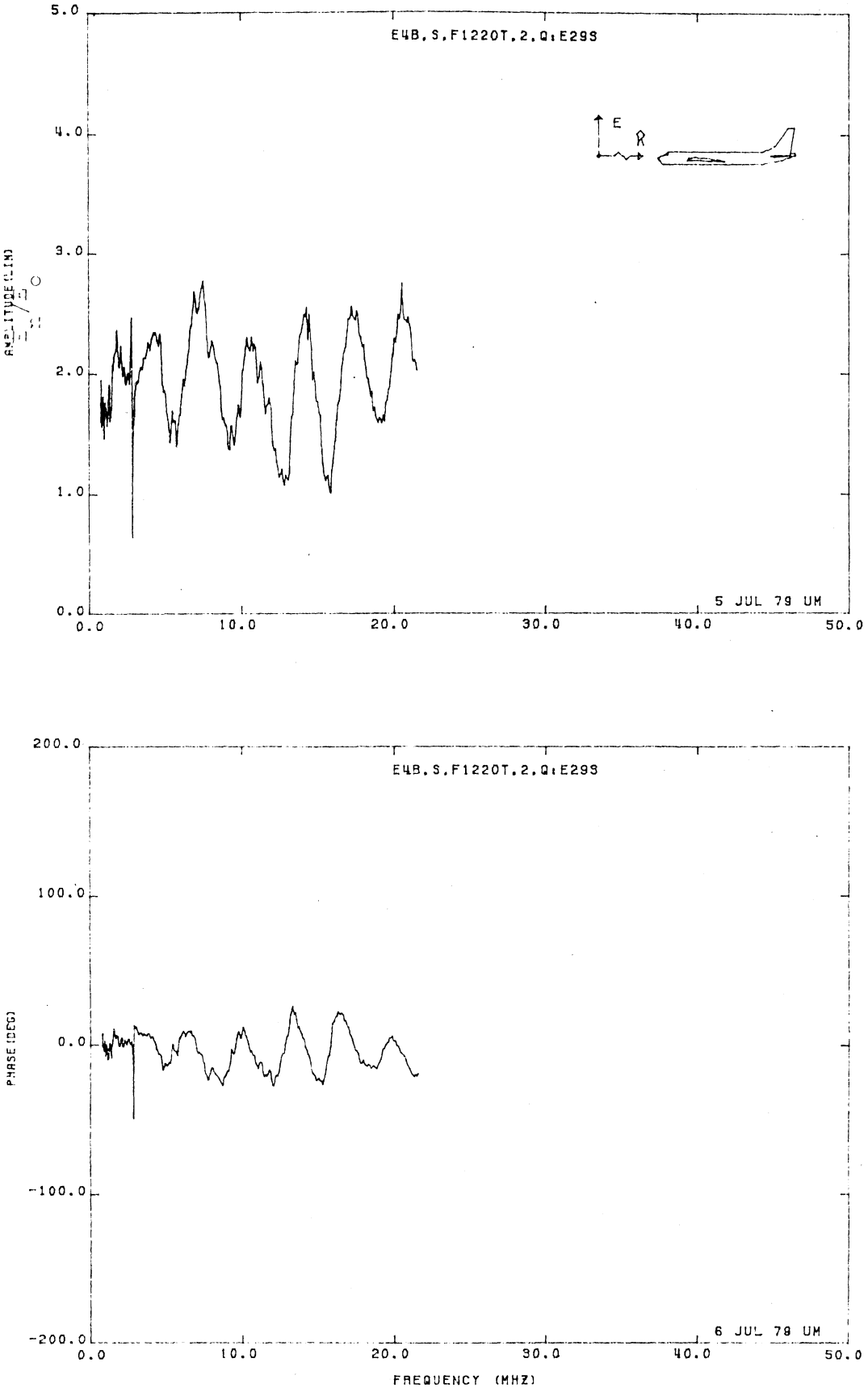

Figure 29S. Normal Electric Field at STA:F1220T, Excitation 2, 1/200 Model.

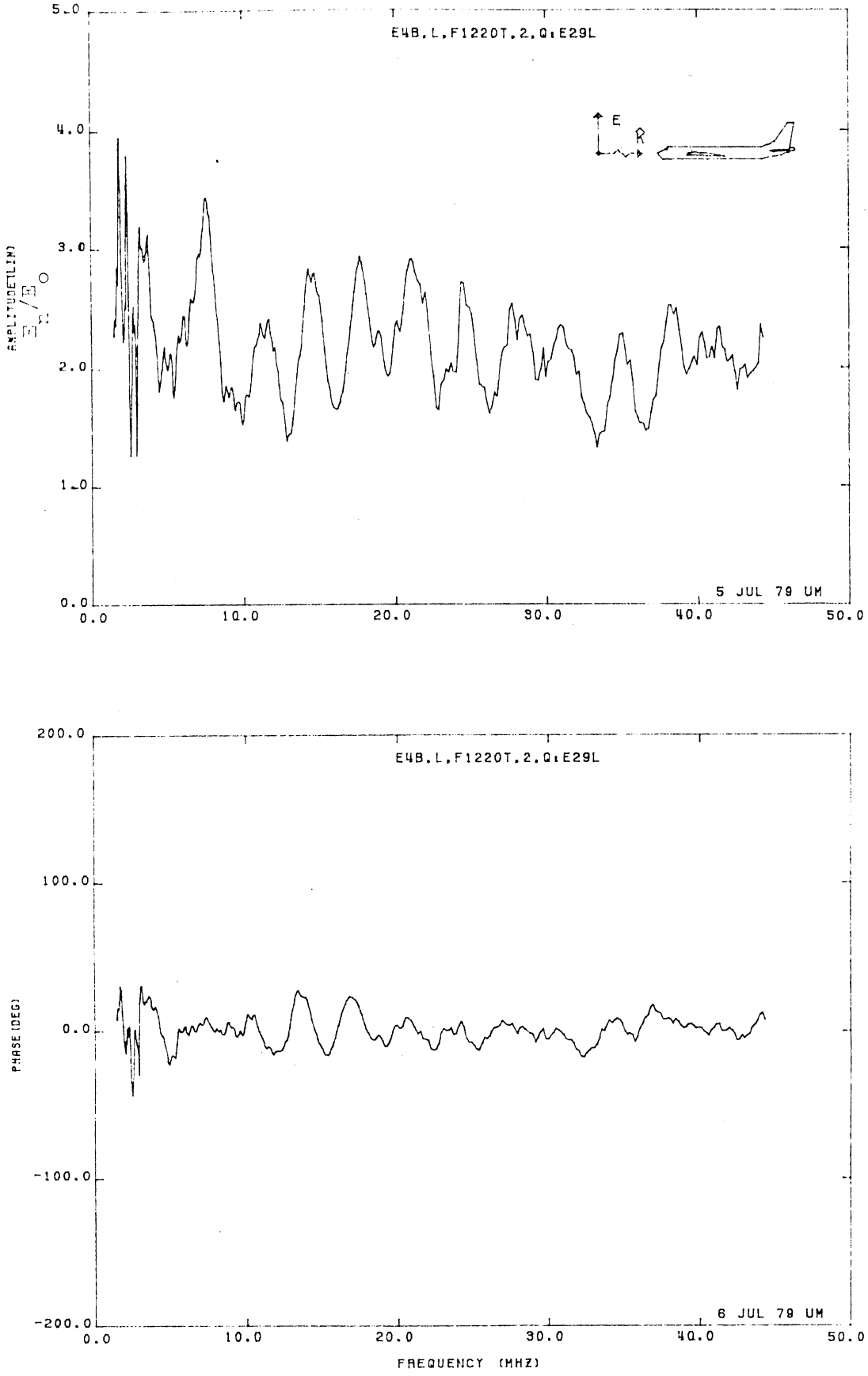

Figure 29L. Normal Electric Field at STA:F1220T, Excitation 2, 1/100 Model.

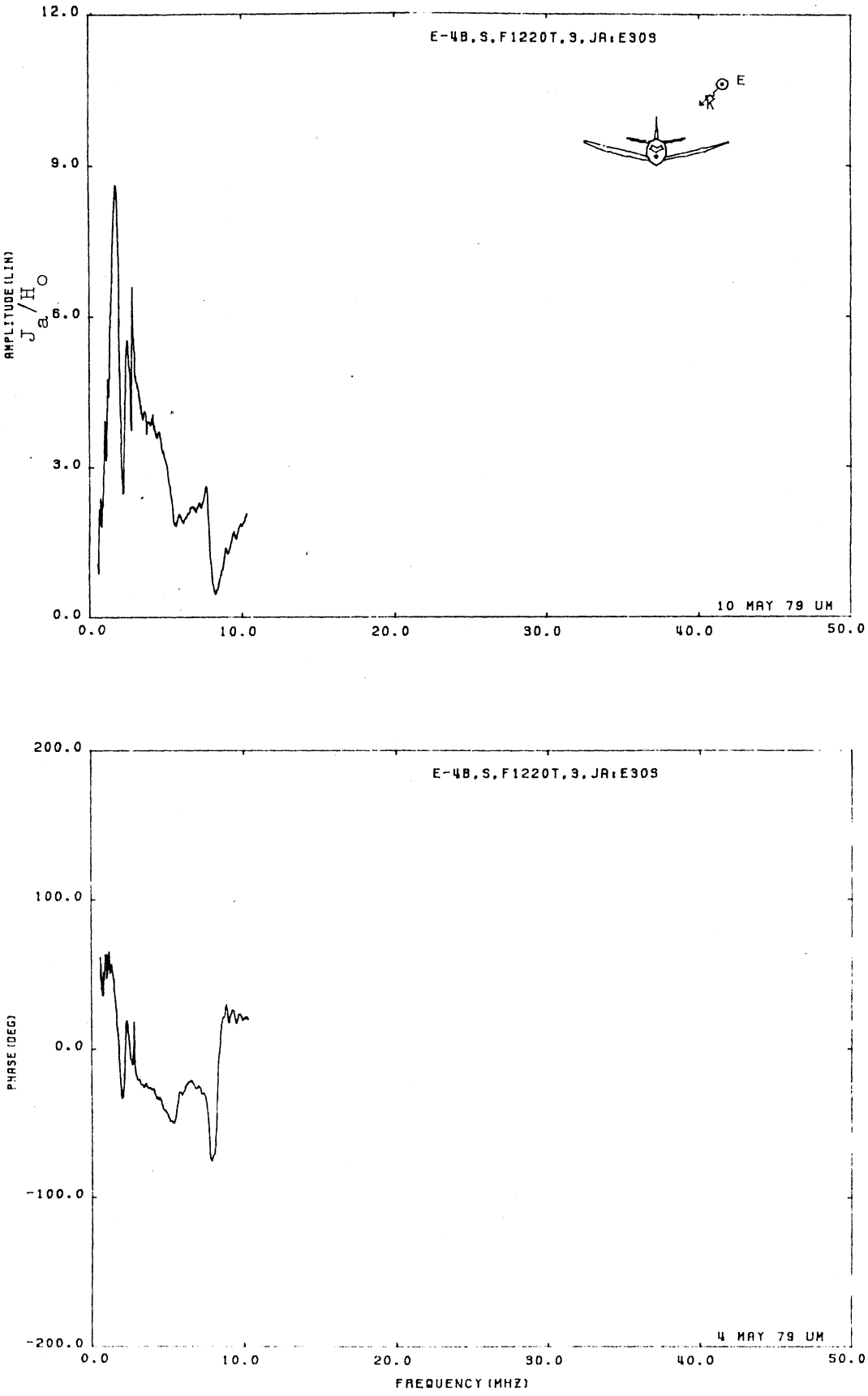

Figure 30S. Axial Current at STA:F1220T, Excitation 3, 1/200 Model.

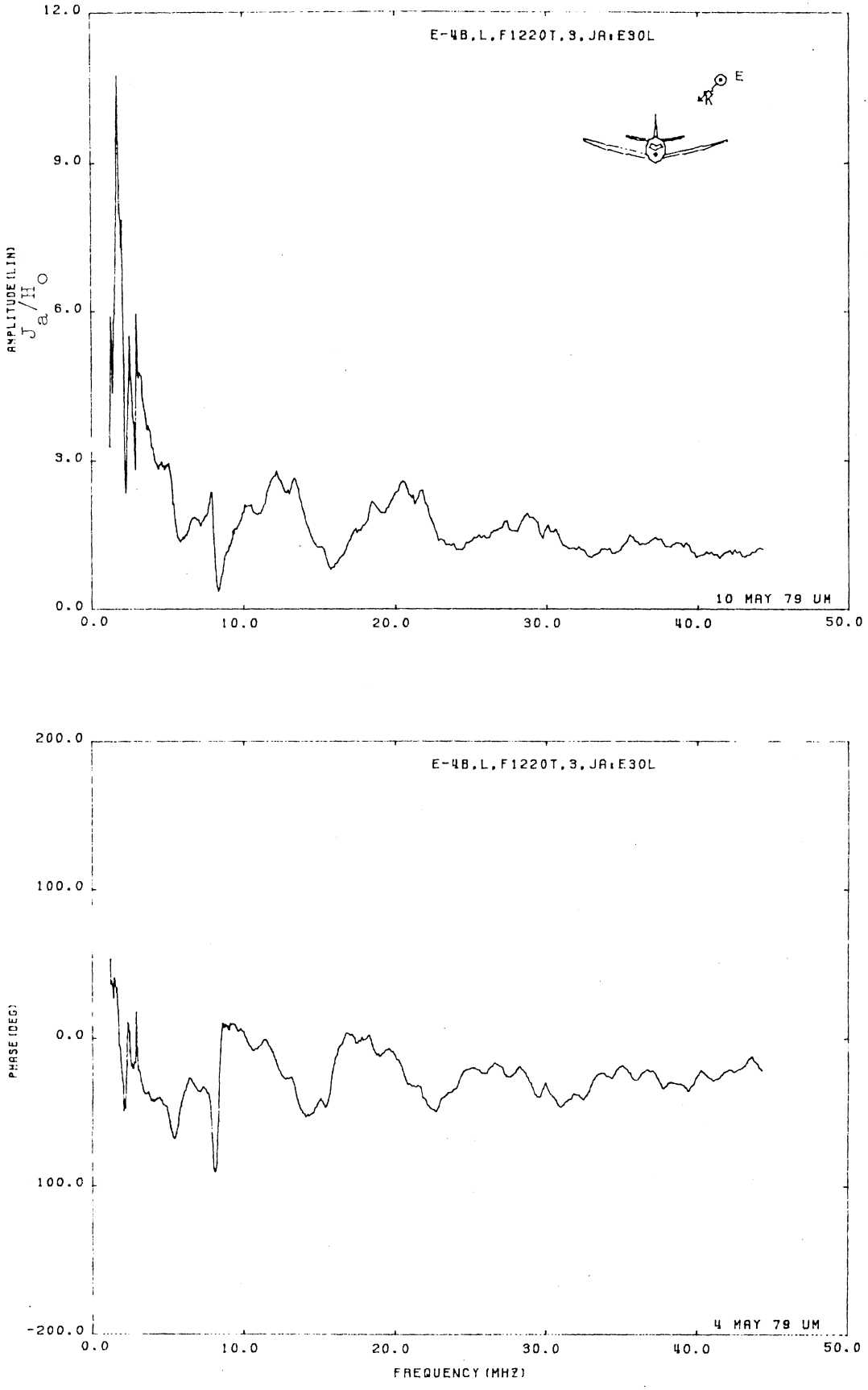

Figure 30L. Axial Current at STA:F1220T, Excitation 3, 1/100 Model.

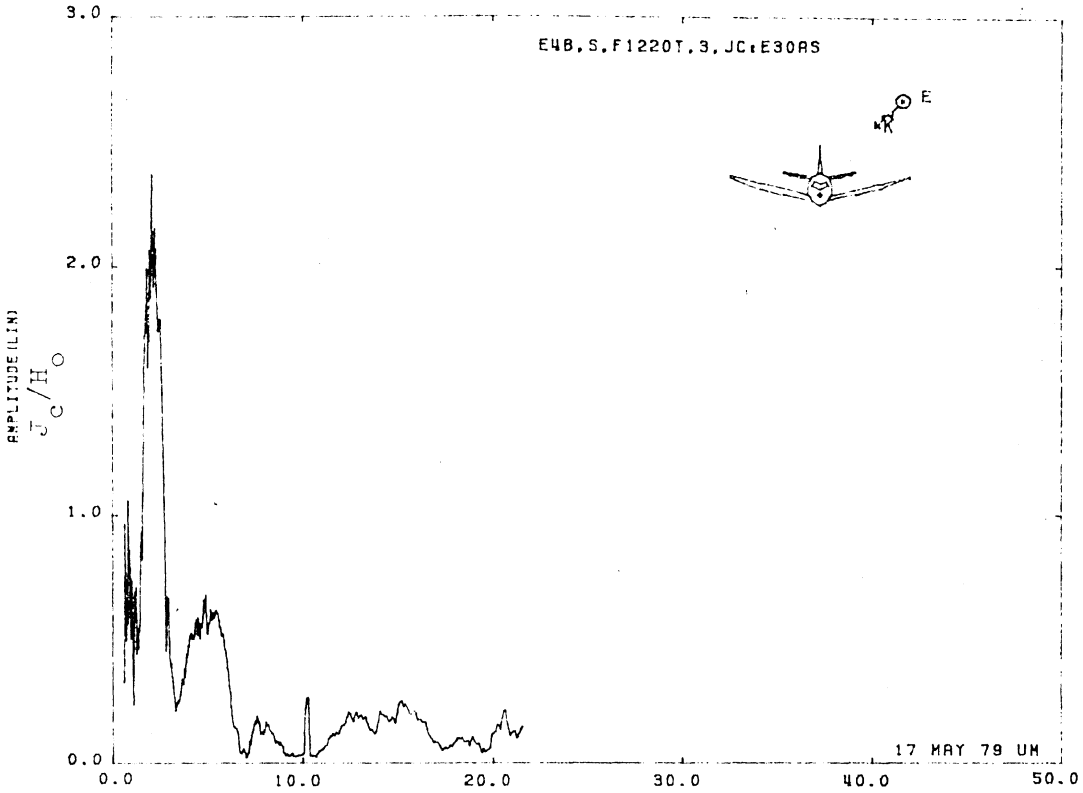

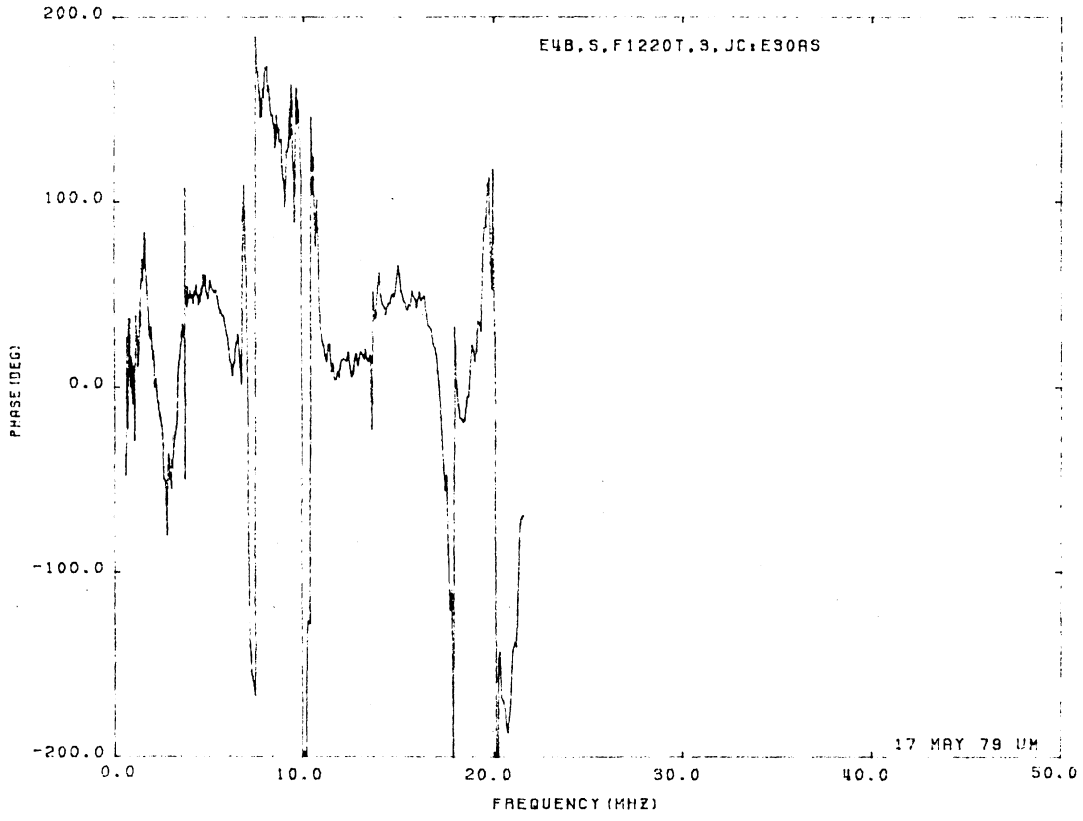

Figure 30AS. Circumferential Current at STA:F1220T, Exctiation 3, 1/200 Model.

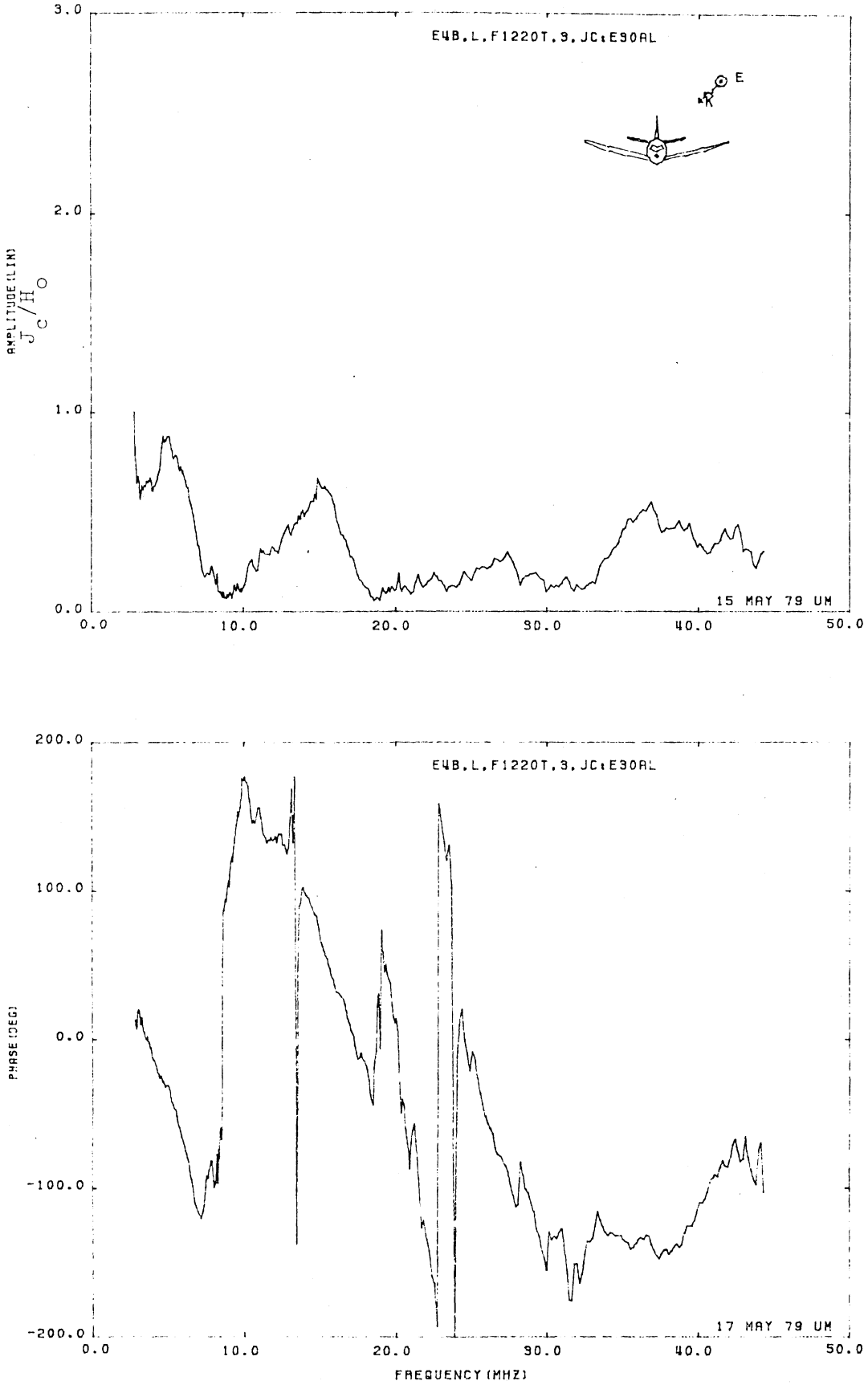

Figure 30AL. Circumferential Current at STA:F1220T, Excitation 3, 1/100 Model.

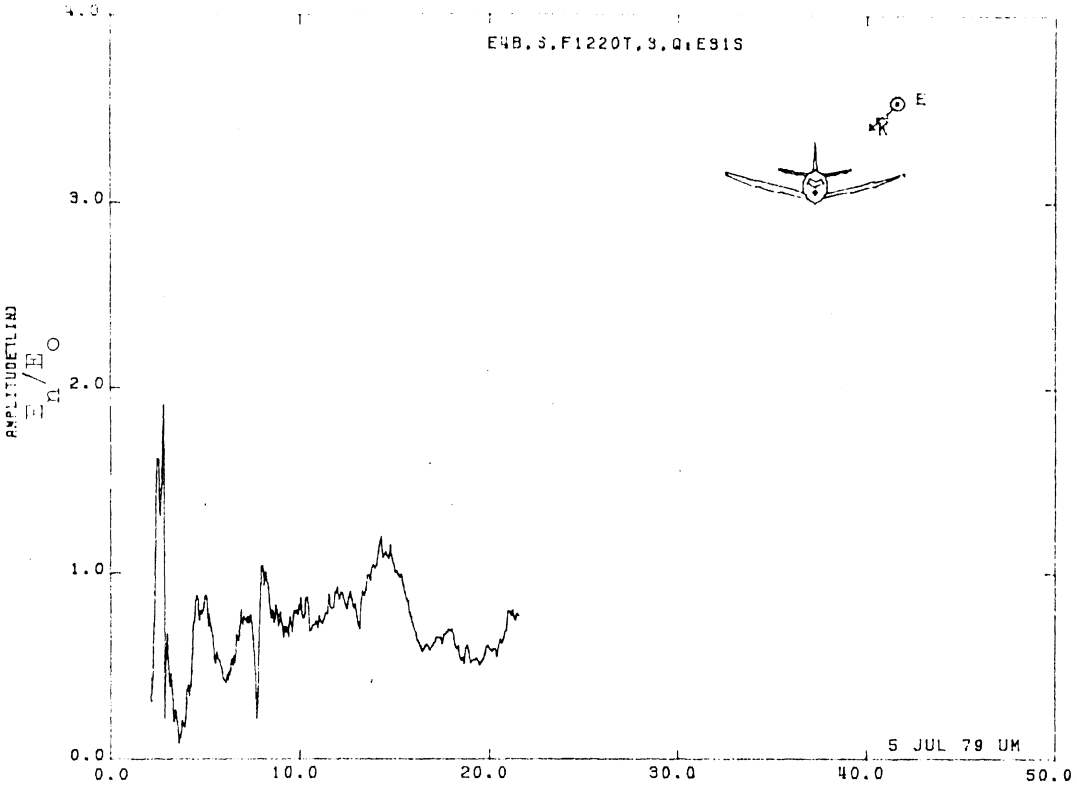

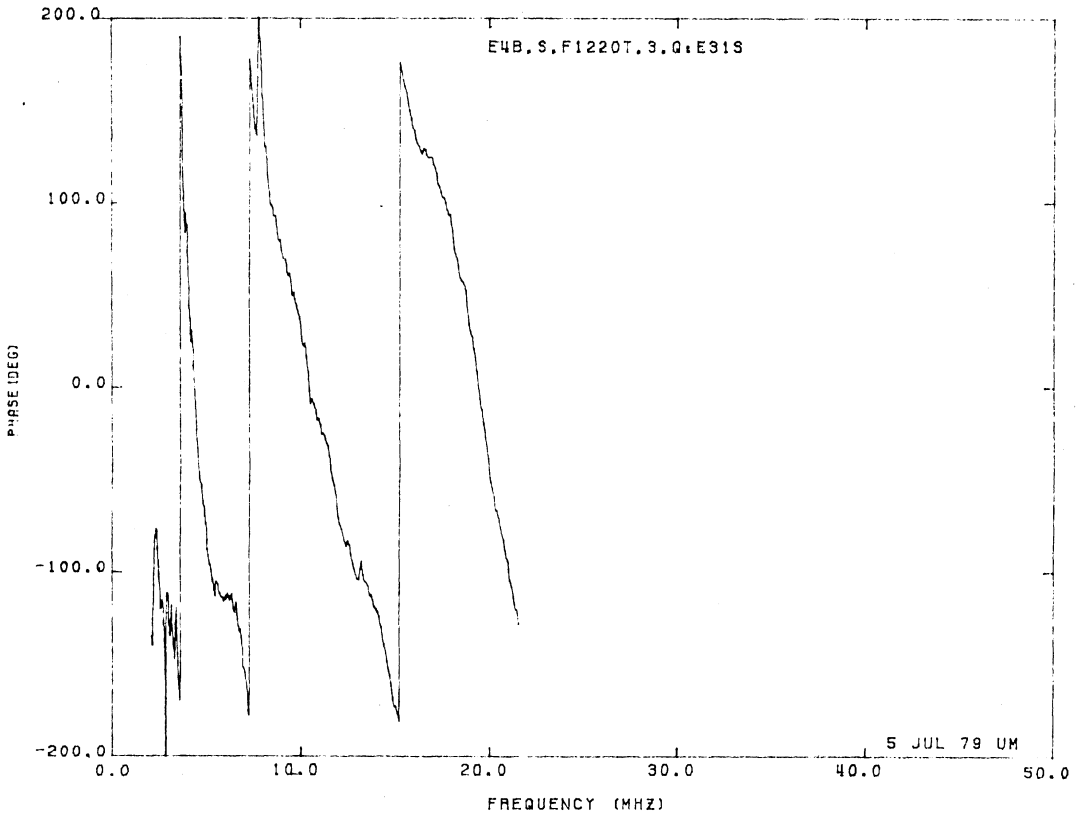

Figure 31S Normal Electric Field at STA:F1220T, Excitation 3, 1/200 Model.

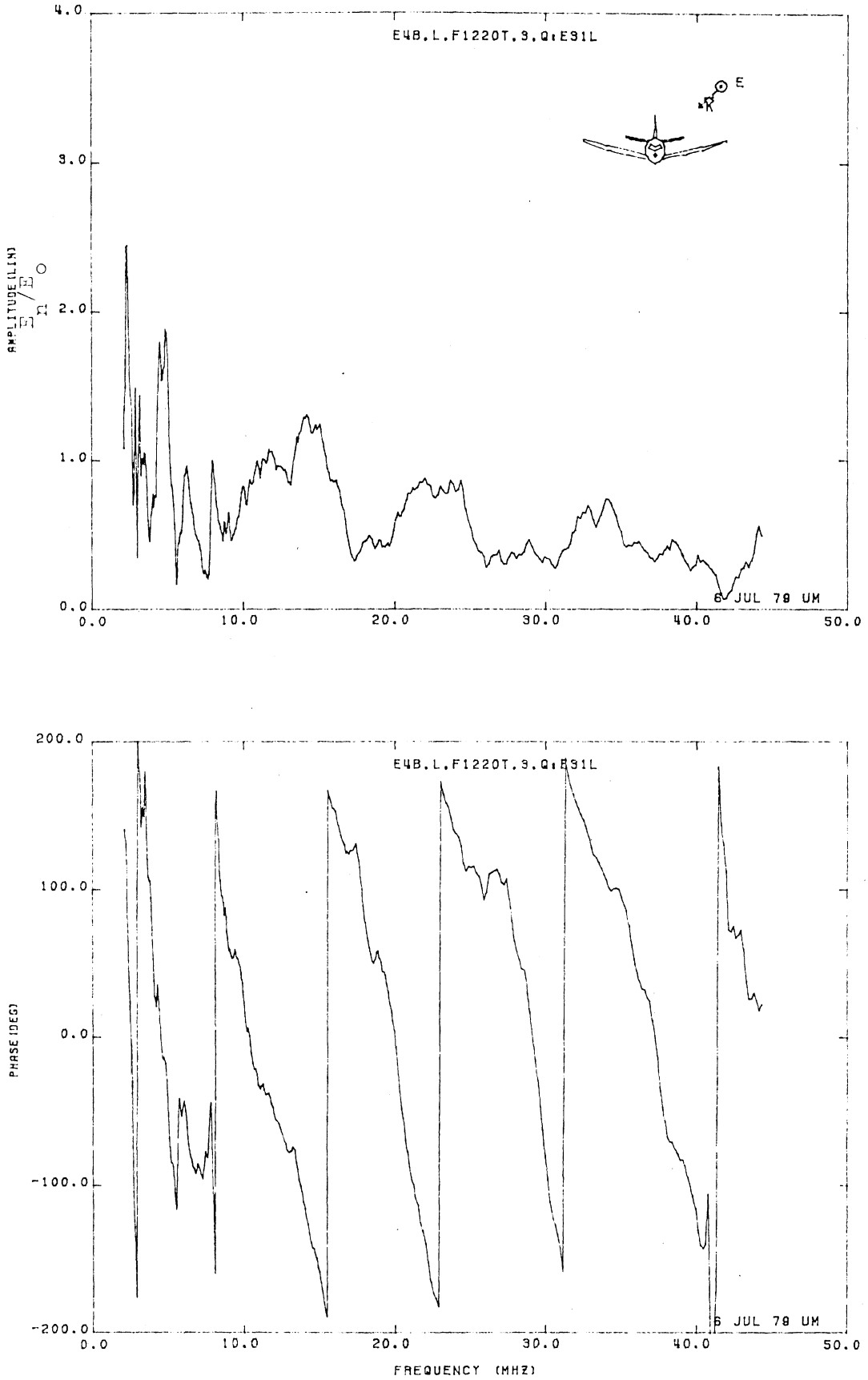

Figure 31L. Normal Electric Field at STA:F1220T, Excitation 3, 1/100 Model.

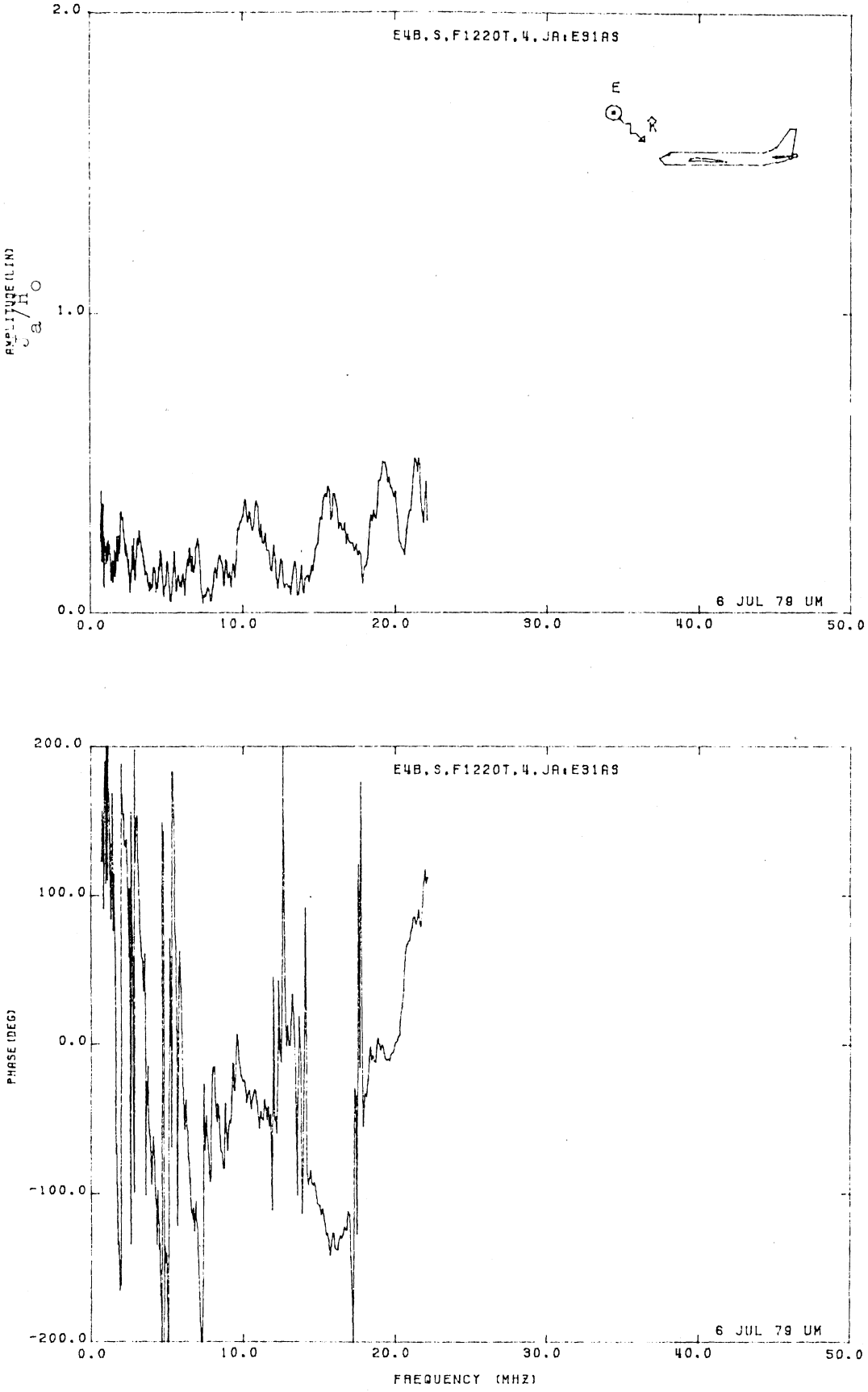

Figure 31AS. Axial Current at STA:F1220T, Excitation 4, 1/200 Model.

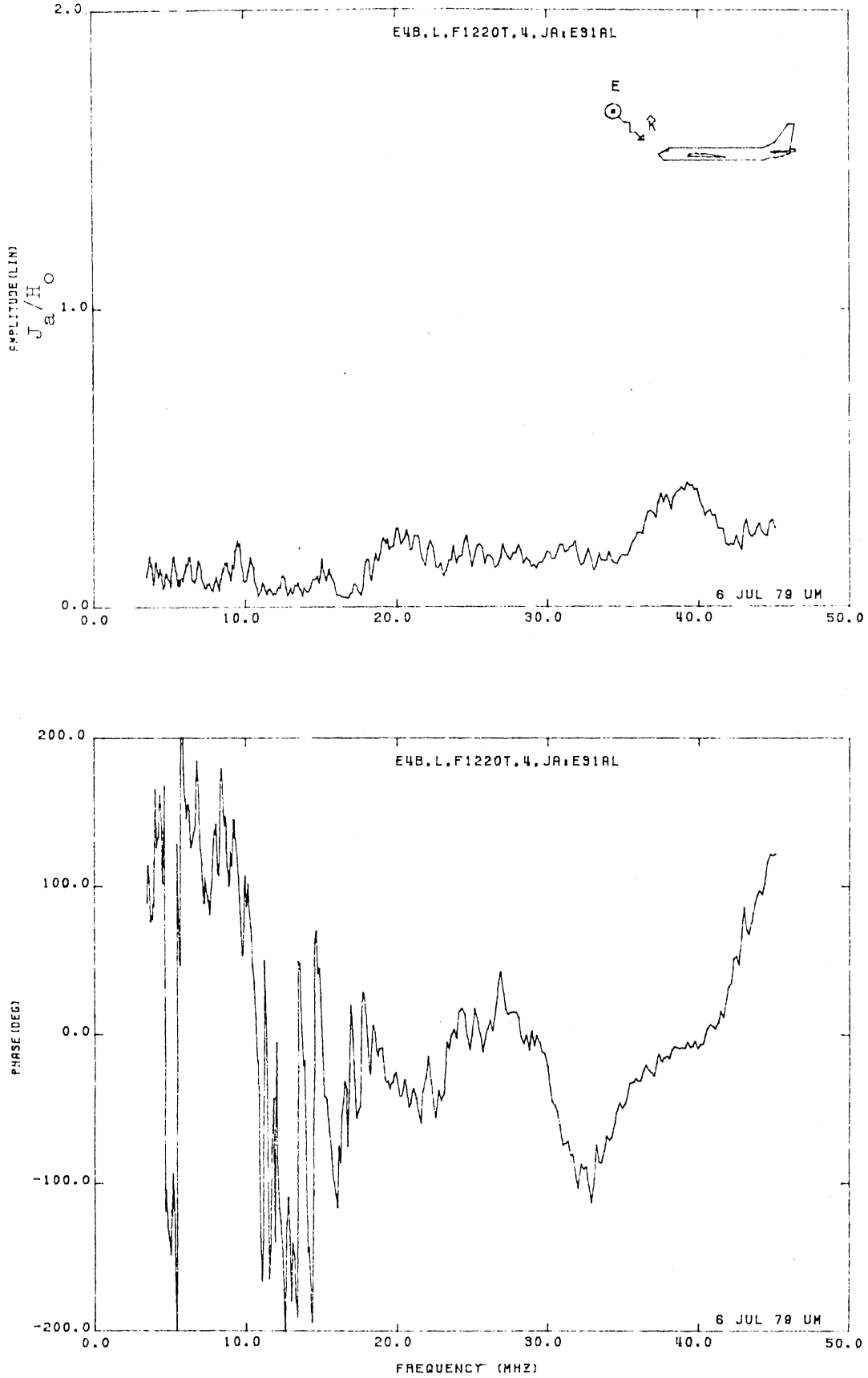

Figure 31AL. Axial Current at STA:F1220T, Excitation 4, 1/100 Model.

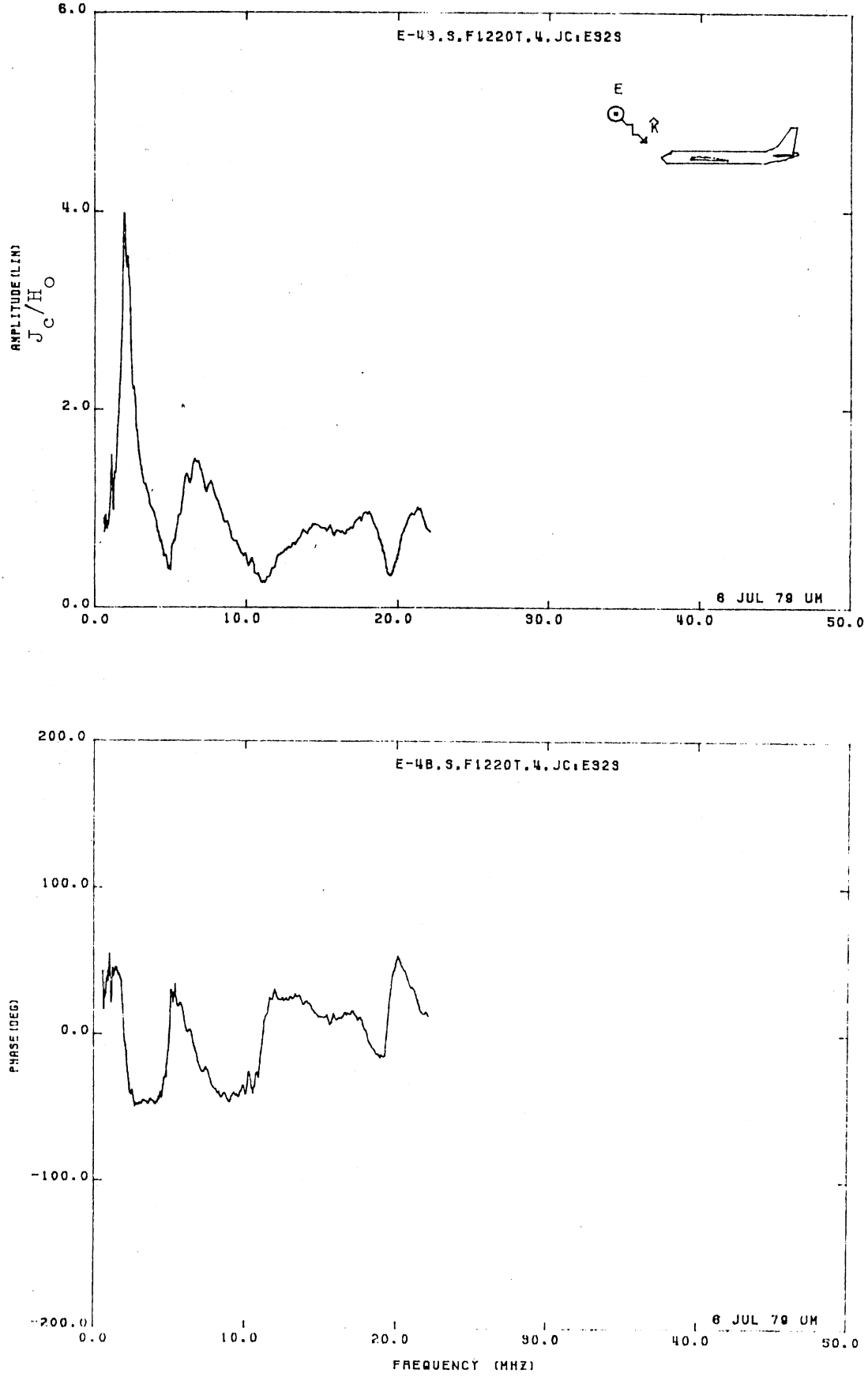

Figure 32S. Circumferential Current at STA:F1220T, Excitation 4, 1/200 Model.

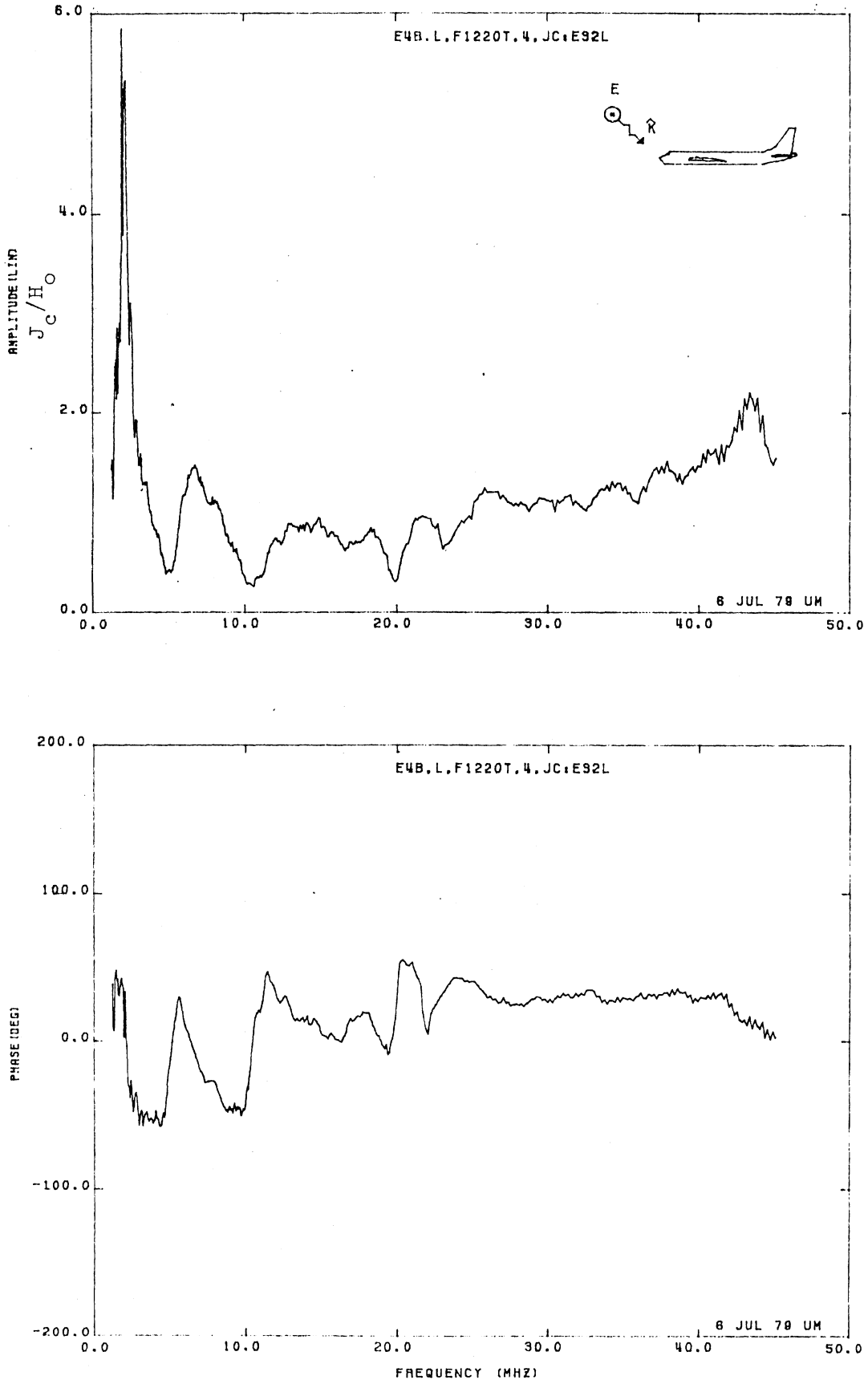

Figure 32L. Circumferential Current at STA:F1220T, Excitation 4, 1/100 Model.

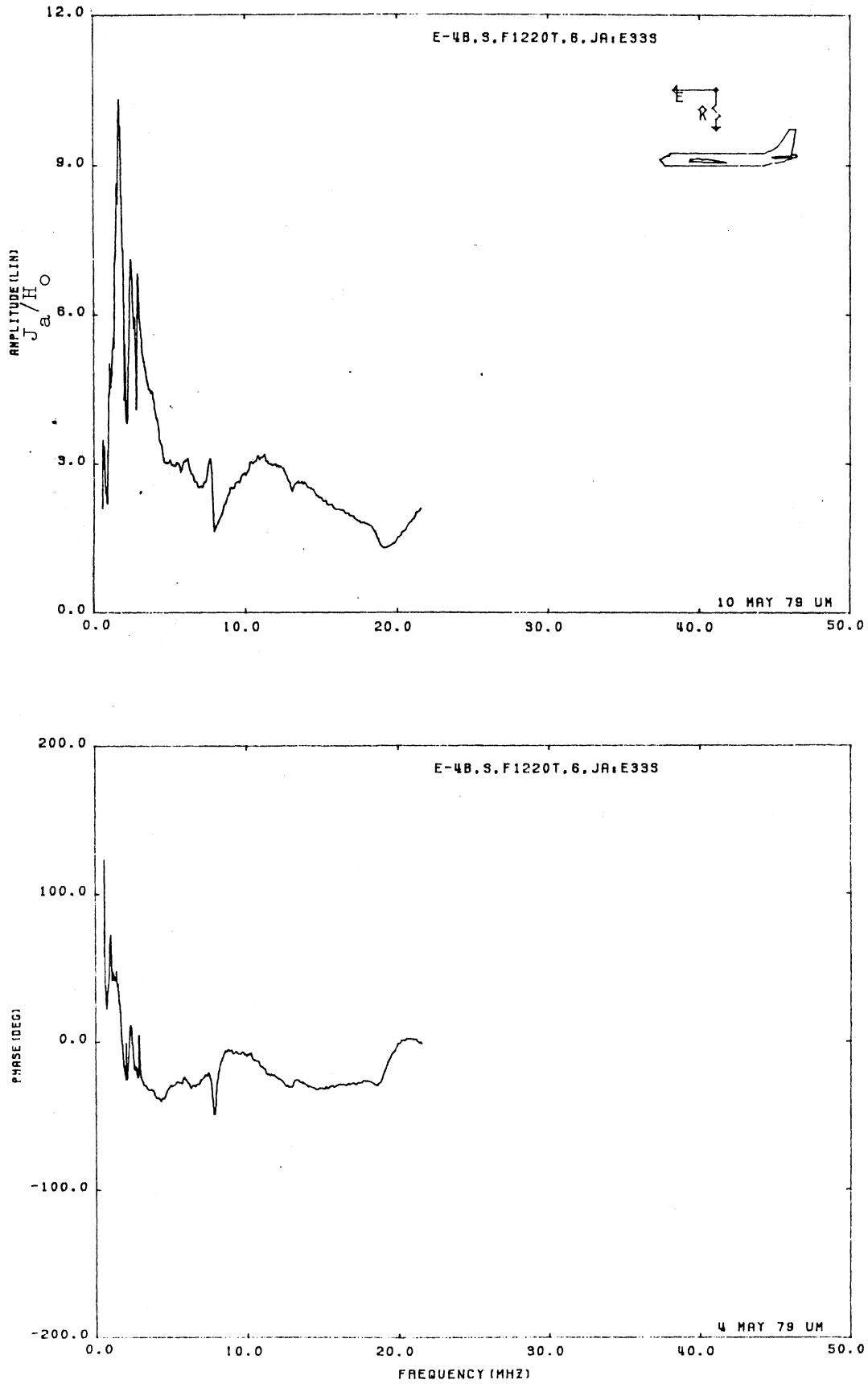

Figure 33S. Axial Current at STA:F1220T, Excitation 6, 1/200 Model.

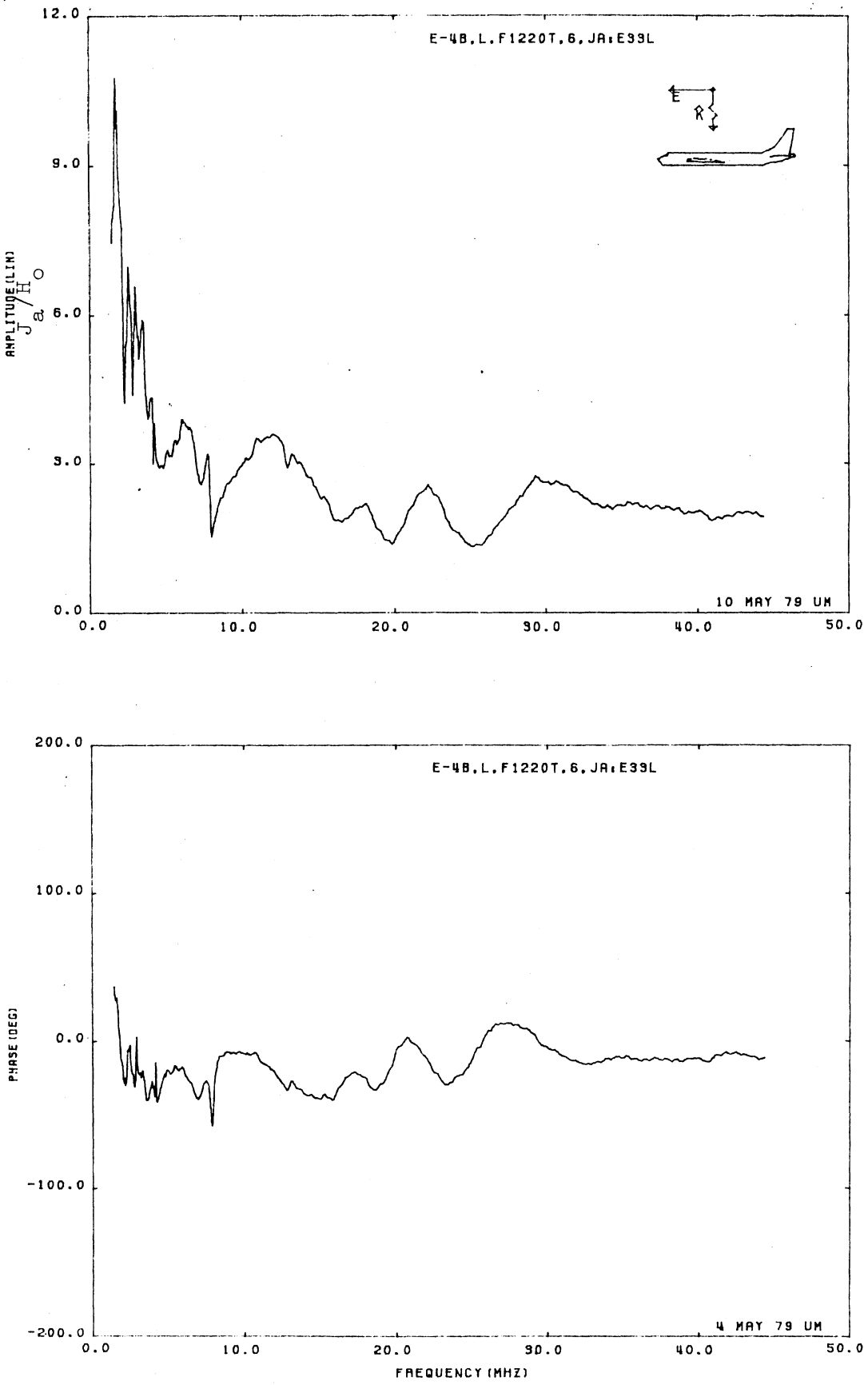

Figure 33L. Axial Current at STA:F1220T, Excitation 6, 1/100 Model.

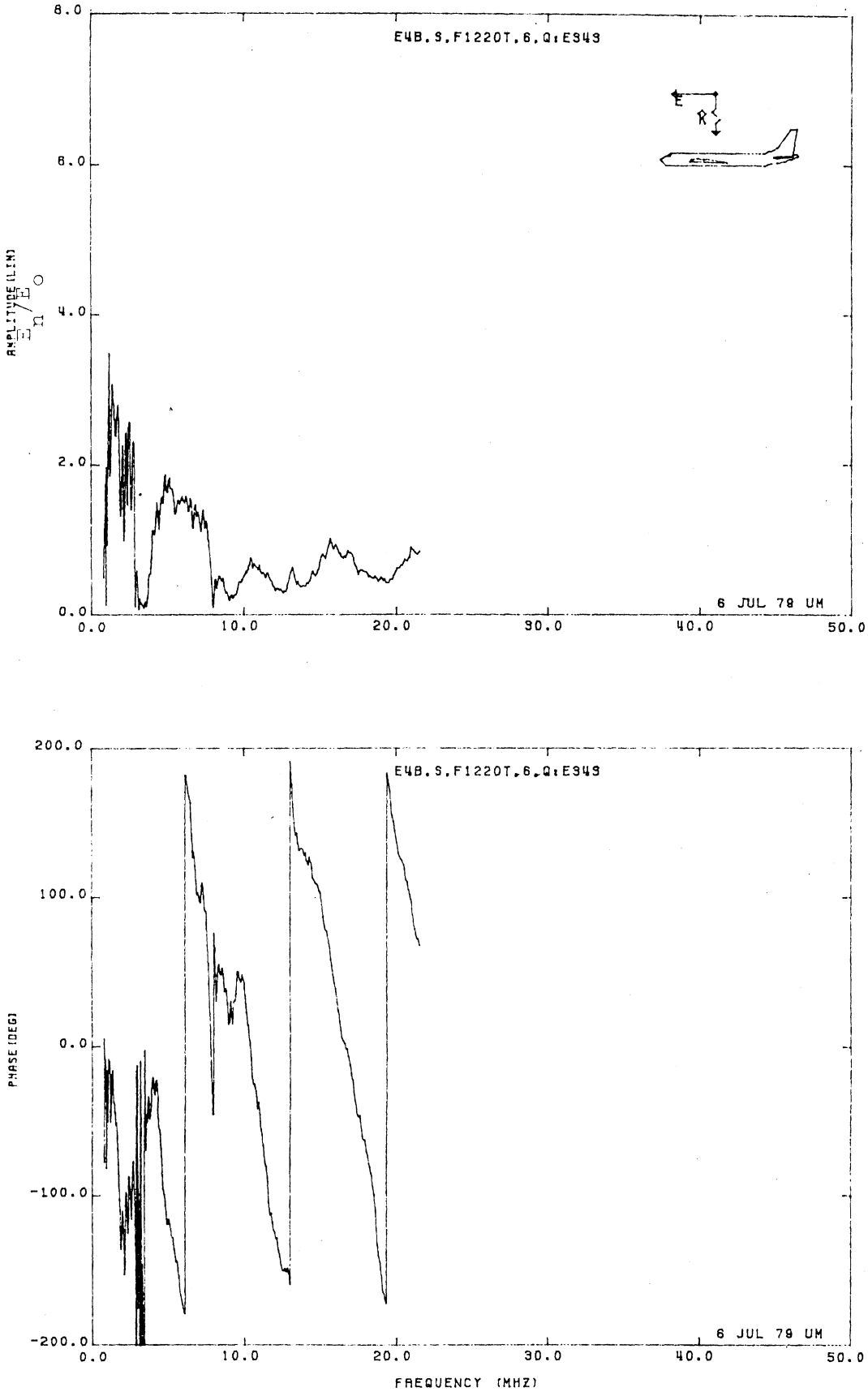

Figure 34S. Normal Electric Field at STA:F1220T, Excitation 6, 1/200 Model.

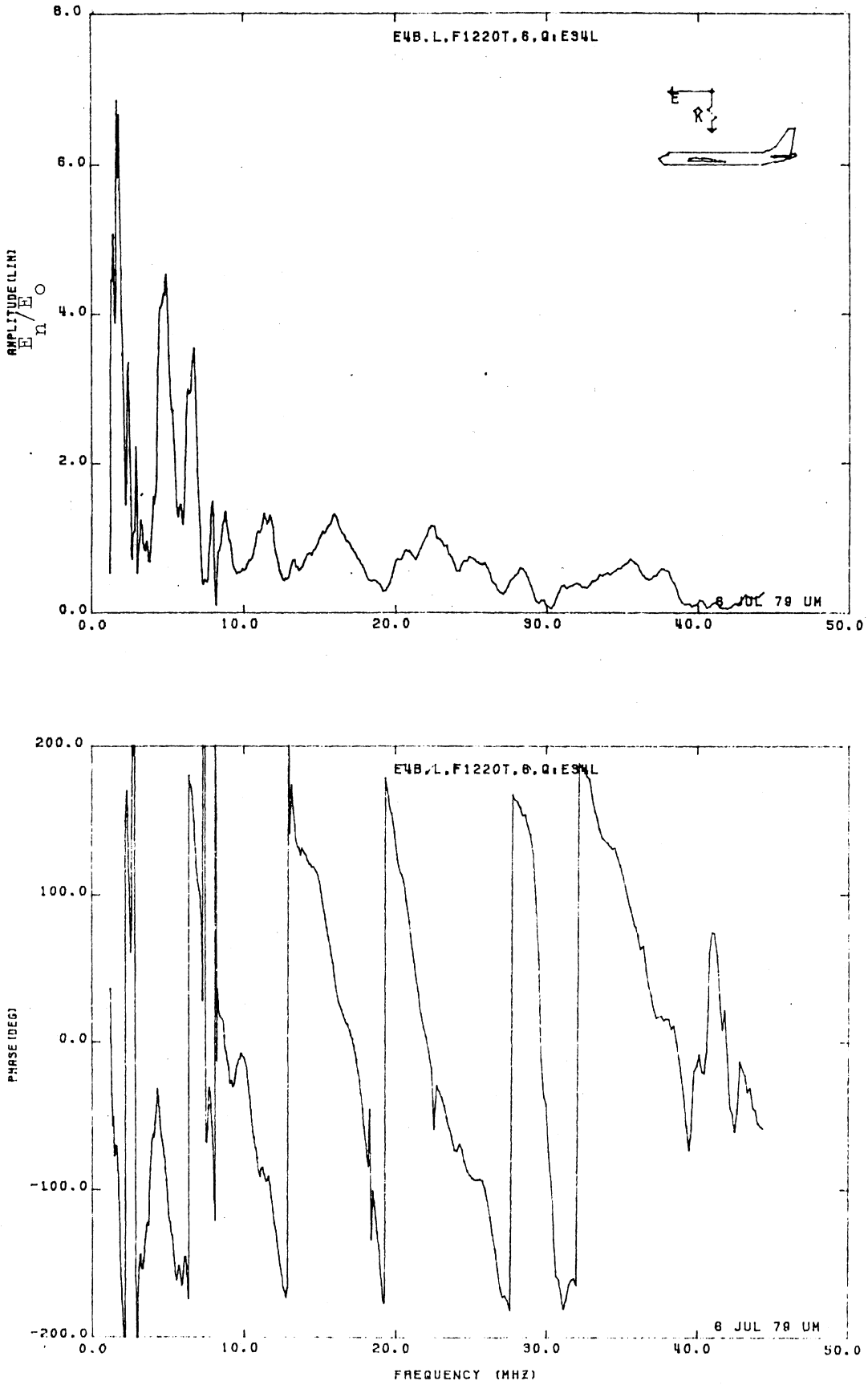

Figure 34L. Normal Electric Field at STA:F1220T, Excitation 6, 1/100 Model.

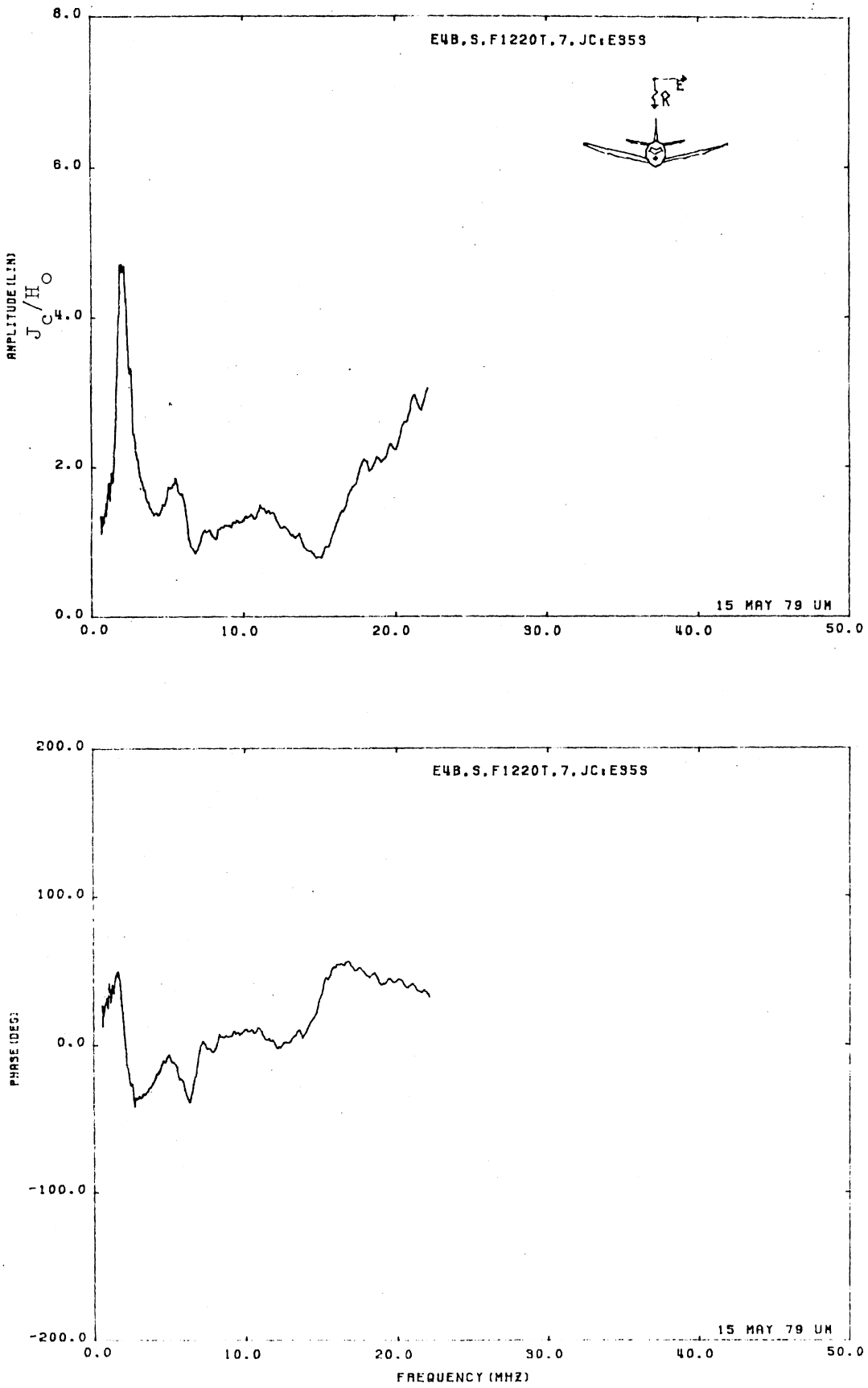

Figure 35S. Circumferential Current at STA:F1220T, Excitation 7, 1/200 Model.

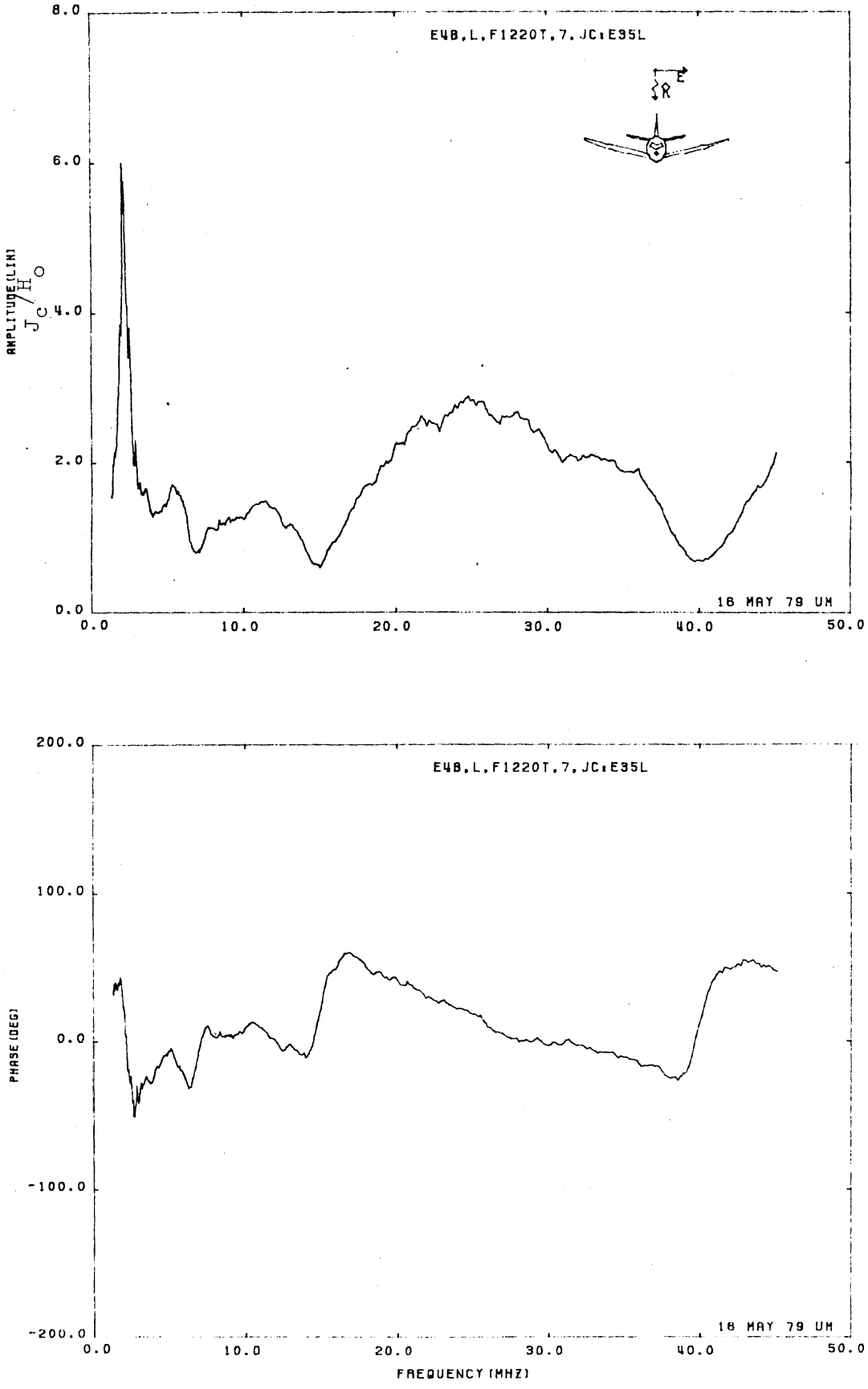

Figure 35L. Circumferential Current at STA:F1220T, Excitation 7, 1/100 Model.

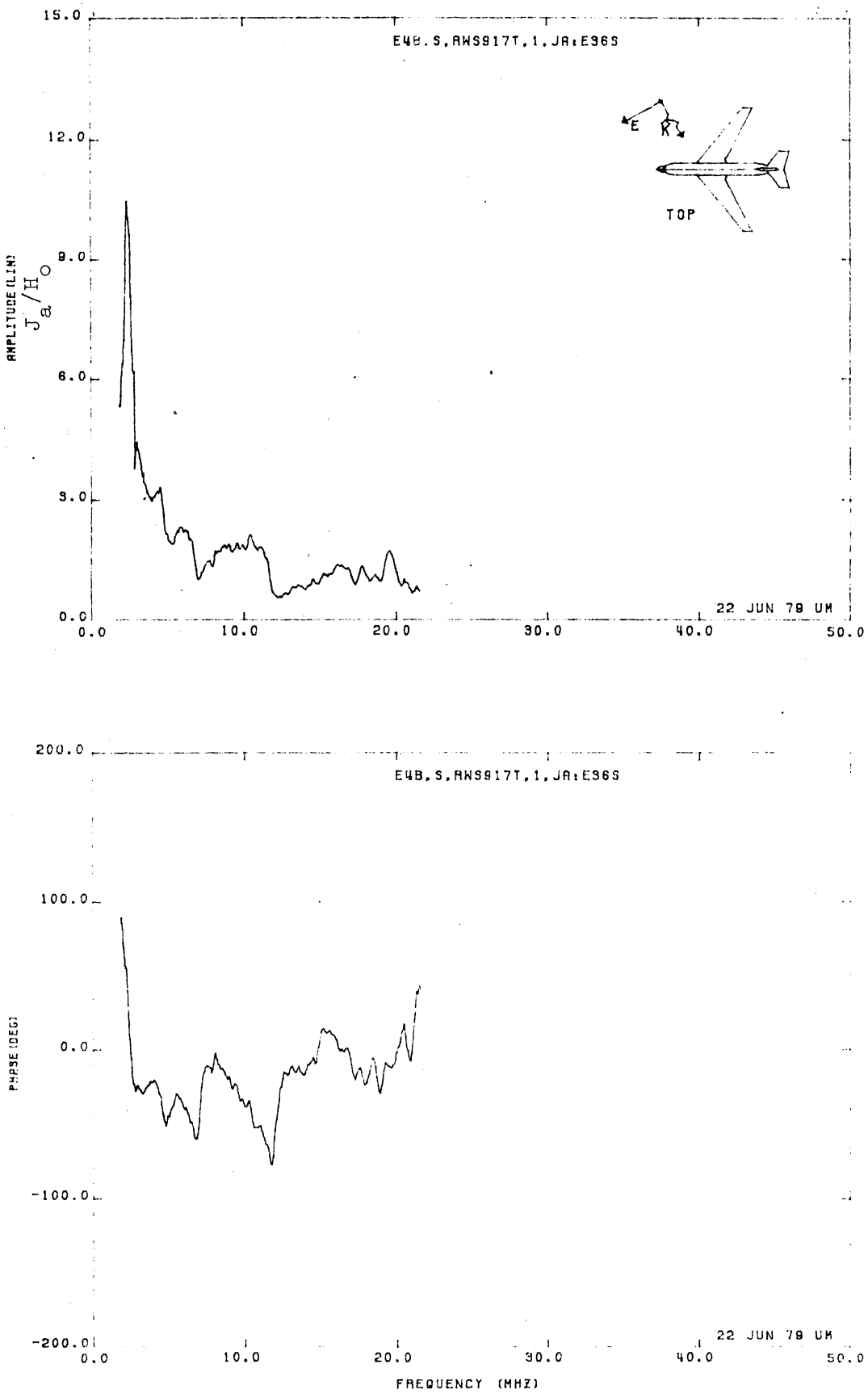

Figure 36S. Axial Current at STA:RWS917T, Excitation 1, 1/200 Model.

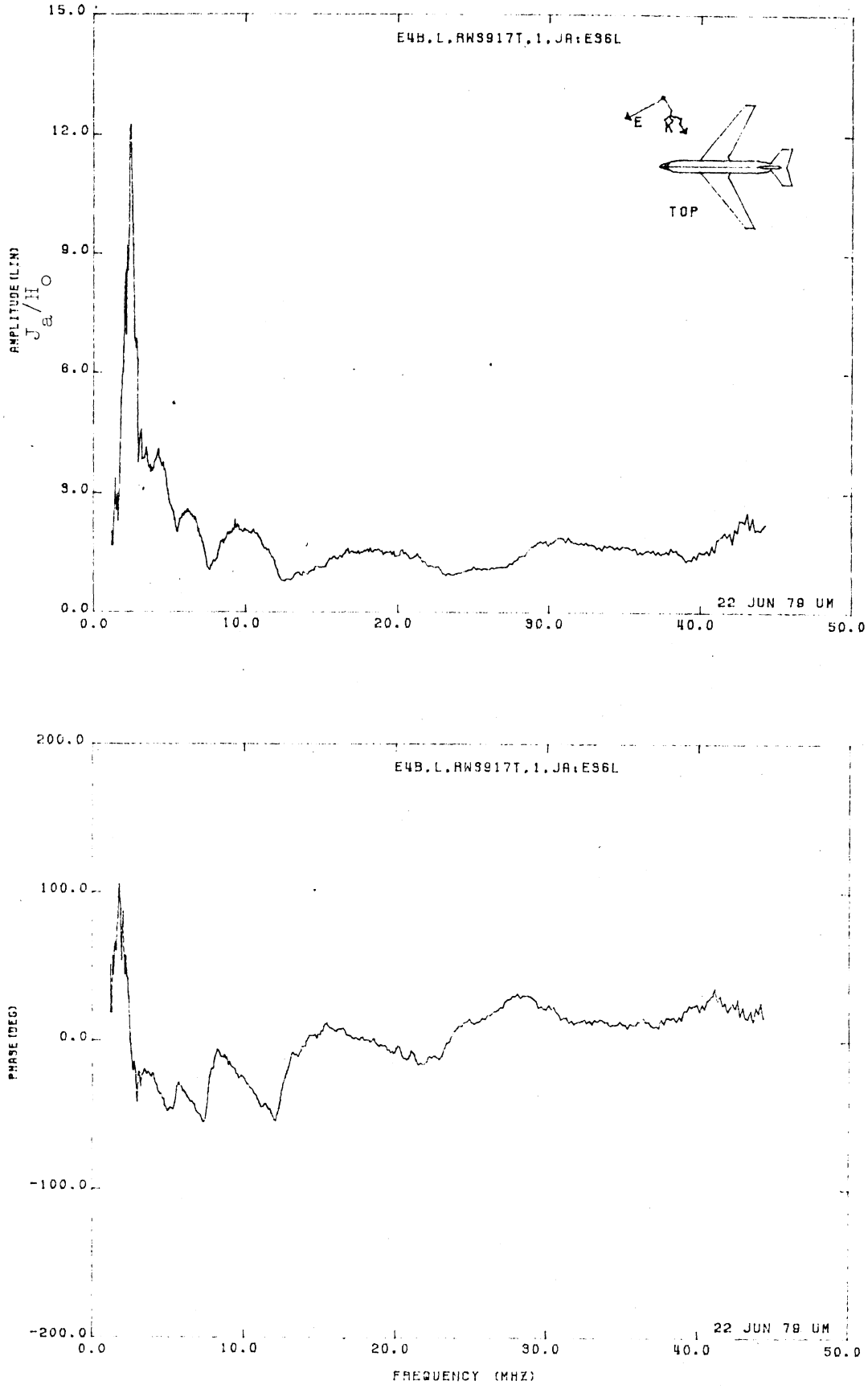

Figure 36L. Axial Current at STA:RWS917T, Excitation 1, 1/100 Model.

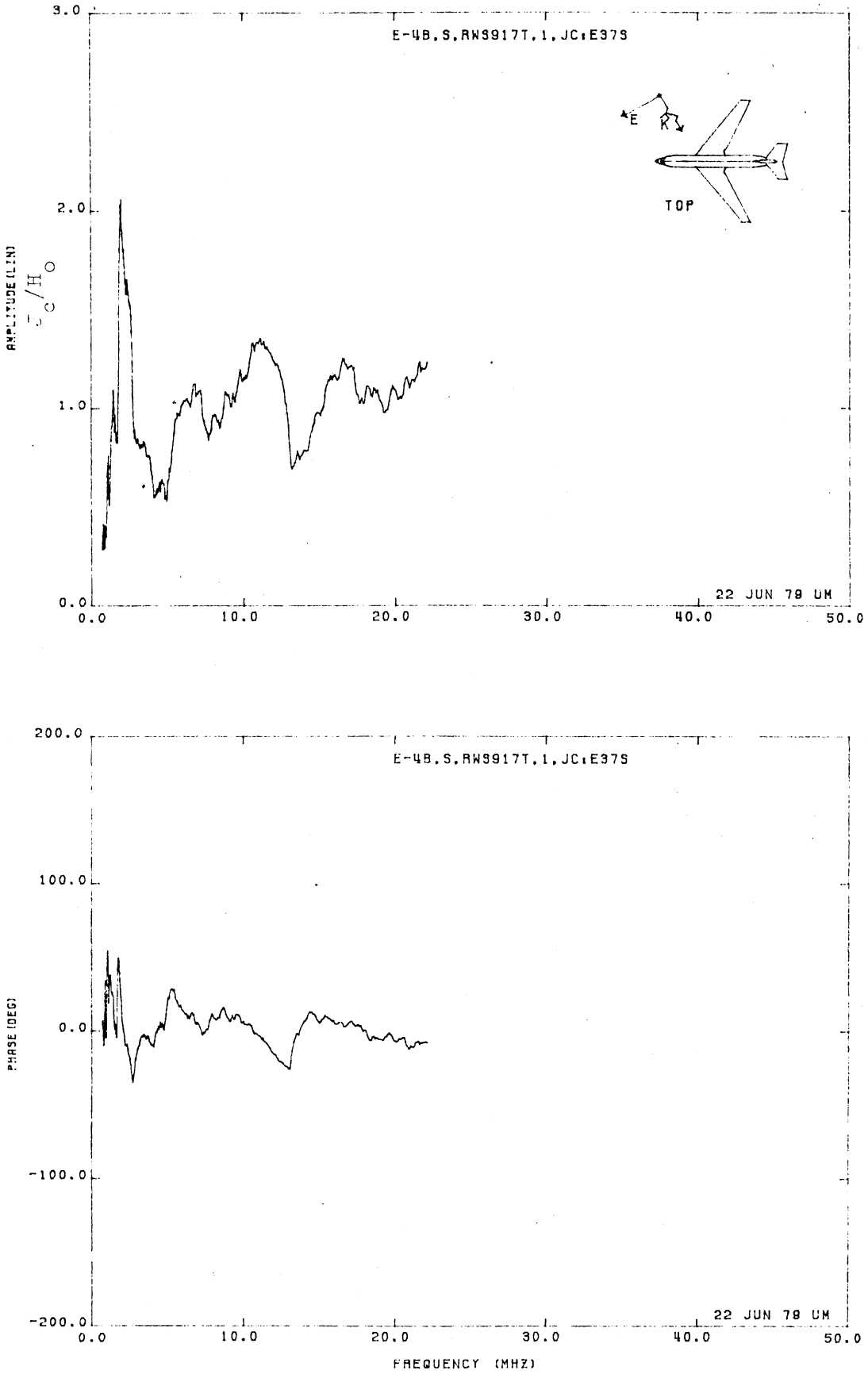

Figure 37S. Circumferential Current at STA:RWS917T, Excitation 1, 1/200 Model.

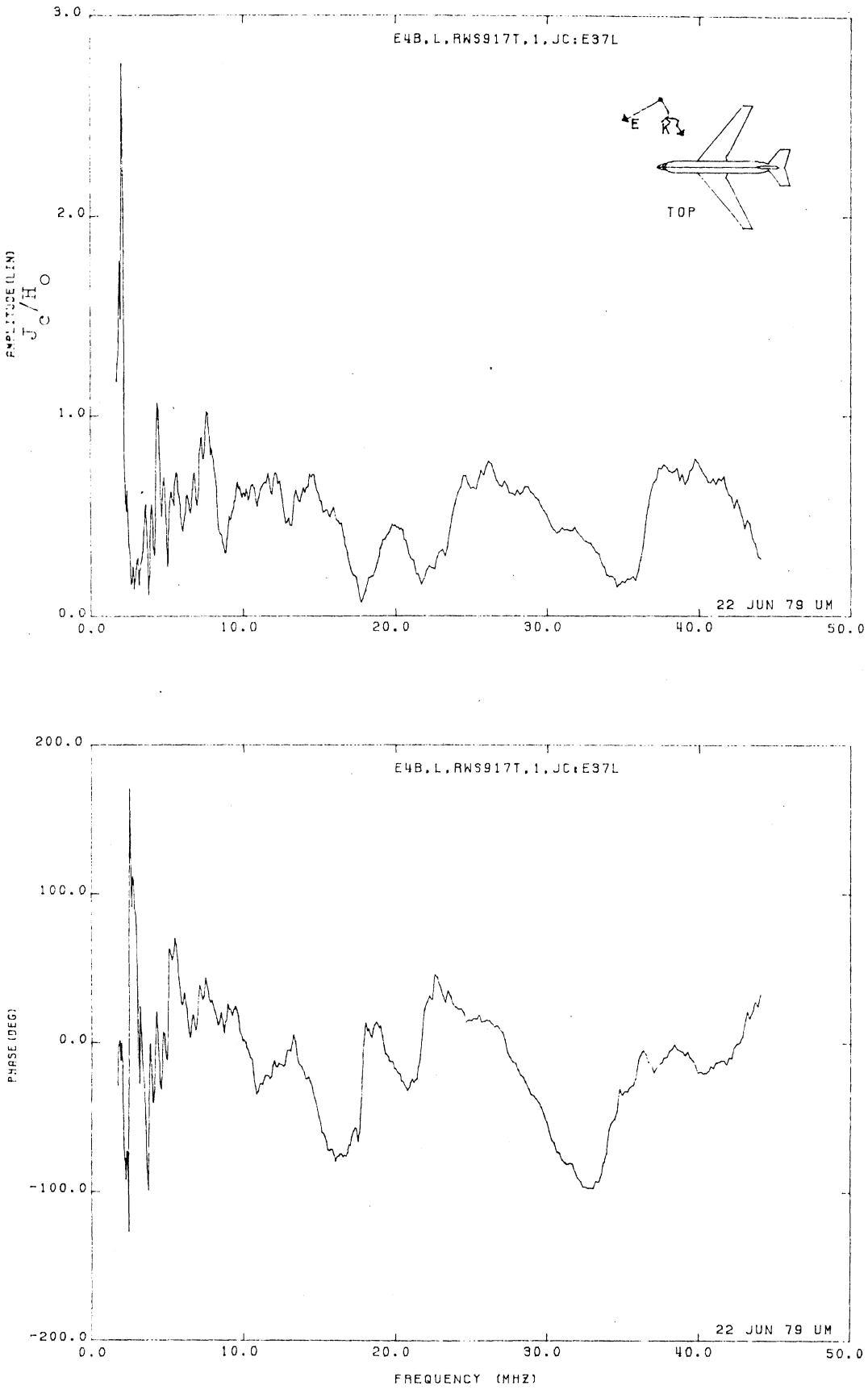

Figure 37L. Circumferential Current at STA:RWS917T, Excitation 1, 1/100 Model.

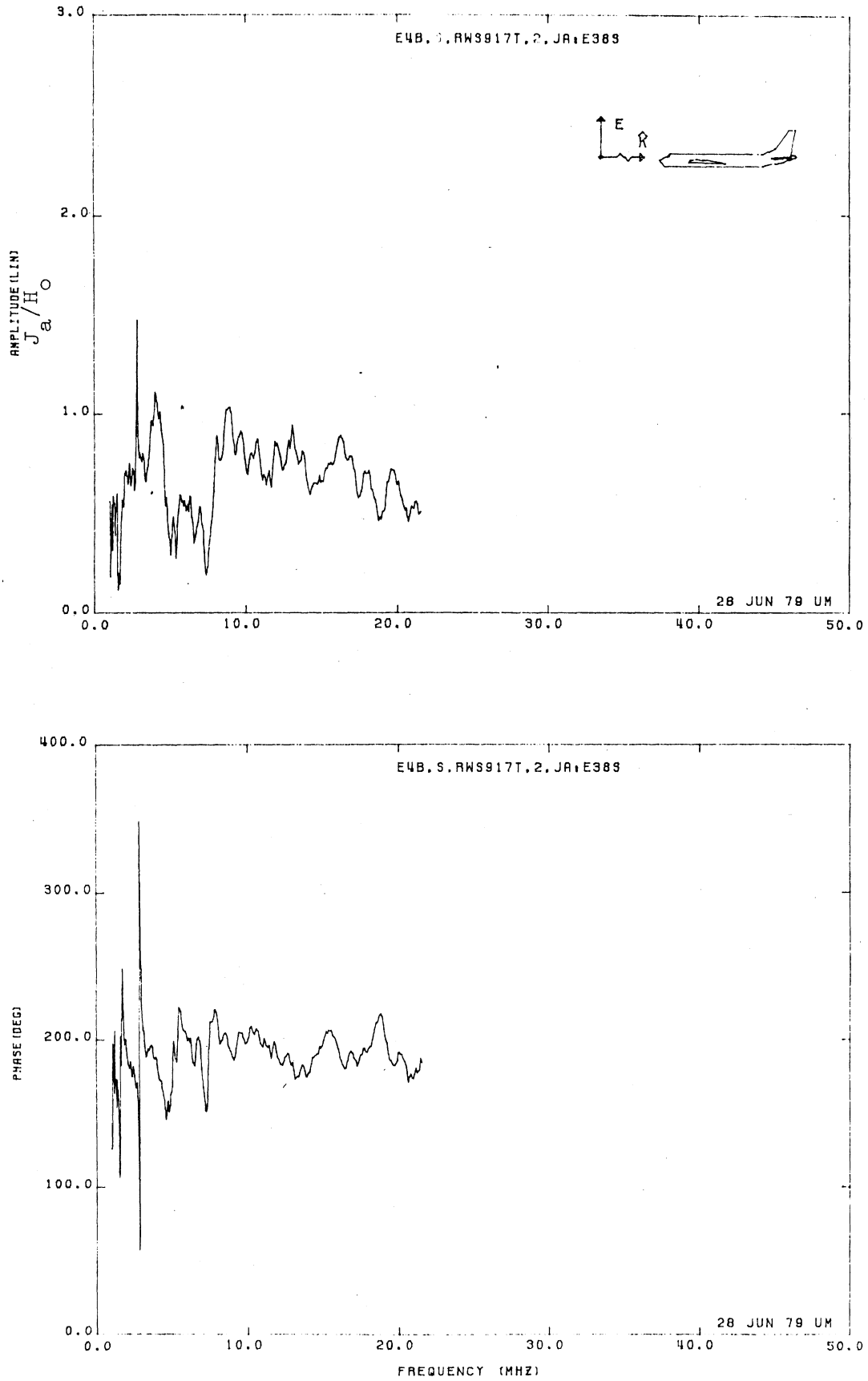

Figure 38S. Axial Current at STA:RWS917T, Excitation 2, 1/200 Model.

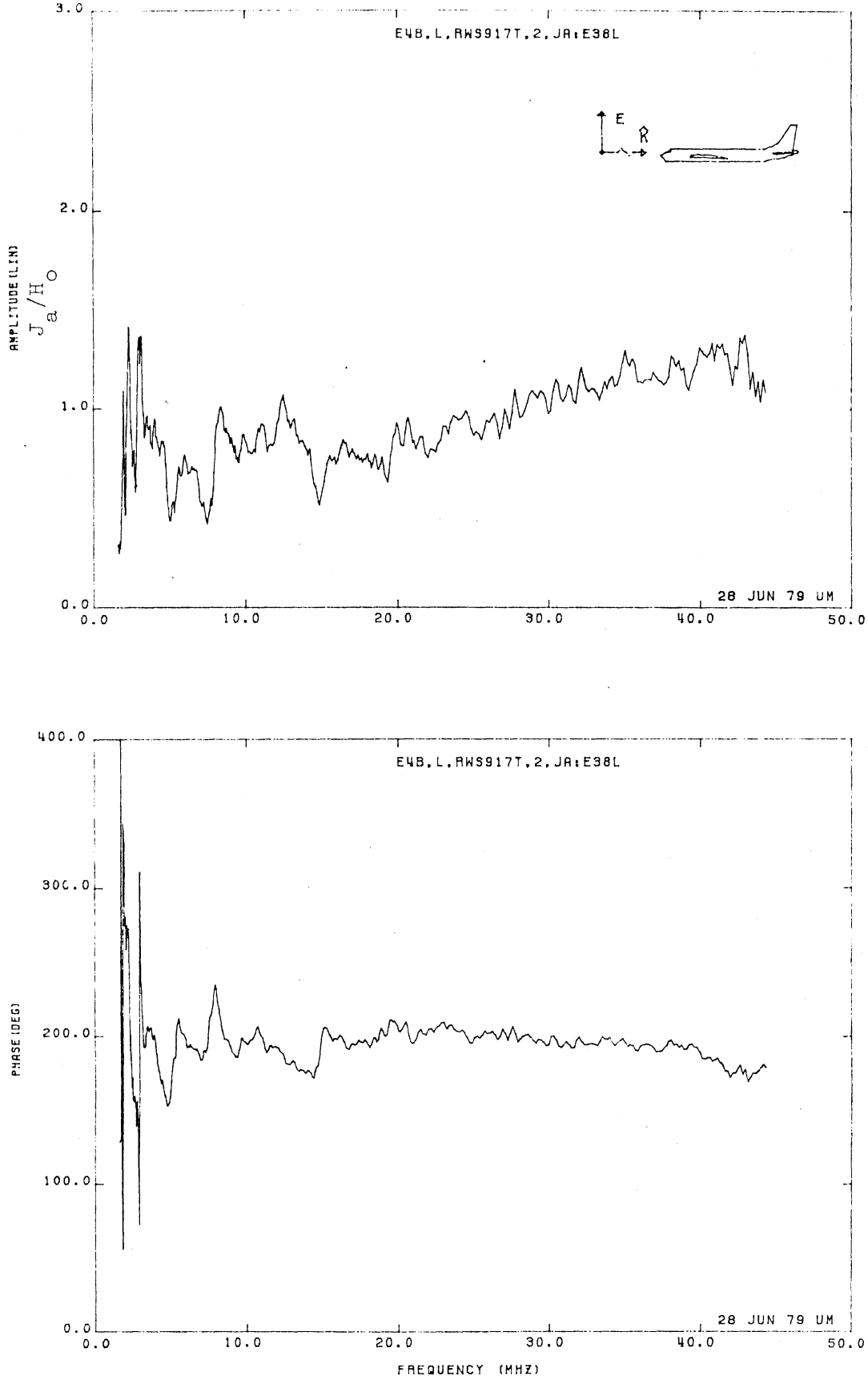

Figure 38L. Axial Current at STA:RWS917T, Excitation 2, 1/100 Model.

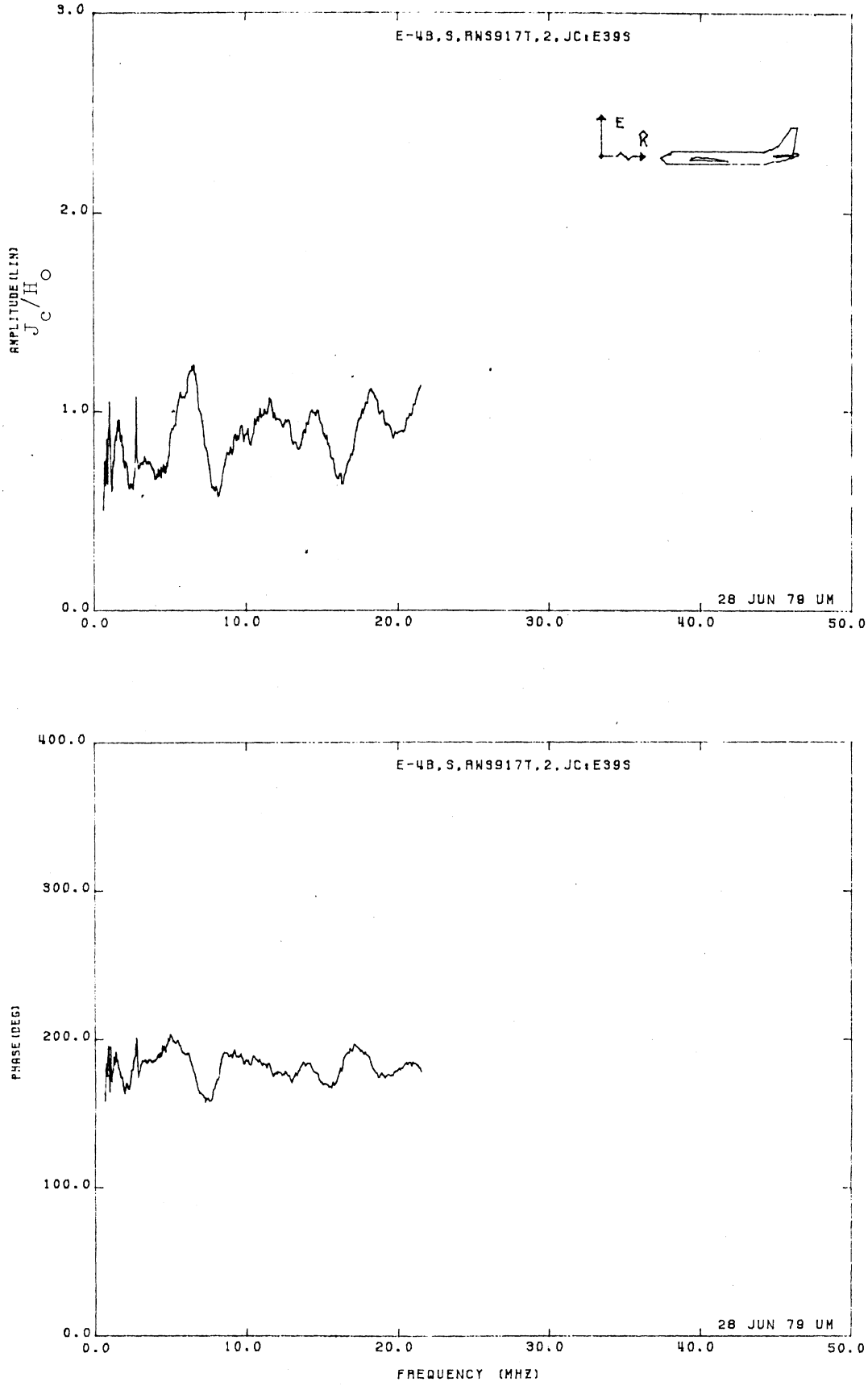

Figure 39S. Circumferential Current at STA:RWS917T, Excitation 2, 1/200 Model.

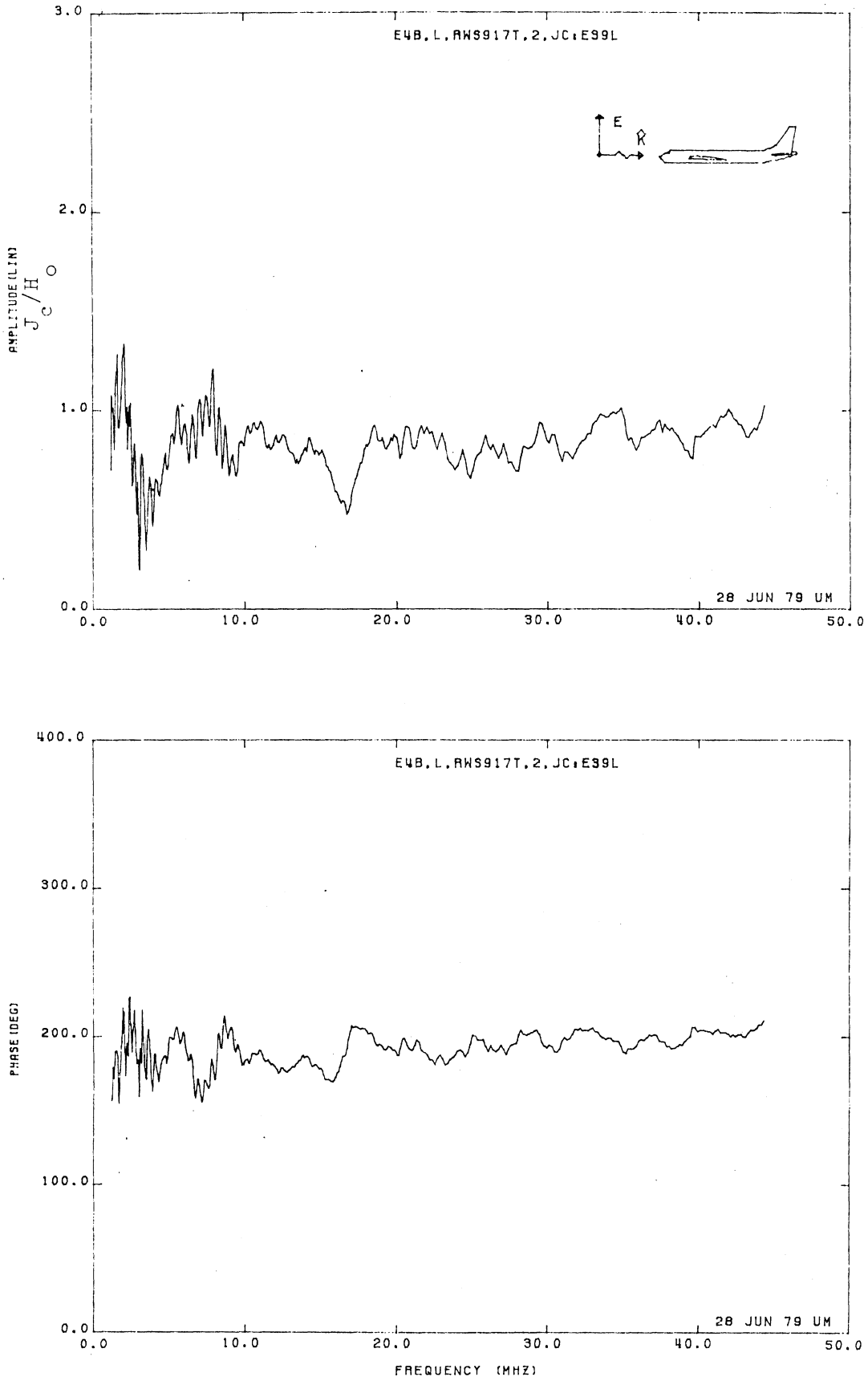

Figure 39L. Circumferential Current at STA:RWS917T, Excitation 2, 1/100 Model.

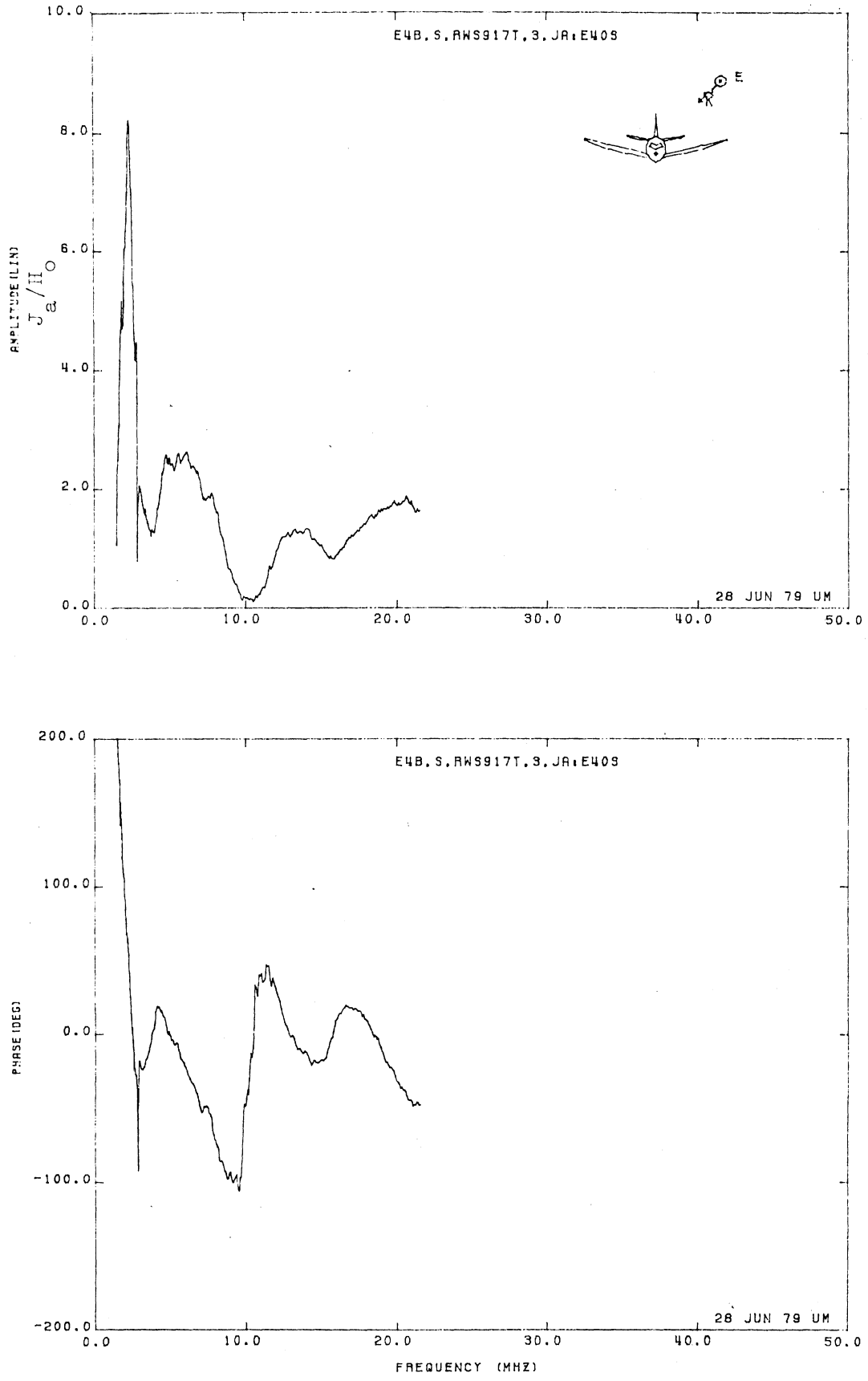

Figure 40S. Axial Current at STA:RWS917T, Excitation 3, 1/200 Model.

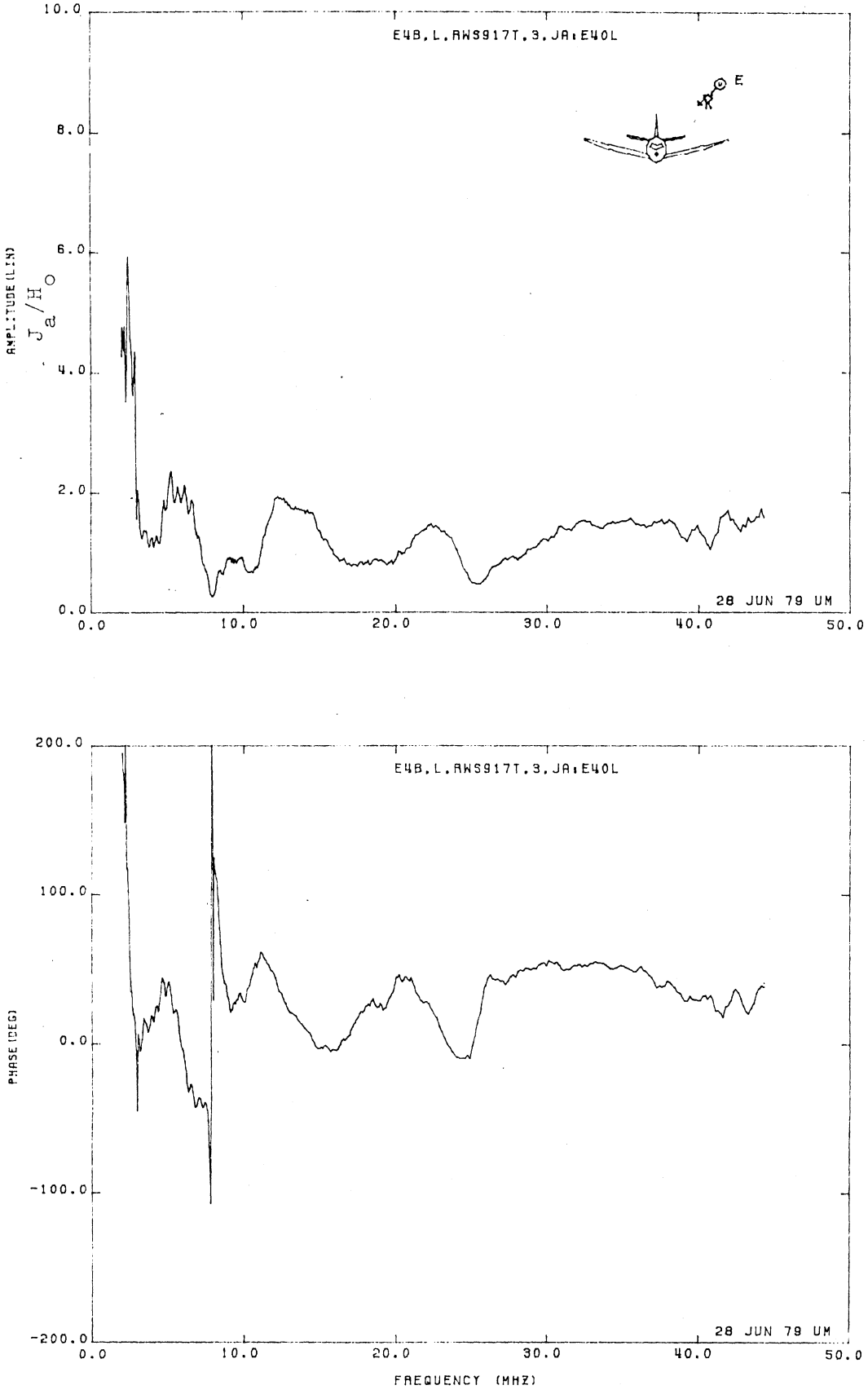

Figure 40L. Axial Current at STA:RWS917T, Excitation 3, 1/100 Model.

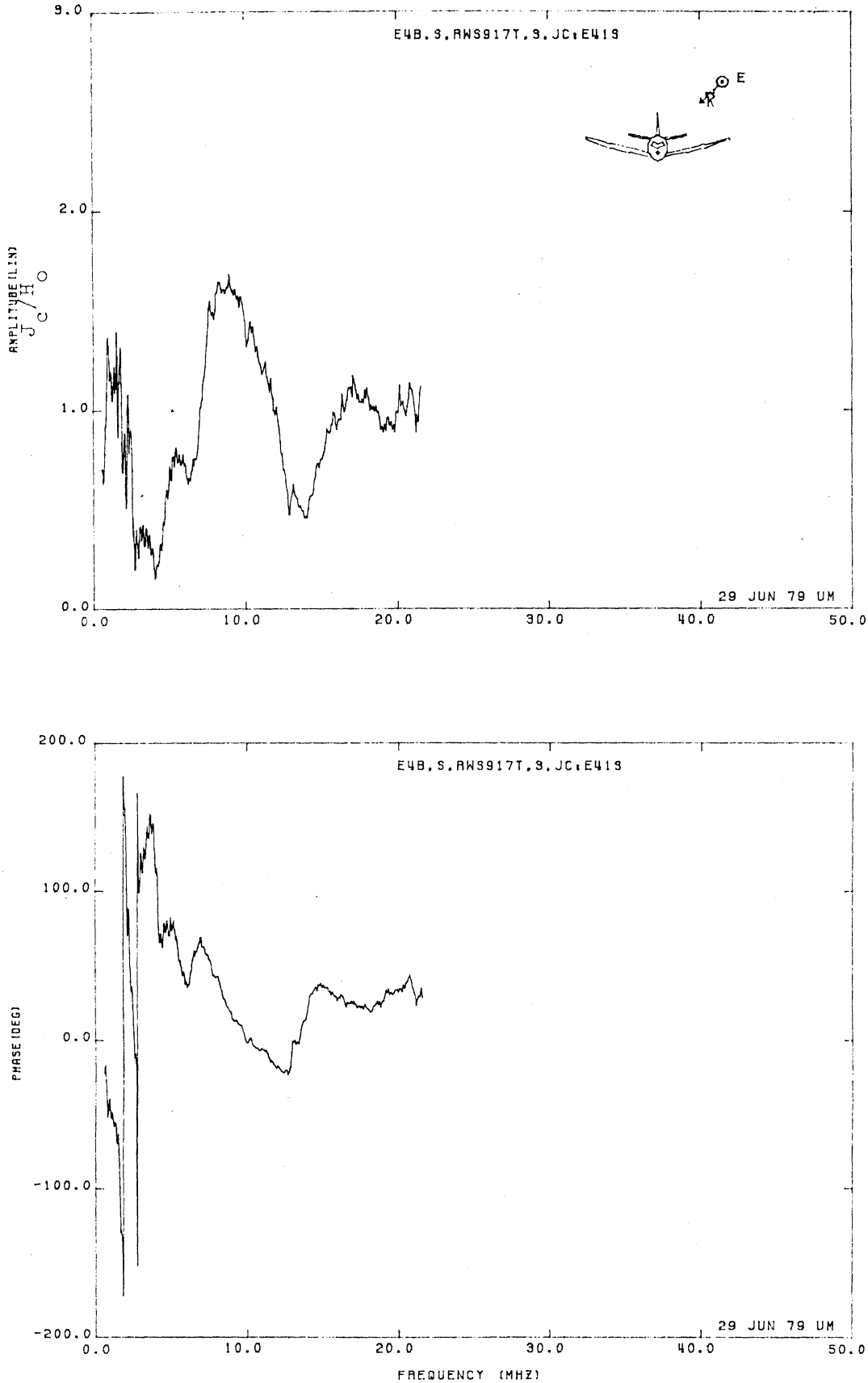

Figure 41S. Circumferential Current at STA:RWS917T, Excitation 3, 1/200 Model.

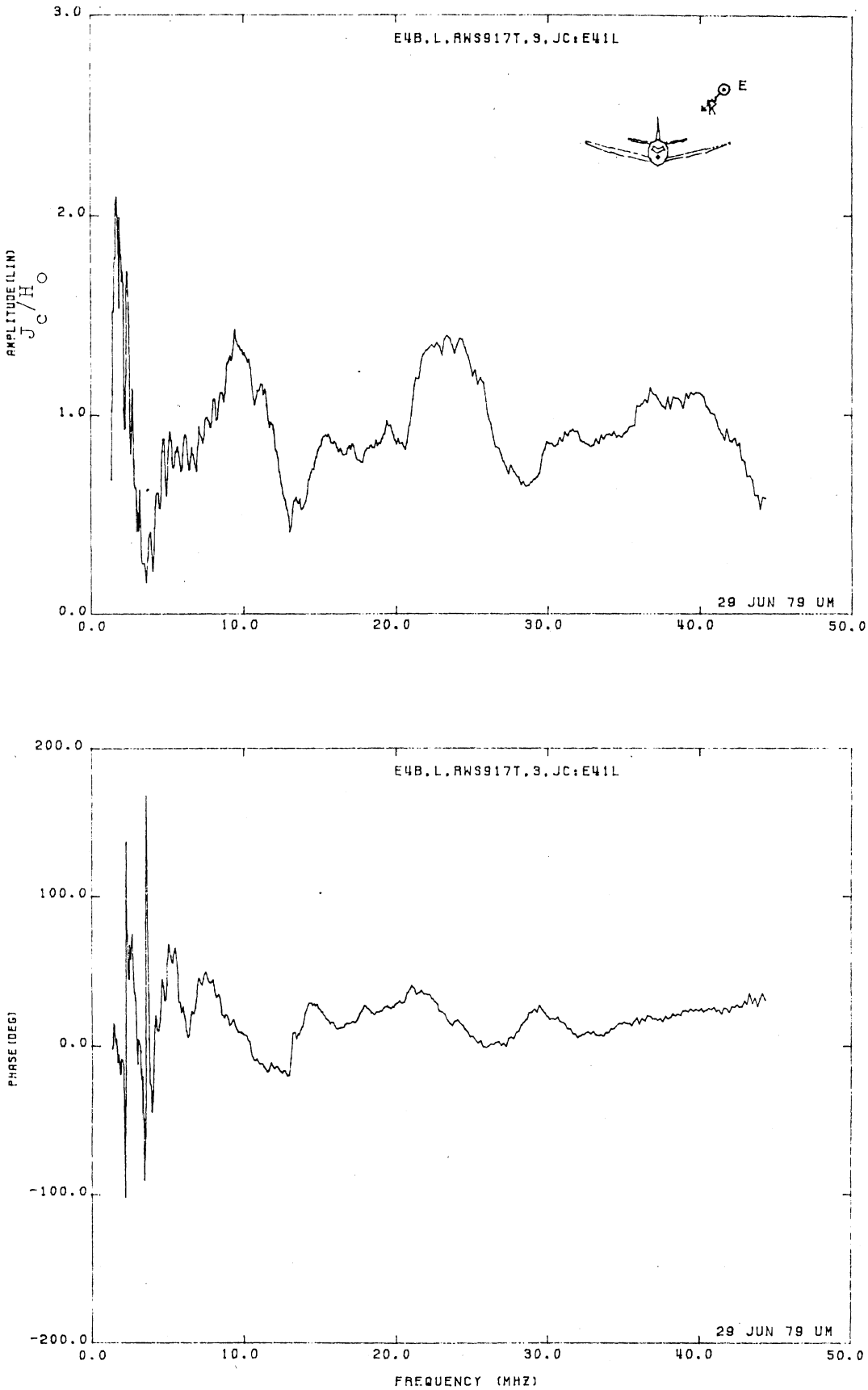

Figure 41L. Circumferential Current at STA:RWS917T, Excitation 3, 1/100 Model.

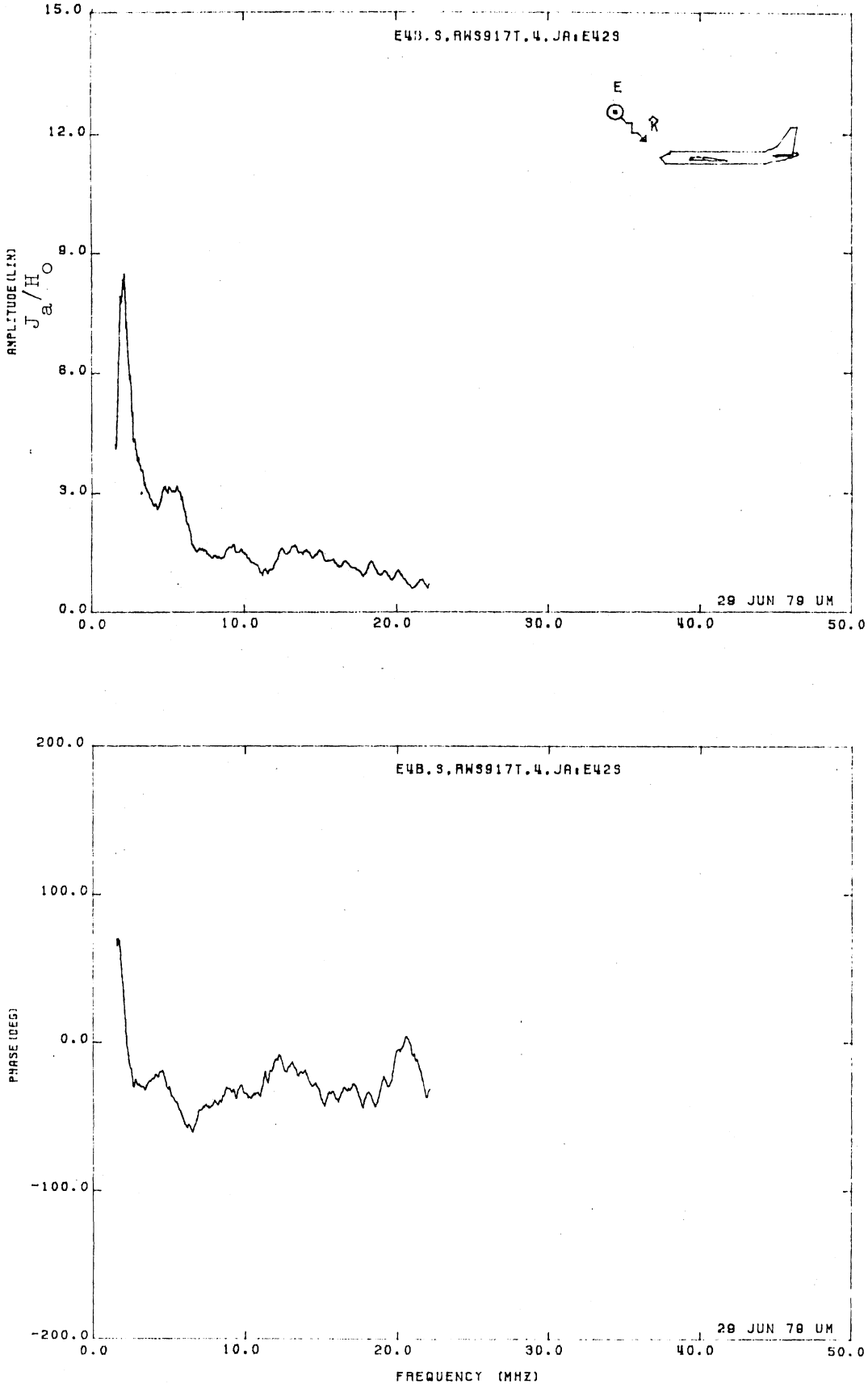

Figure 42S. Axial Current at STA:RWS917T, Excitation 4, 1/200 Model.

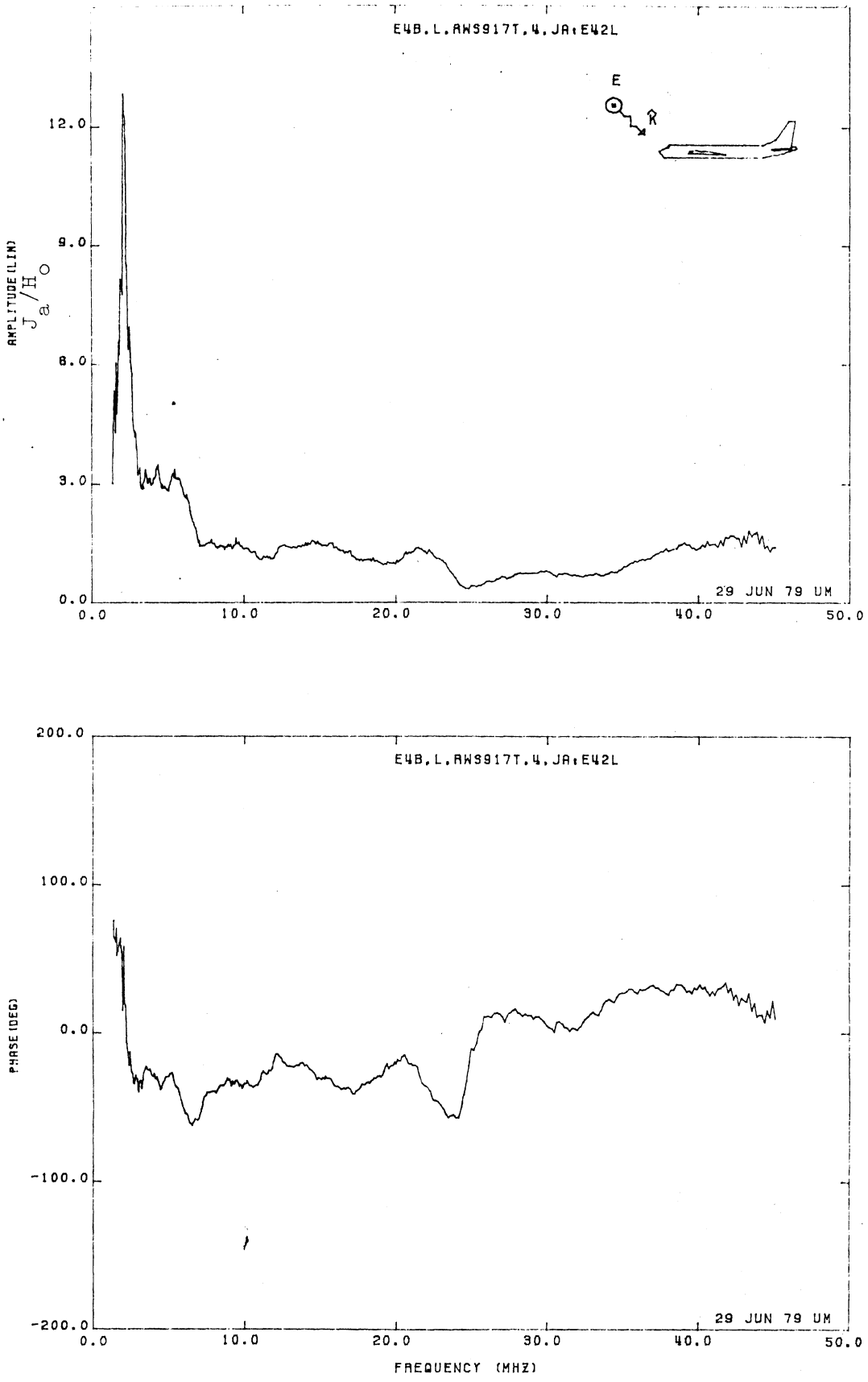

Figure 42L. Axial Current at STA:RWS917T, Excitation 4, 1/100 Model.

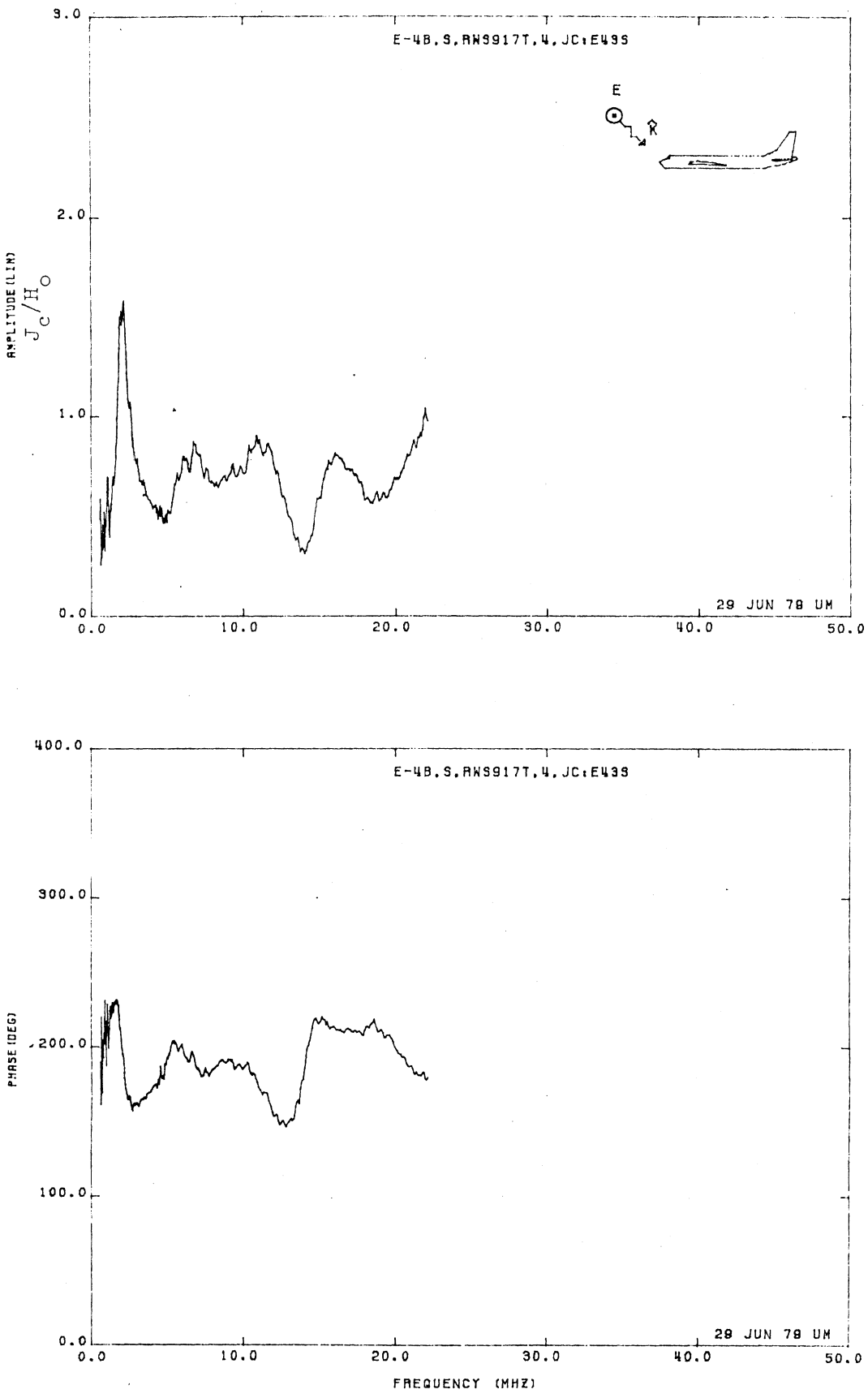

Figure 43S. Circumferential Current at STA:RWS917T, Excitation 4, 1/200 Model.

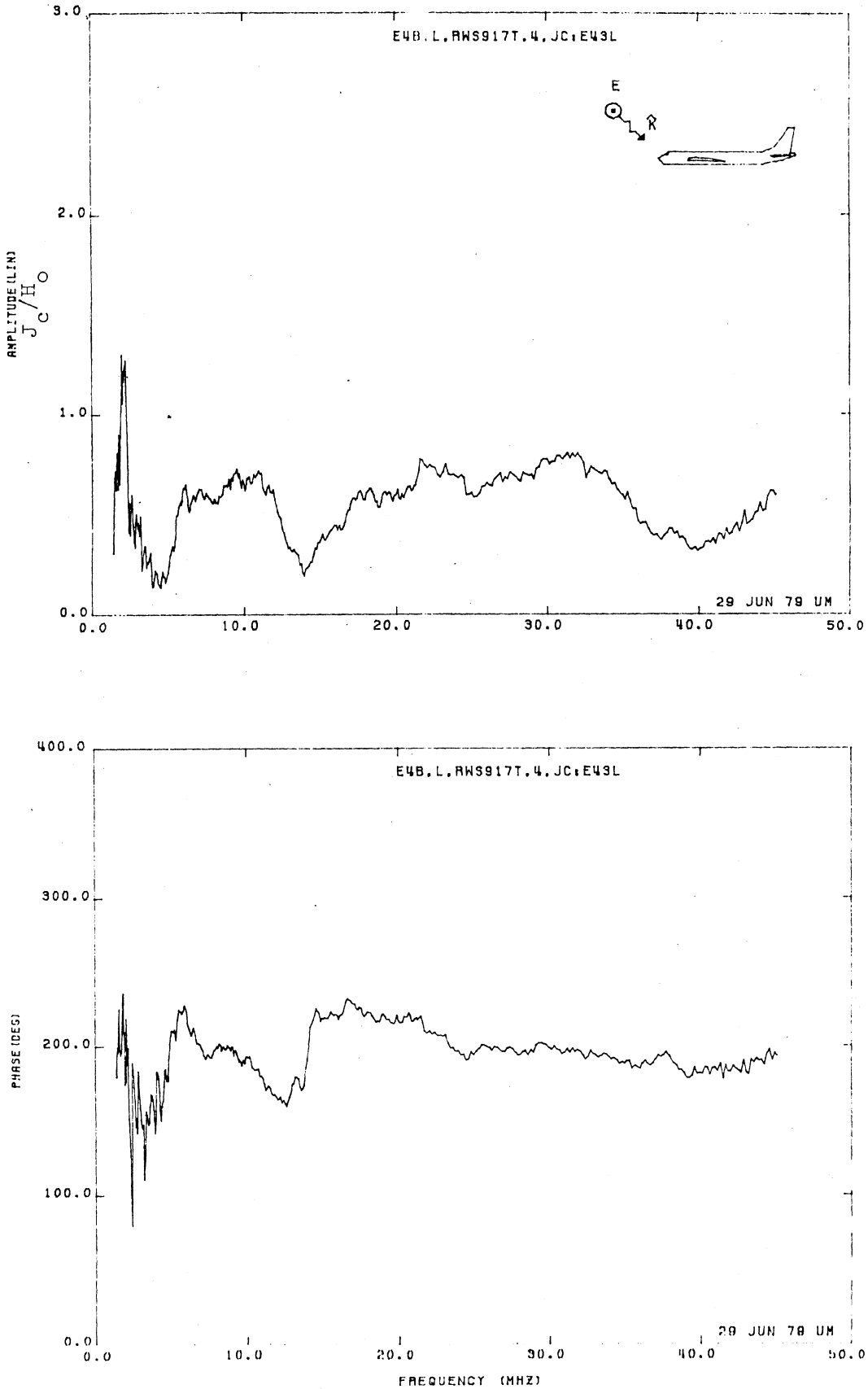

Figure 43L. Circumferential Current at STA:RWS917T, Excitation 4, 1/100 Model.

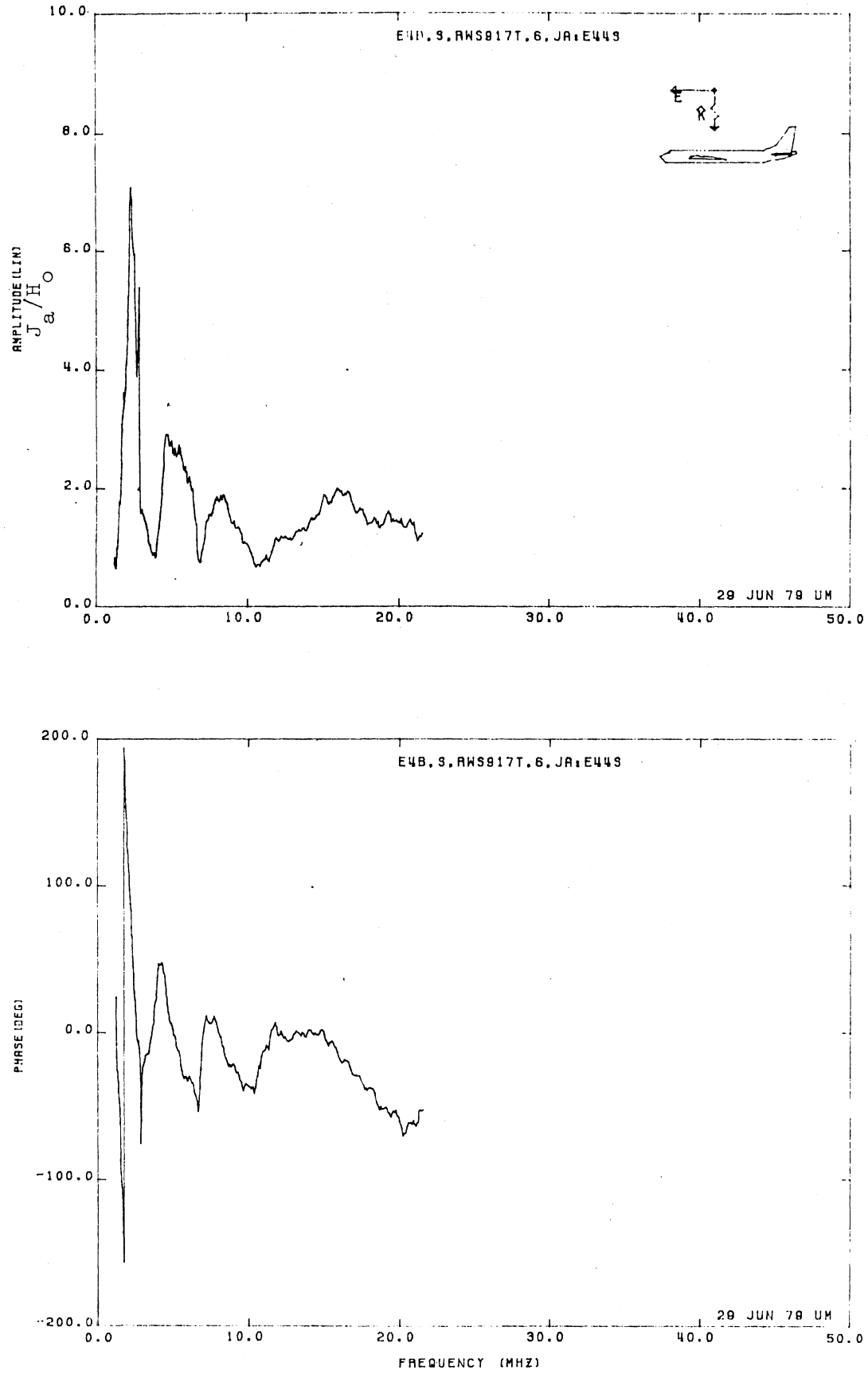

Figure 44S. Axial Current at STA:44S, Excitation 6, 1/200 Model.

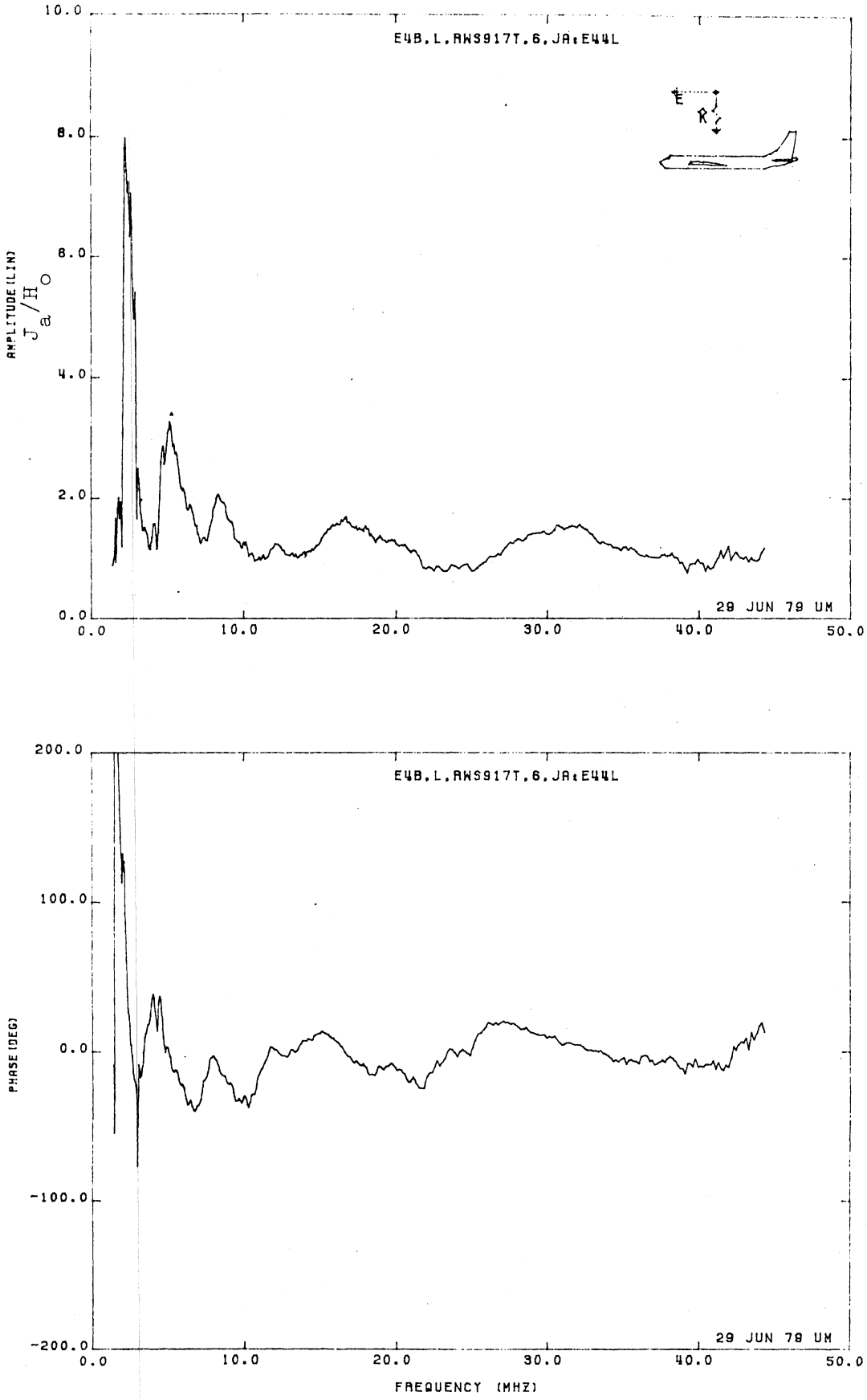

Figure 44L. Axial Current at STA:RWS917T, Excitation 6, 1/100 Model.

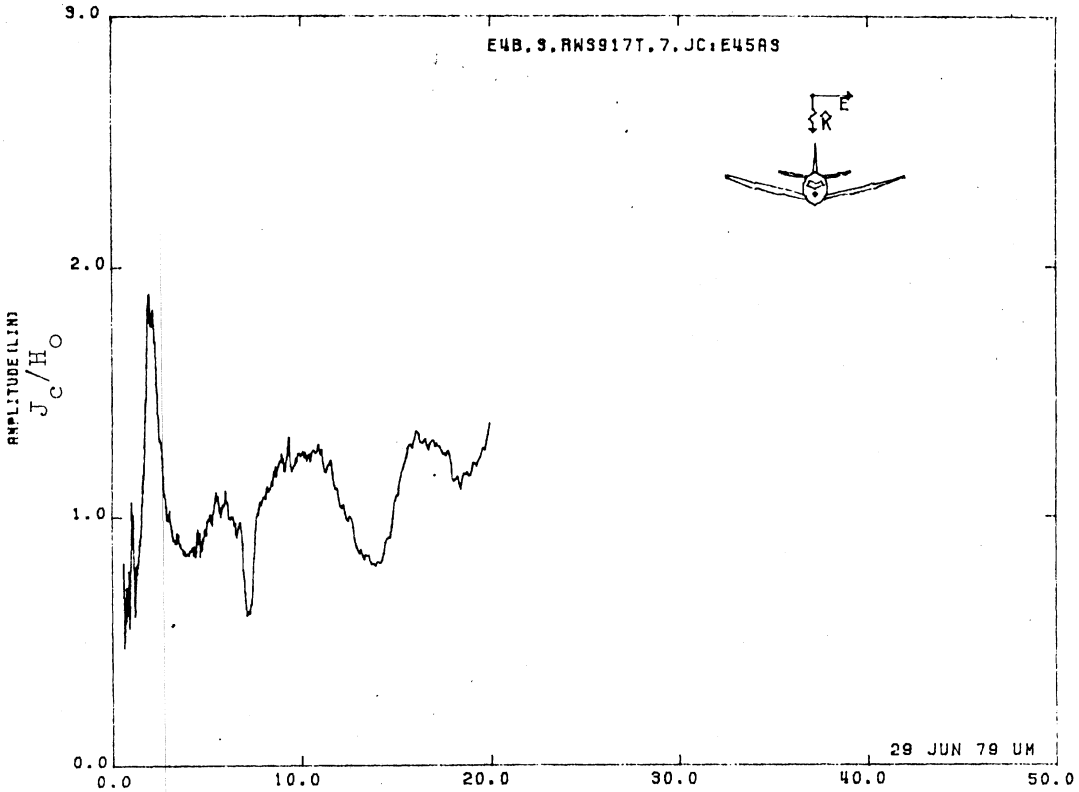

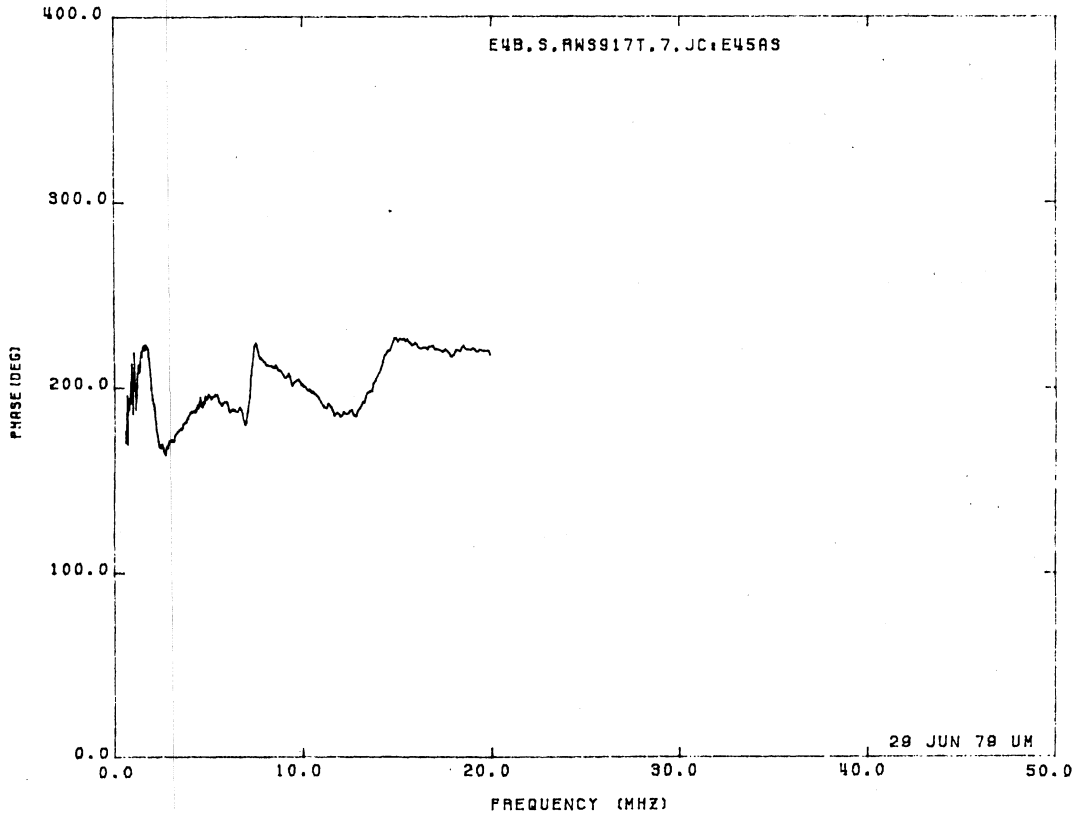

Figure 45AS. Circumferential Current at STA:RWS917T, Excitation 7, 1/200 Model.

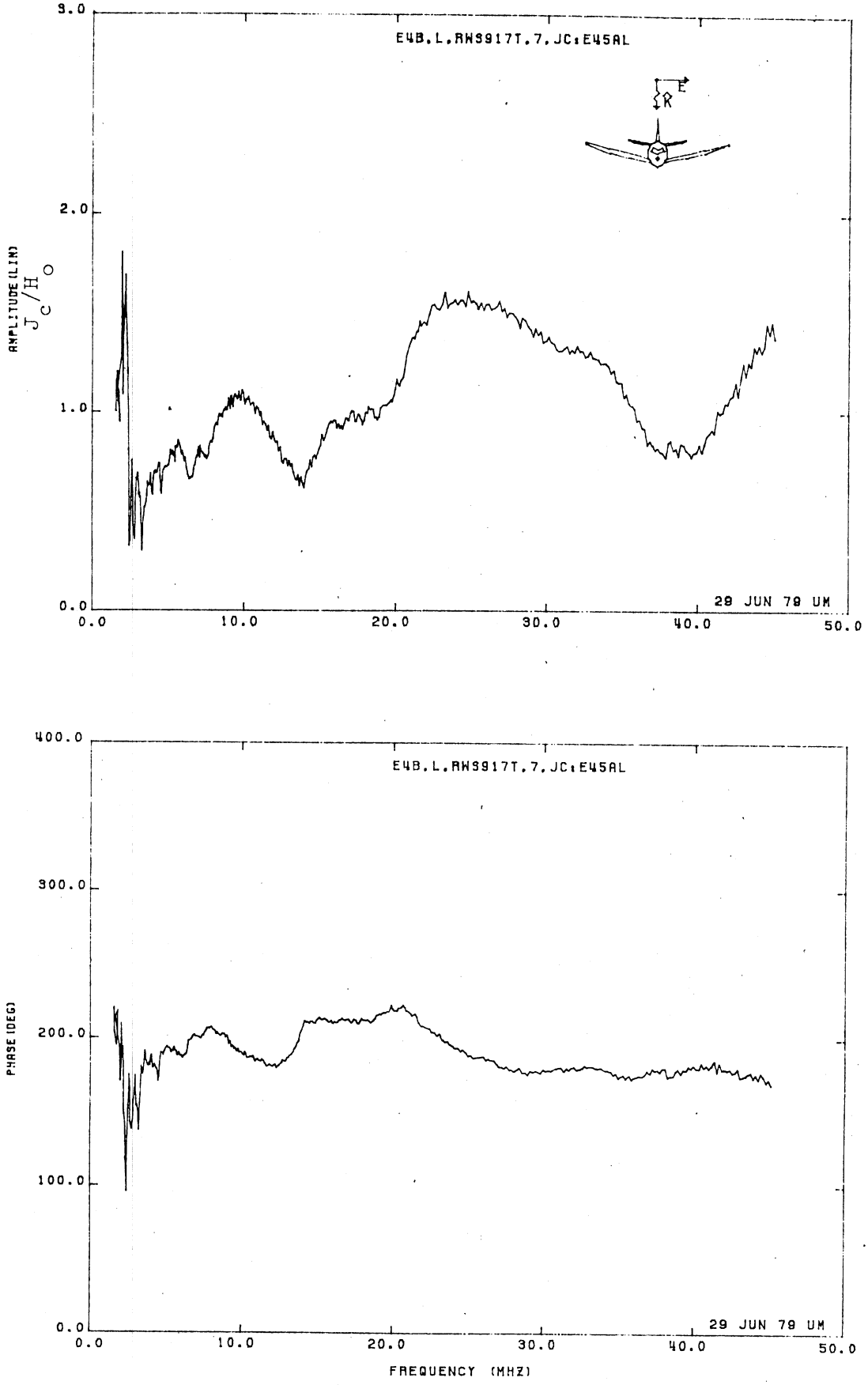

Figure 45AL. Circumferential Current at STA:RWS917T, Excitation 7, 1/100 Model.

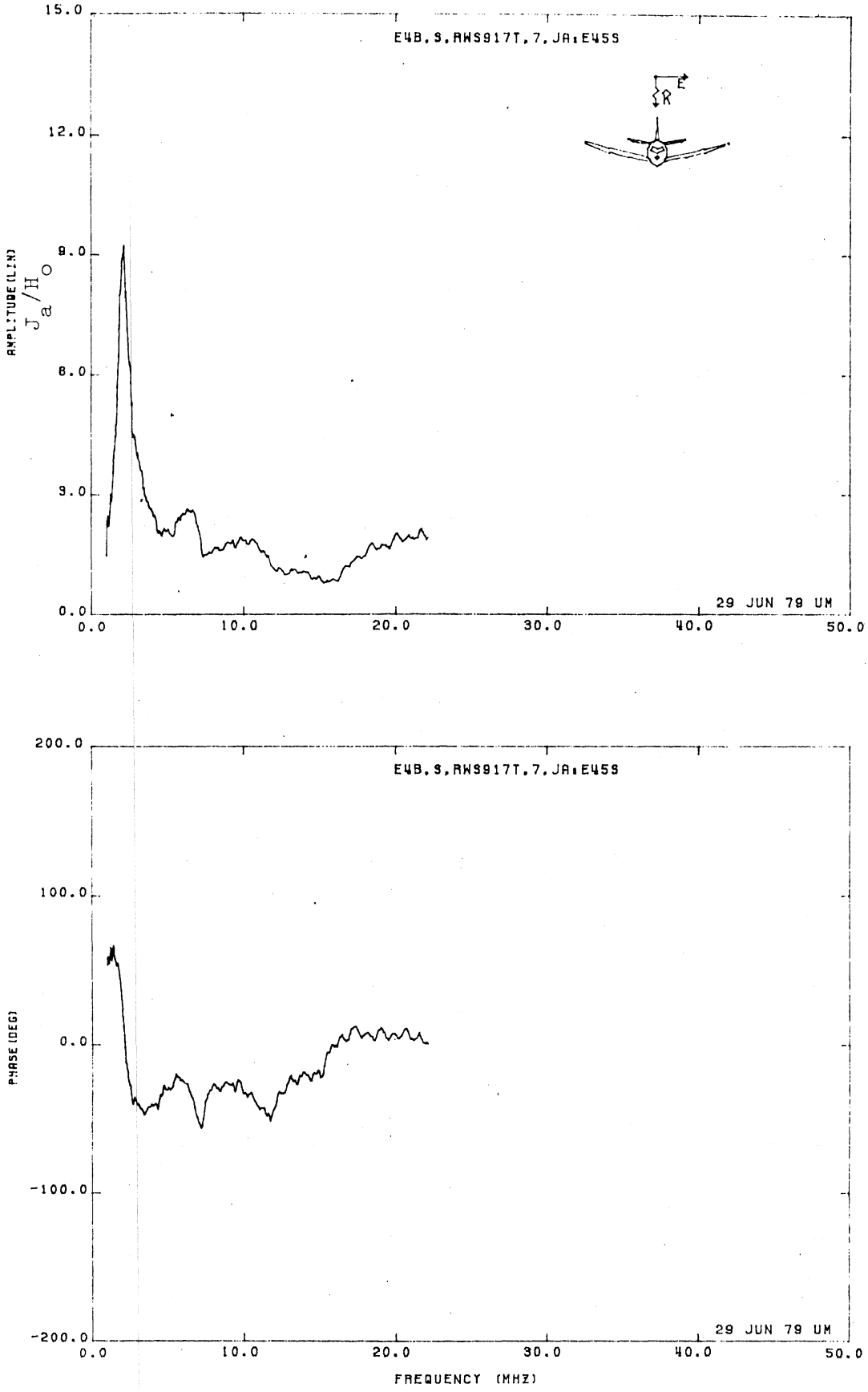

Figure 45S. Axial Current at STA:RWS917T, Excitation 7, 1/200 Model.

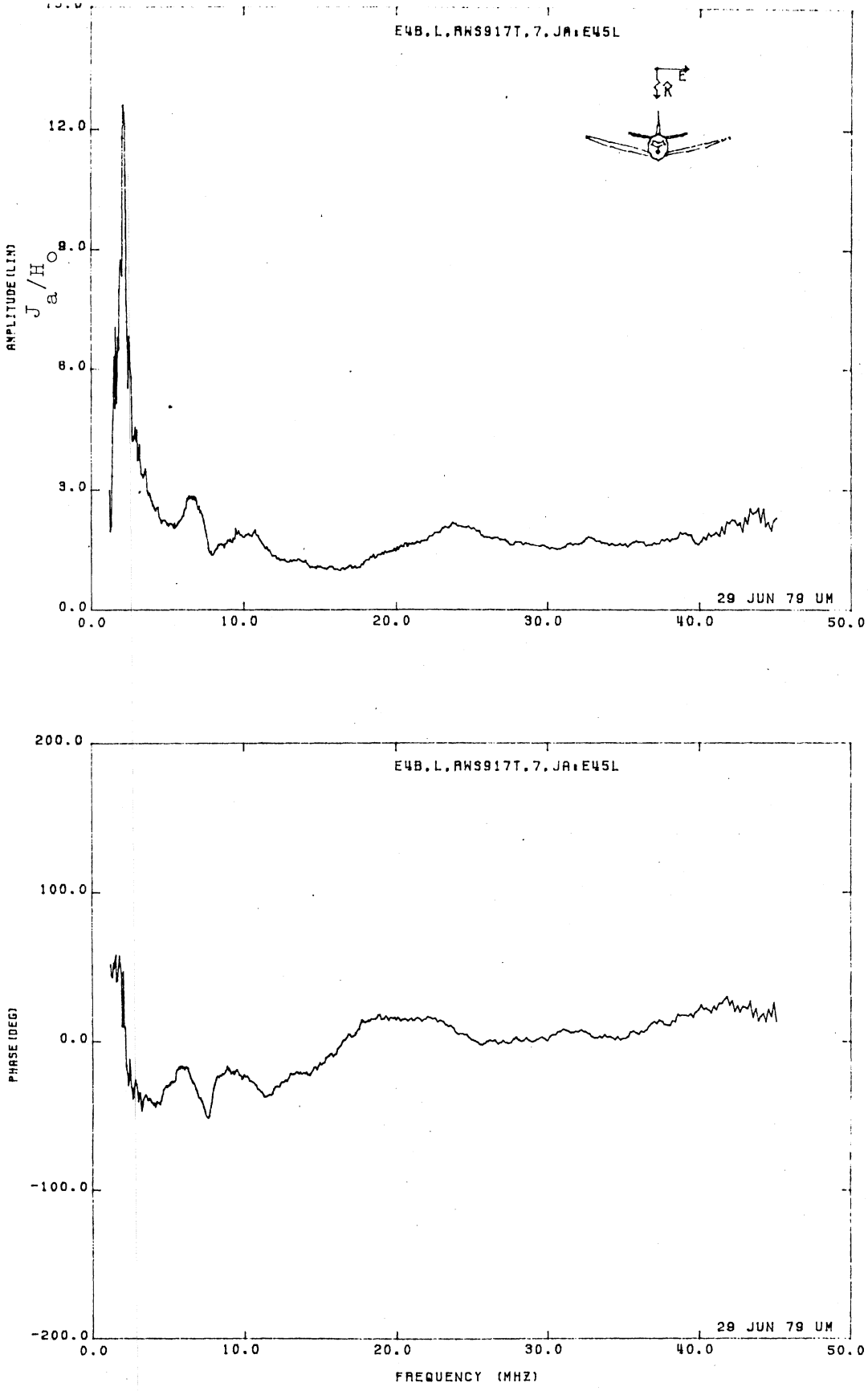

Figure 45L. Axial Current at STA:RWS917T, Excitation 7, 1/100 Model.

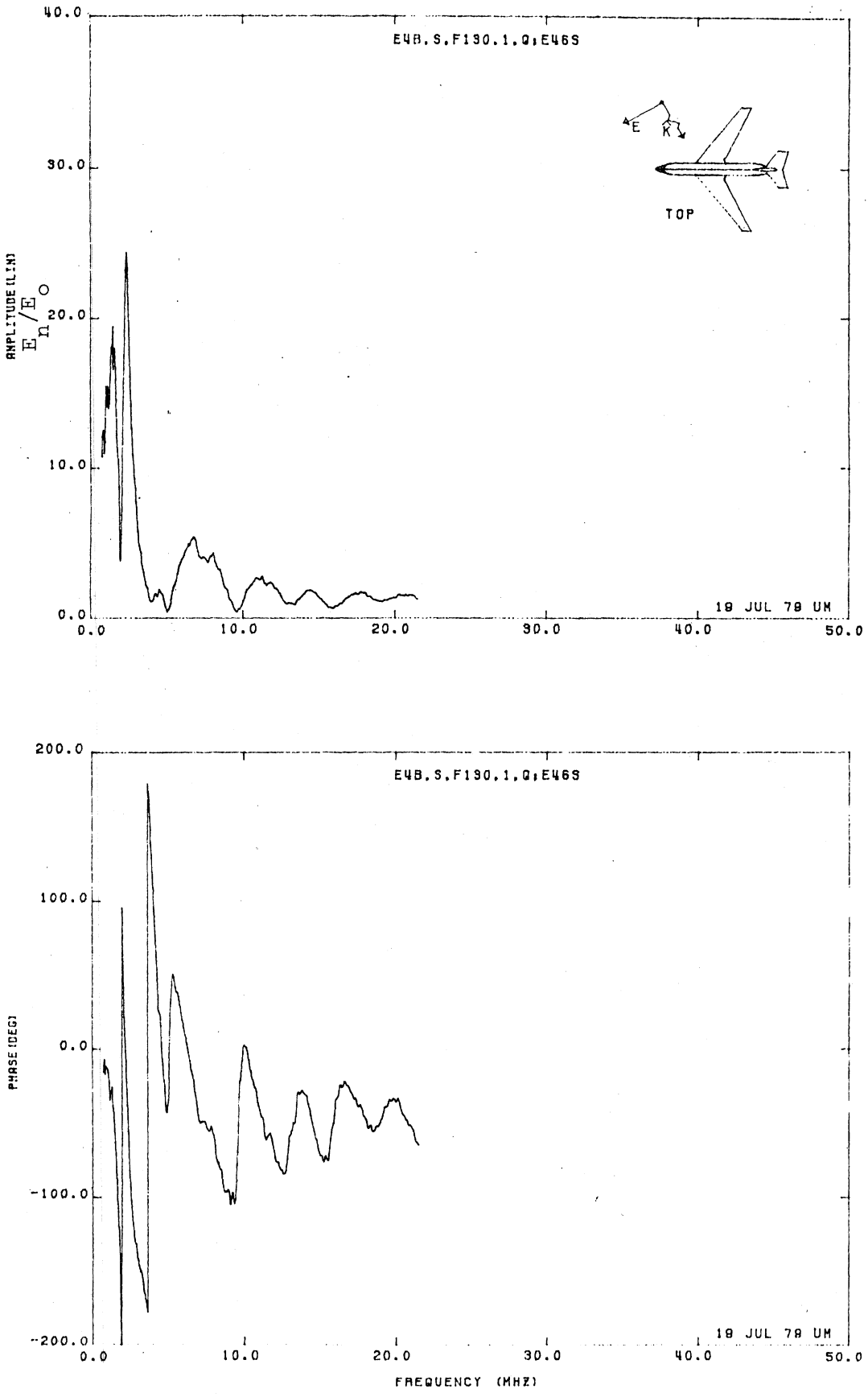

Figure 46S. Normal Electric Field at STA:F130, Excitation 1, 1/200 Model.

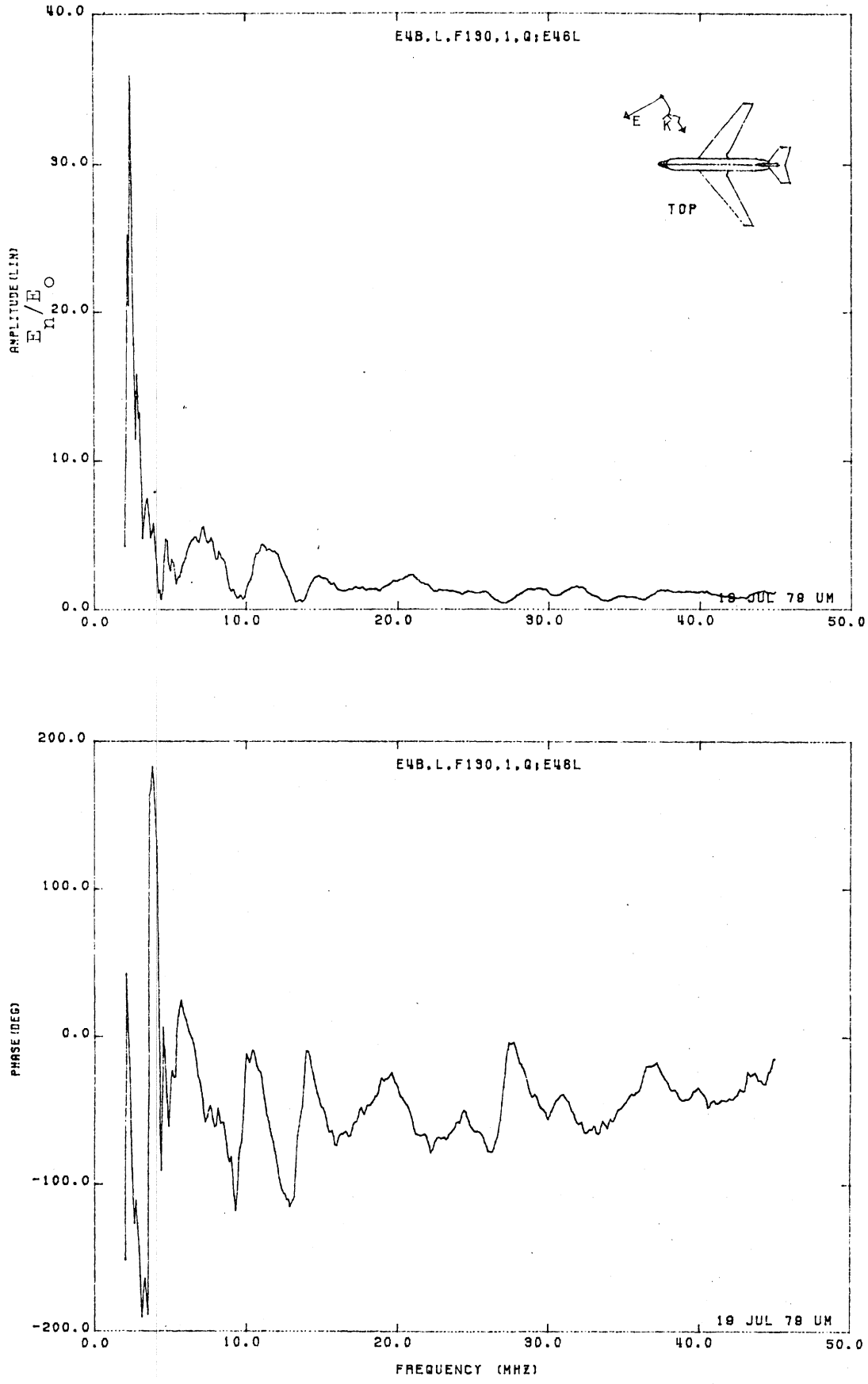

Figure 46L. Normal Electric Field at STA:F130, Excitation 1, 1/100 Model.

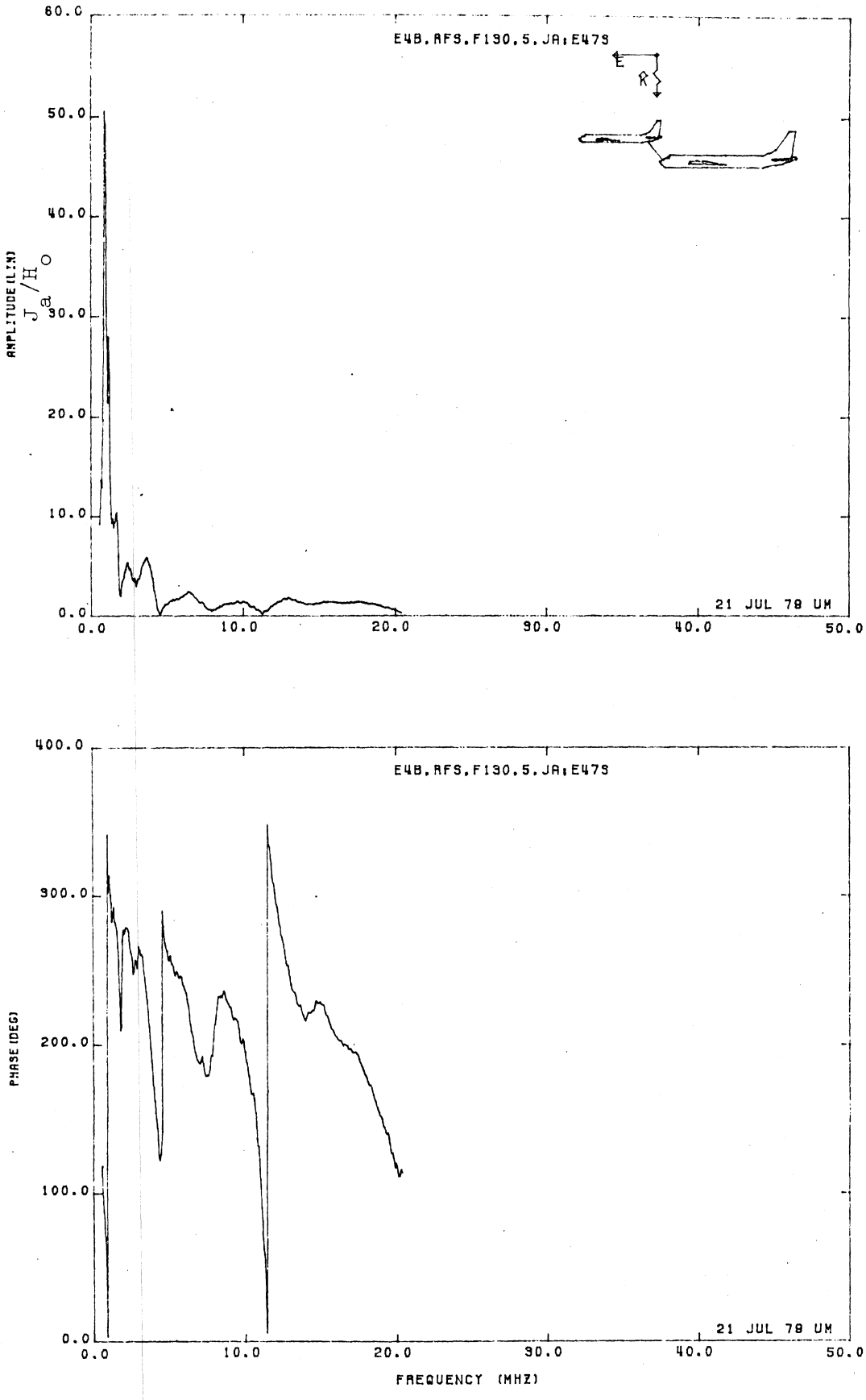

Figure 47S. Axial Current at STA:F130, Excitation 5, 1/215 Model. (Refueling Mode)

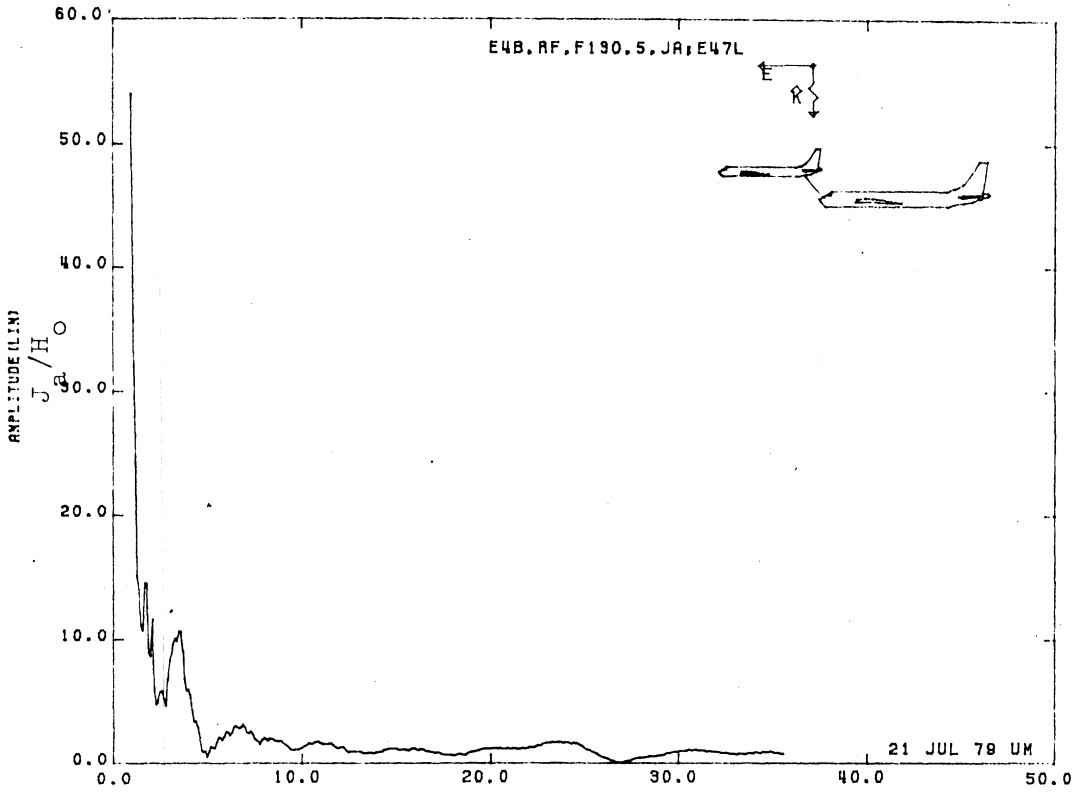

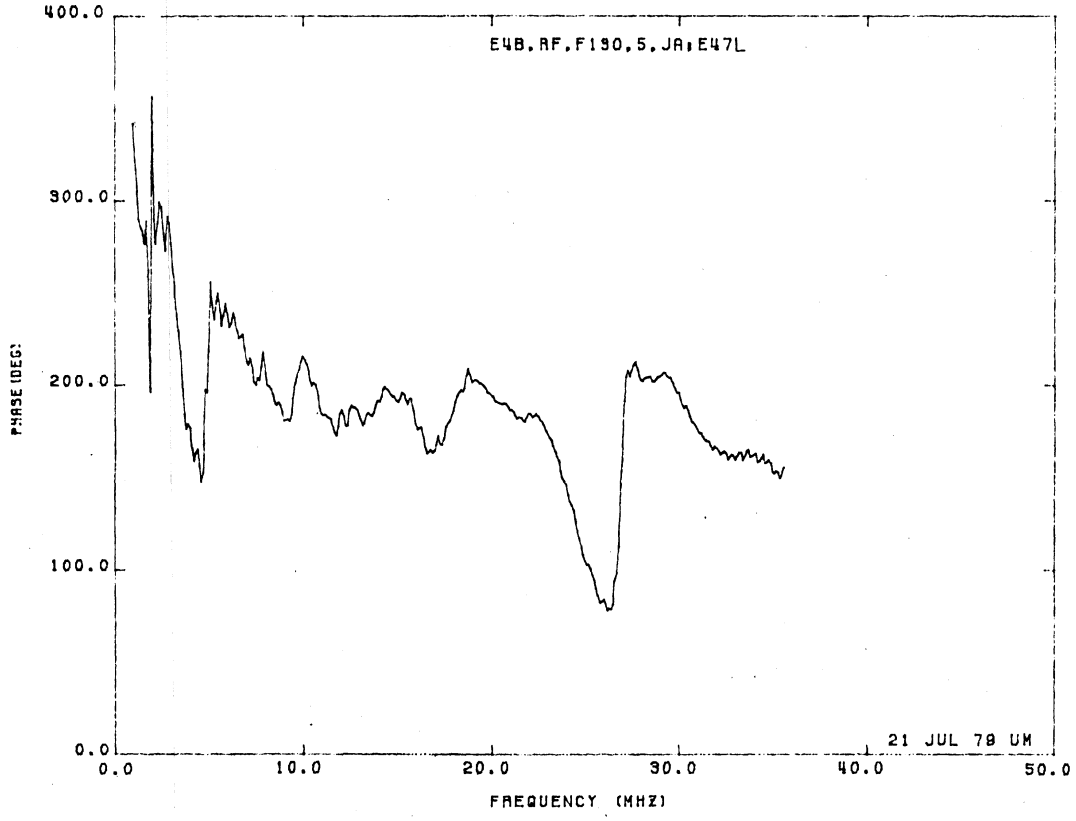

Figure 47L. Axial Current at STA:F130, Excitation 5, 1/125 Model. (Refueling Mode)

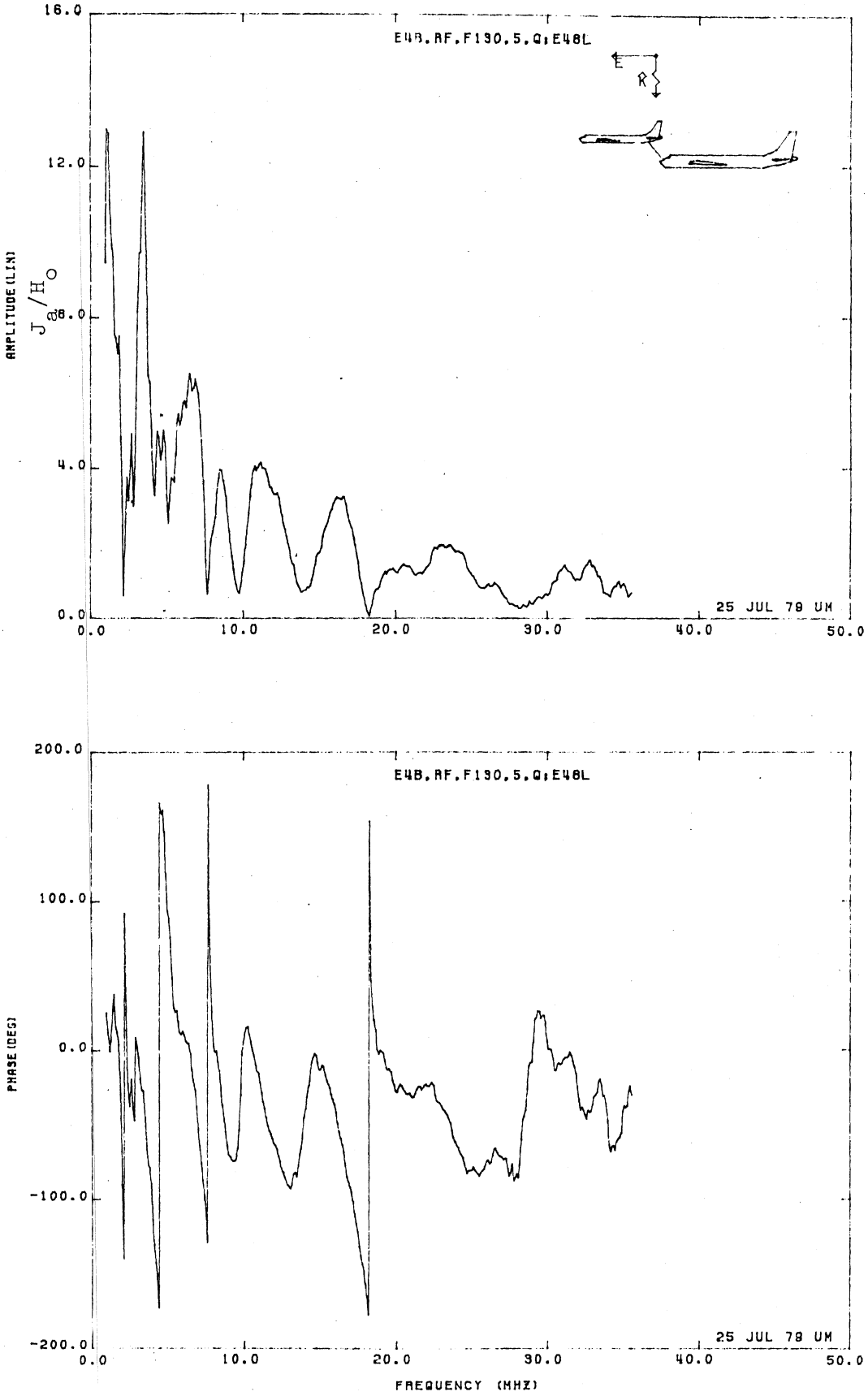

Figure 48L. Normal Electric Field at STA:130, Excitation 5, 1/125 Model. (Refueling Mode)

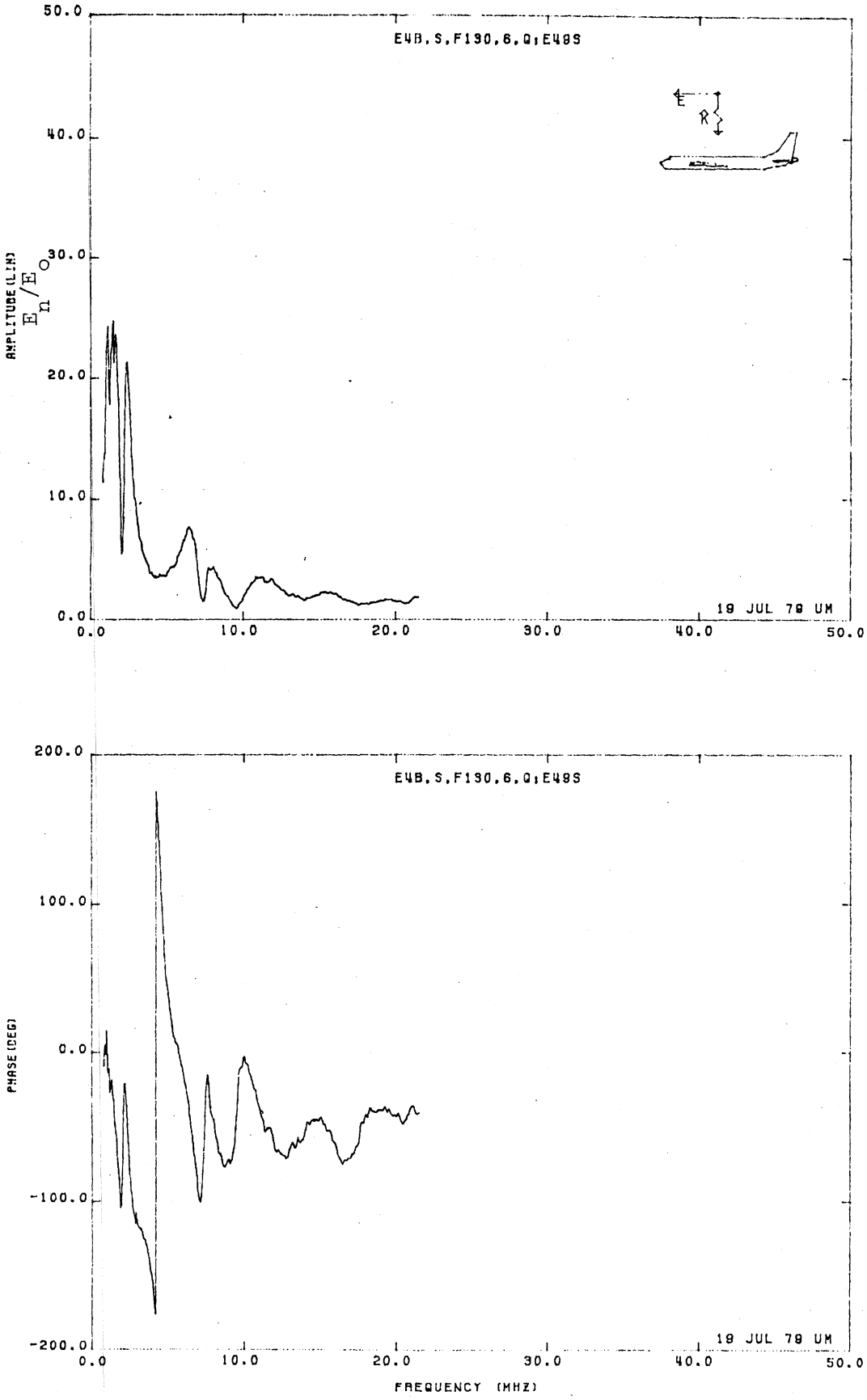

Figure 49S. Normal Electric Field at STA:F130, Excitation 6, 1/200 Model.

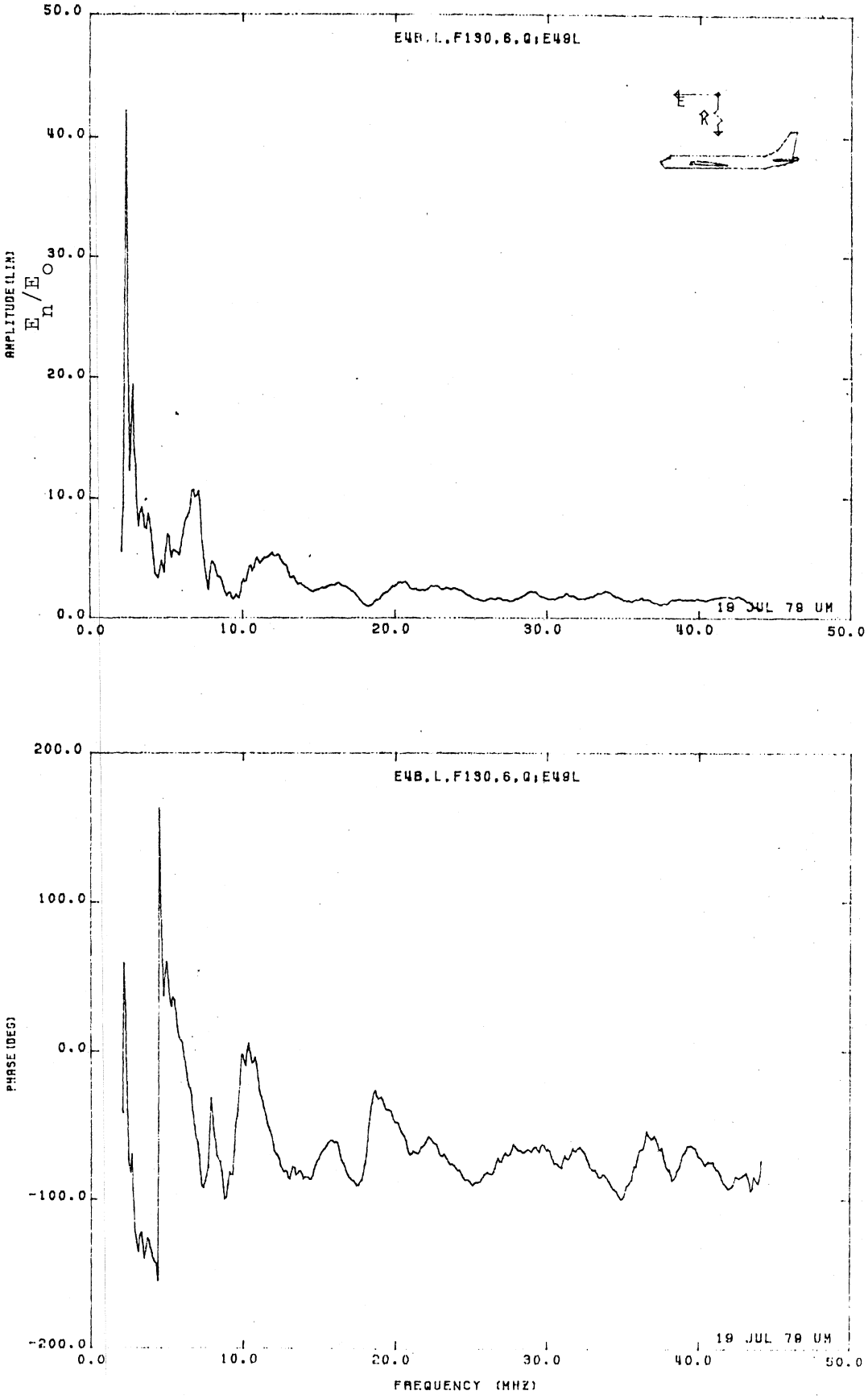

Figure 49L. Normal Electric Field at STA:F130, Excitation 6, 1/100 Model.

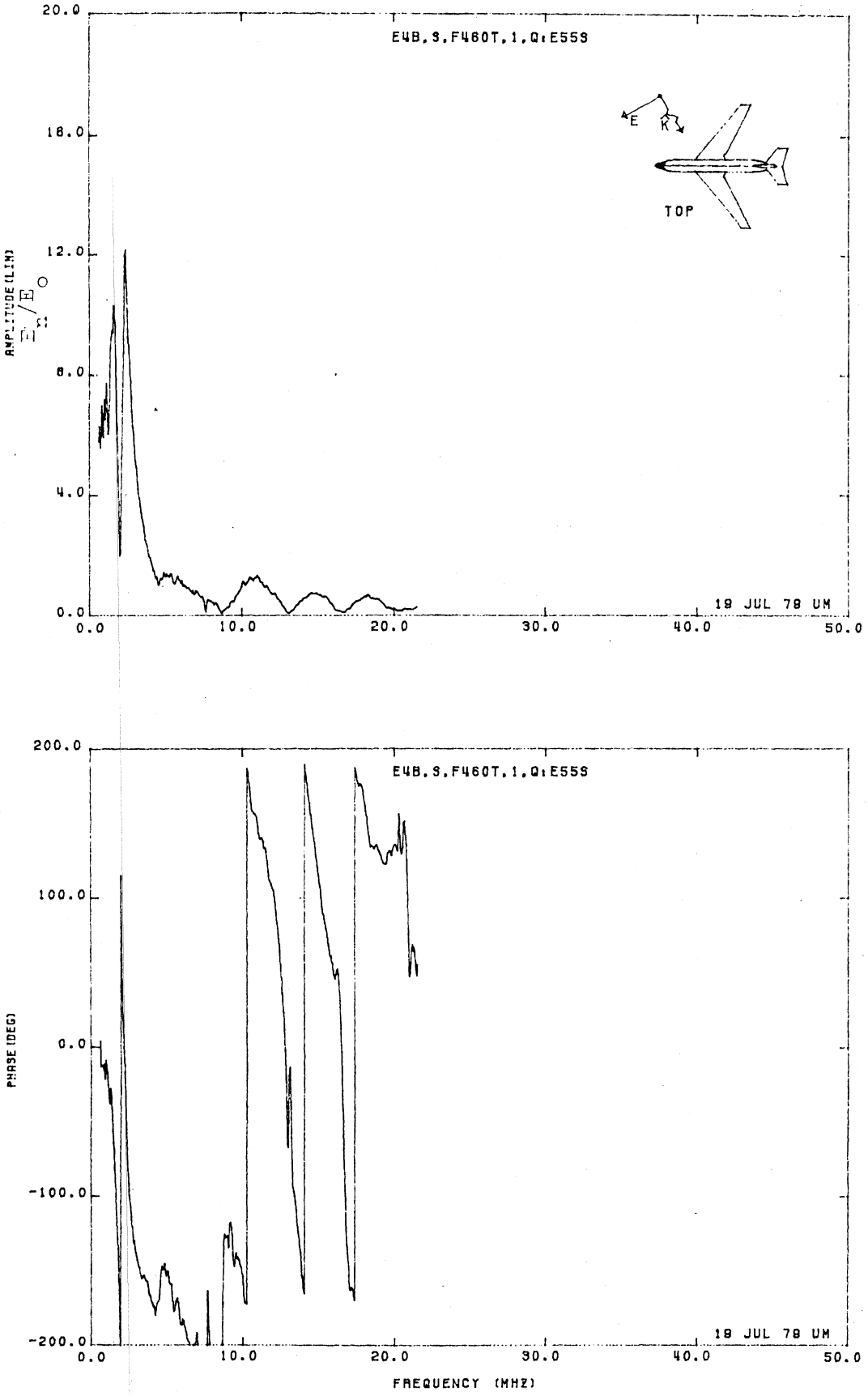

Figure 55S. Normal Electric Field at STA:F460T, Excitation 1, 1/200 Model.

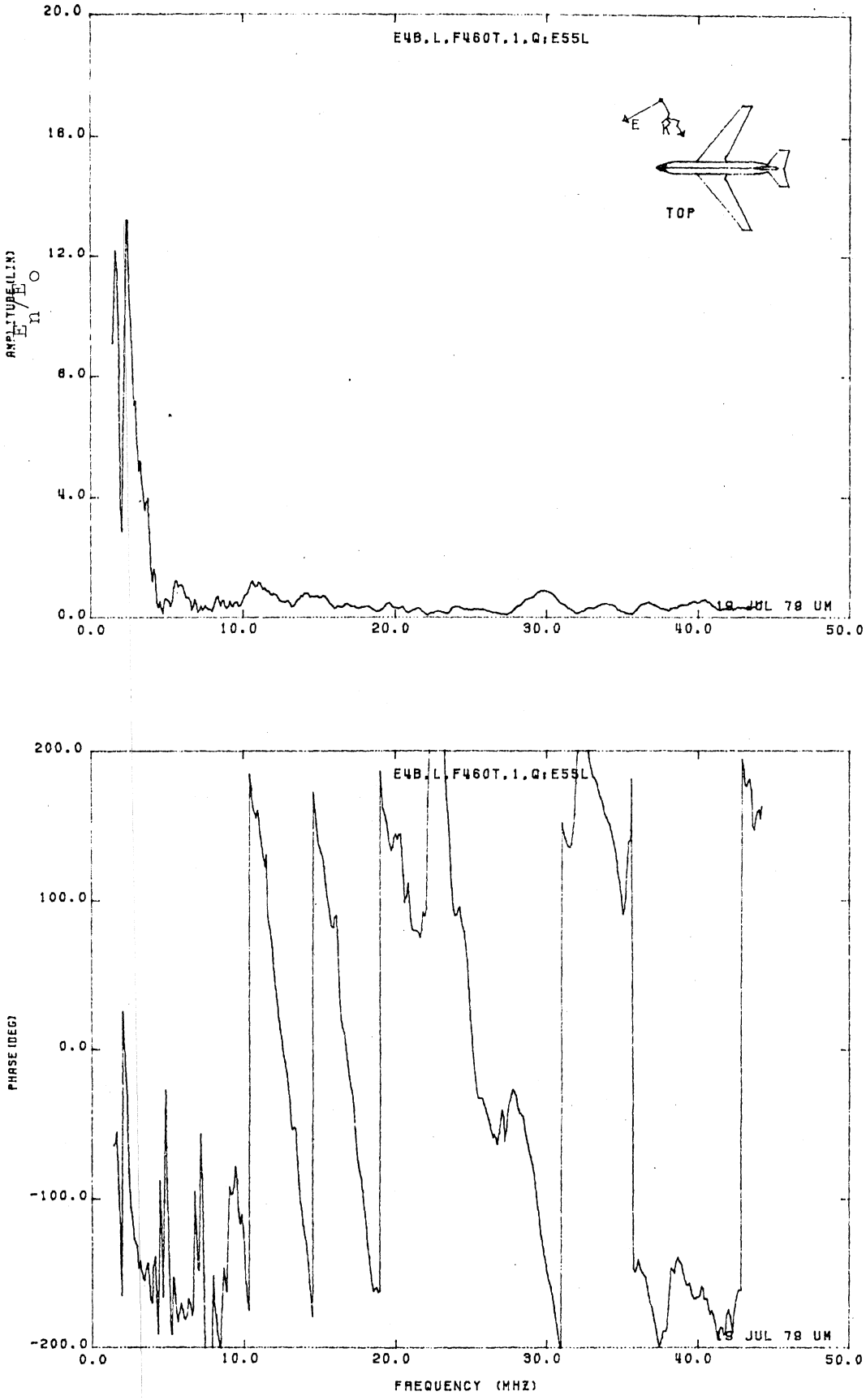

Figure 55L. Normal Electric Field at STA:F460T, Excitation 1, 1/100 Model.

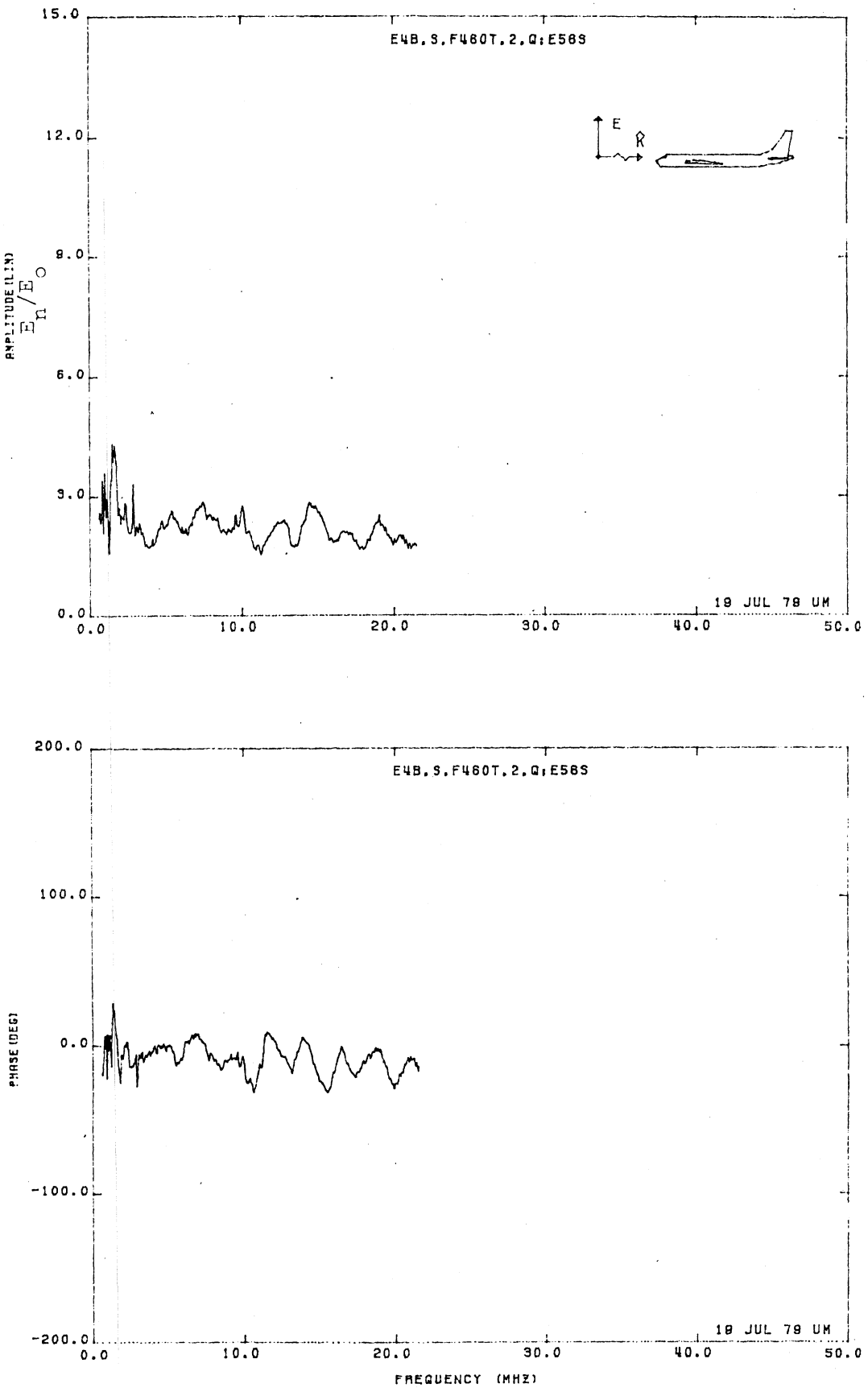

Figure 56S. Normal Electric Field at STA:F460T, Excitation 2, 1/200 Model.

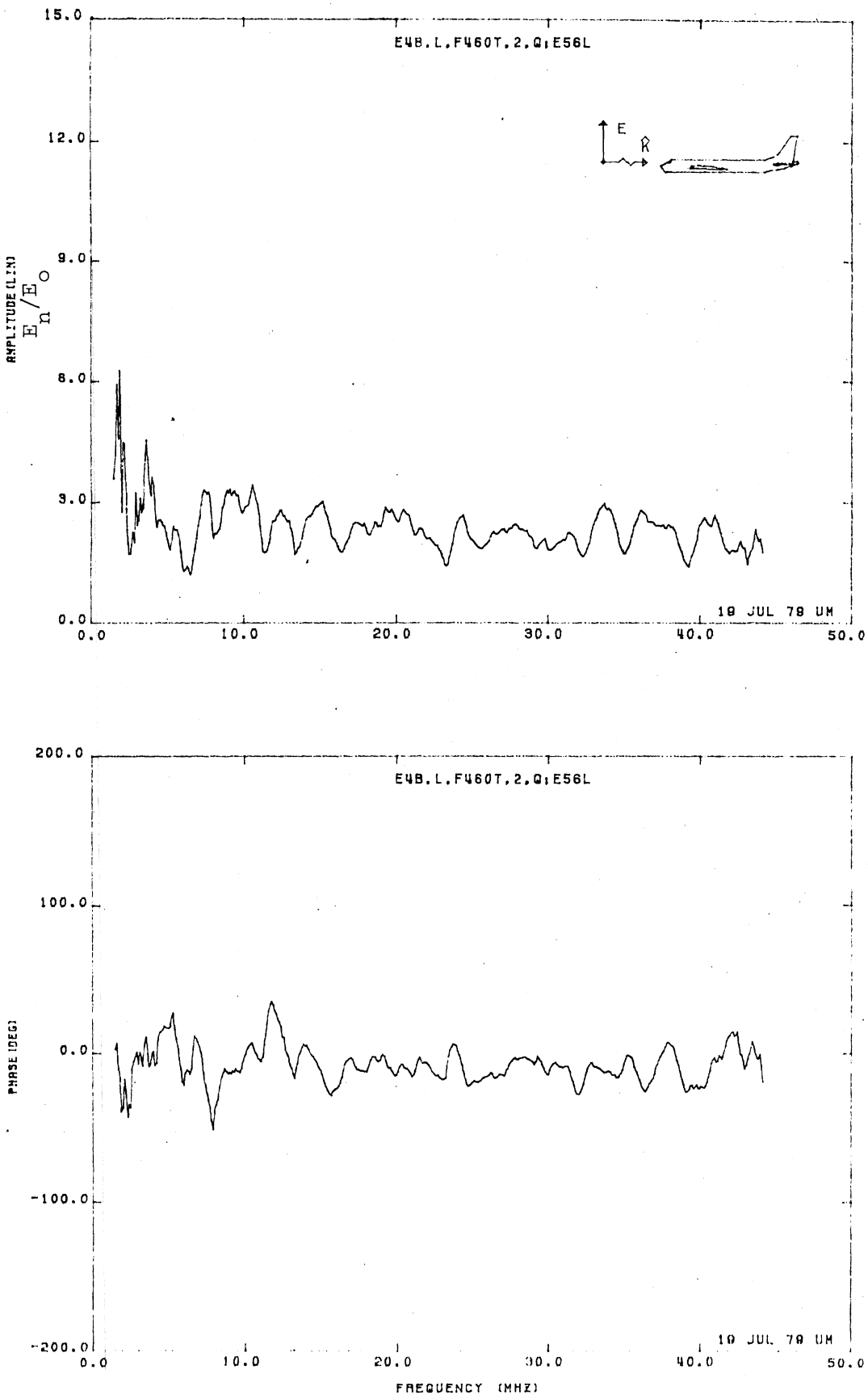

Figure 56L. Normal Electric Field at STA:F460T, Excitation 2, 1/100 Model.

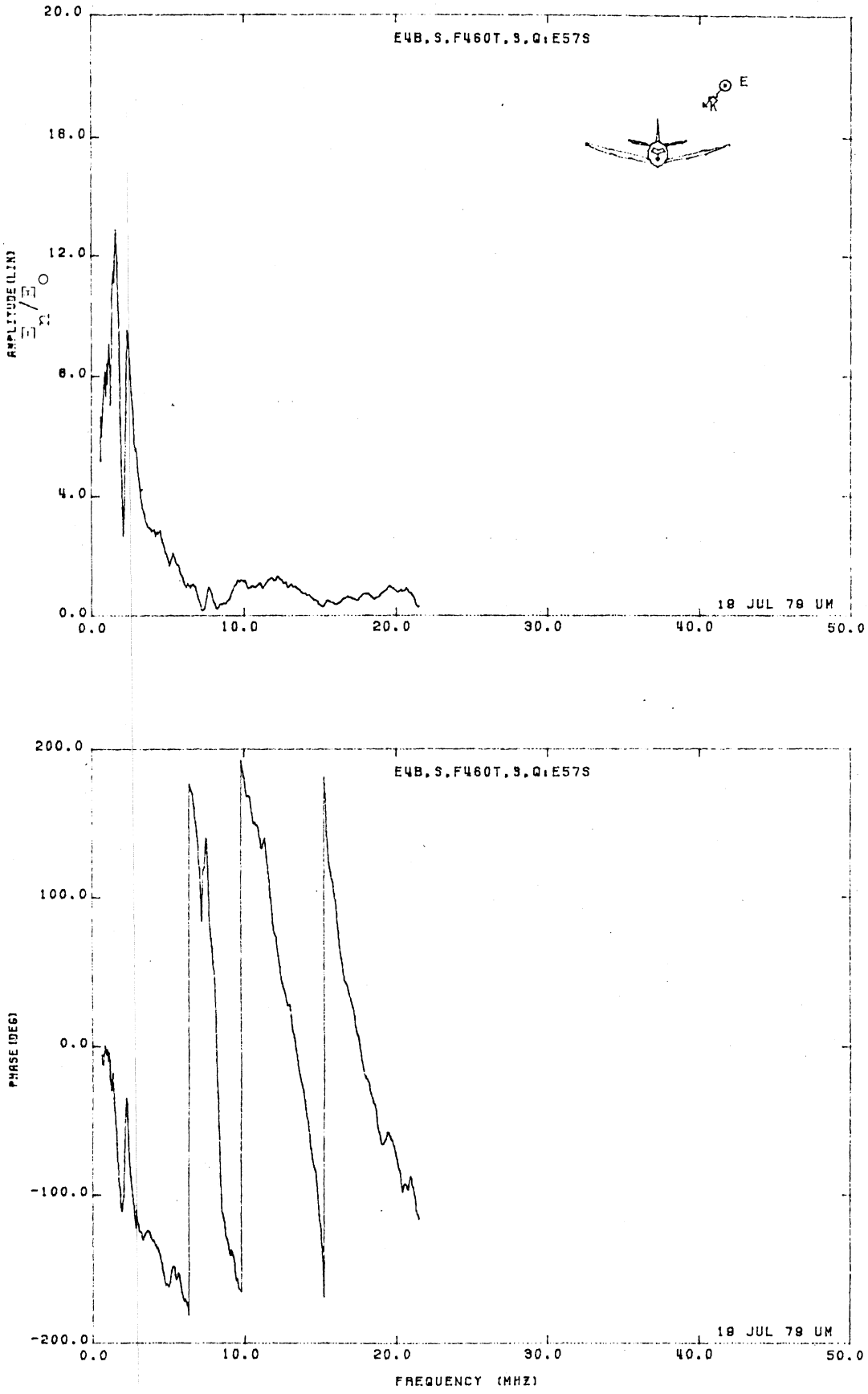

Figure 57S. Normal Electric Field at STA:F460T, Excitation 3, 1/200 Model.

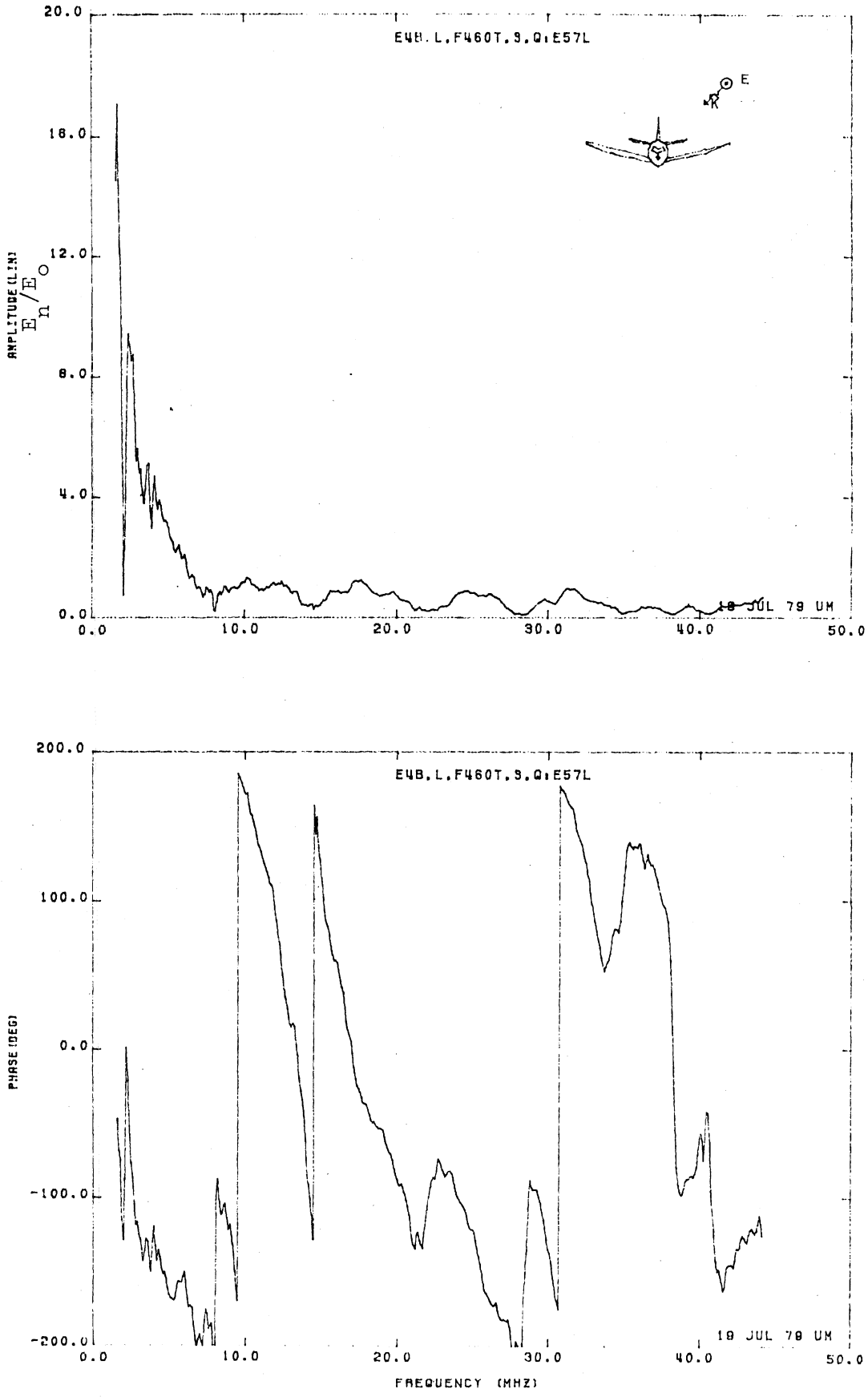

Figure 57L. Normal Electric Field at STA:F460T, Excitation 3, 1/100 Model.

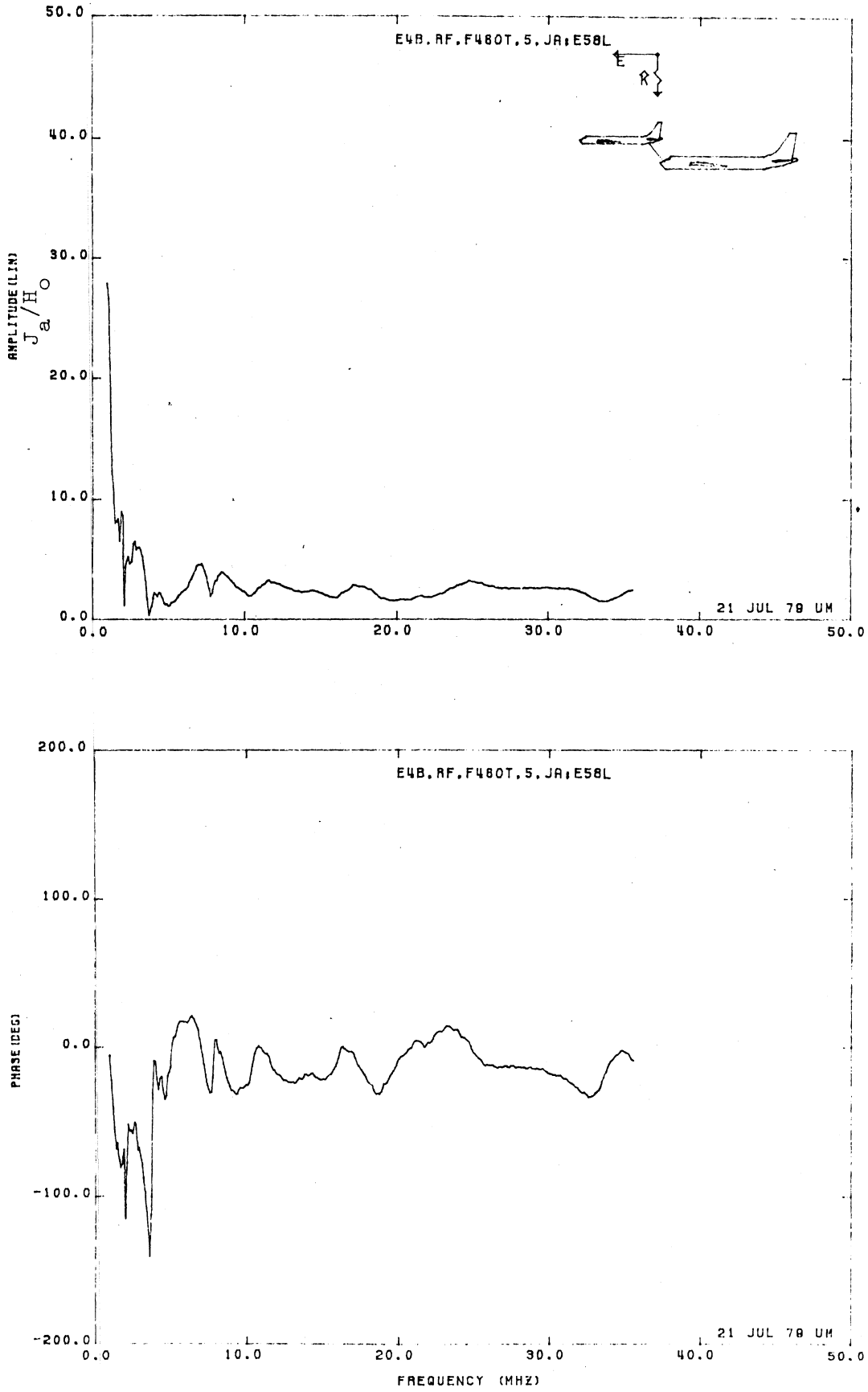

Figure 58L. Axial Current at STA: F460T, Excitation 5, 1/125 Model. (Refueling Mode)

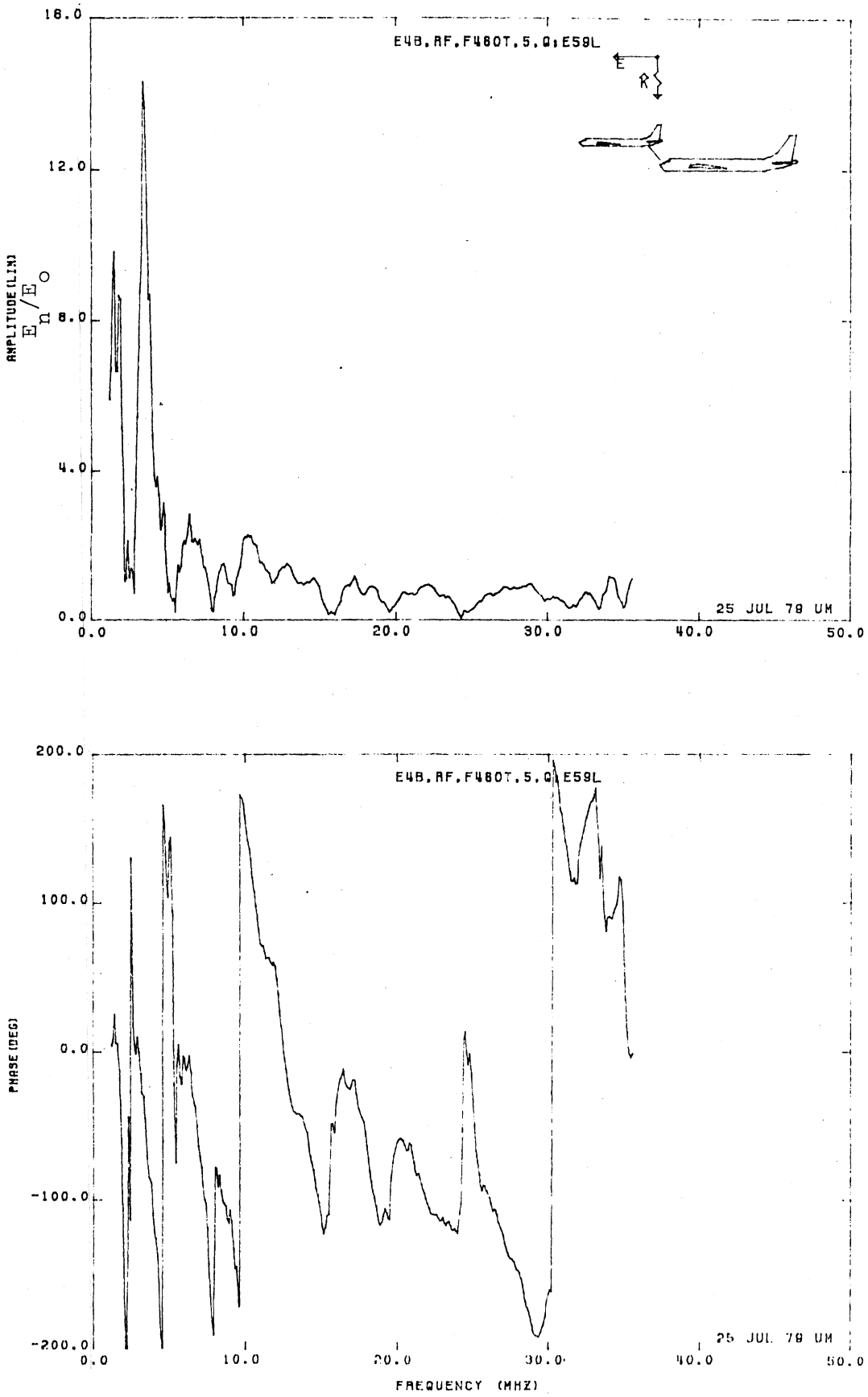

Figure 59L. Normal Electric Field at STA:F460T, Excitation 5, 1/125 Model. (Refueling Mode)

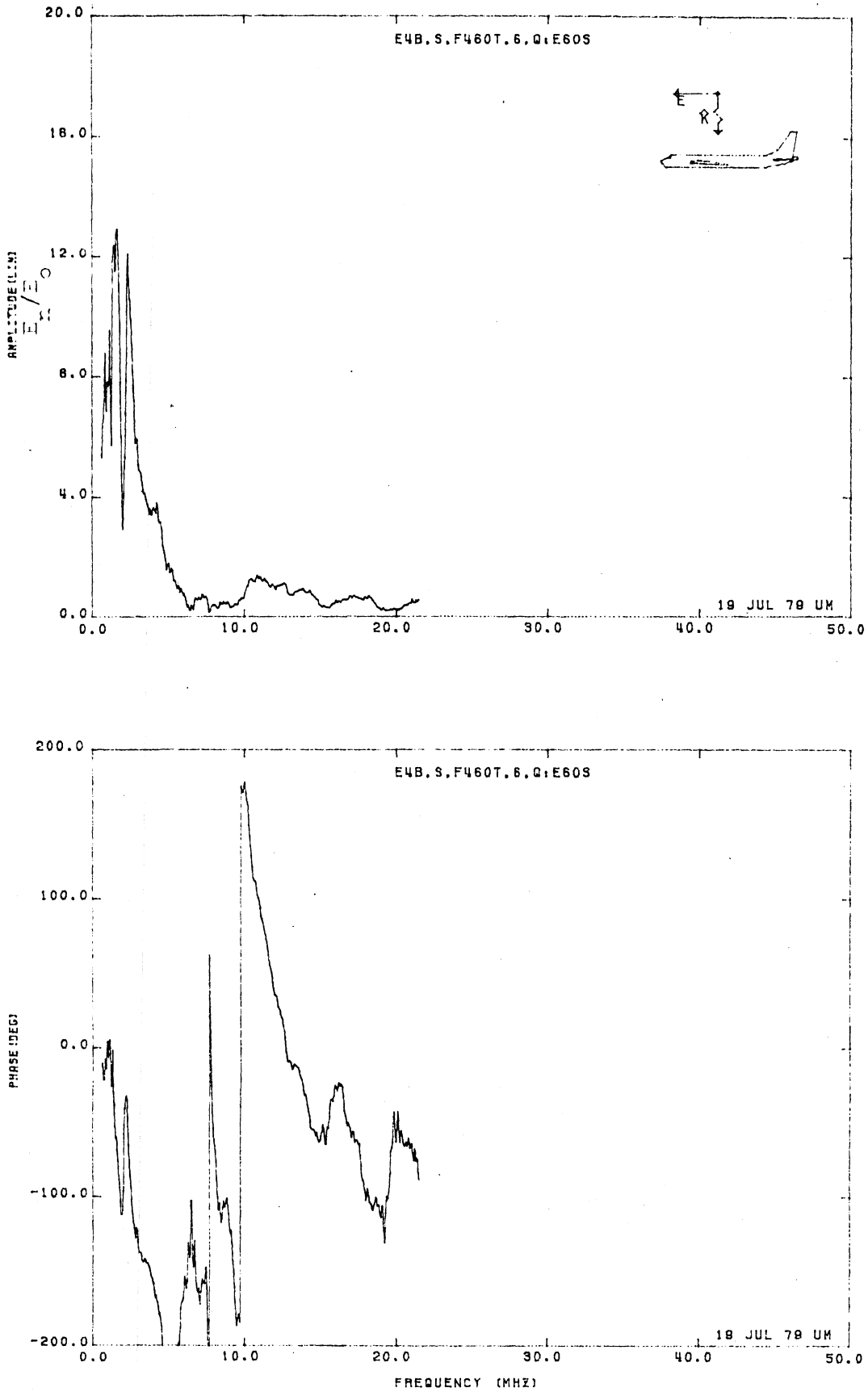

Figure 60S. Normal Electric Field at STA:F460T, Excitation 6, 1/200 Model.

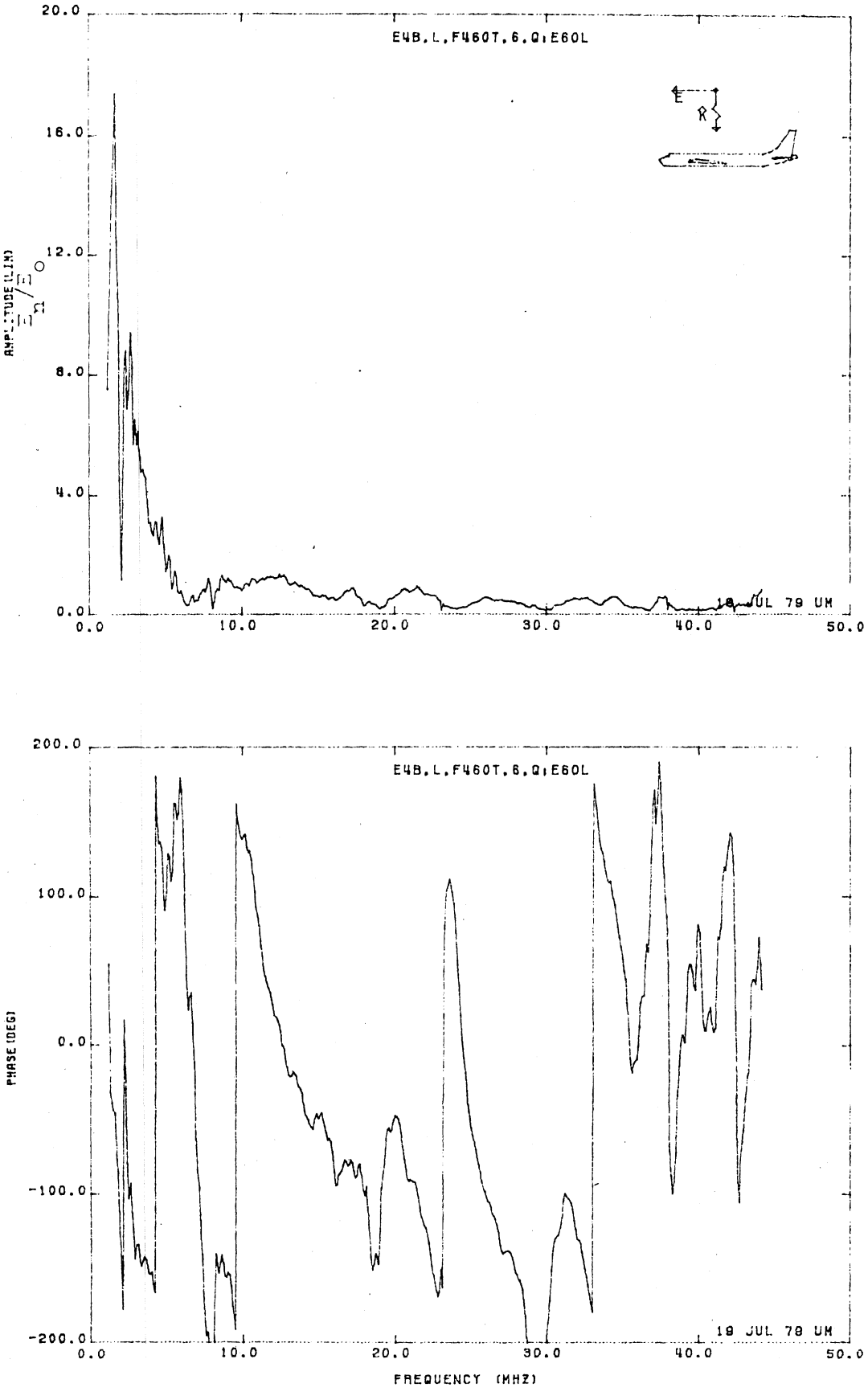

Figure 60L. Normal Electric Field at STA:F460T, Excitation 6, 1/100 Model.

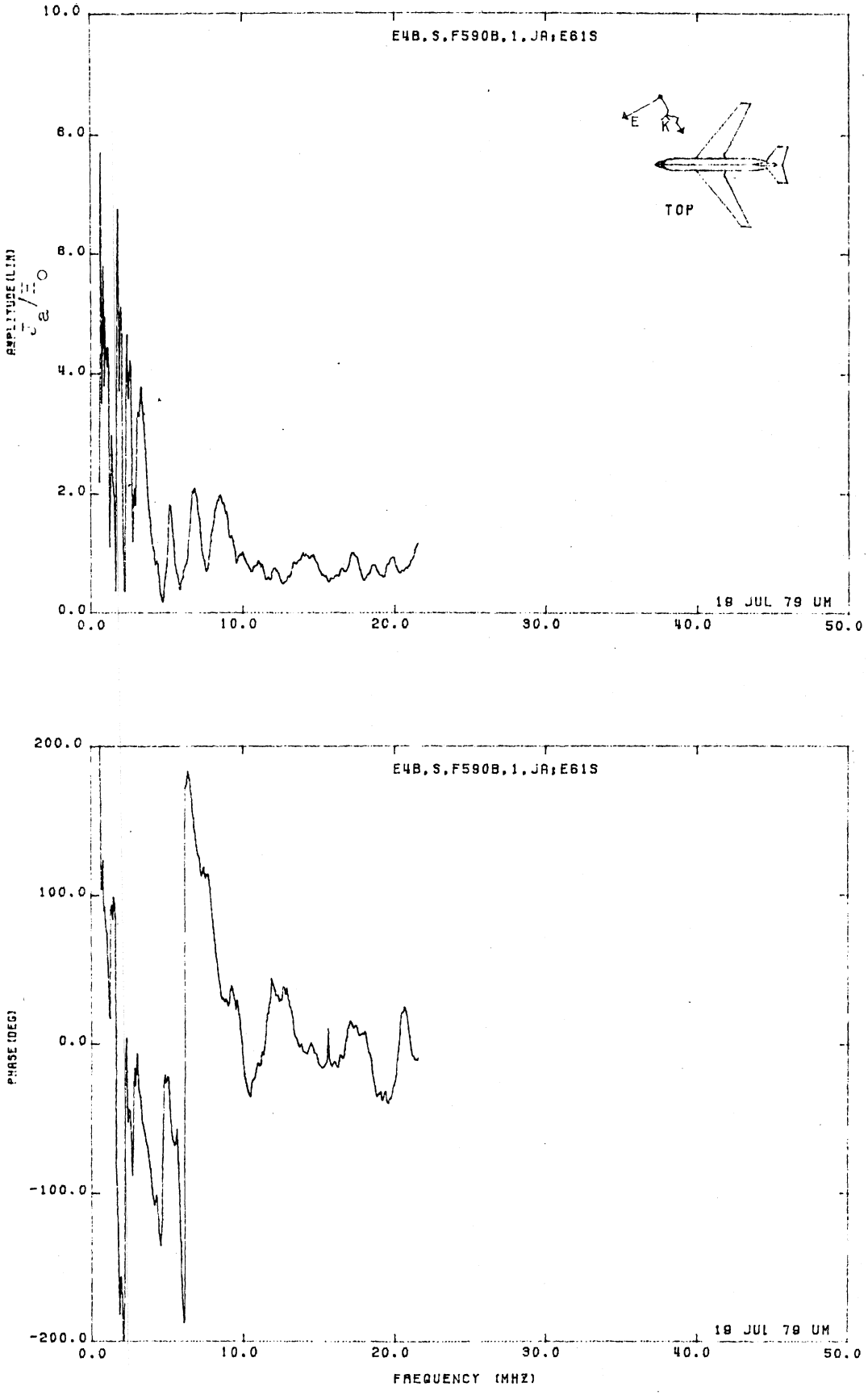

Figure 61S. Axial Current at STA:F590B, Excitation 1, 1/200 Model.

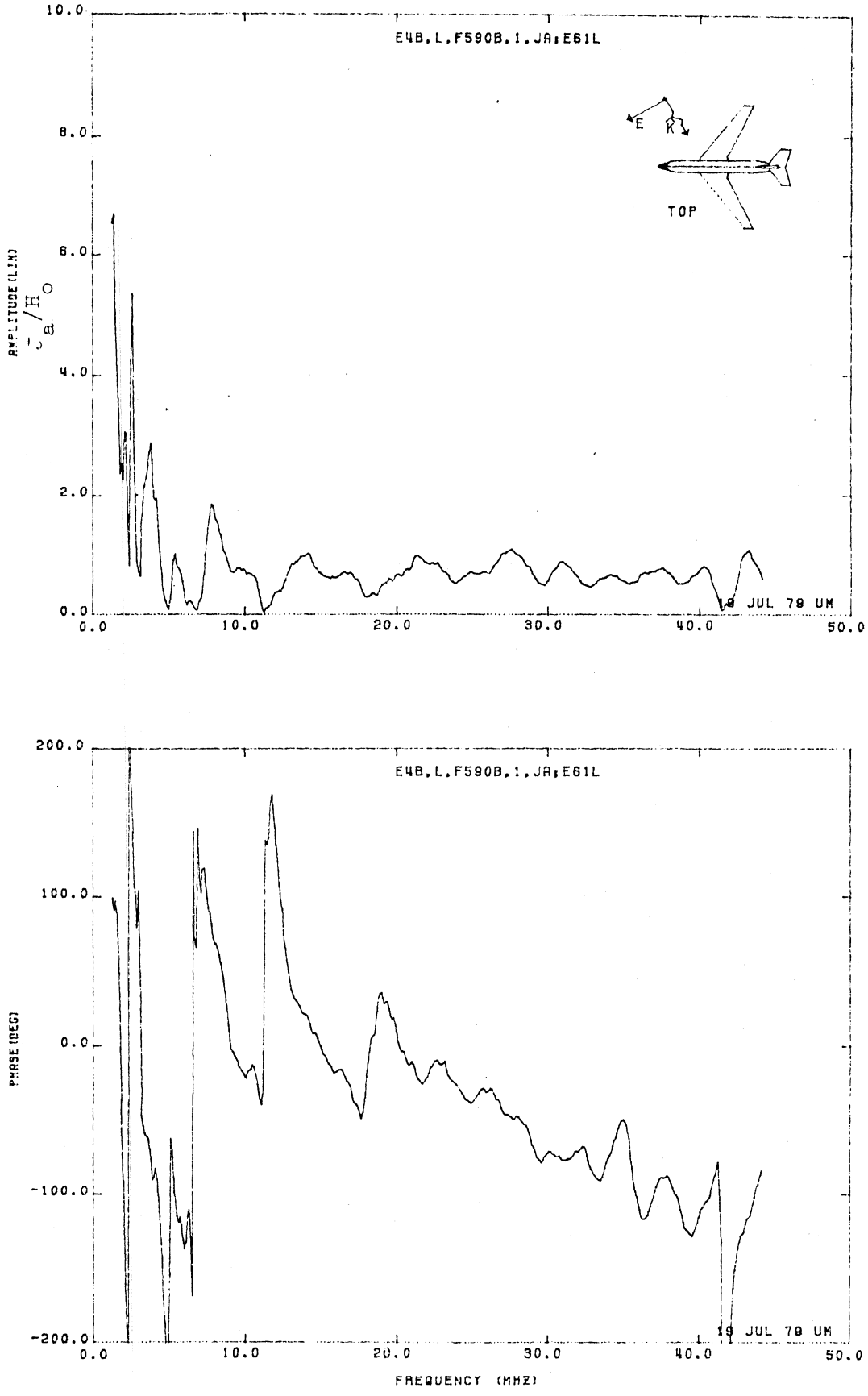

Figure 61L. Axial Current at STA:F590B, Excitation 1, 1/100 Model.

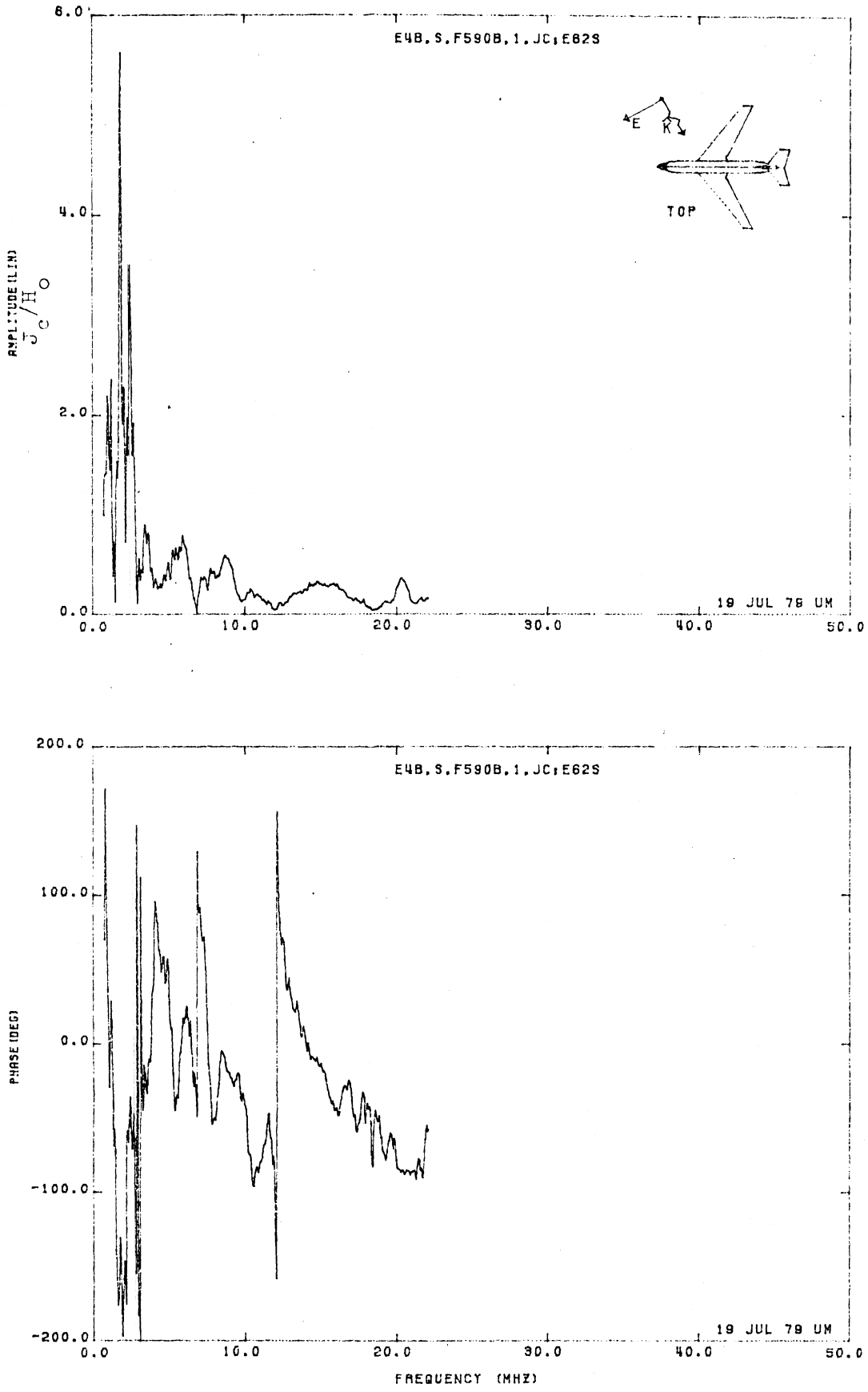

Figure 62S. Circumferential Current at STA:F590B, Excitation 1, 1/200 Model.

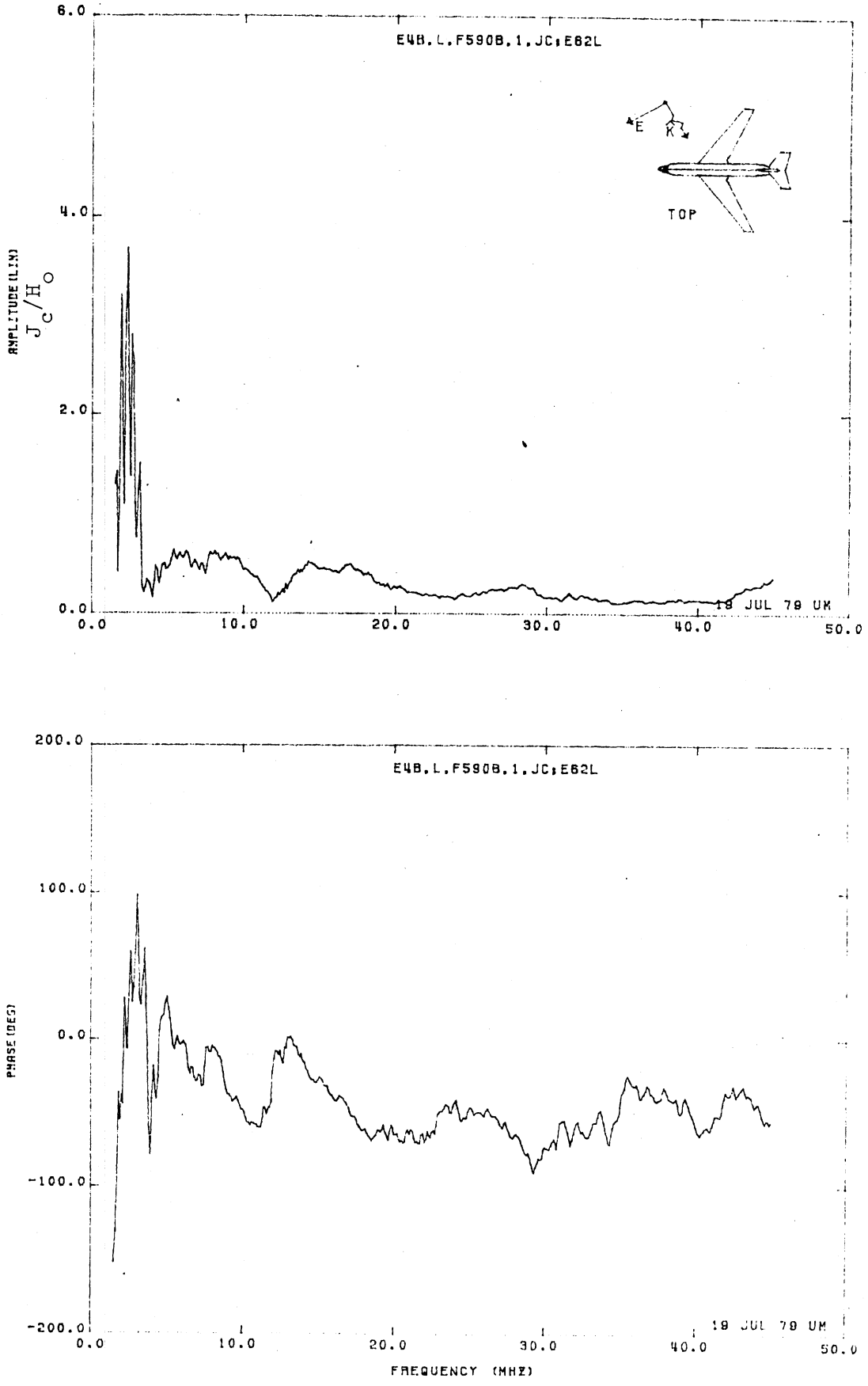

Figure 62L. Circumferential Current at STA:F590B, Excitation 1, 1/100 Model.

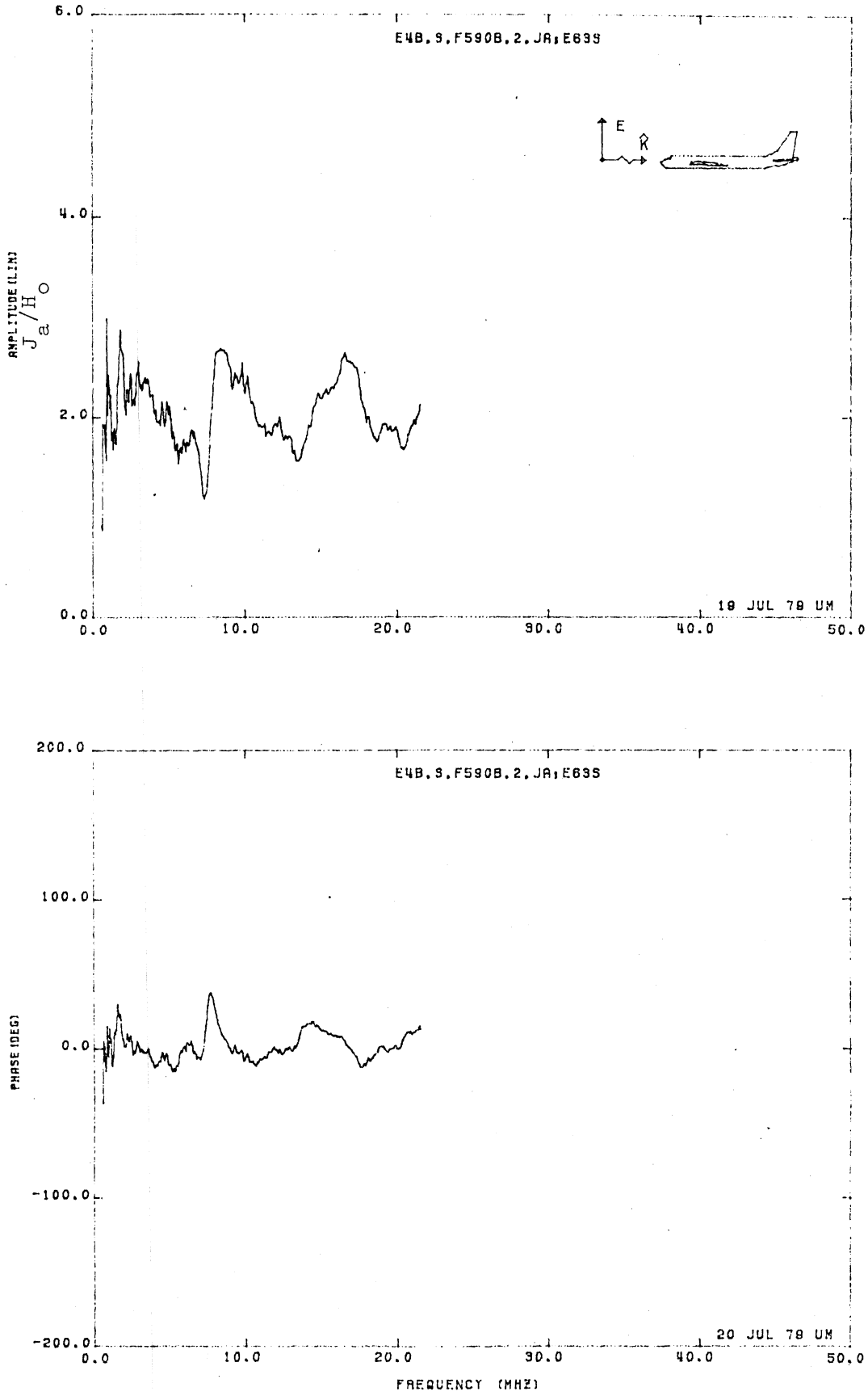

Figure 63S. Axial Current at STA:F590B, Excitation 2, 1/200 Model.

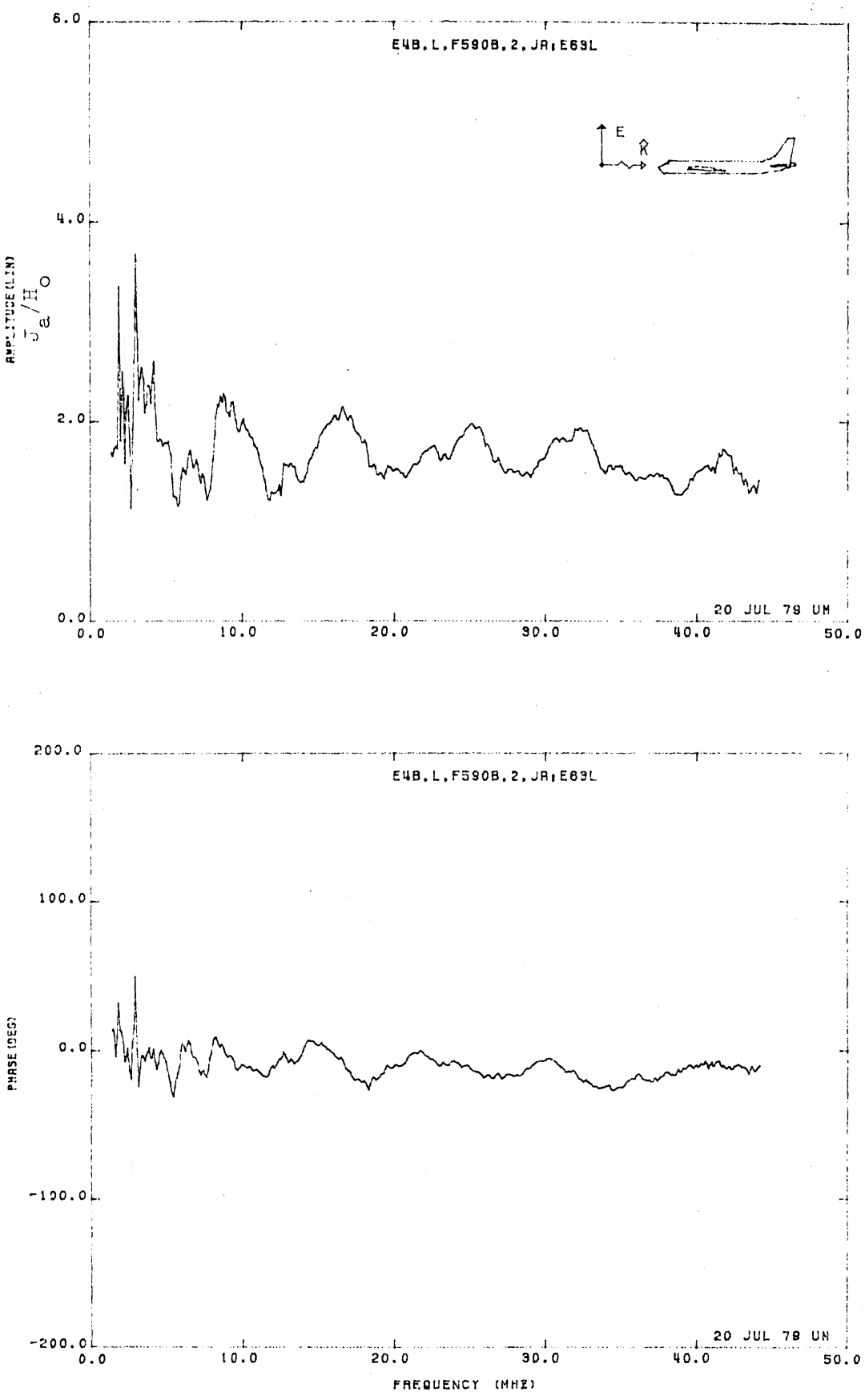

Figure 63L. Axial Current at STA:F590B, Excitation 2, 1/100 Model.

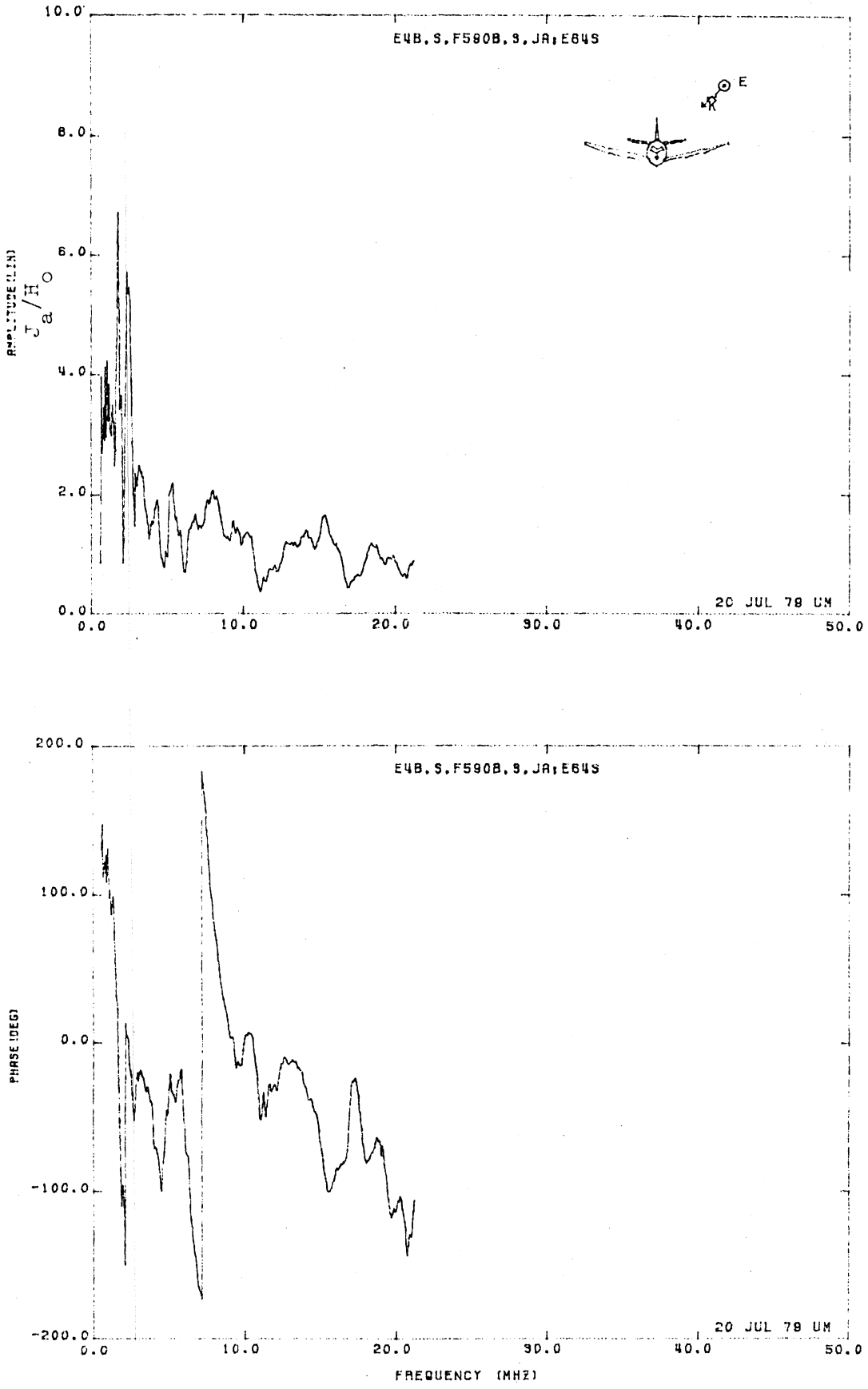

Figure 64S. Axial Current at STA:F590B, Excitation 3, 1/200 Model.

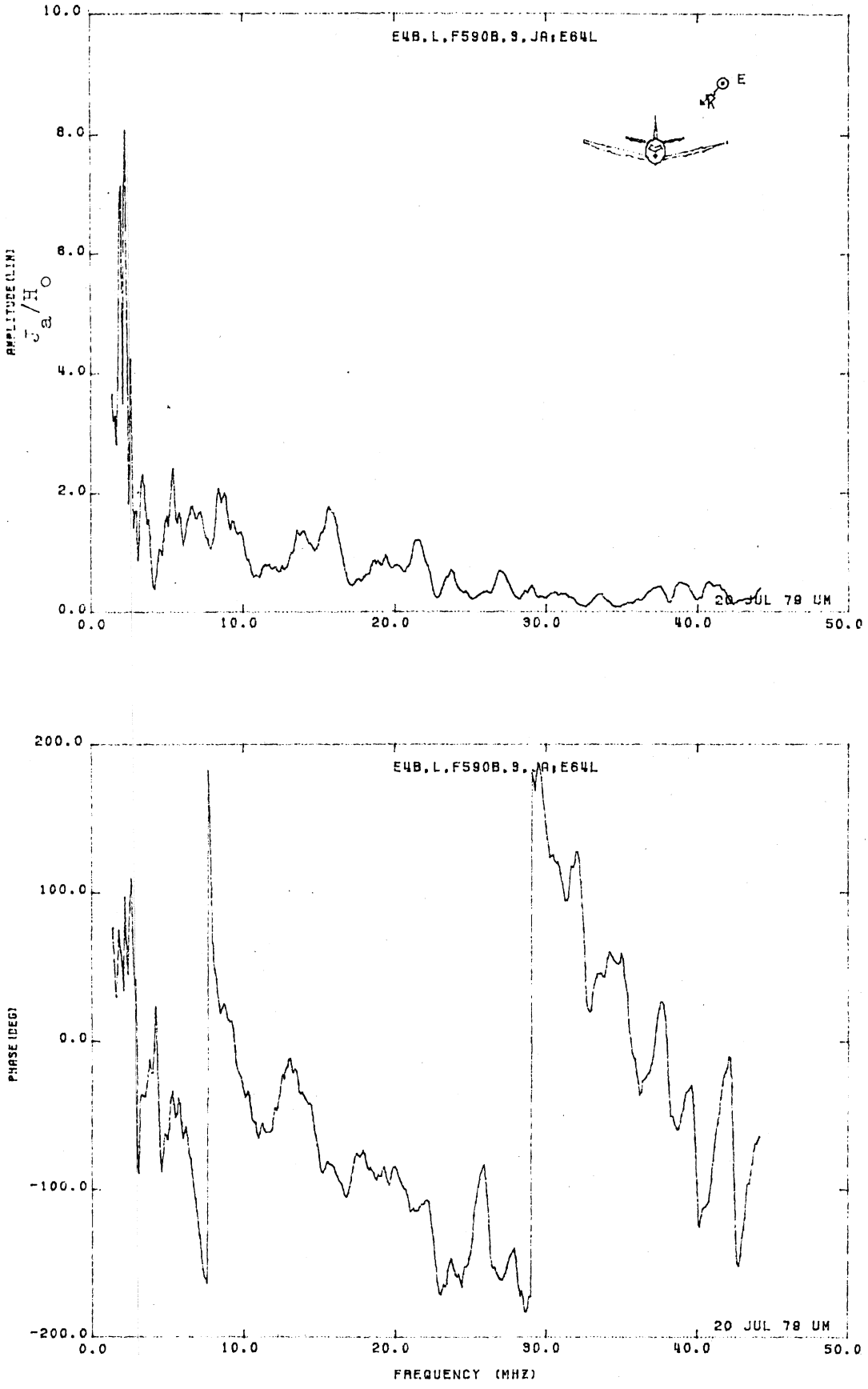

Figure 64L. Axial Current at STA:F590B, Excitation 3, 1/100 Model.

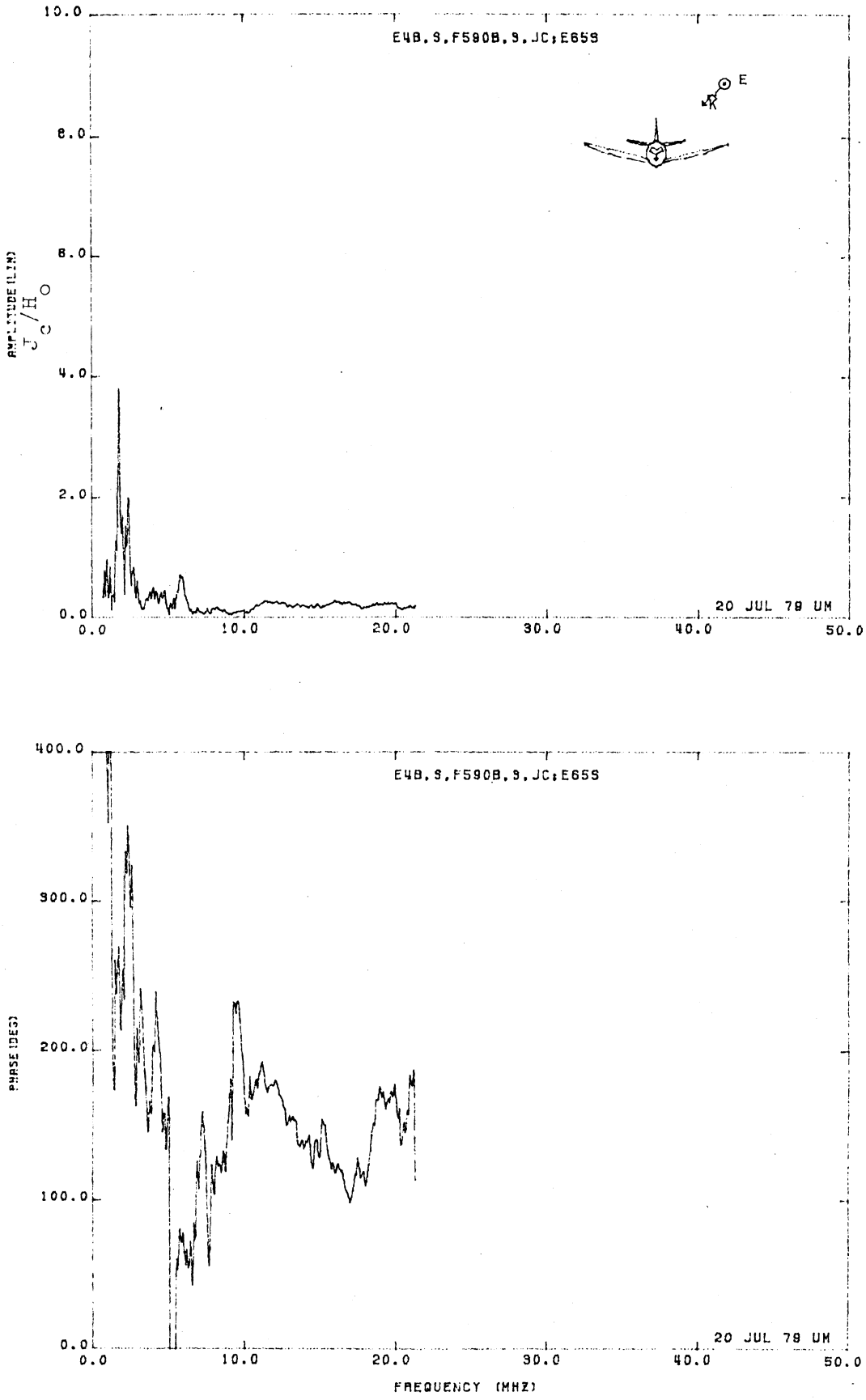

Figure 65S. Circumferential Current at STA:F590B, Excitation 3, 1/200 Model.

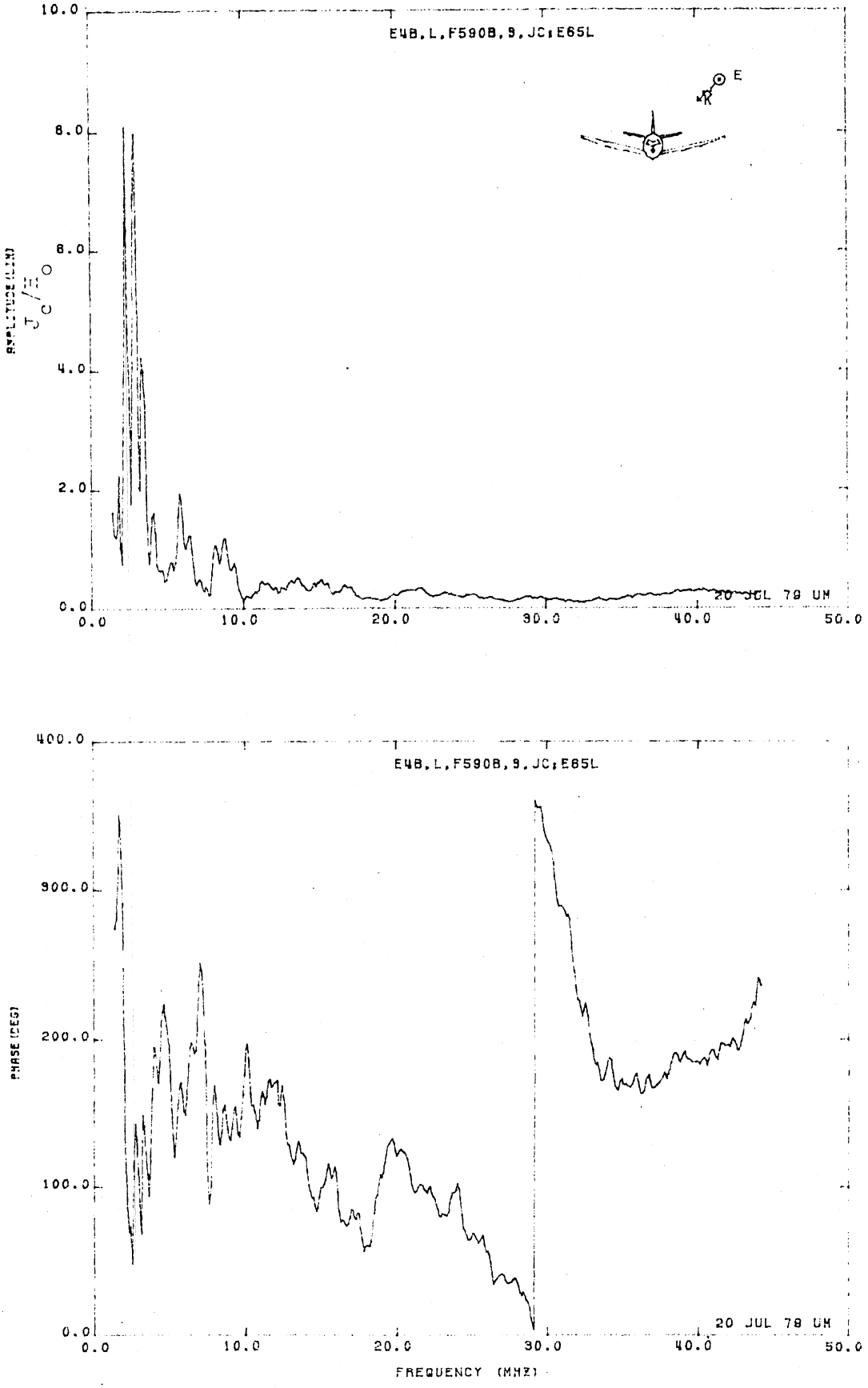

Figure 65L. Circumferential Current at STA:F590B, Excitation 3, 1/100 Model.

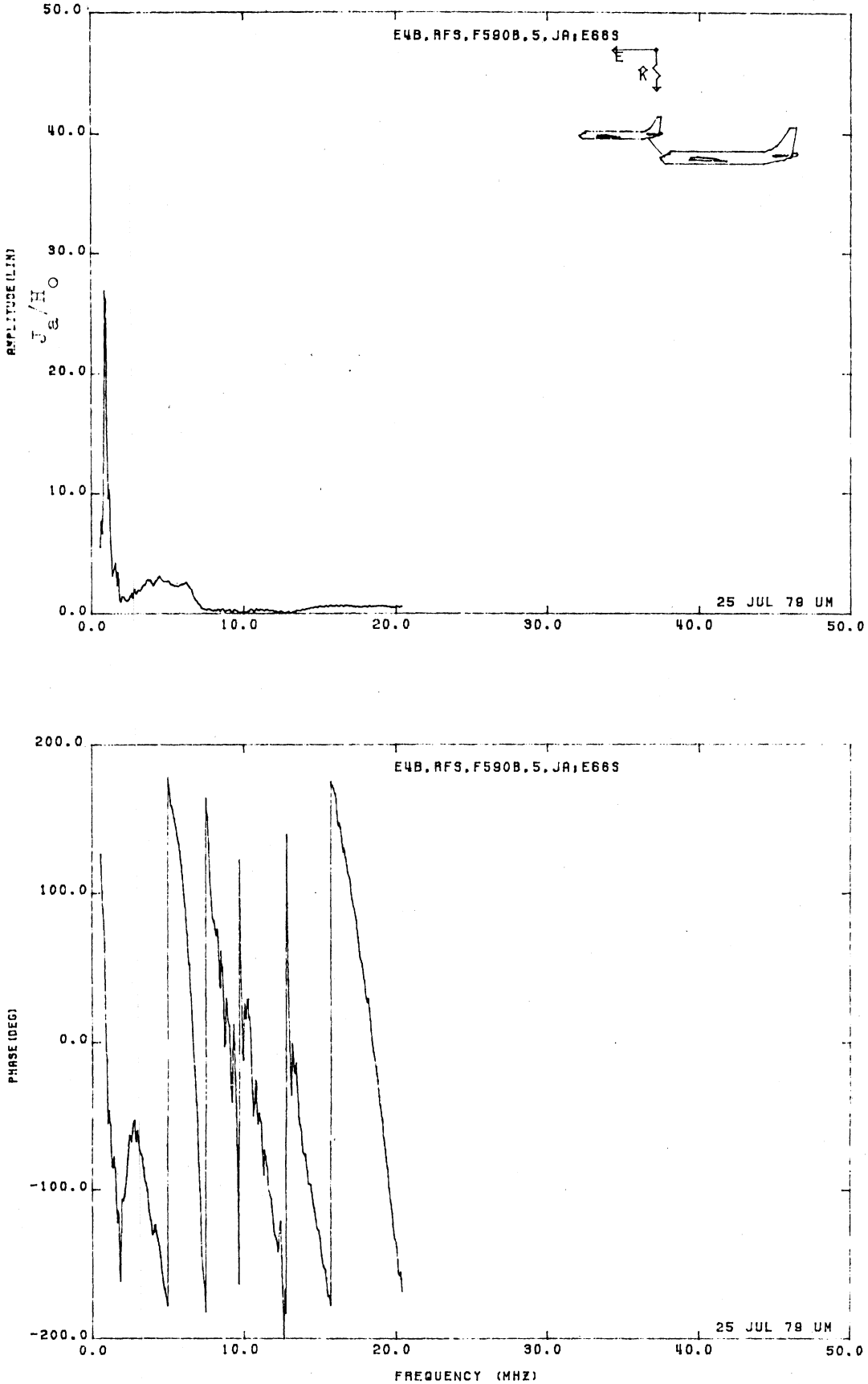

Figure 66S. Axial Current at STA:F590B, Excitation 5, 1/215 Model. (Refueling Mode)

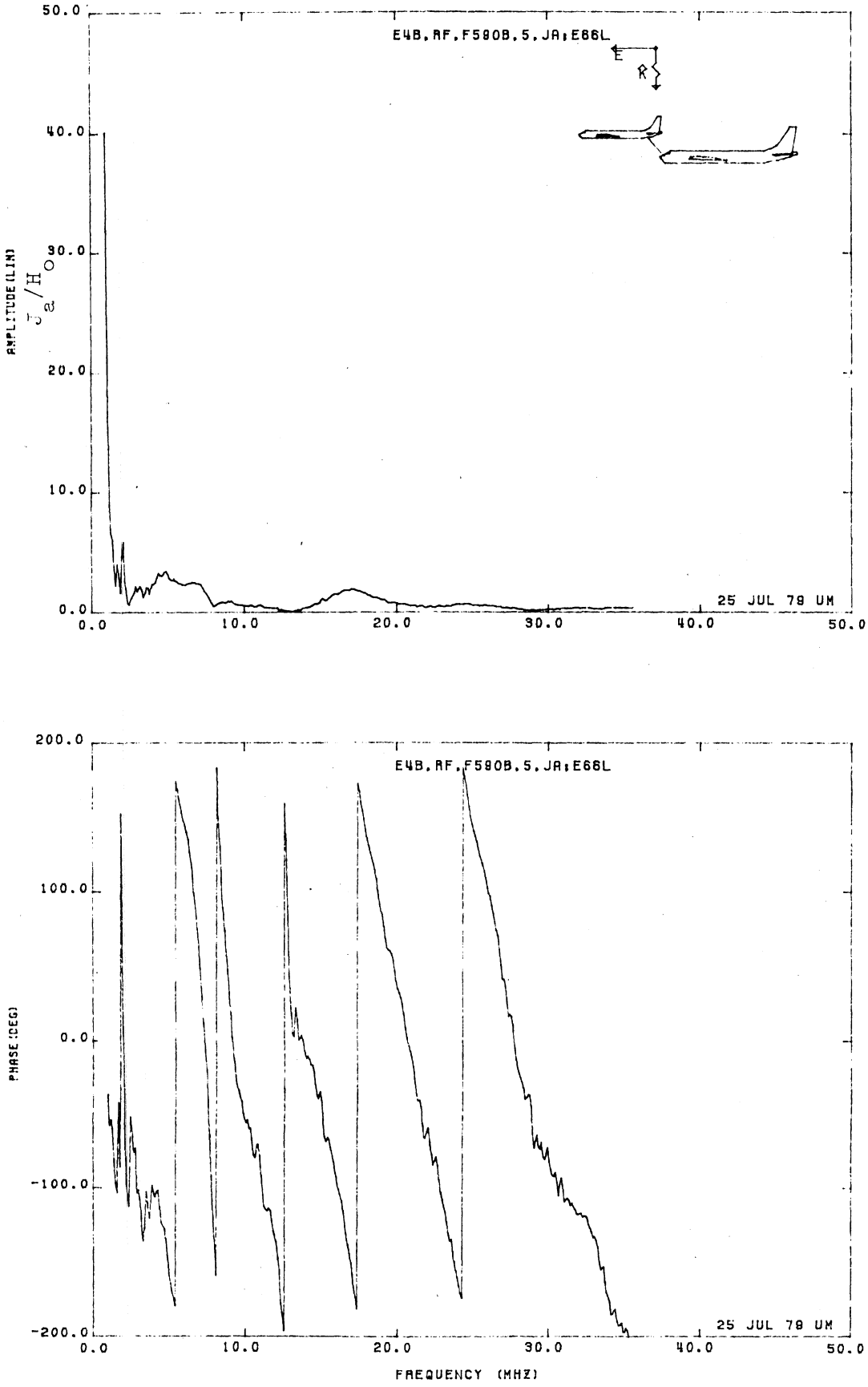

Figure 66L. Axial Current at STA:F590B, Excitation 5, 1/125 Model. (Refueling Mode)

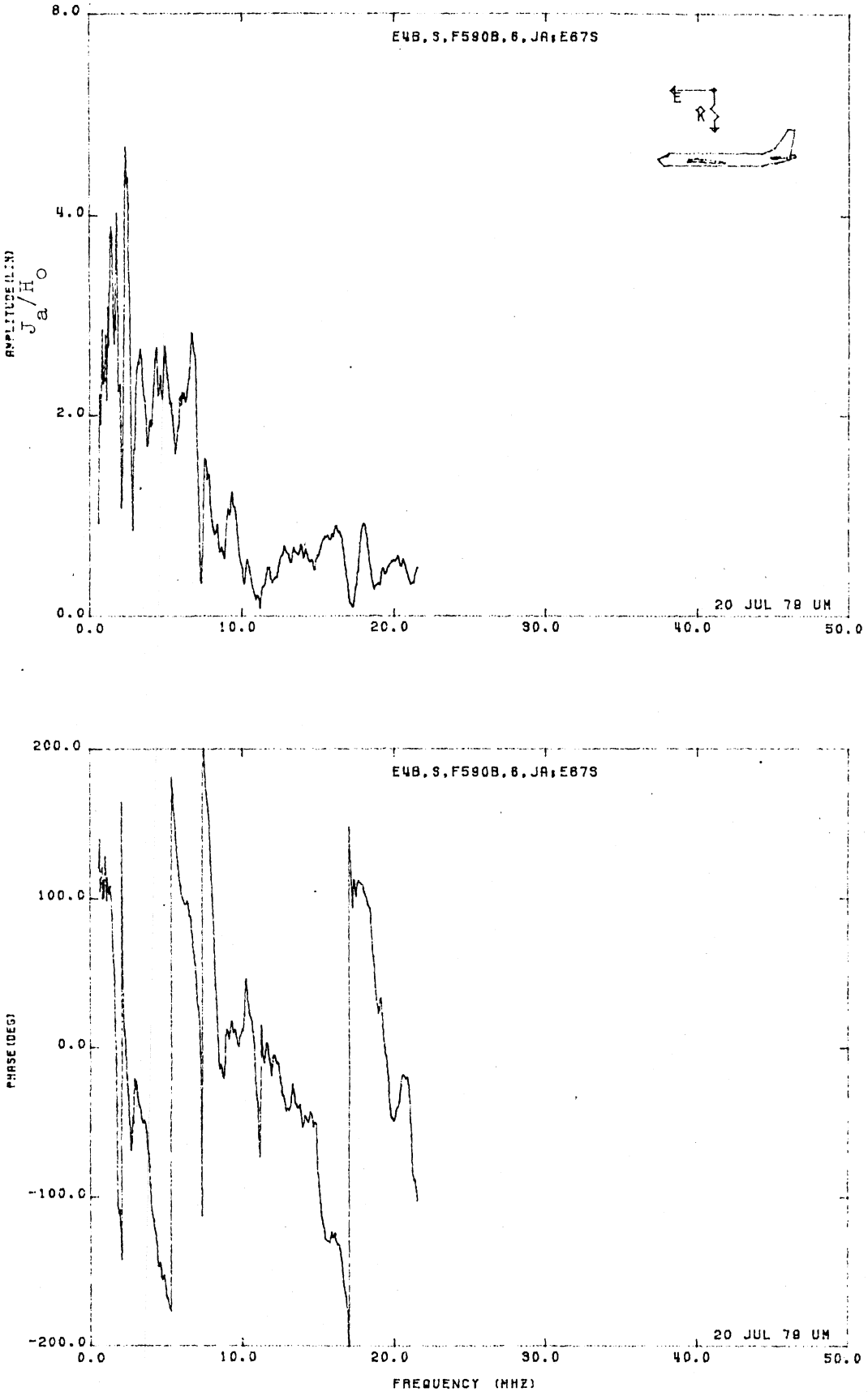

Figure 67S. Axial Current at STA:F590B, Excitation 6, 1/200 Model.

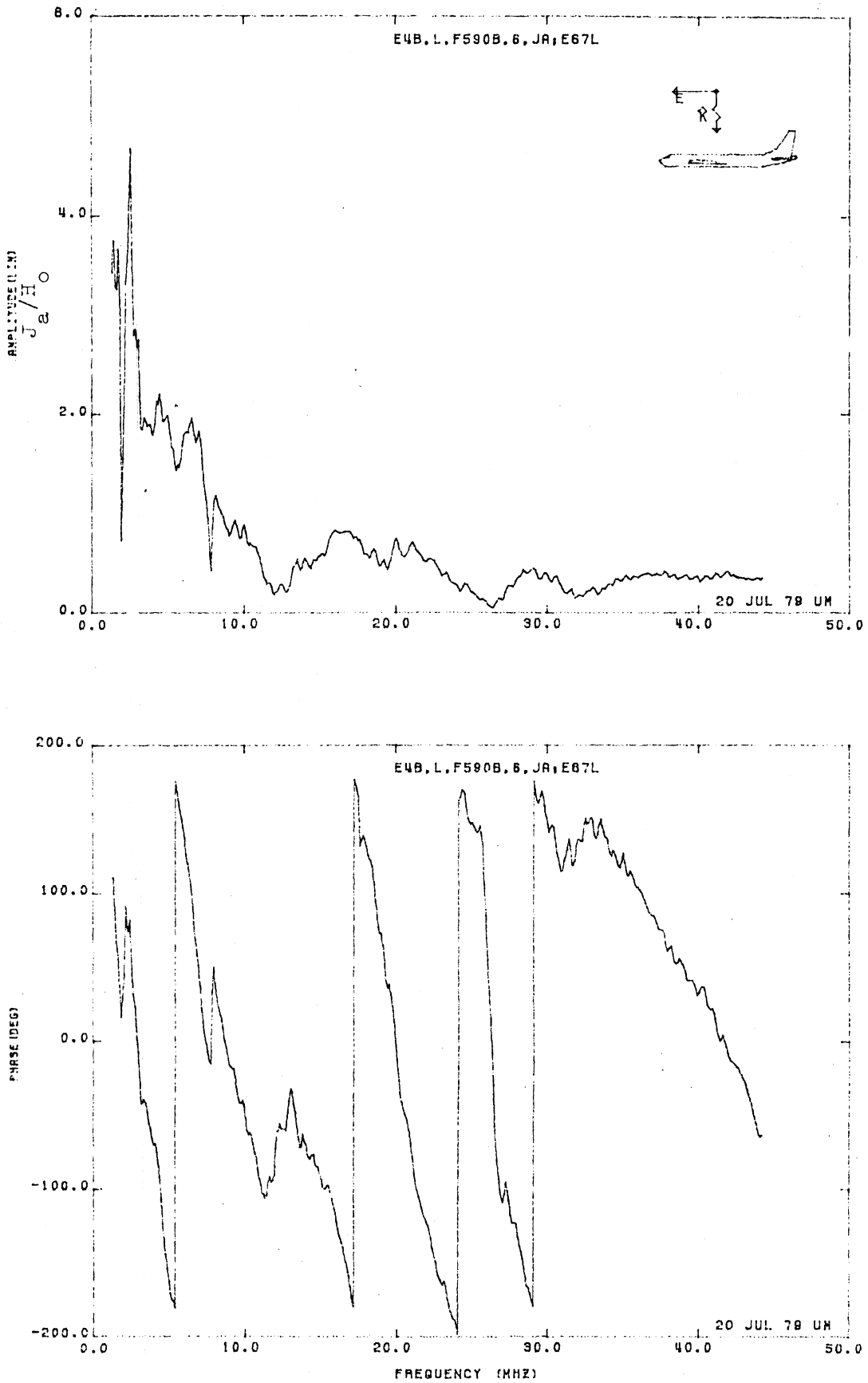

Figure 67L. Axial Current at STA:F590B, Excitation 6, 1/100 Model.

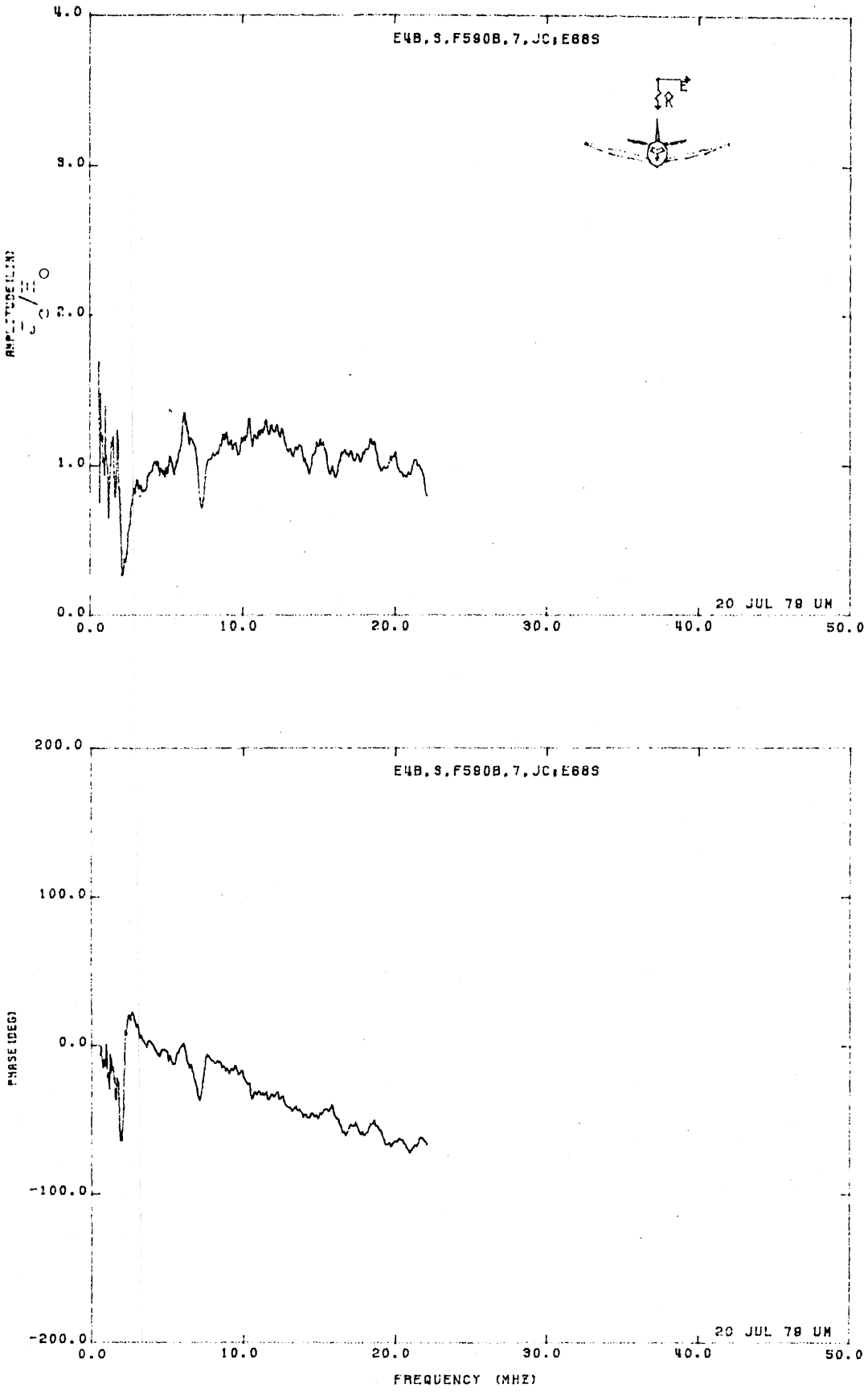

Figure 68S. Circumferential Current at STA:F590B, Excitation 7, 1/200 Model.

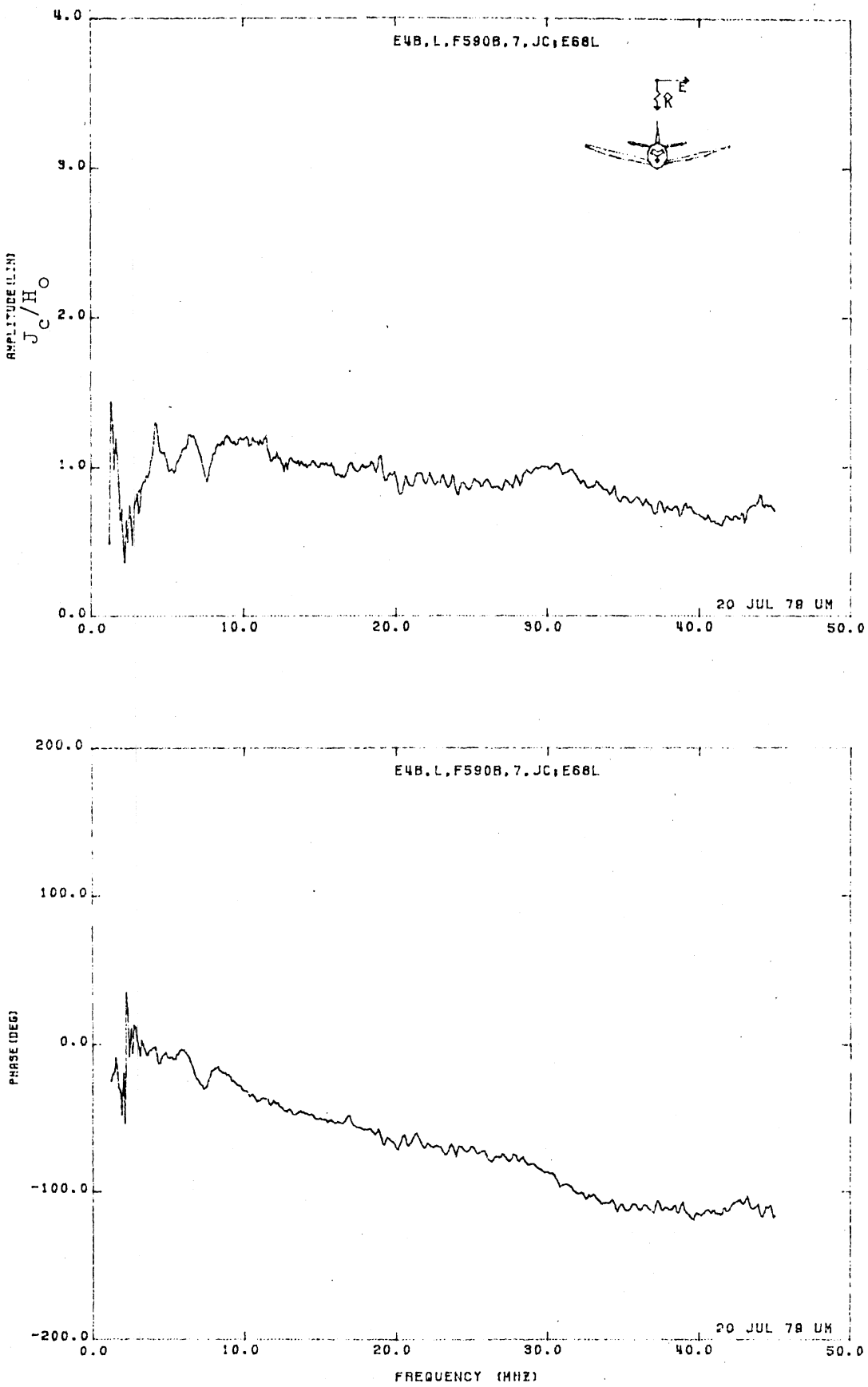

Figure 68L. Circumferential Current at STA:F590B, Excitation 7, 1/100 Model.

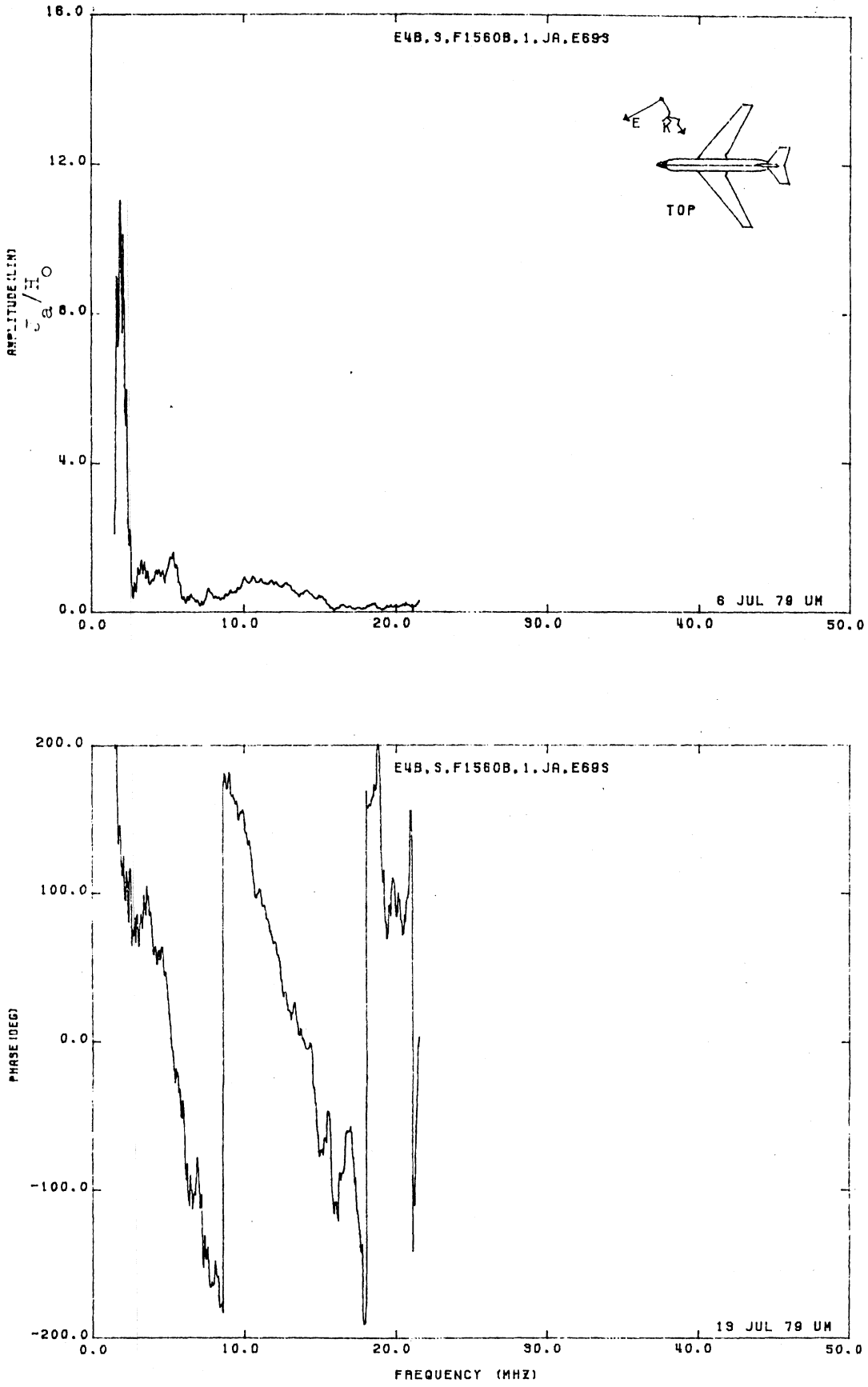

Figure 69S. Axial Current at STA:F1560B, Excitation 1, 1/200 Model.

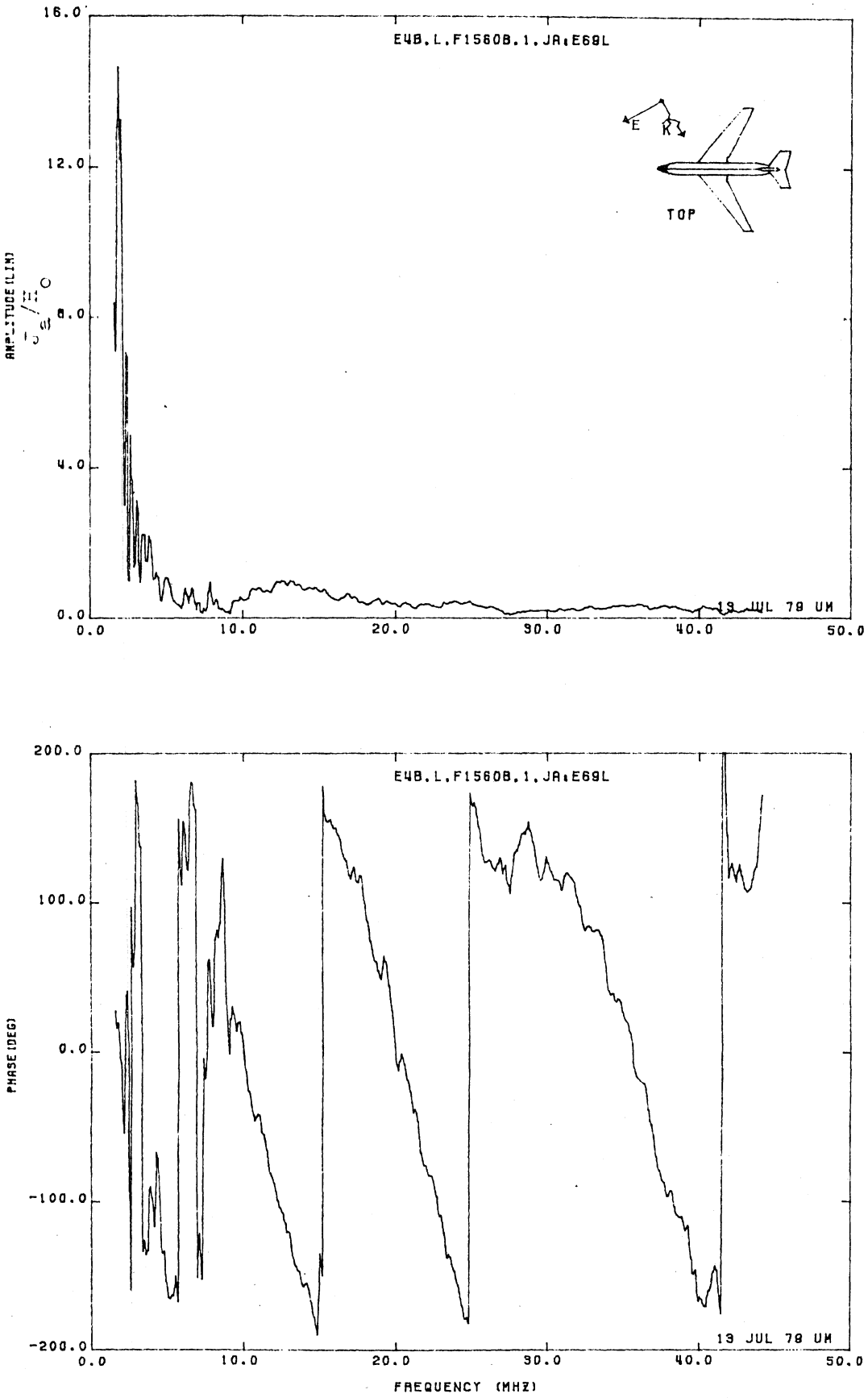

Figure 69L. Axial Current at STA:F1560B, Excitation 1, 1/100 Model.

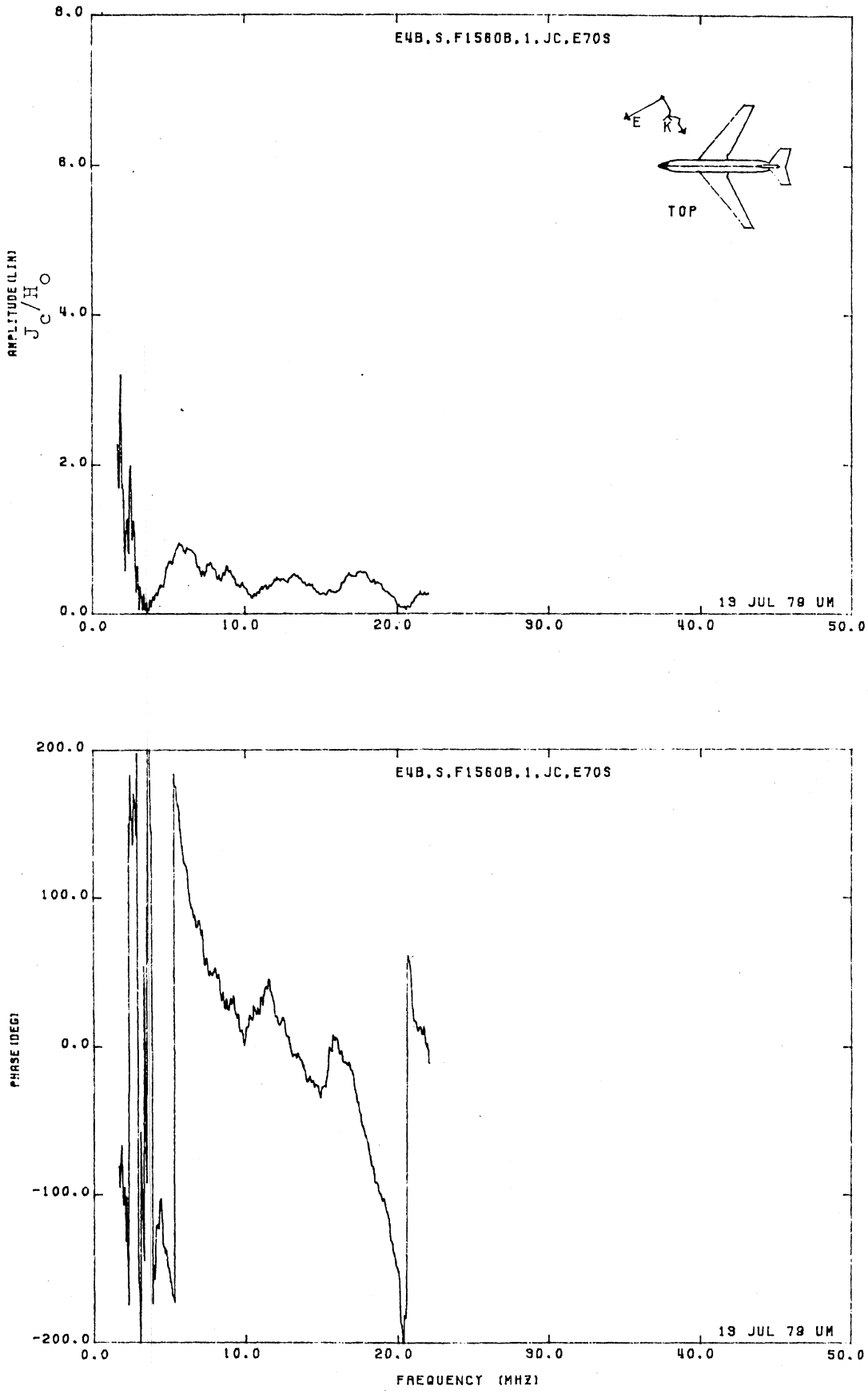

Figure 70S. Circumferential Current at STA:F1560B, Excitation 1, 1/200 Model.

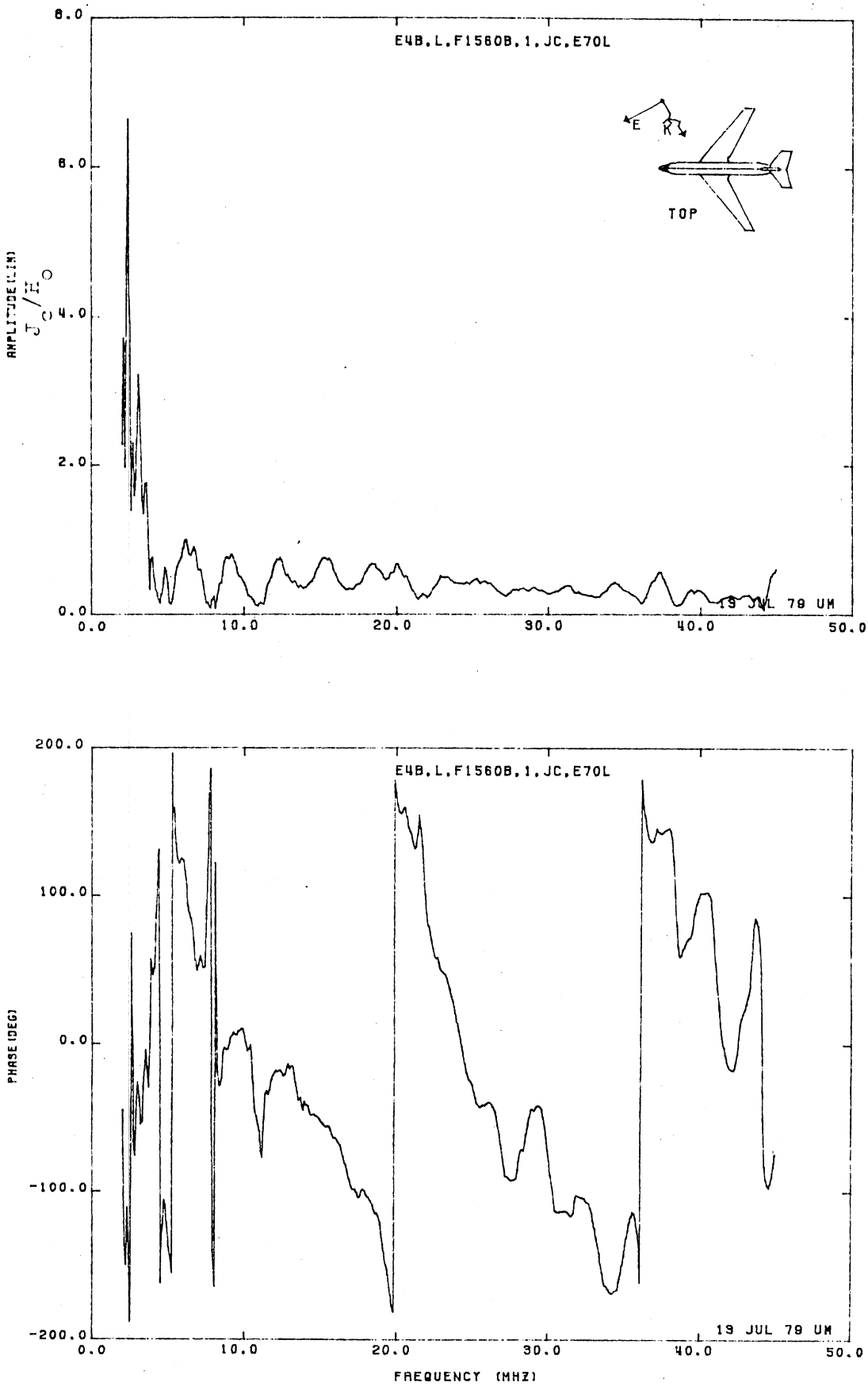

Figure 70L. Circumferential Current at STA:F1560B, Excitation 1, 1/100 Model.

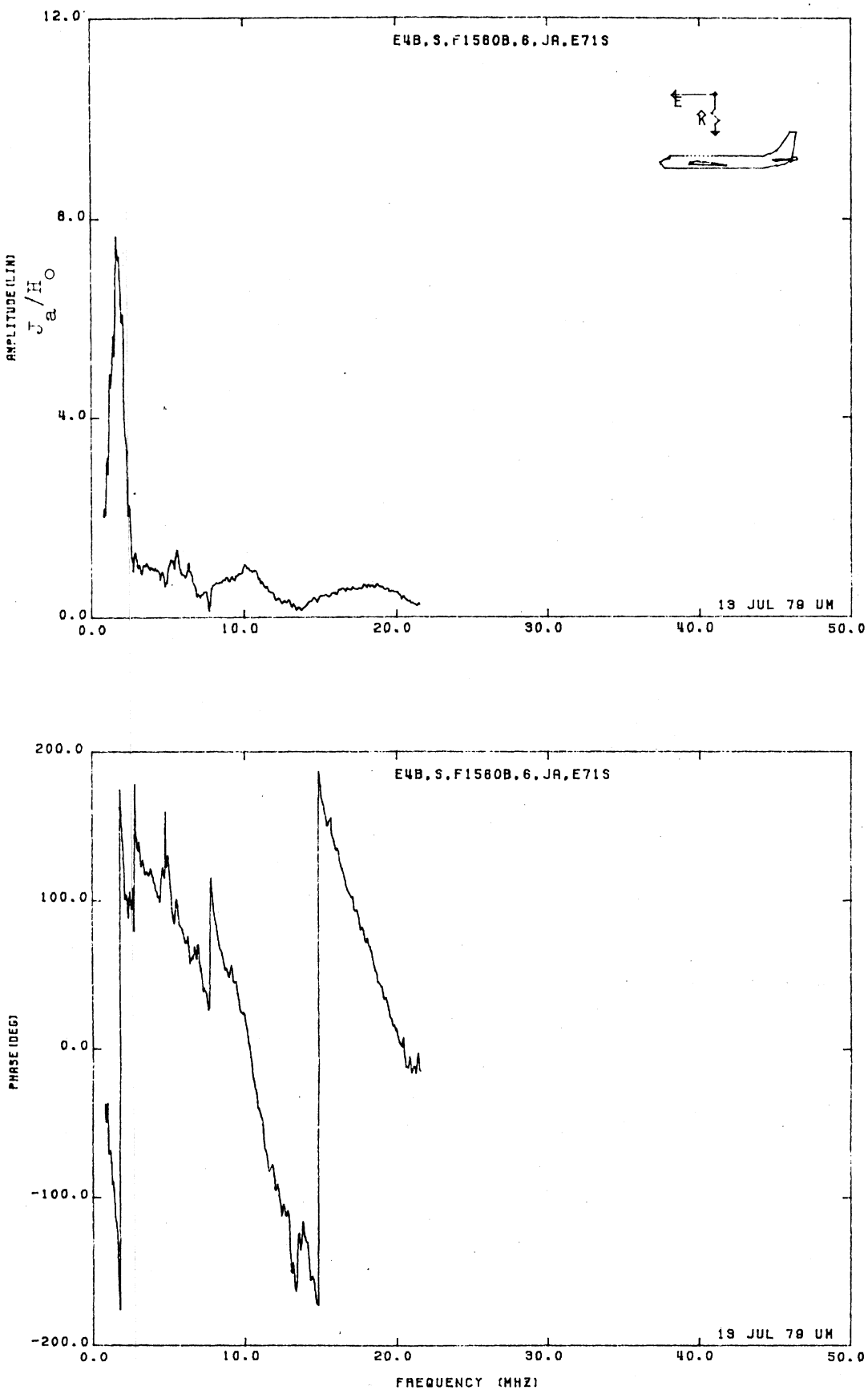

Figure 71S. Axial Current at STA:F1560B, Excitation 6, 1/200 Model.

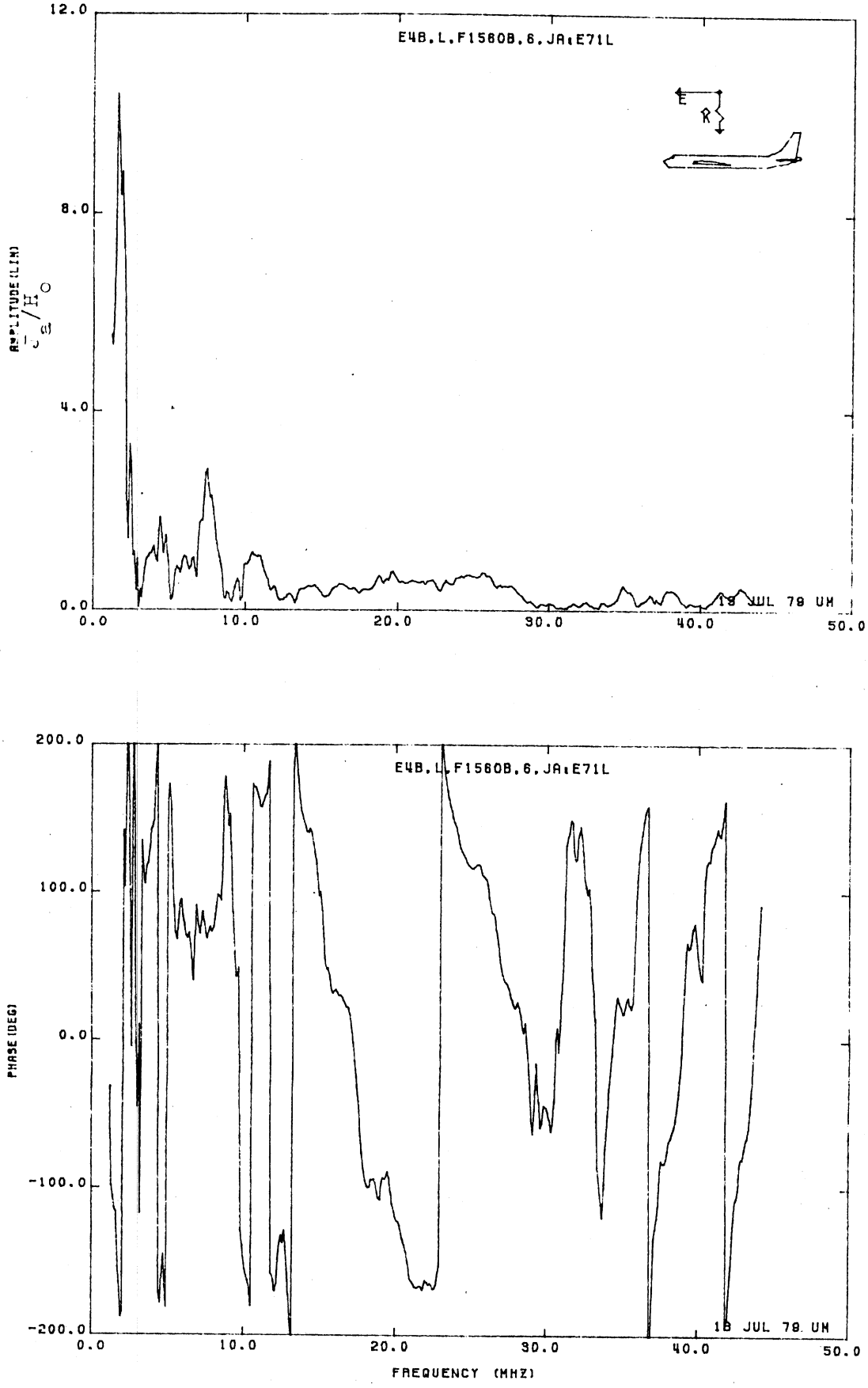

Figure 71L. Axial Current at STA:F1560B, Excitation 6, 1/100 Model.

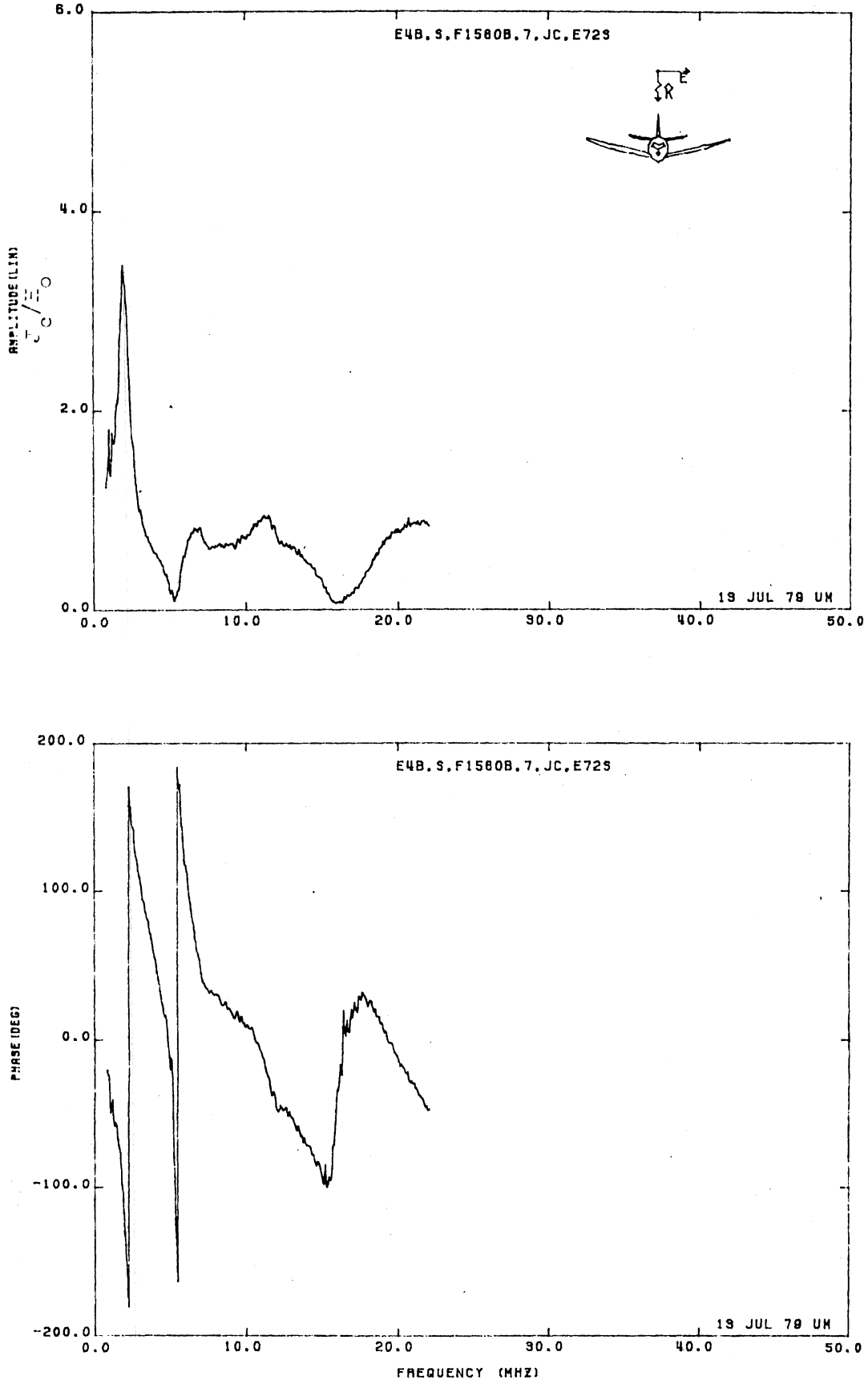

Figure 72S. Circumferential Current at STA:F1560B, Excitation 7, 1/200 Model.

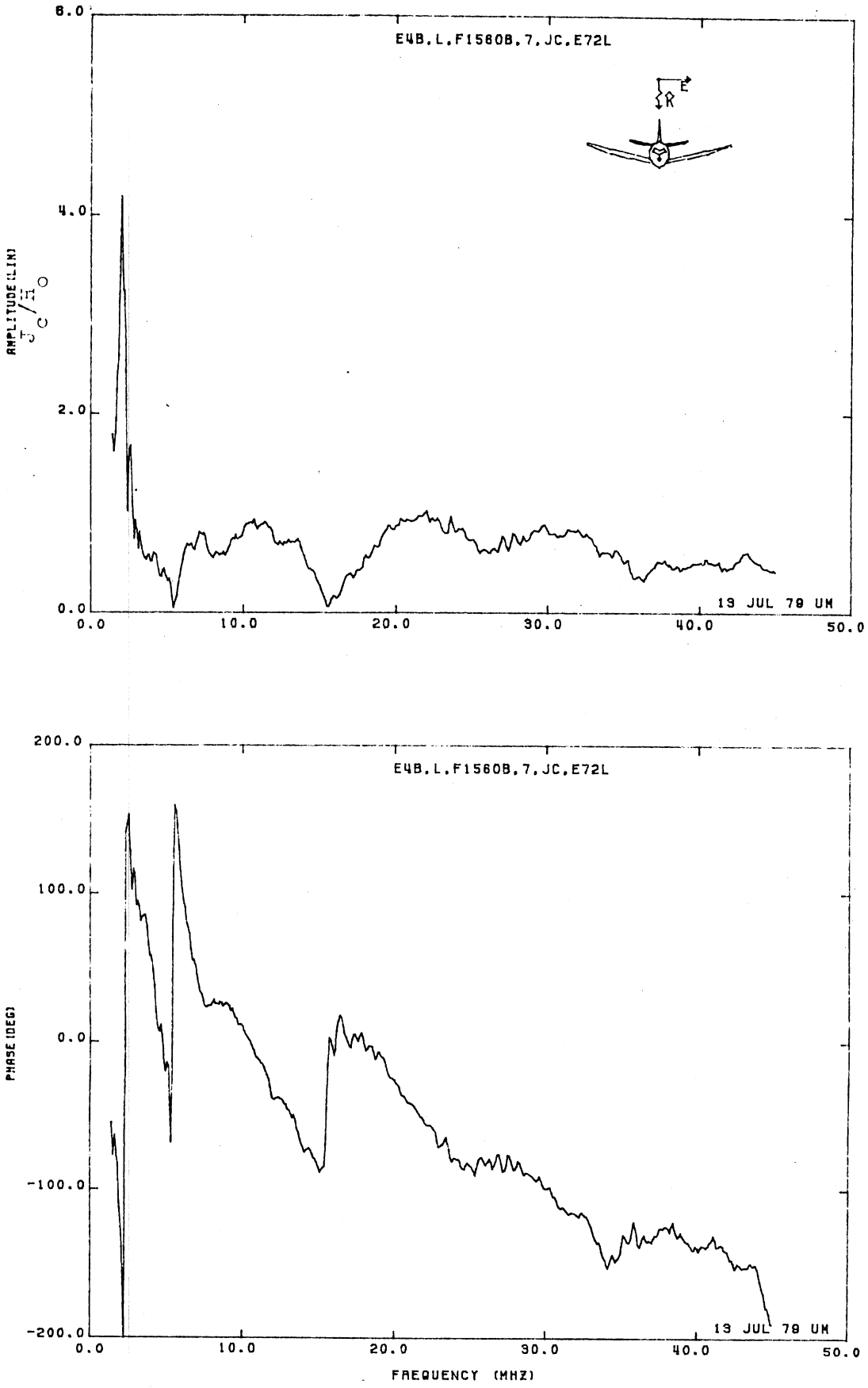

Figure 72L. Circumferential Current at STA:F1560B, Excitation 7, 1/100 Model.

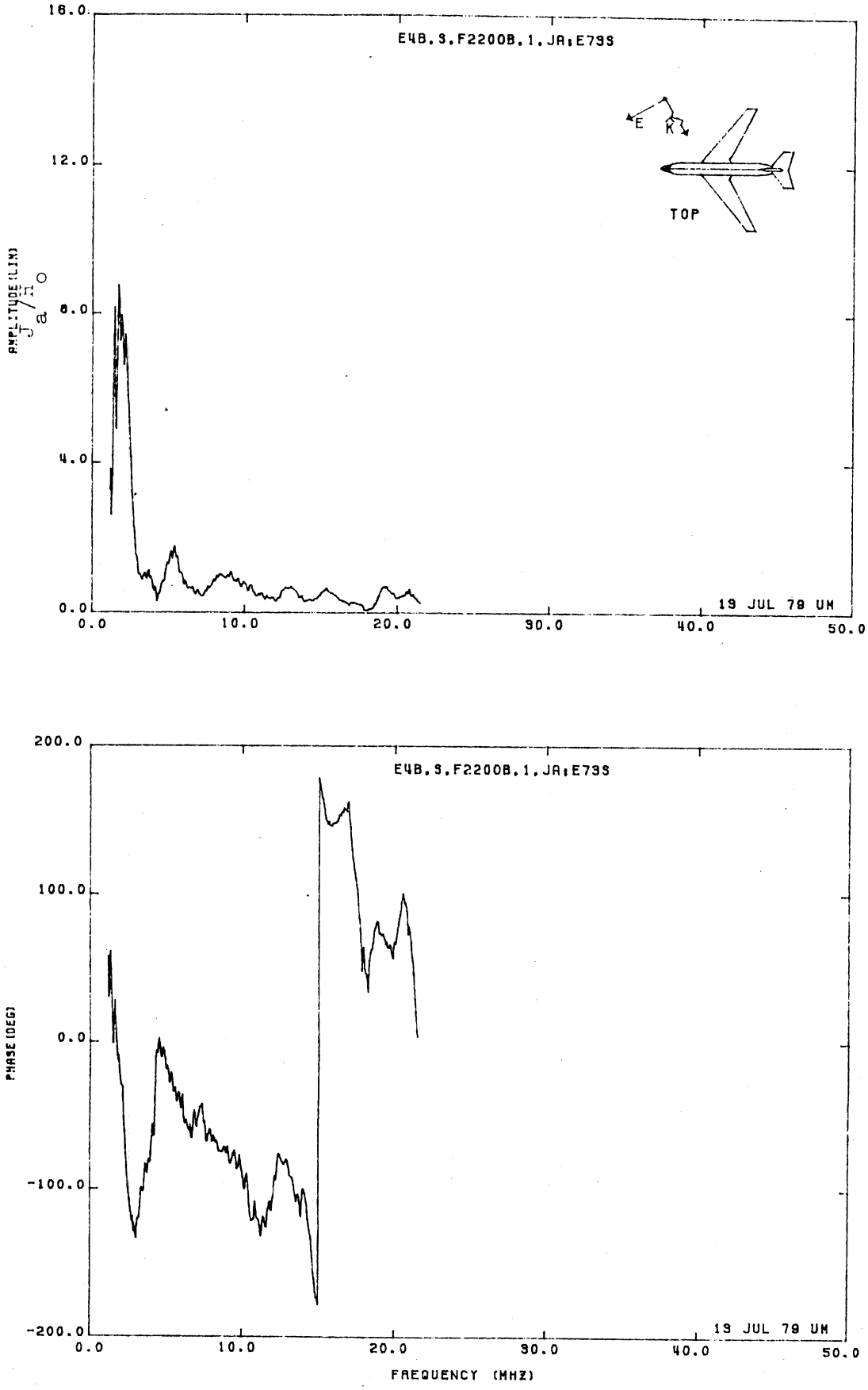

Figure 73S. Axial Current at STA:F2200B, Excitation 1, 1/200 Model.

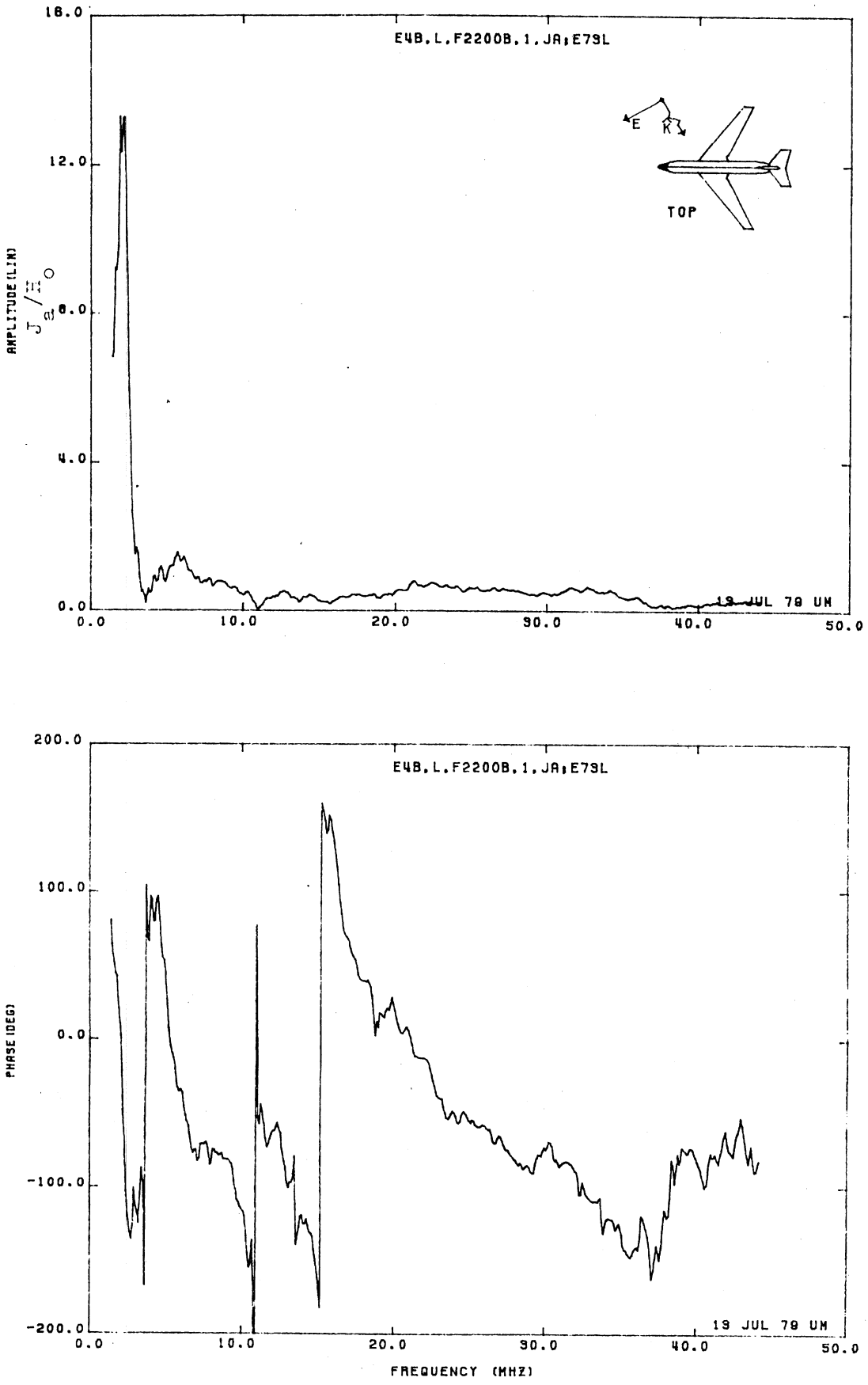

Figure 73L. Axial Current at STA:F2200B, Excitation 1, 1/100 Model.

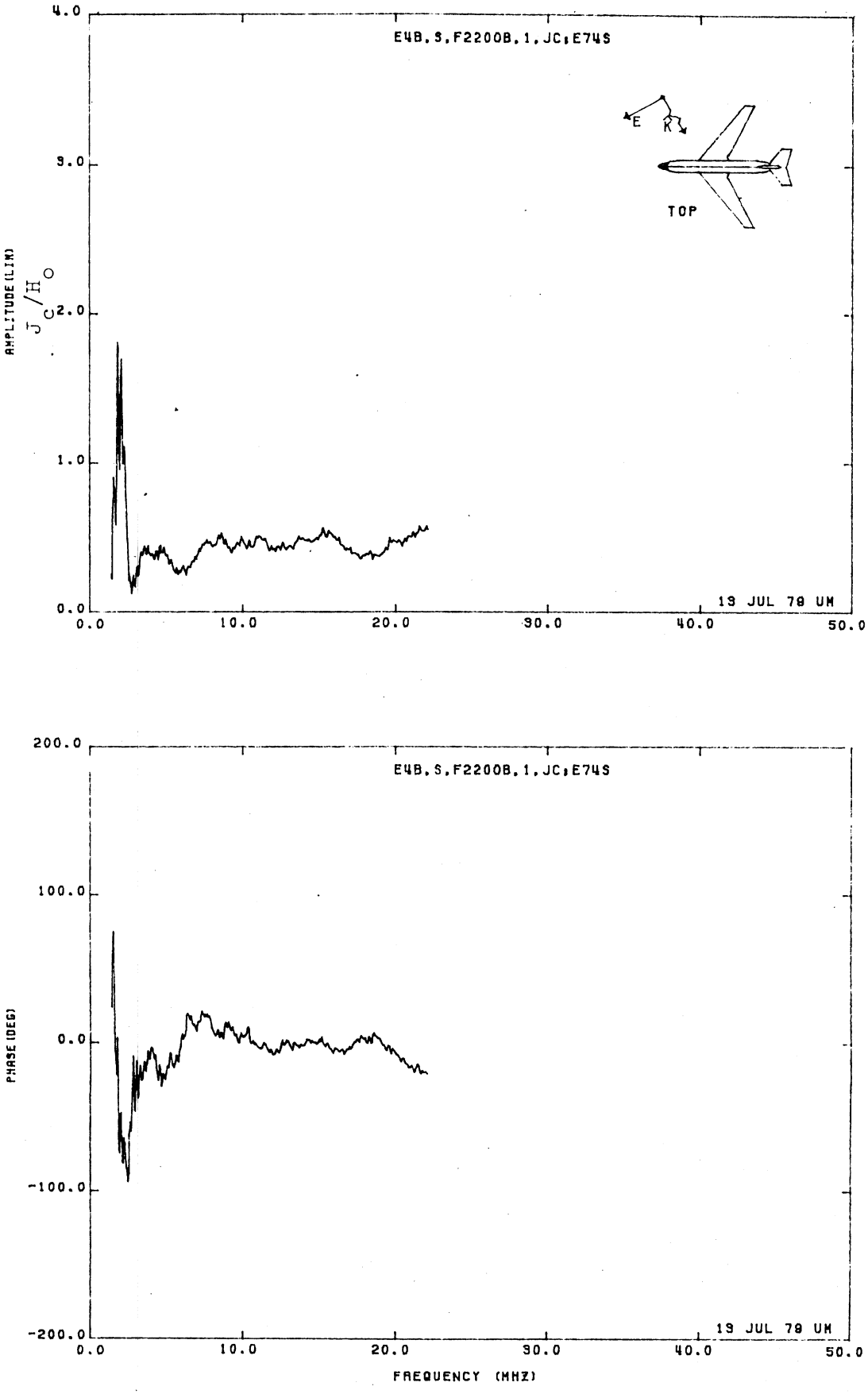

Figure 74S. Circumferential Current at STA:F2200B, Excitation 1, 1/200 Model.

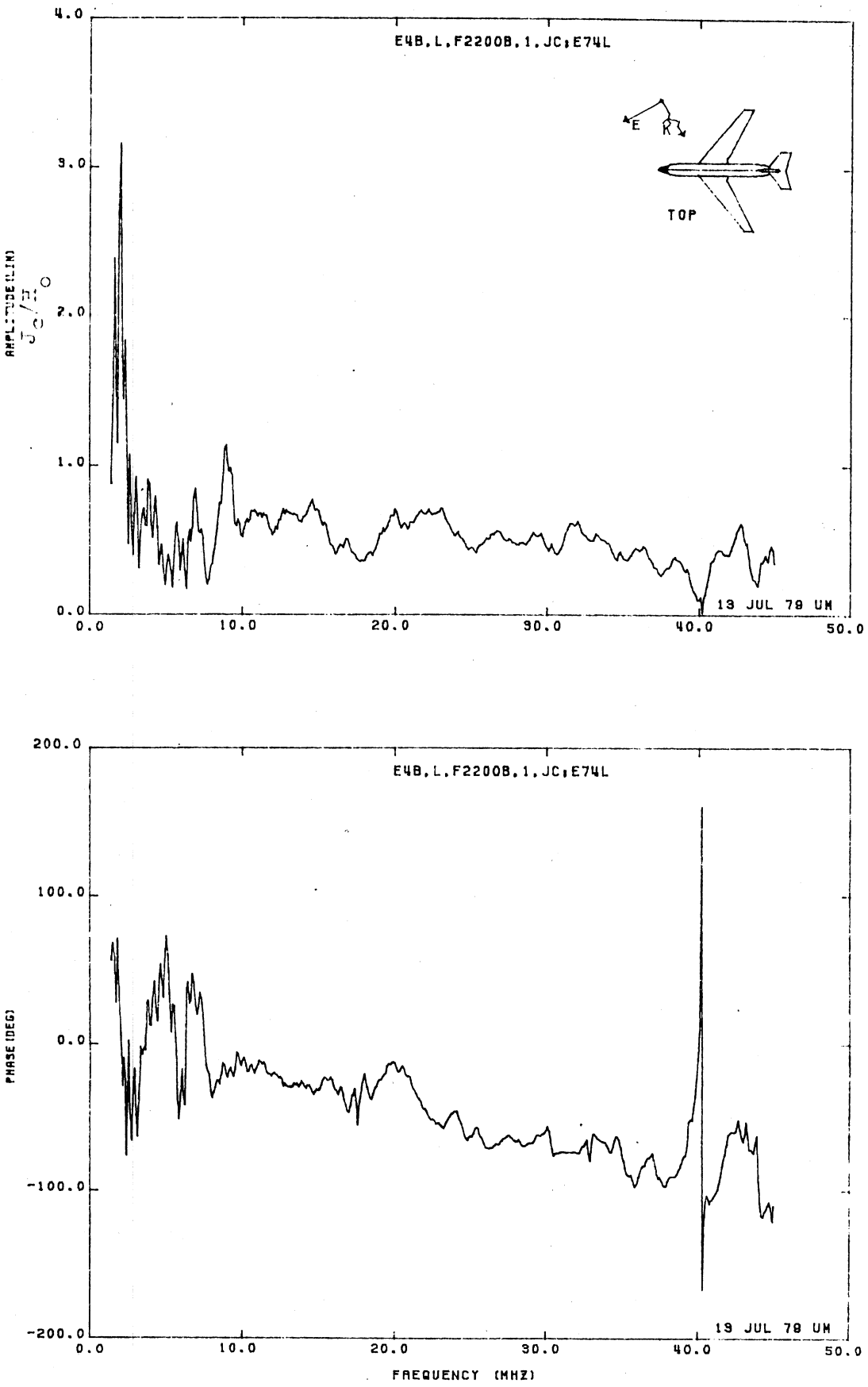

Figure 74L. Circumferential Current at STA:F2200B, Excitation 1, 1/100 Model.

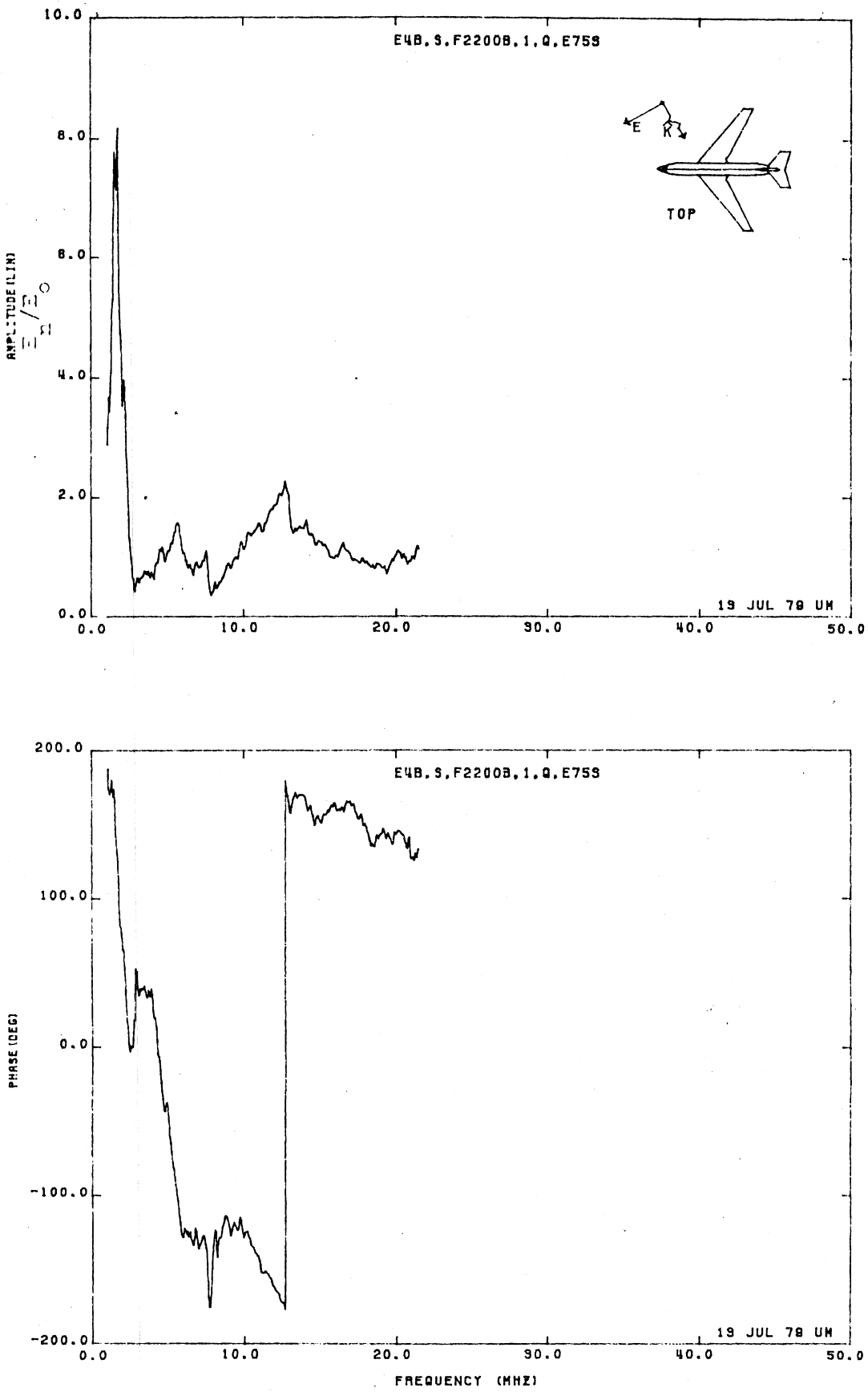

Figure 75S. Normal Electric Field at STA:F2200B, Excitation 2, 1/200 Model.

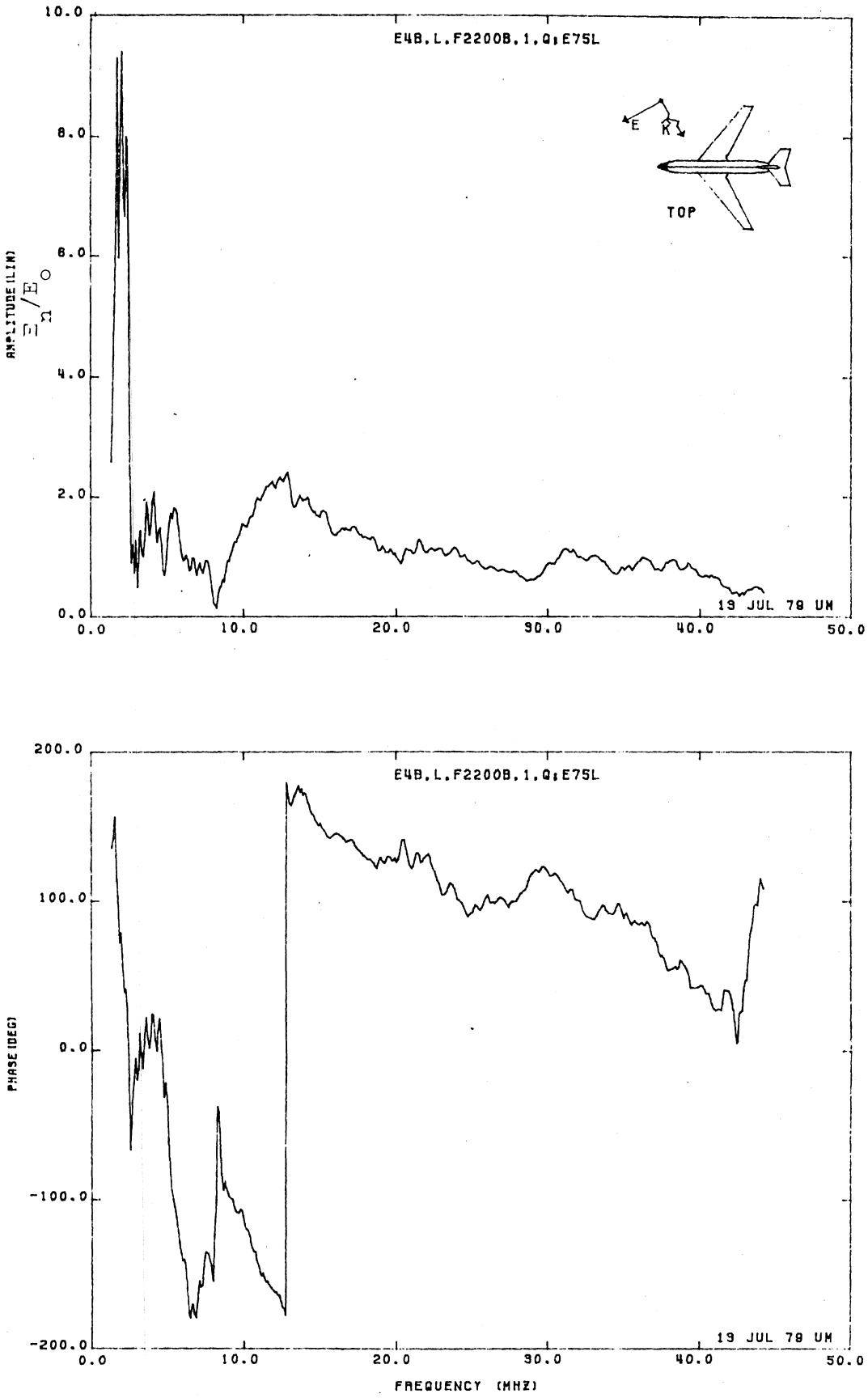

Figure 75L. Normal Electric Field at STA:F2200B, Excitation 1, 1/100 Model.

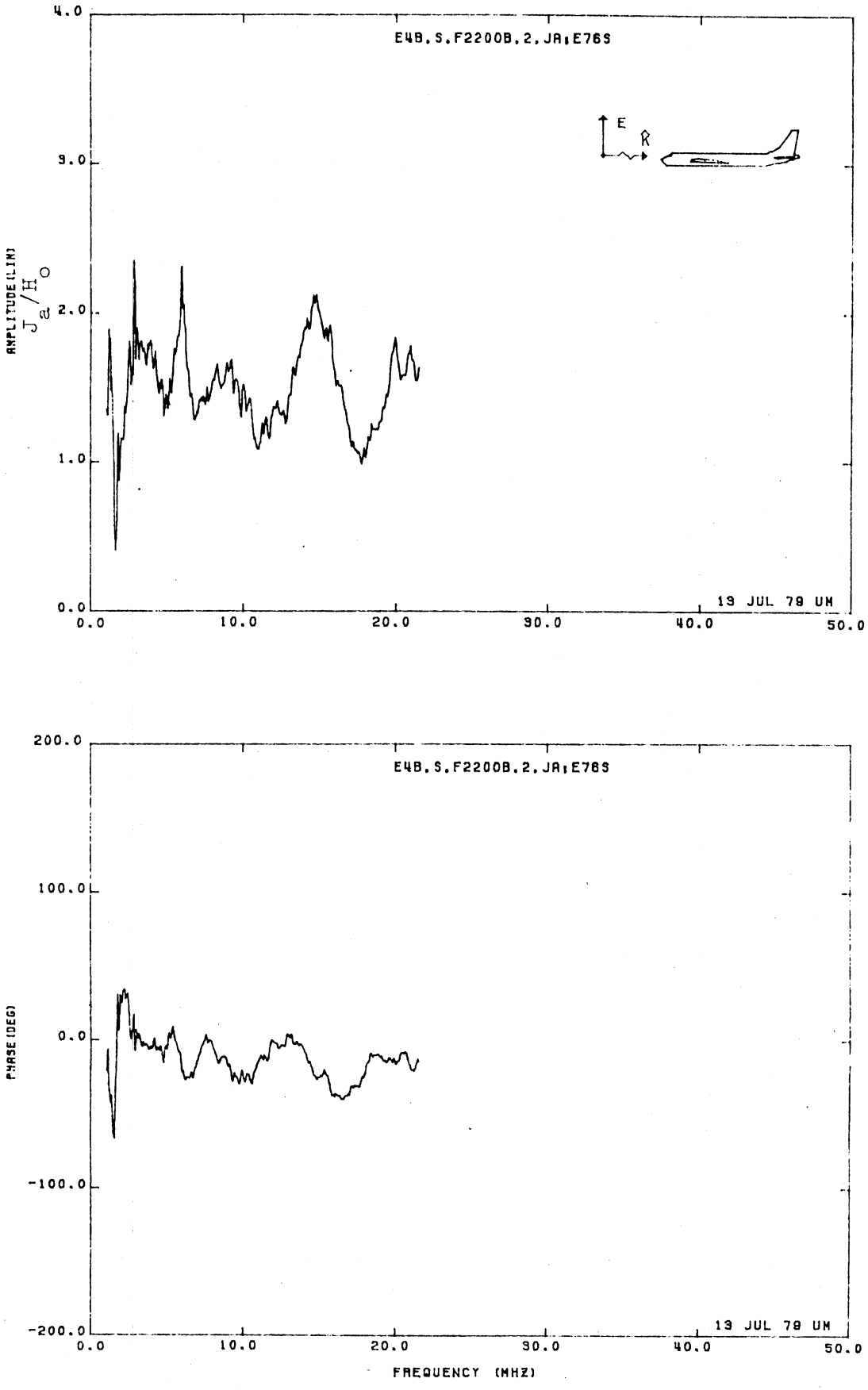

Figure 76S. Axial Current at STA:F2200B, Excitation 2, 1/200 Model.

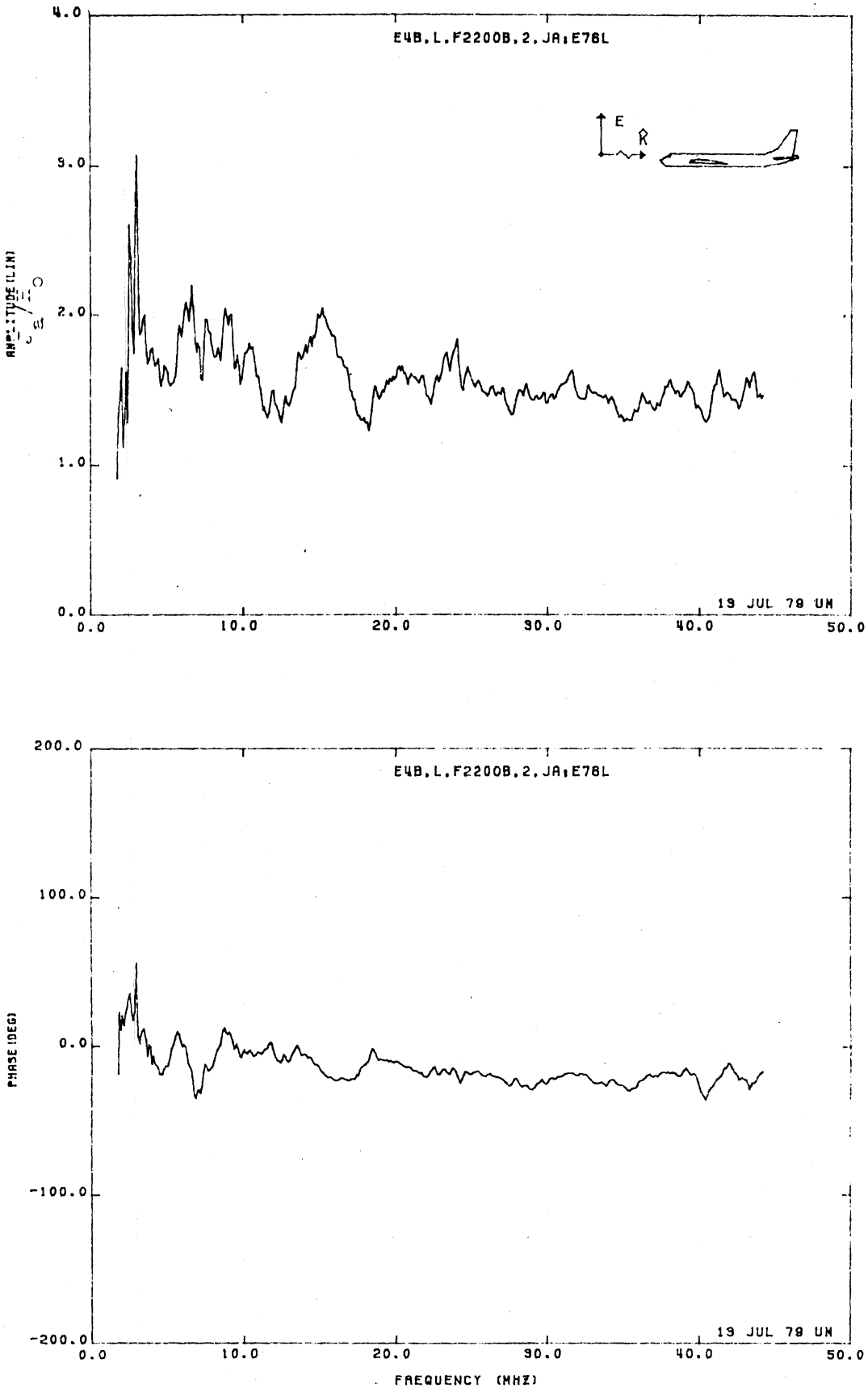

Figure 76L. Axial Current at STA:F2200B, Excitation 2, 1/100 Model.

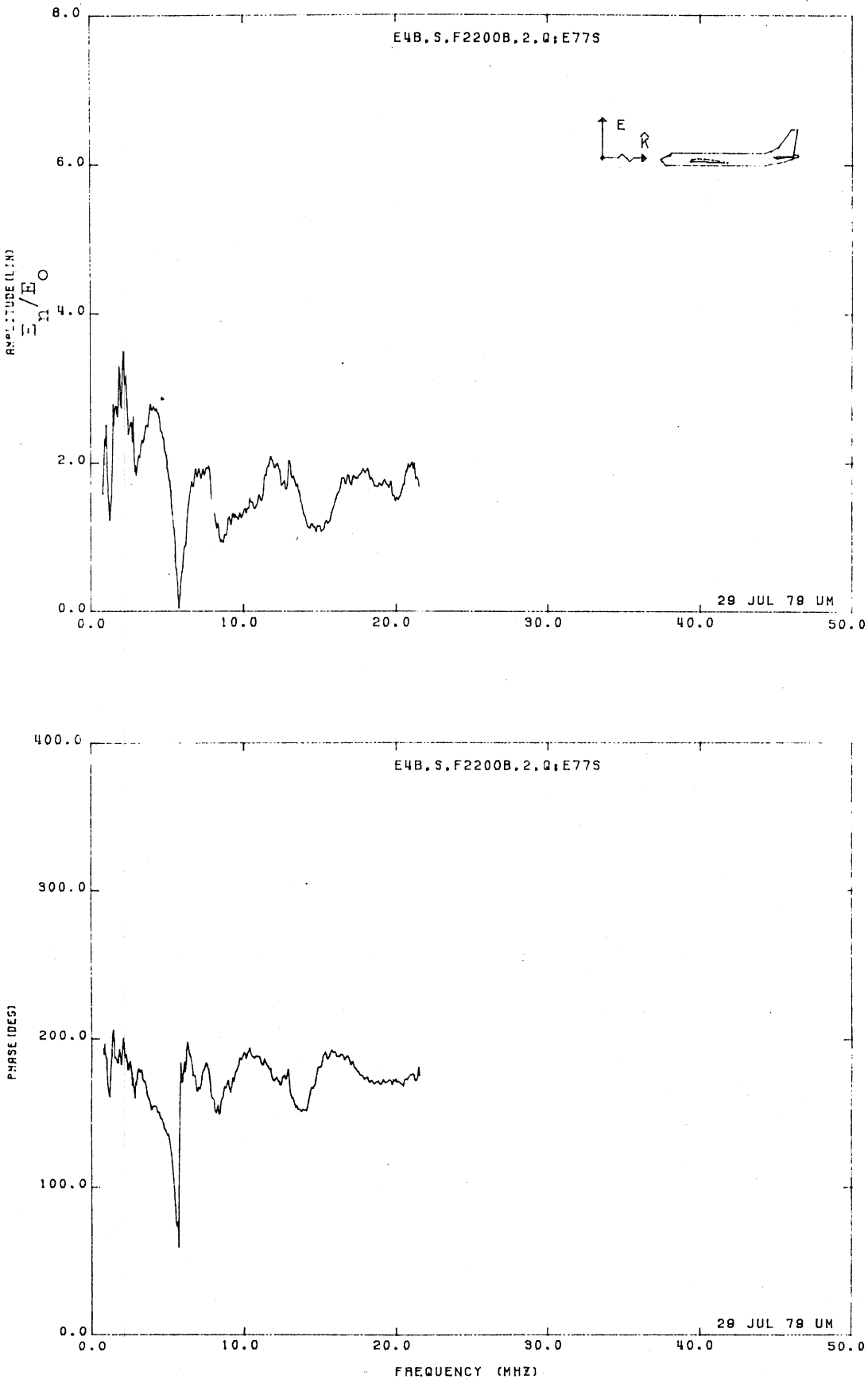

Figure 77S. Normal Electric Field at STA:F2200B, Excitation 2, 1/200 Model.

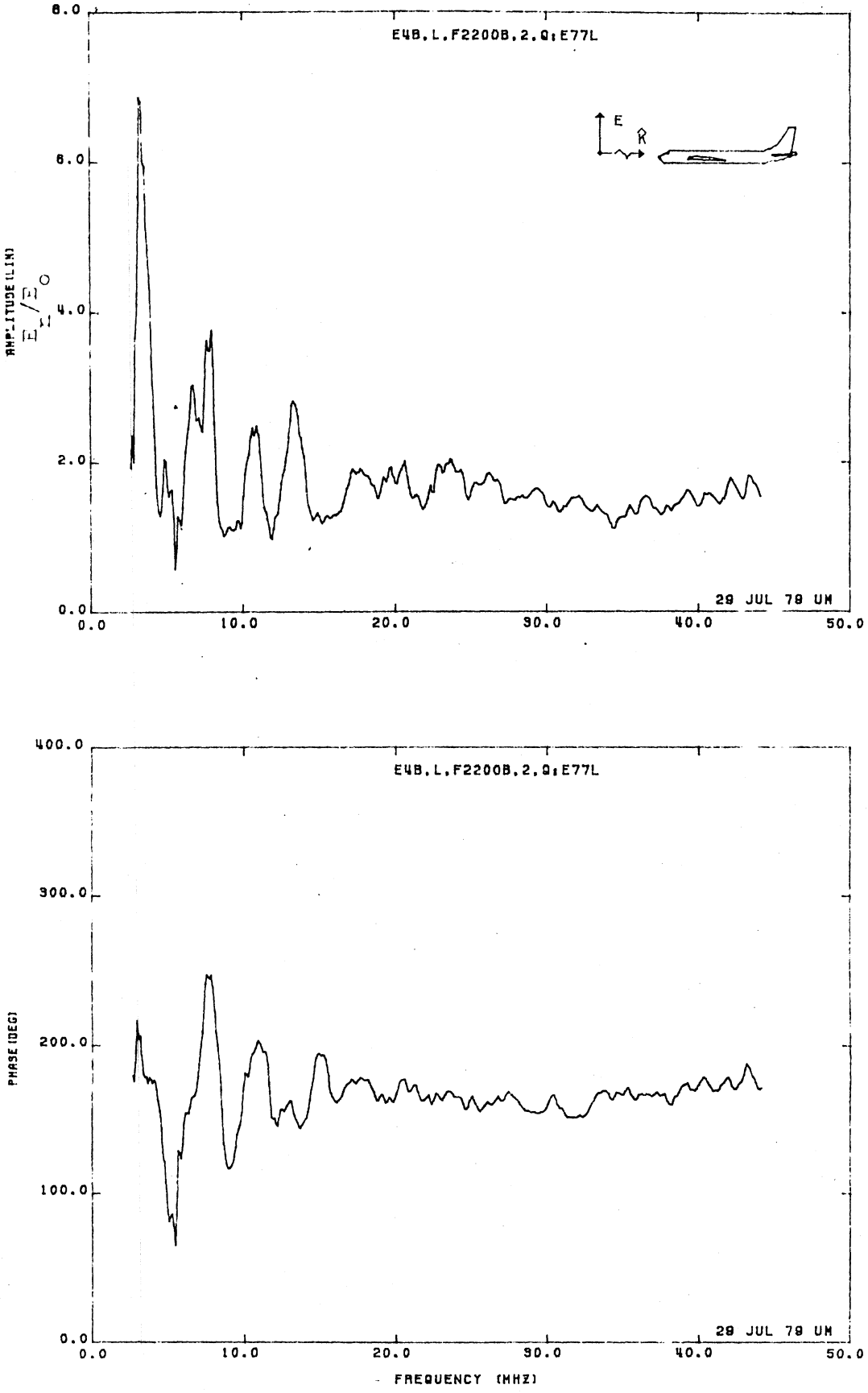

Figure 77L. Normal Electric Field at STA:F2200B, Excitation 2, 1/100 Model.

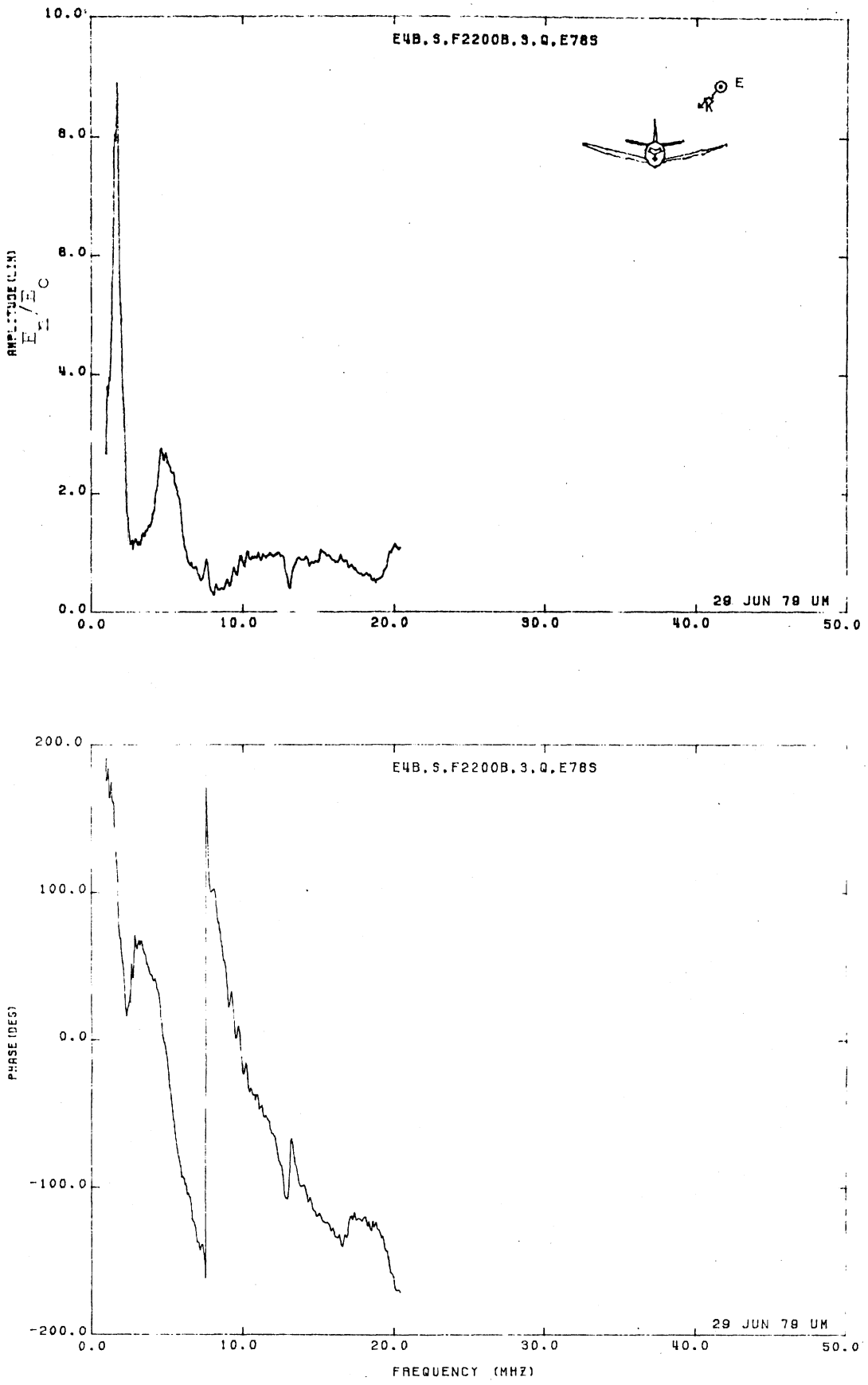

Figure 78S. Normal Electric Field at STA:F2200B, Excitation 3, 1/200 Model.

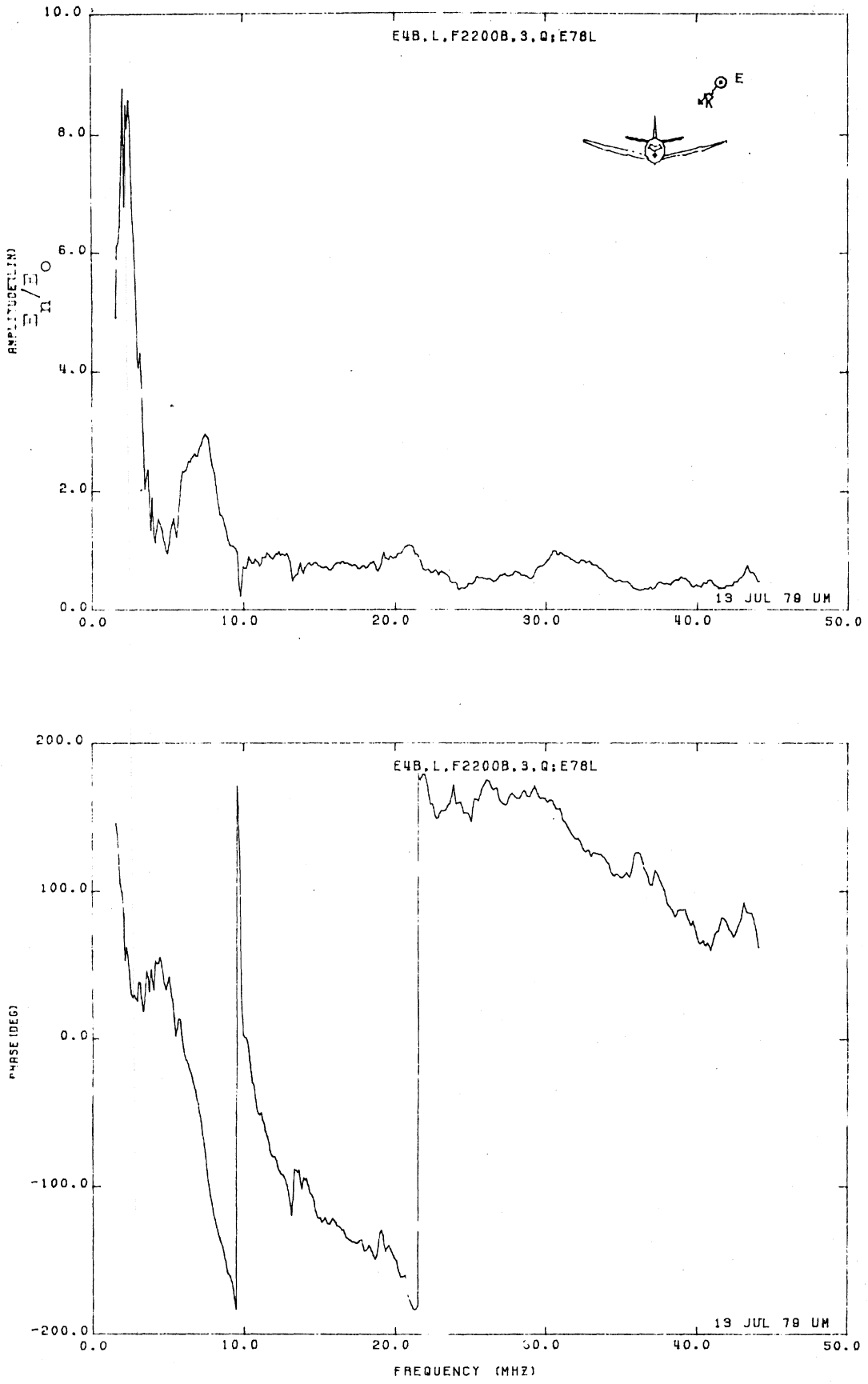

Figure 78L. Normal Electric Field at STA:F2200B, Excitation 3, 1/100 Model.

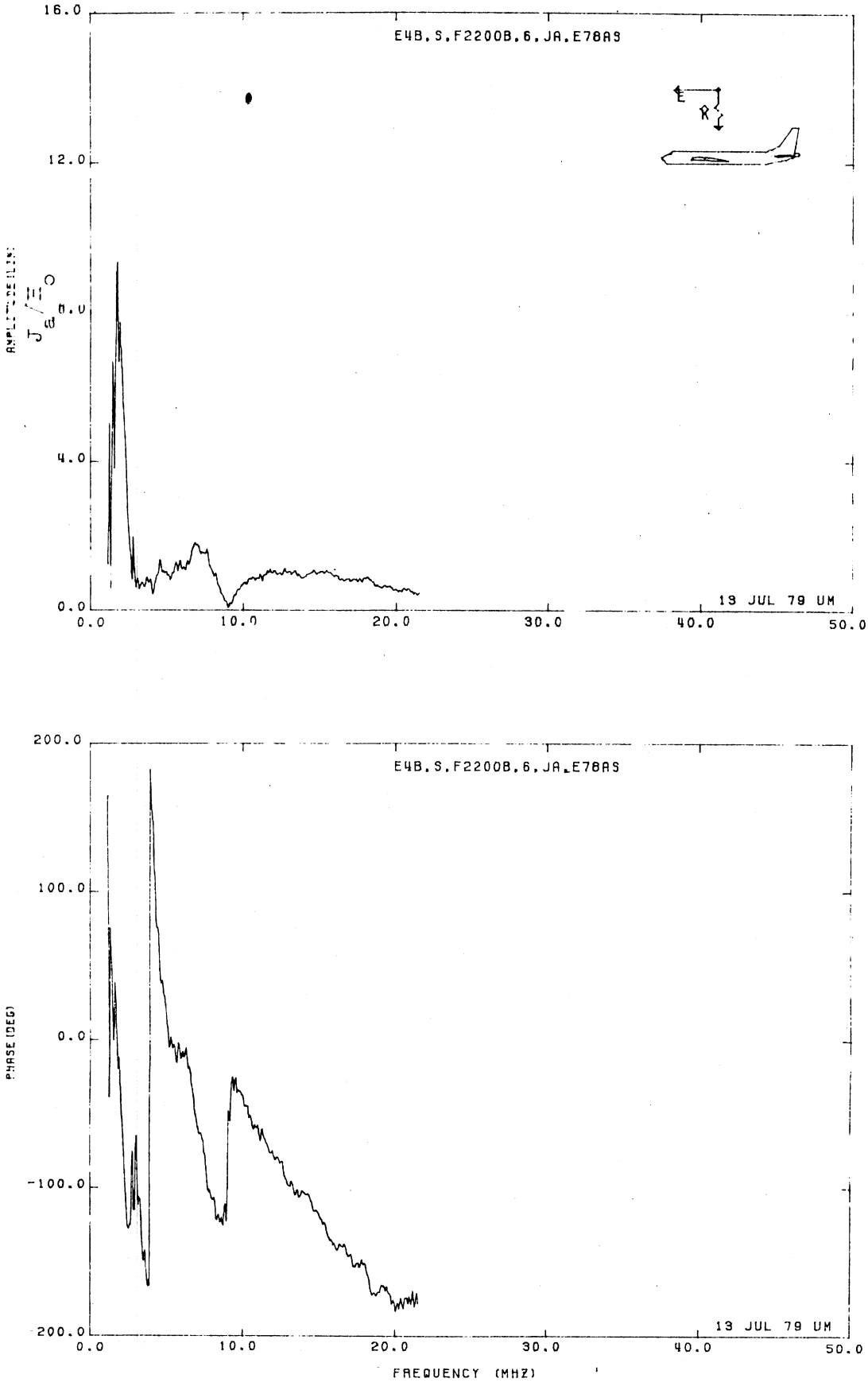

Figure 78AS. Axial Current at STA:F2200B, Excitation 6, 1/200 Model.

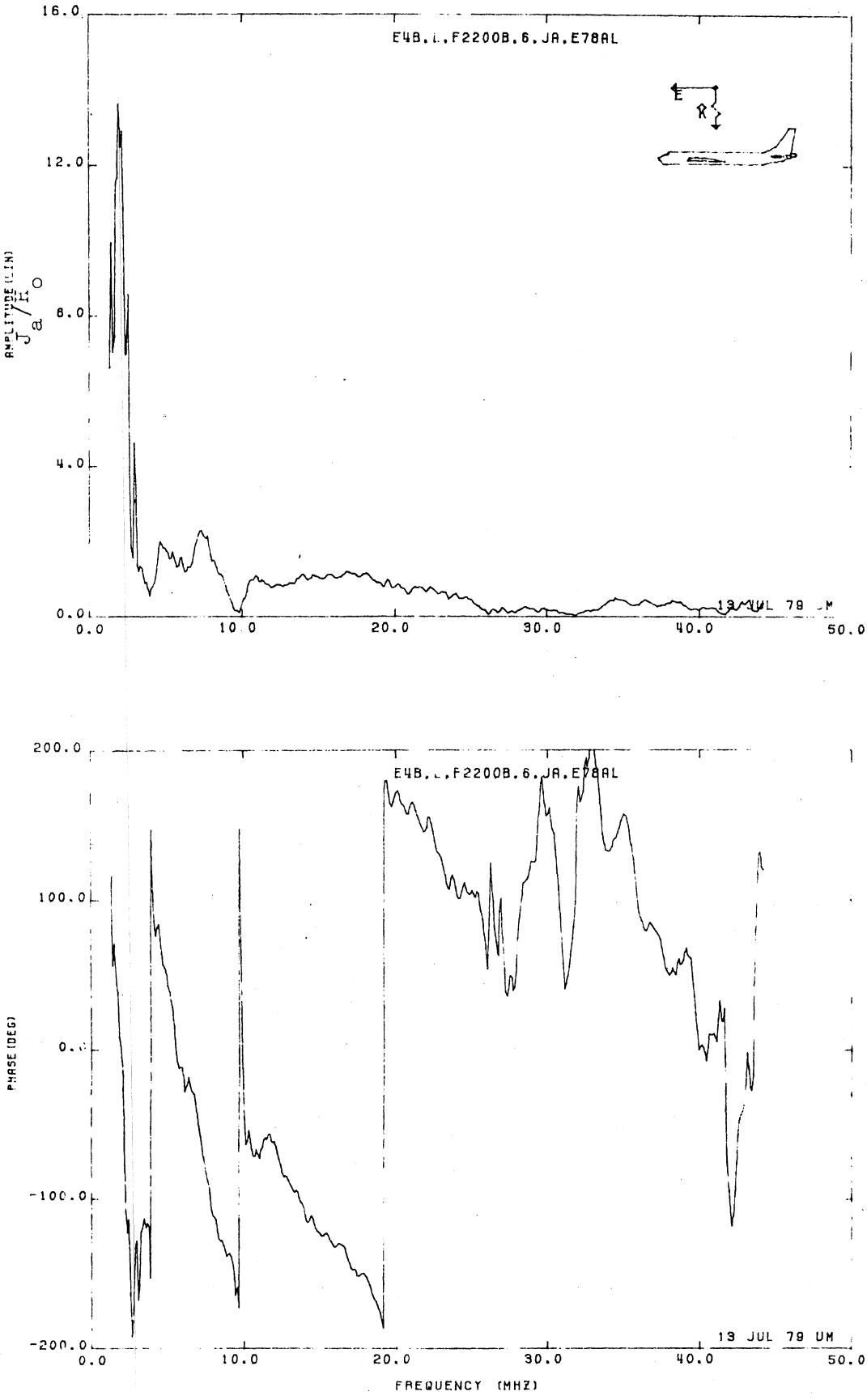

Figure 78AL. Axial Current at STA:F2200B, Excitation 6, 1/100 Model.

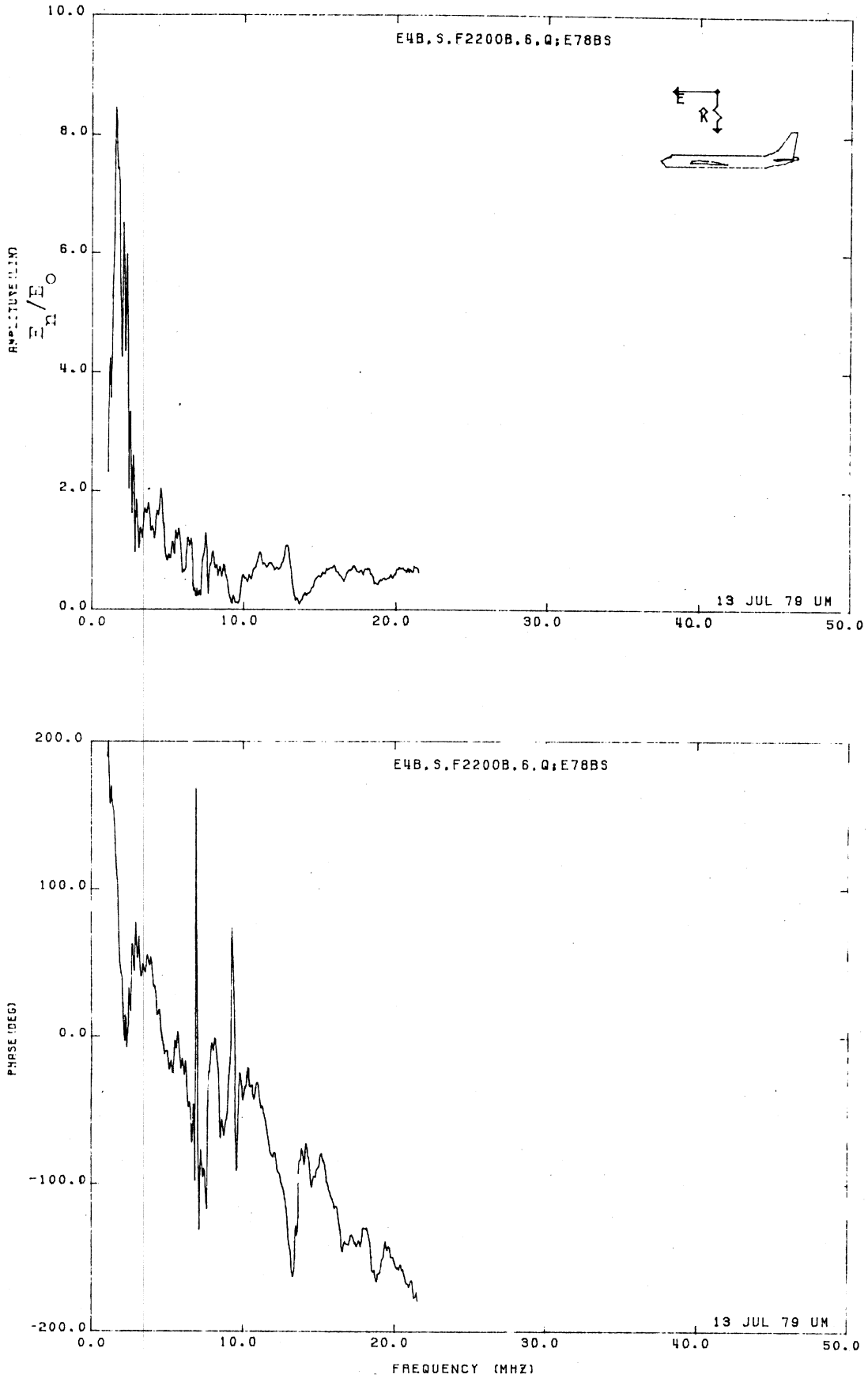

Figure 78BS. Normal Electric Field at STA:F2200B, Excitation 6, 1/200 Model.

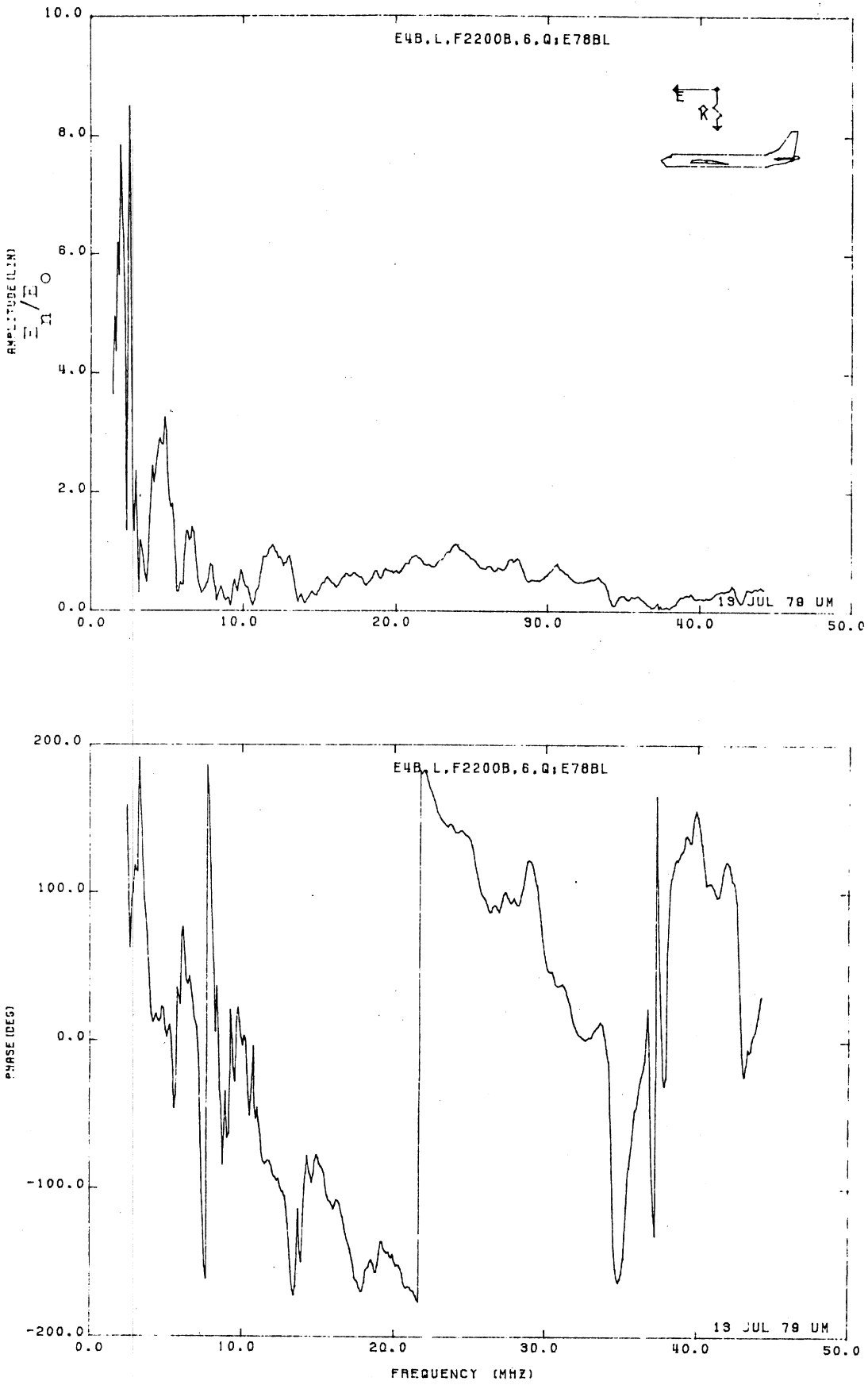

Figure 78BL. Normal Electric Field at STA:F2200B, Excitation 6, 1/100 Model.

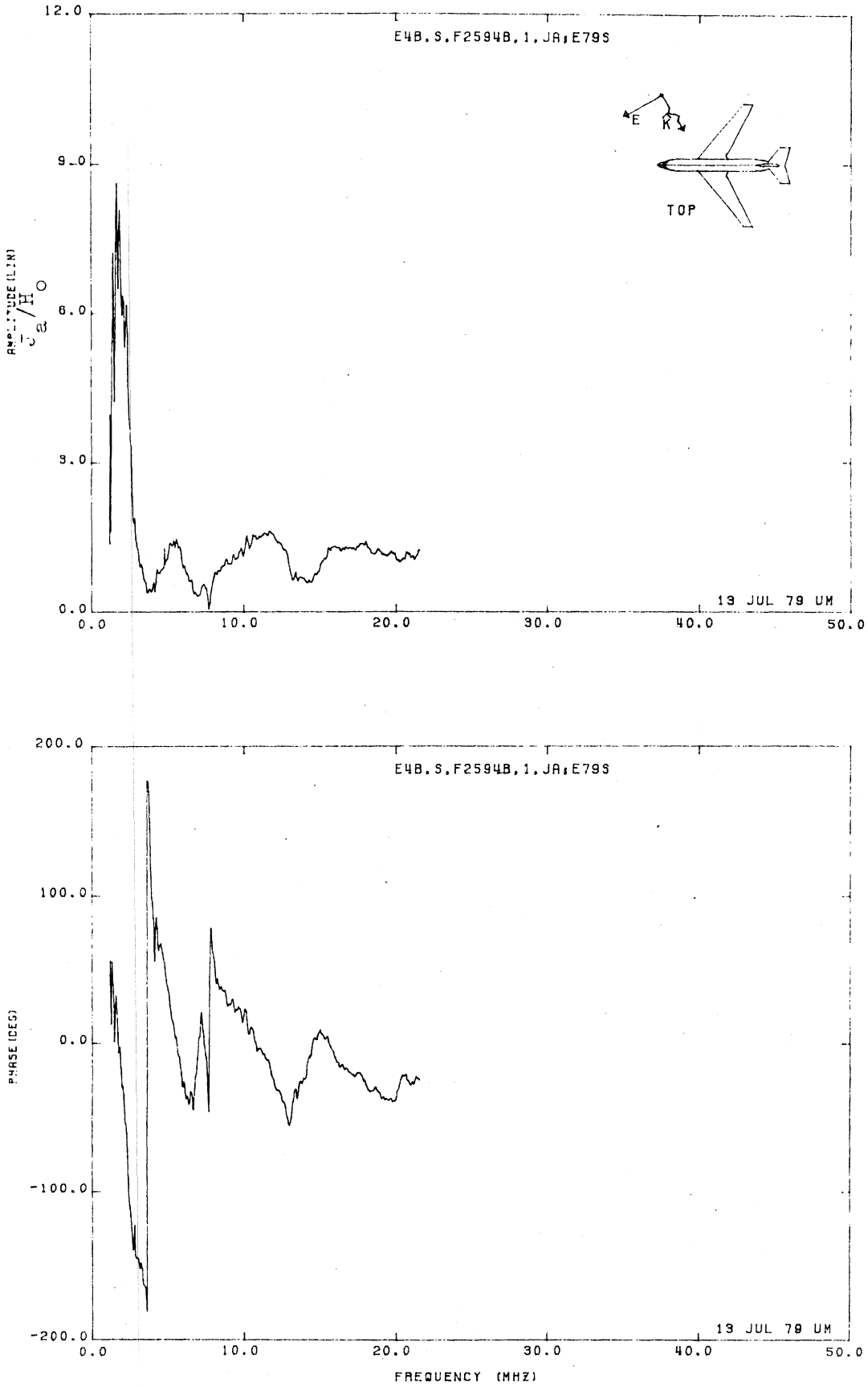

Figure 79S. Axial Current at STA:F2594B, Excitation 1, 1/200 Model.

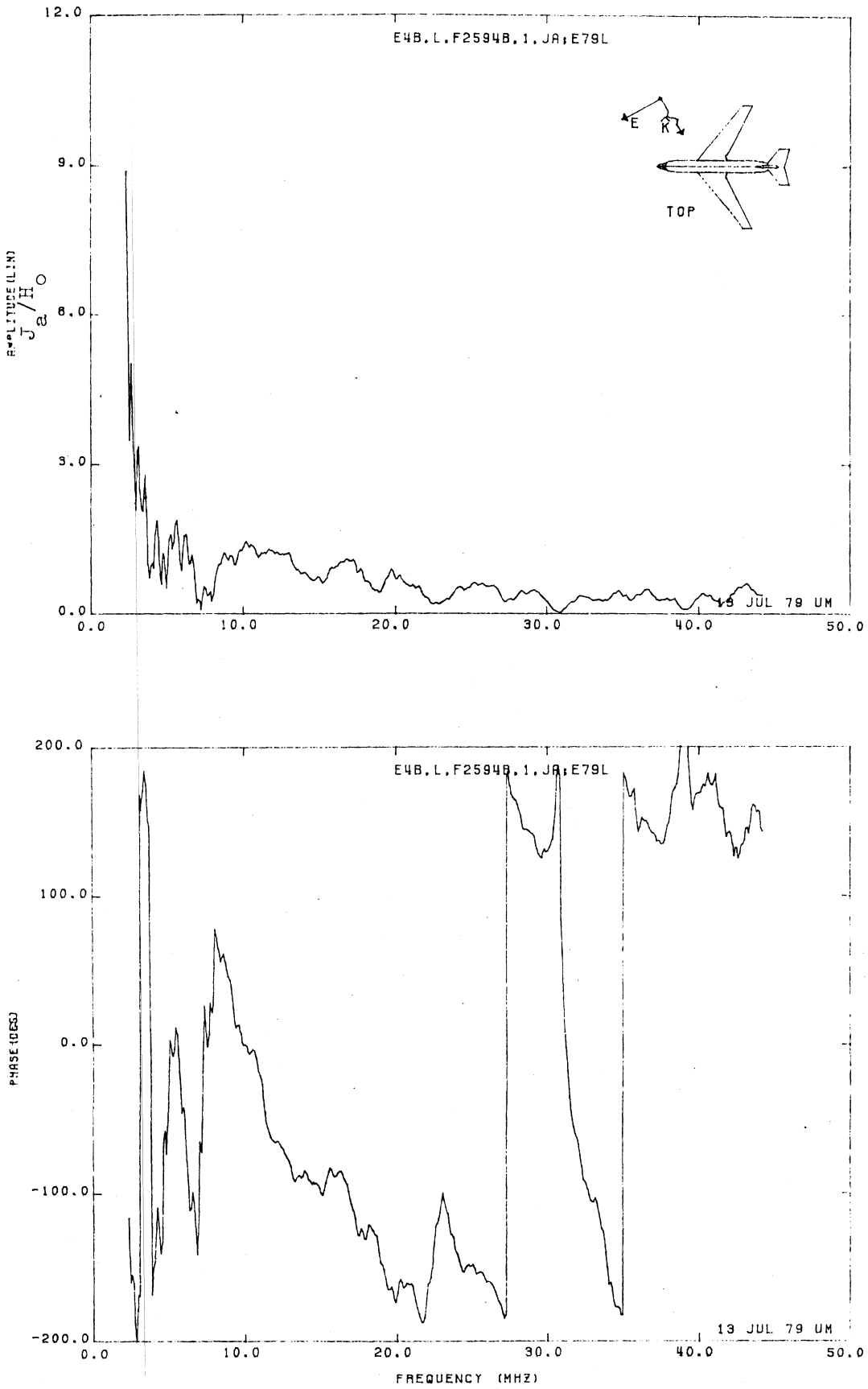

Figure 79L. Axial Current at STA:F2594B, Excitation 1, 1/100 Model.

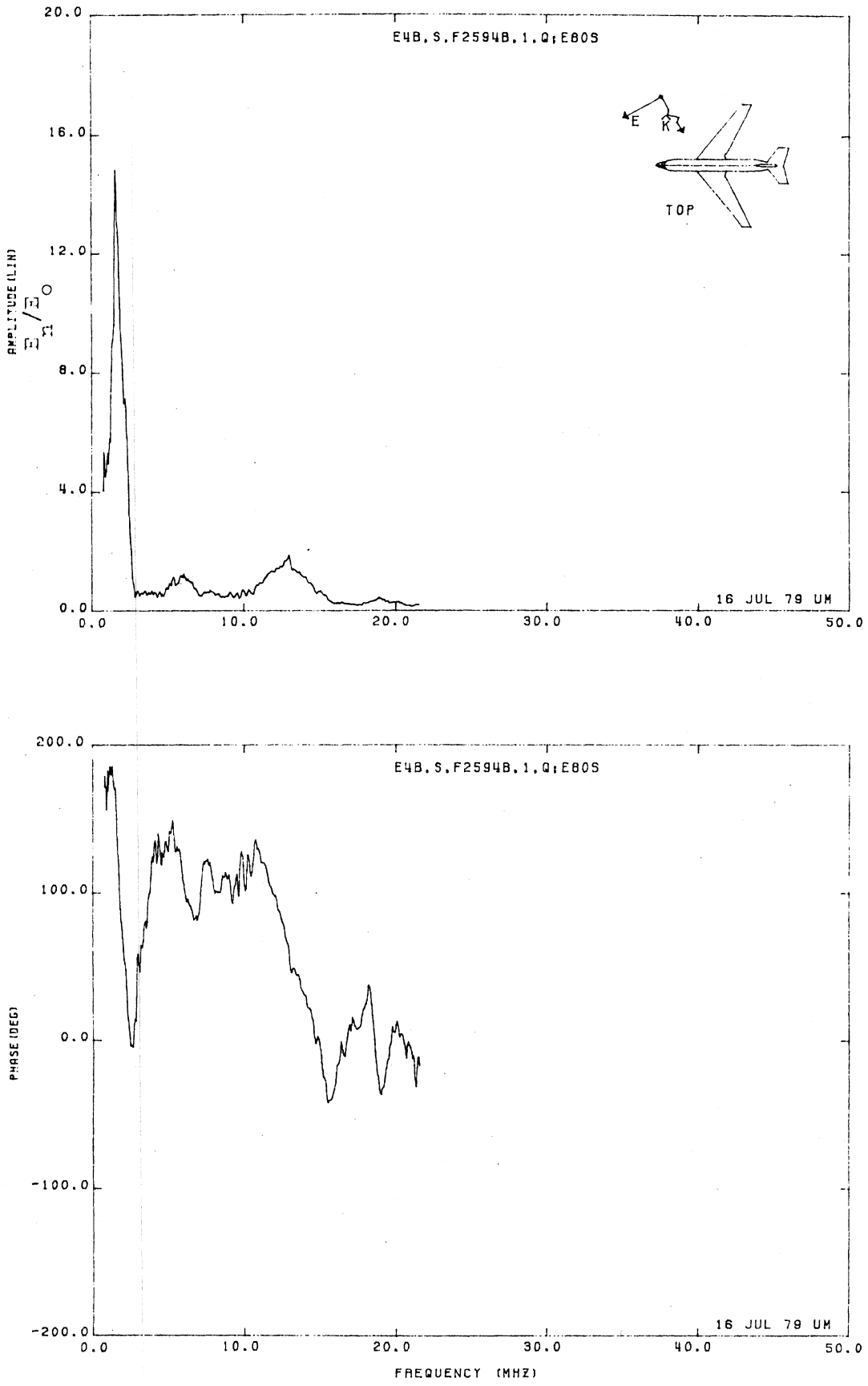

Figure 80S. Normal Electric Field at STA:F2594B, Excitation 1, 1/200 Model.

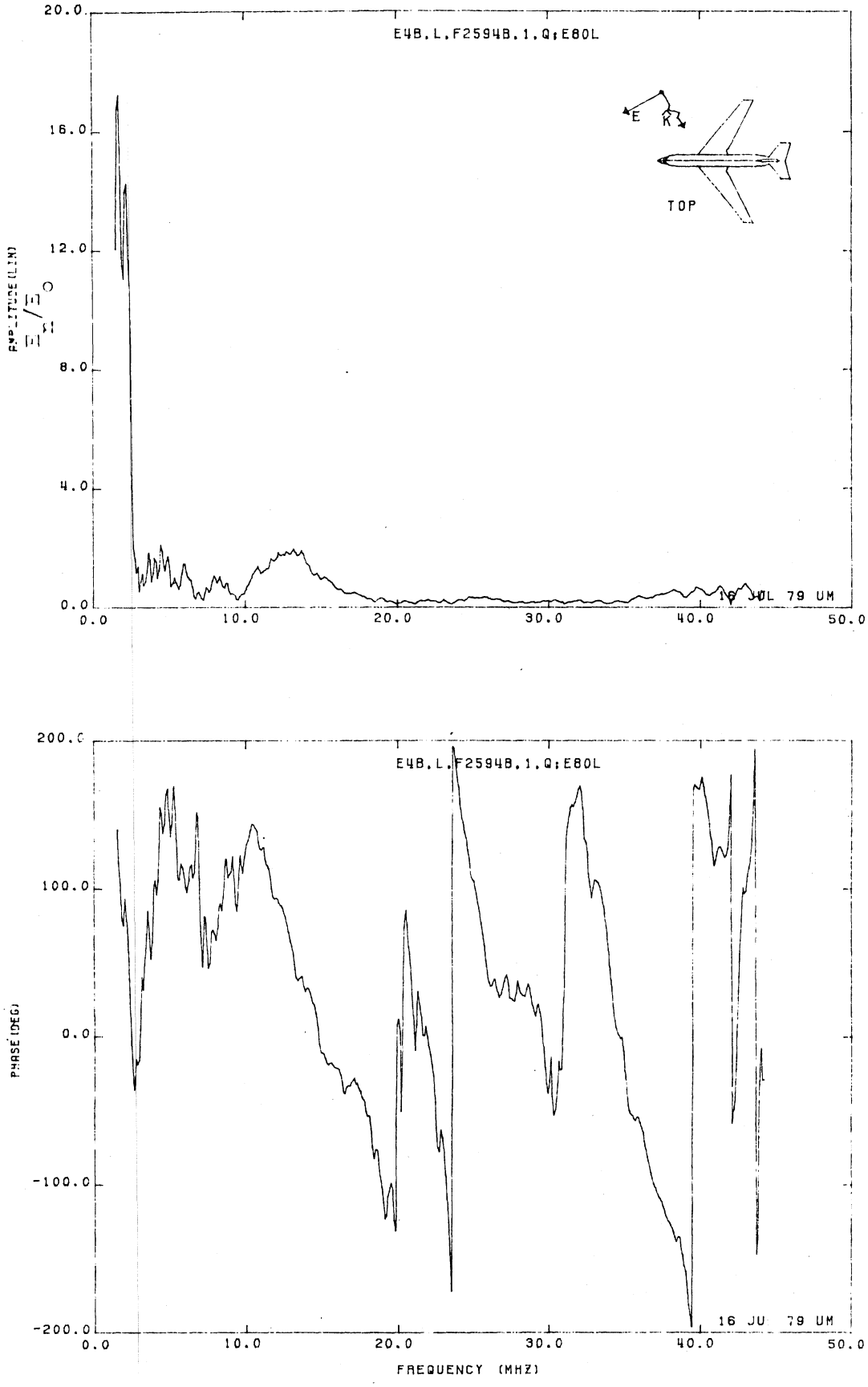

Figure 80L. Normal Electric Field at STA:F2594B, Excitation 1, 1/100 Model.

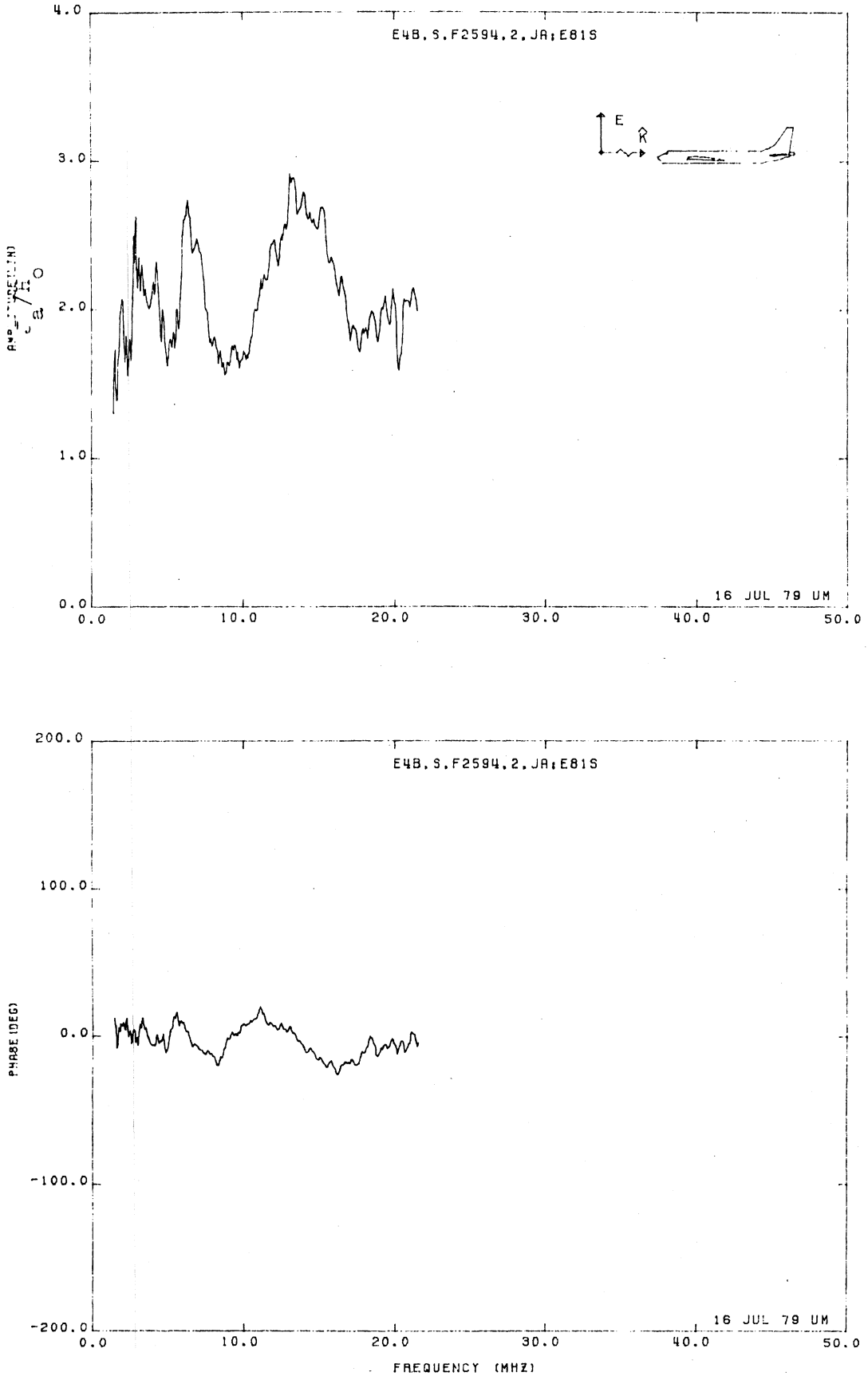

Figure 81S. Axial Current at STA:F2594B, Excitation 2, 1/200 Model.

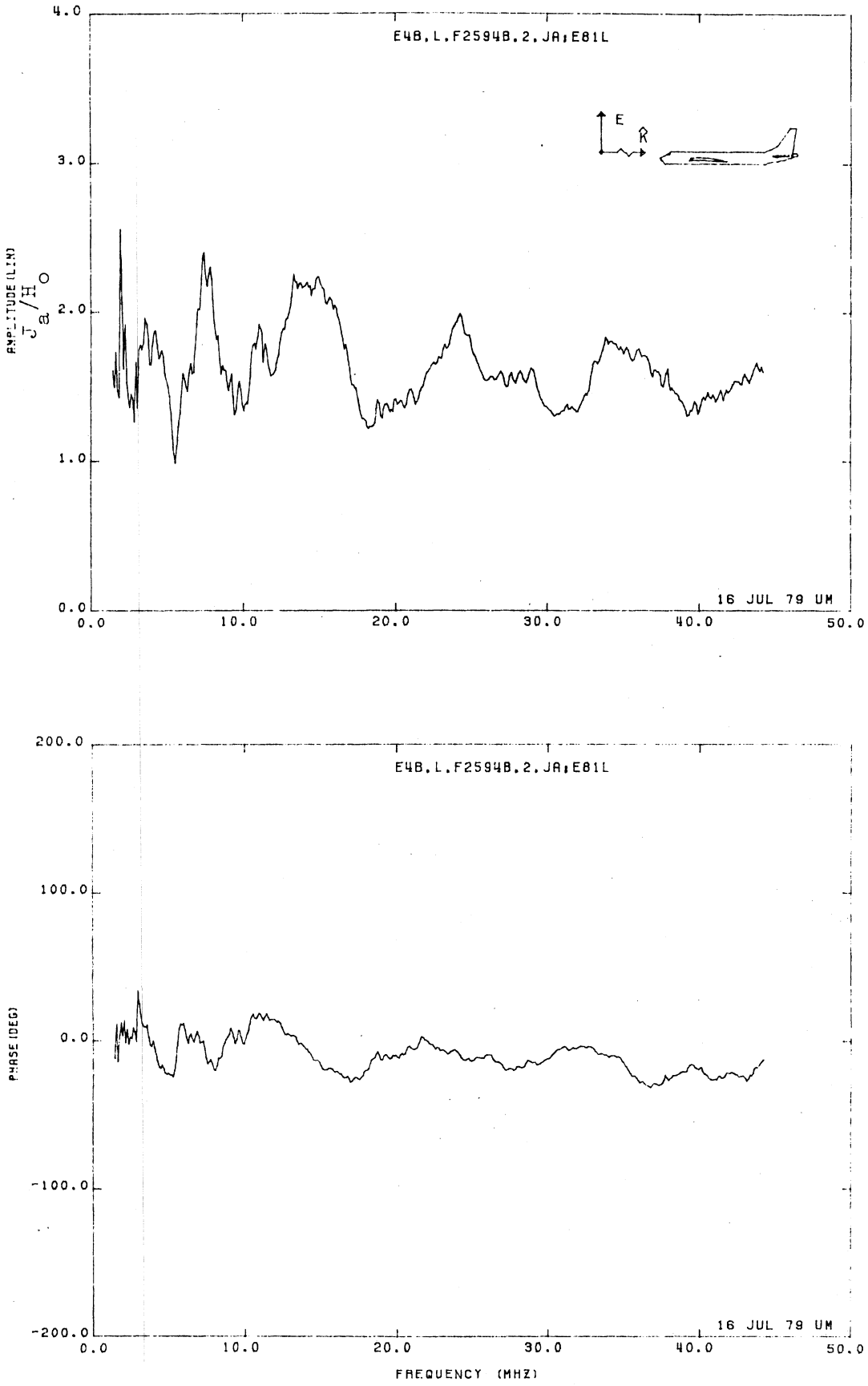

Figure 81L. Axial Current at STA:F2594B, Excitation 2, 1/100 Model.

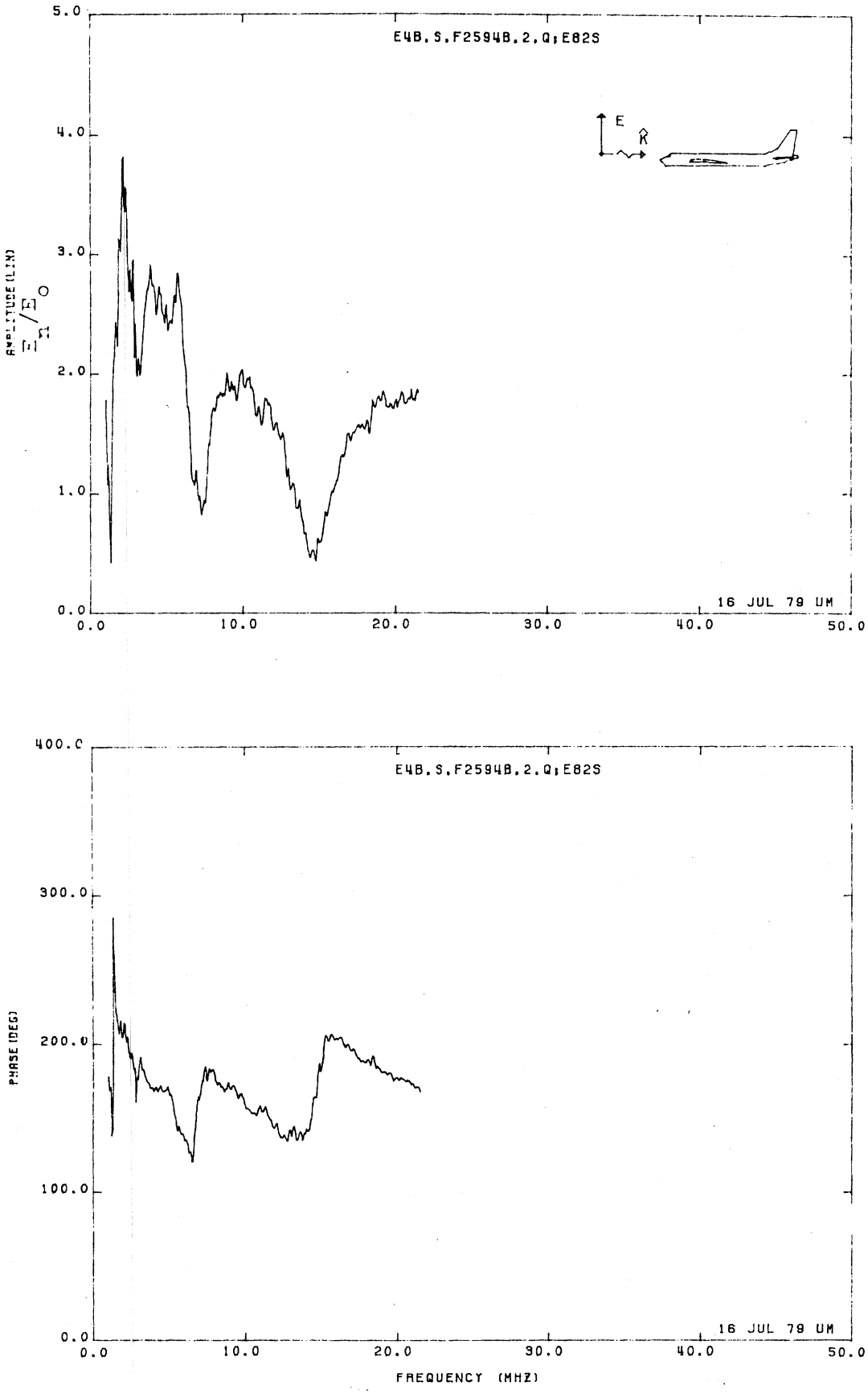

Figure 82S. Normal Electric Field at STA:F2594B, Excitation 2, 1/200 Model.

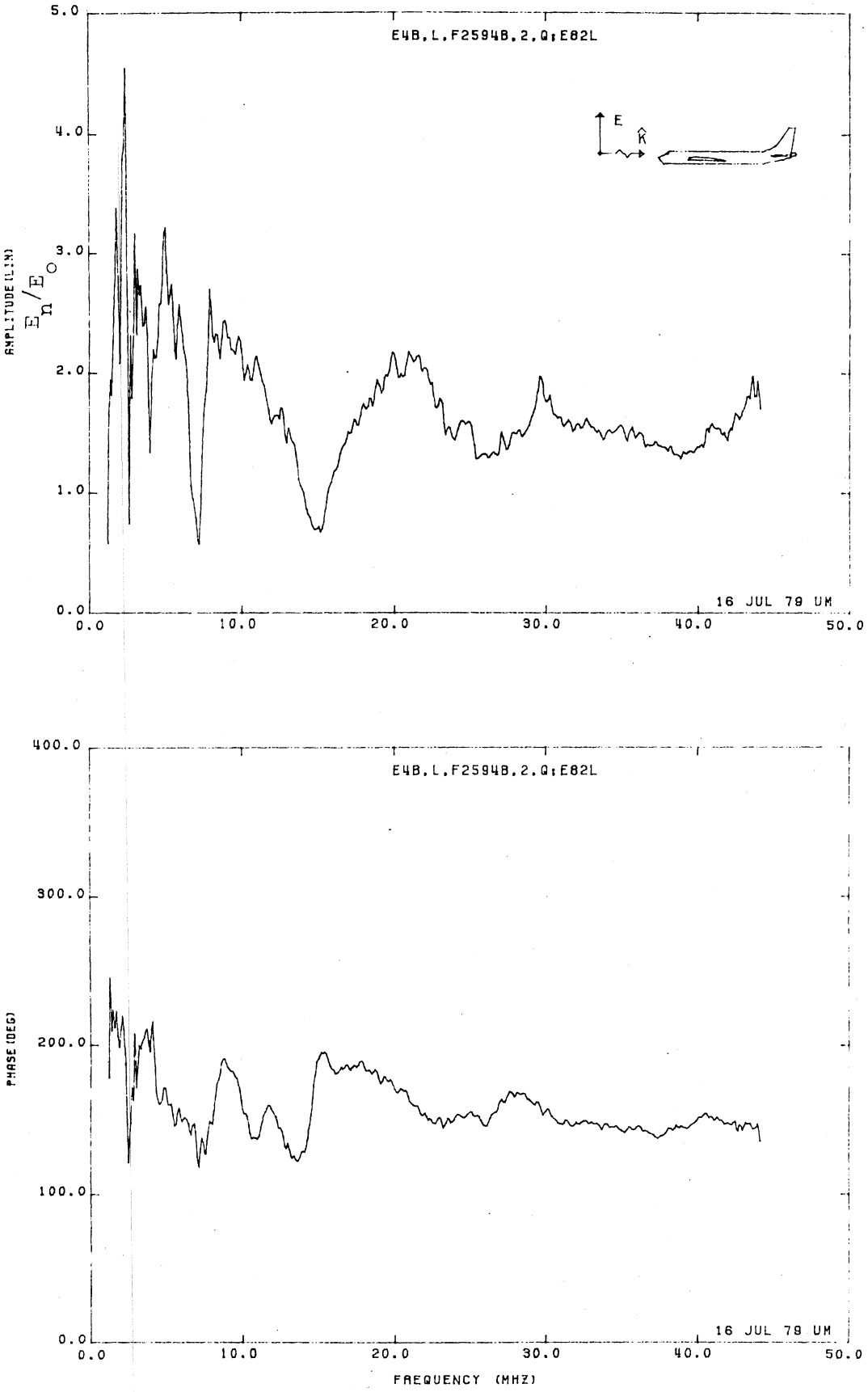

Figure 82L. Normal Electric Field at STA:F2594B, Excitation 2, 1/100 Model.

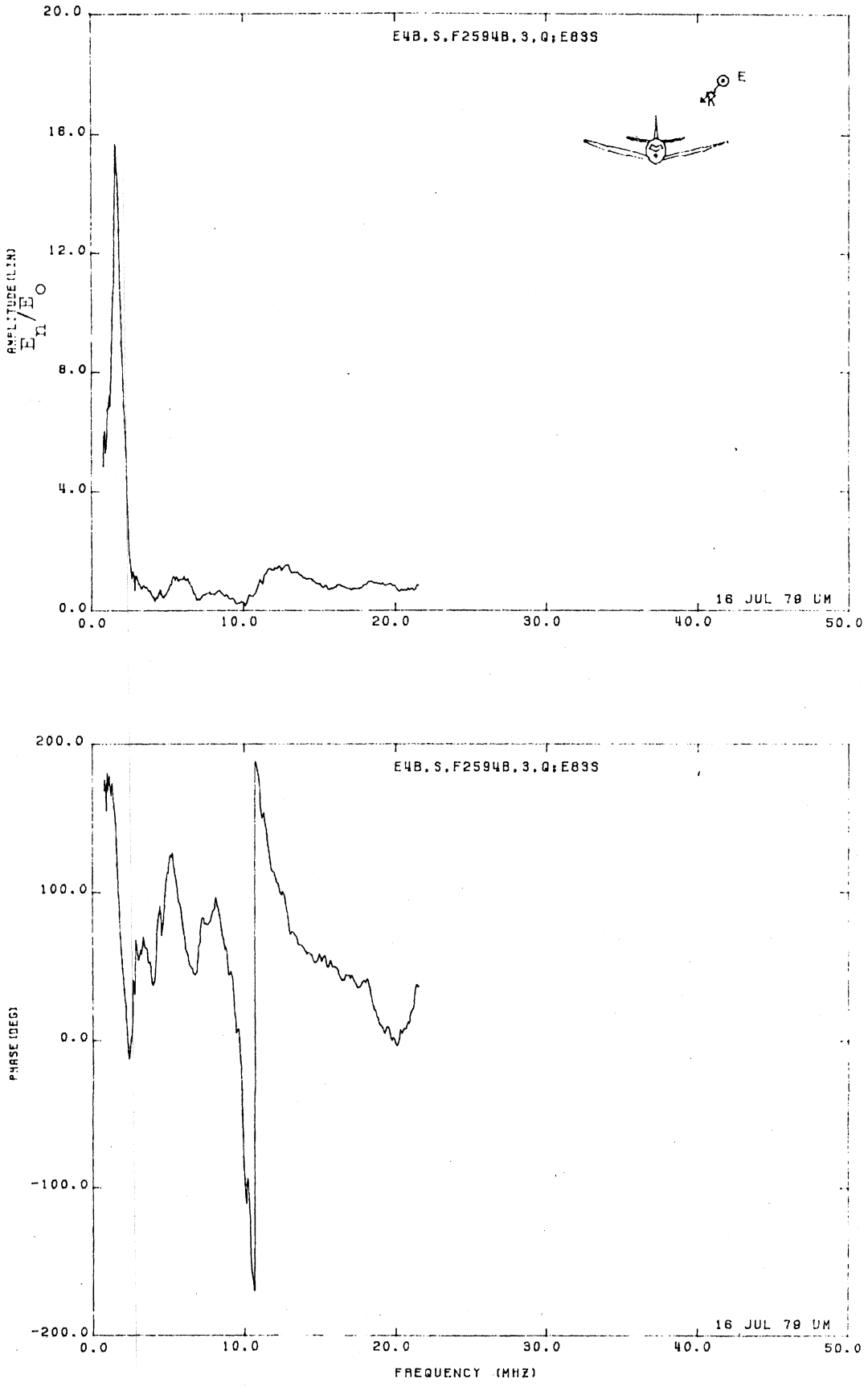

Figure 83S. Normal Electric Field at STA:F2594B, Excitation 3, 1/200 Model.

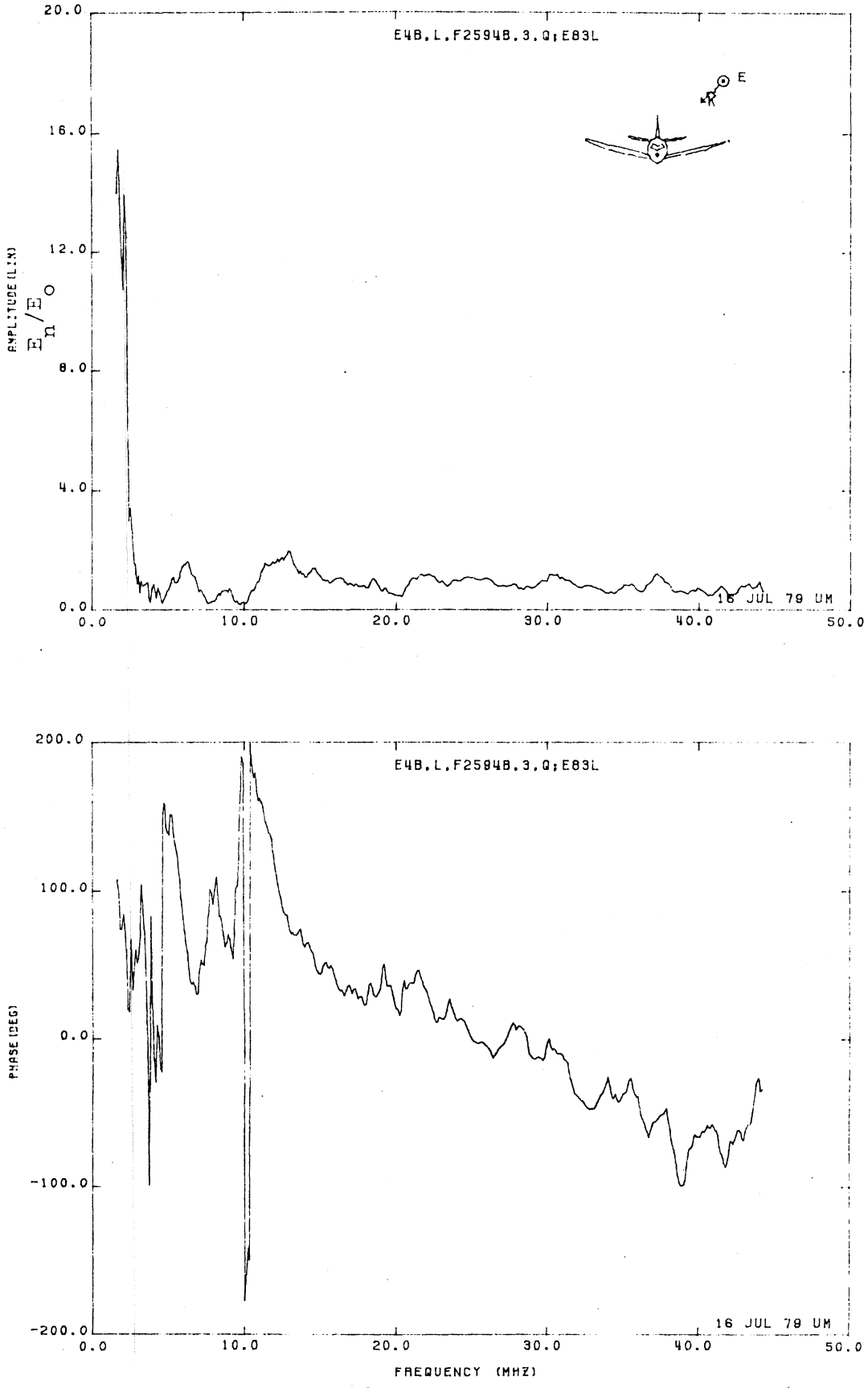

Figure 83L, Normal Electric Field at STA:F2594B, Excitation 3, 1/100 Model.

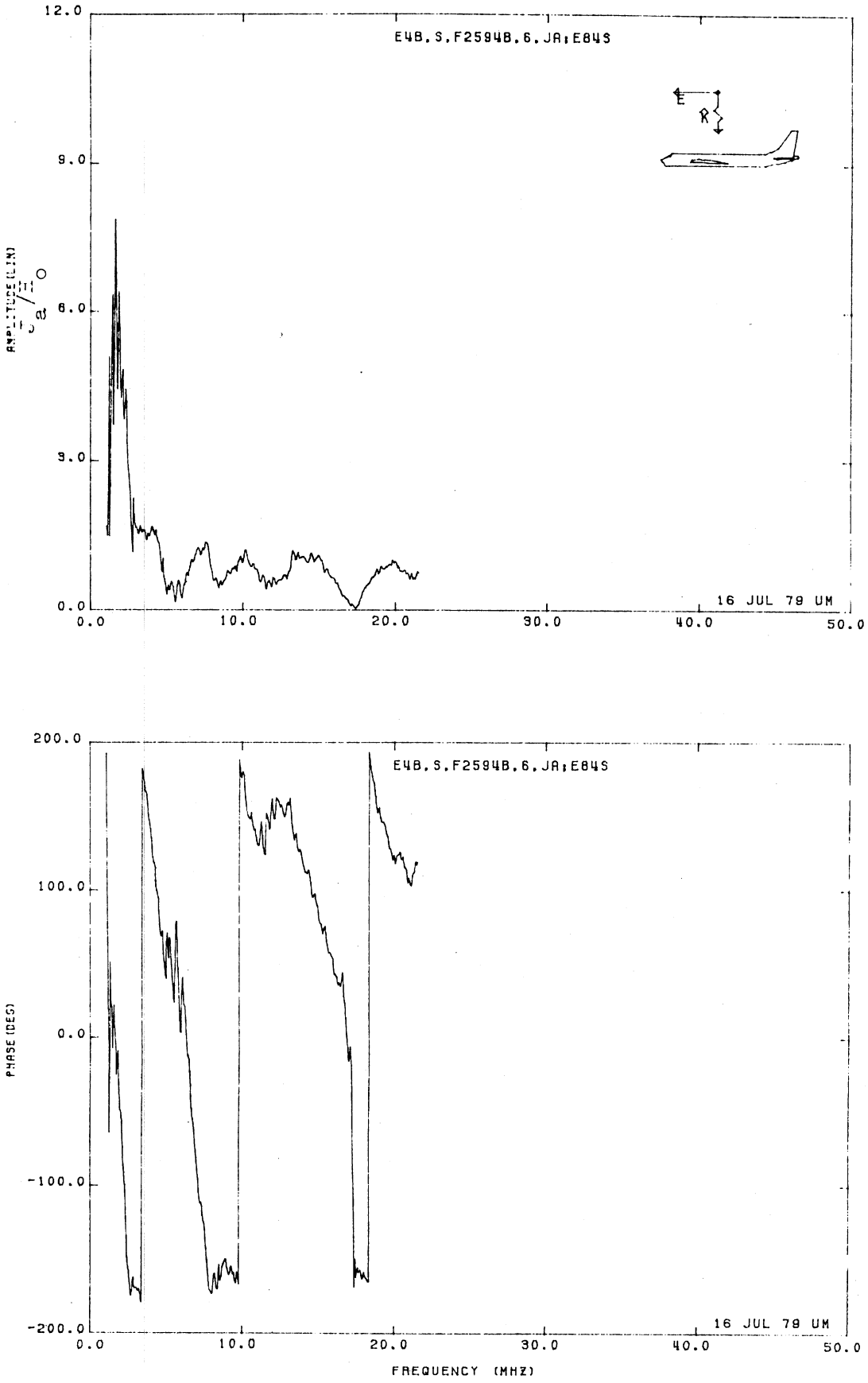

Figure 84S. Axial Current at STA:F2594B, Excitation 6, 1/200 Model.

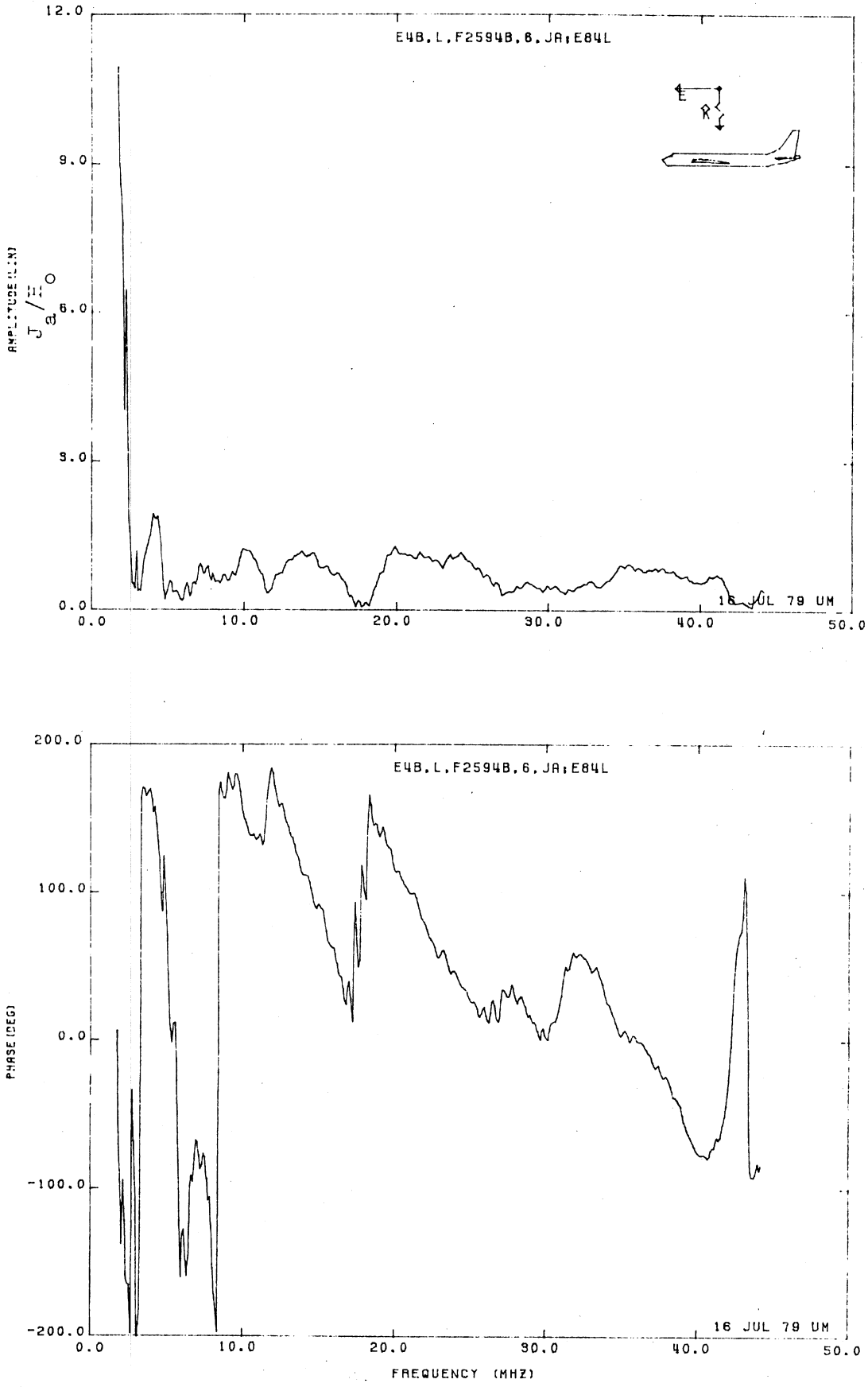

Figure 84L. Axial Current at STA:2594B, Excitation 6, 1/100 Model.

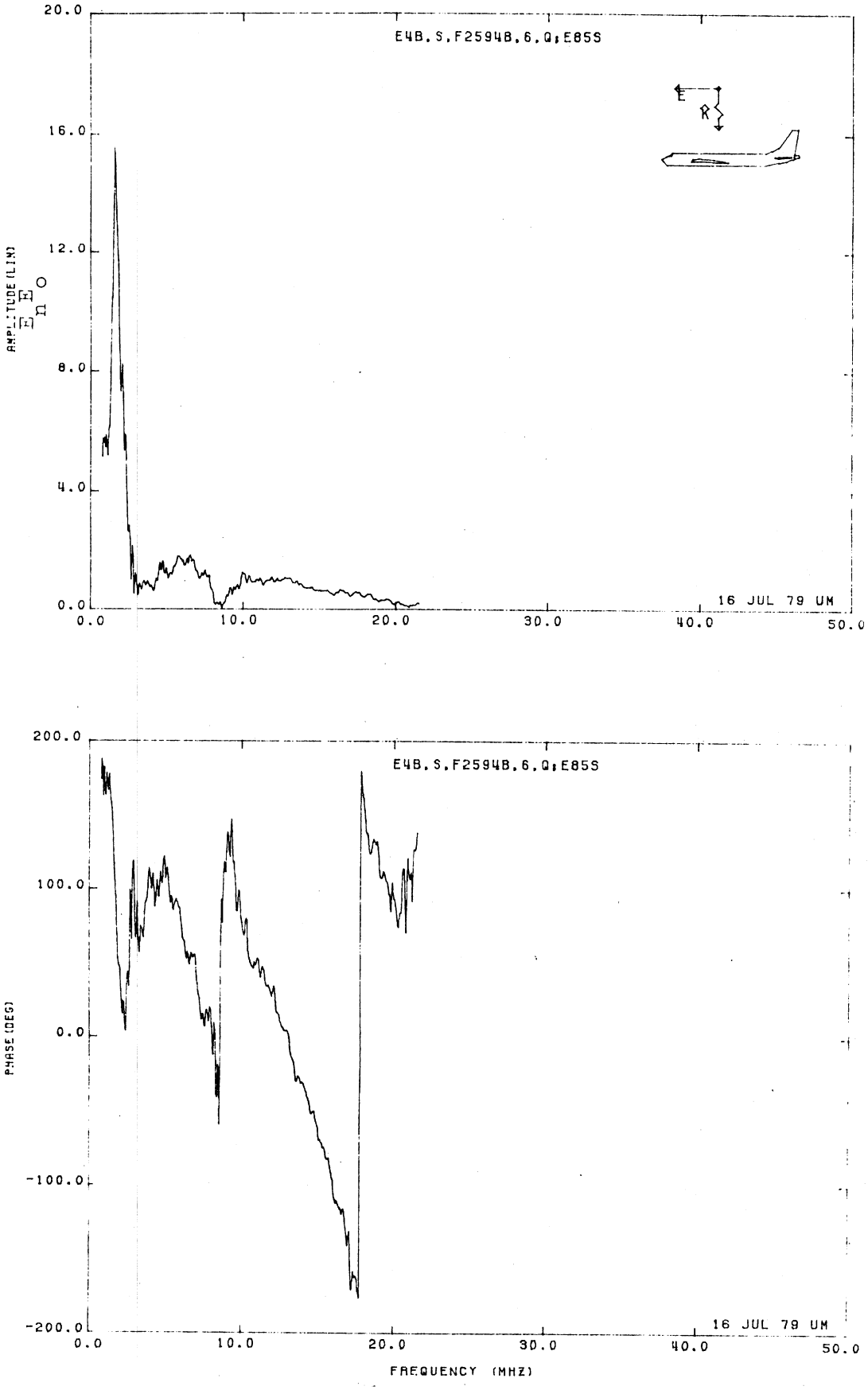

Figure 85S. Normal Electric Field at STA:F2594B, Excitation 6, 1/200 Model.

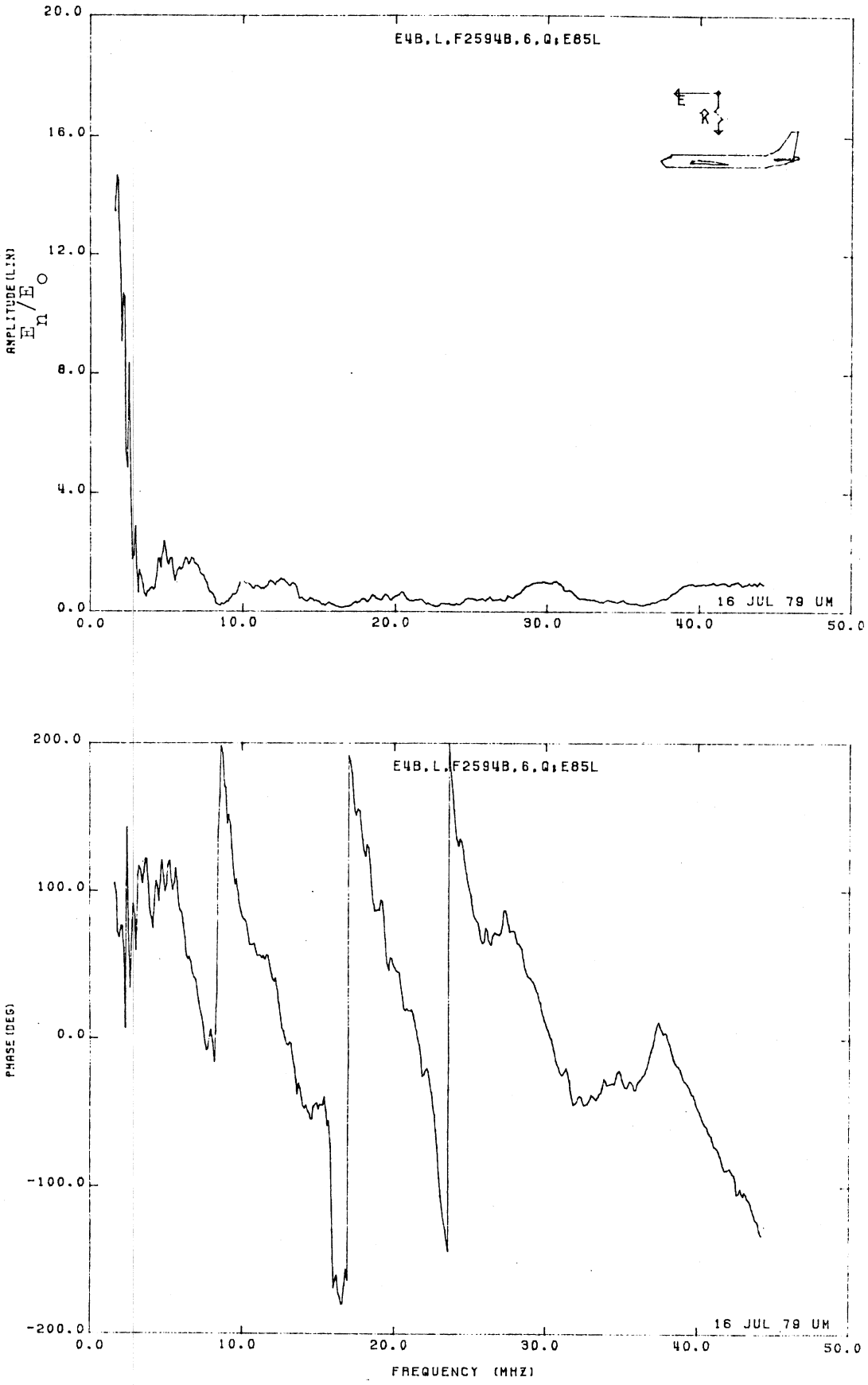

Figure 85L. Normal Electric Field at STA:F2594B, Excitation 6, 1/100 Model.

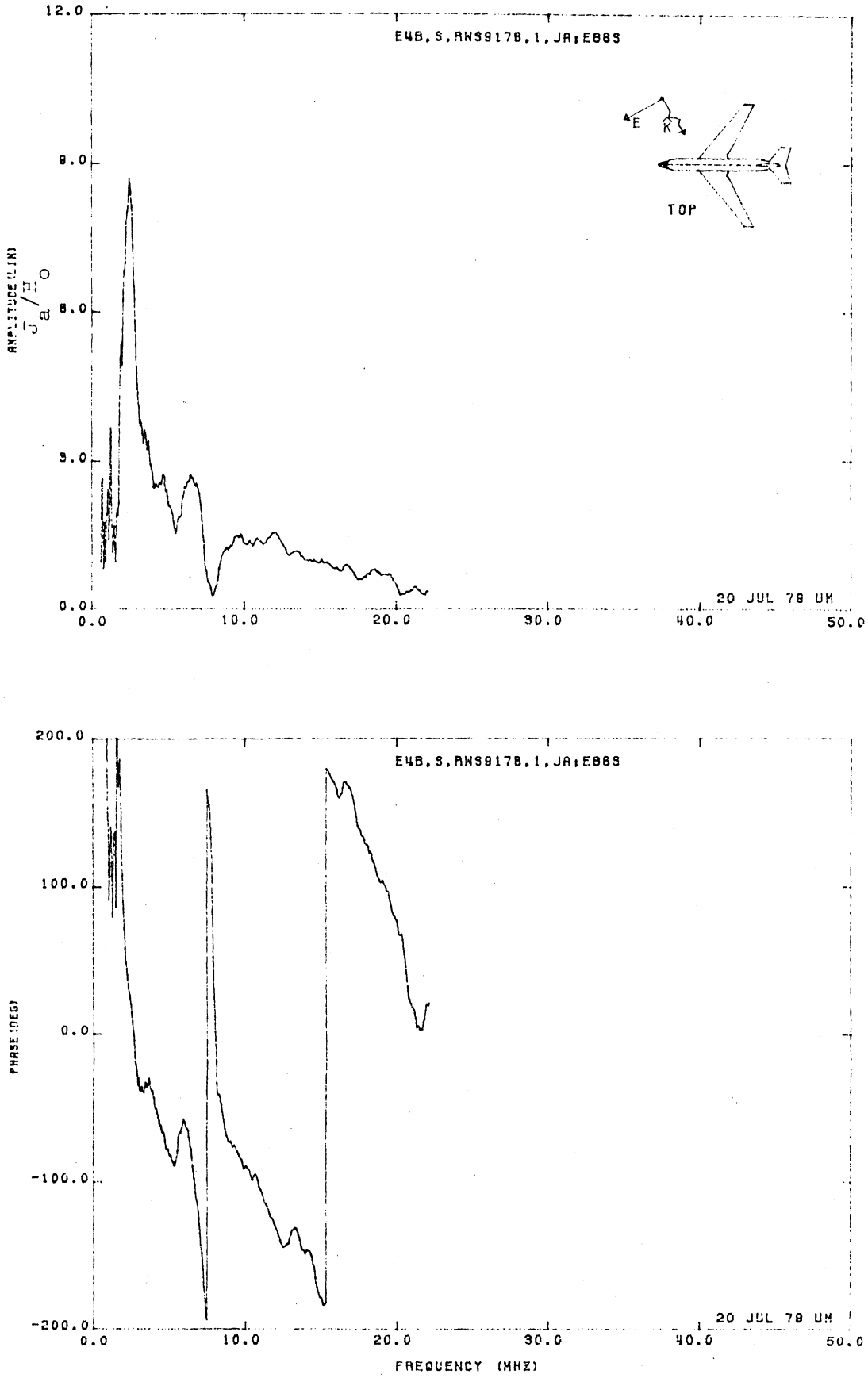

Figure 86S. Axial Current at STA:RWS917B, Excitation 1, 1/200 Model.

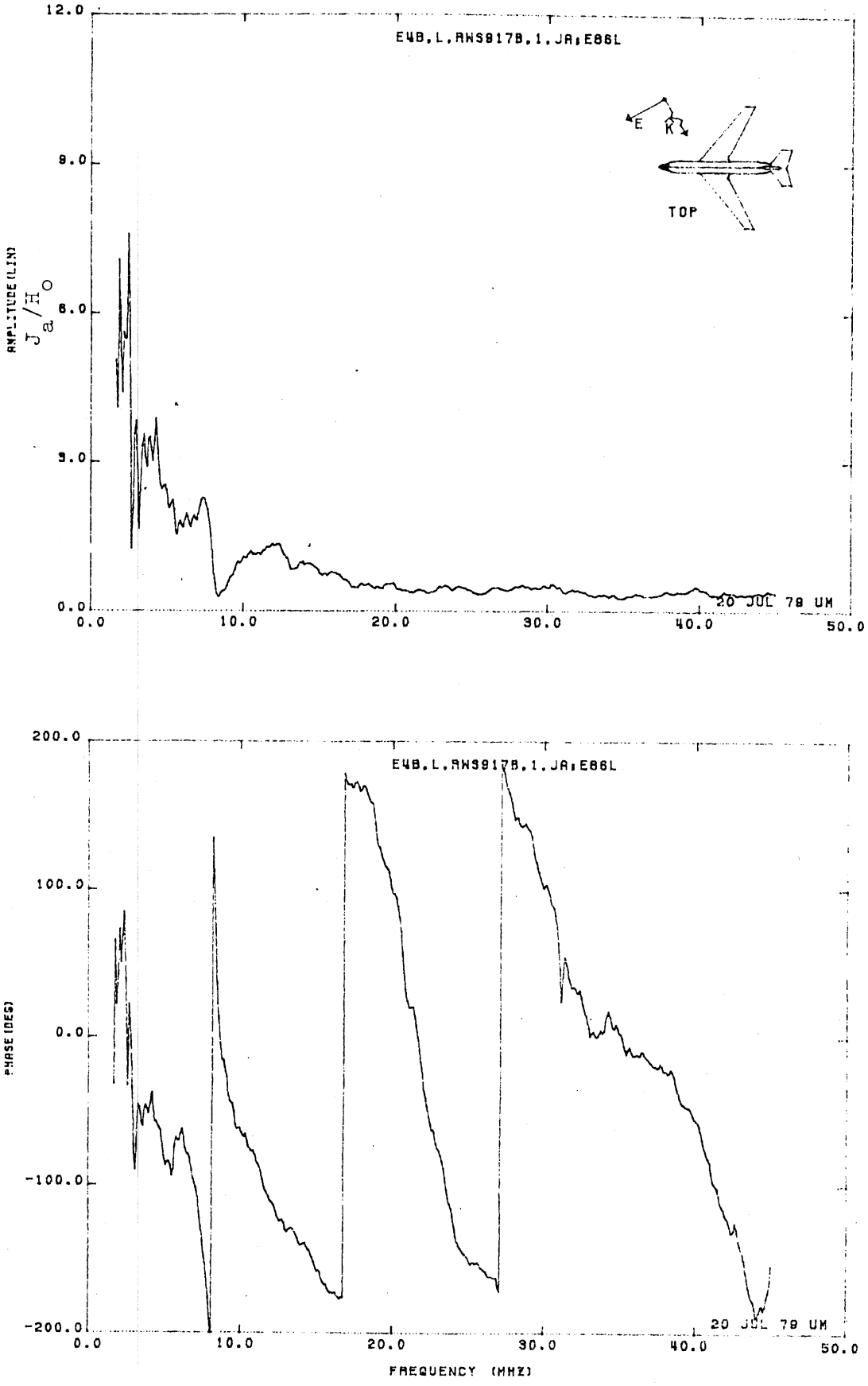

Figure 86L. Axial Current at STA:RWS917B, Excitation 1, 1/100 Model.

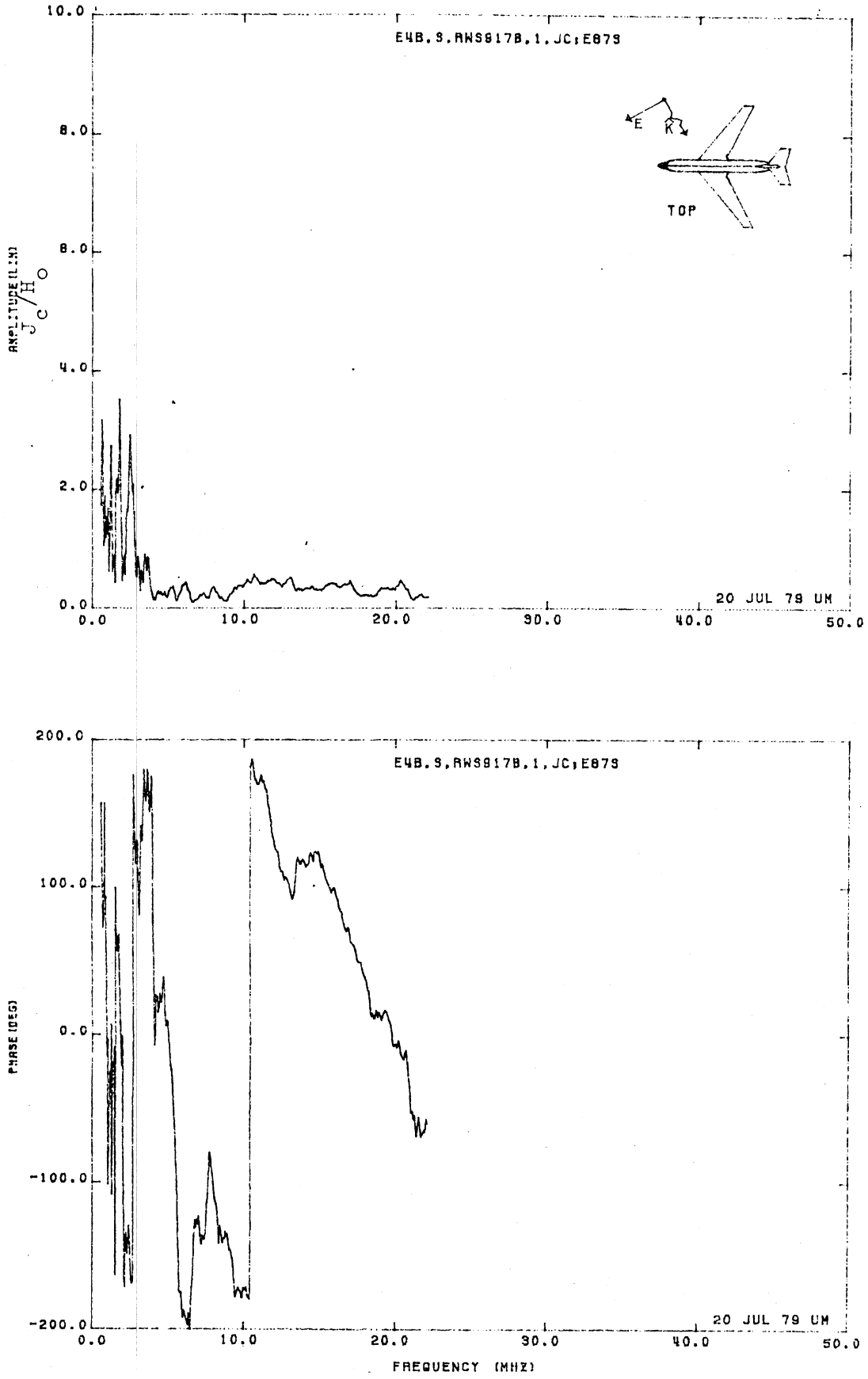

Figure 87S. Circumferential Current at STA:RWS917B, Excitation 1, 1/200 Model.

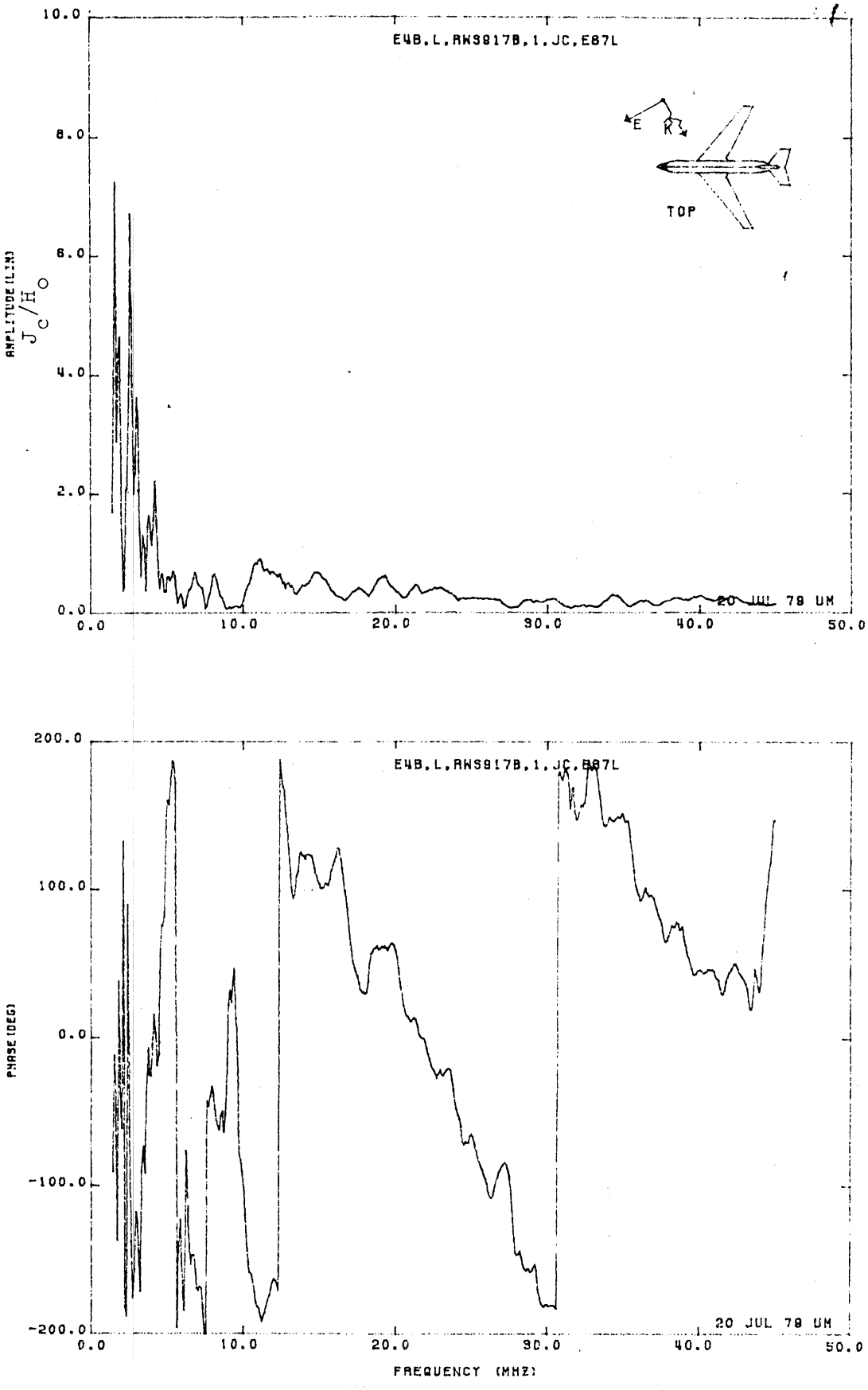

Figure 87L. Circumferential Current at ST:RWS917B, Excitation 1, 1/100 Model.

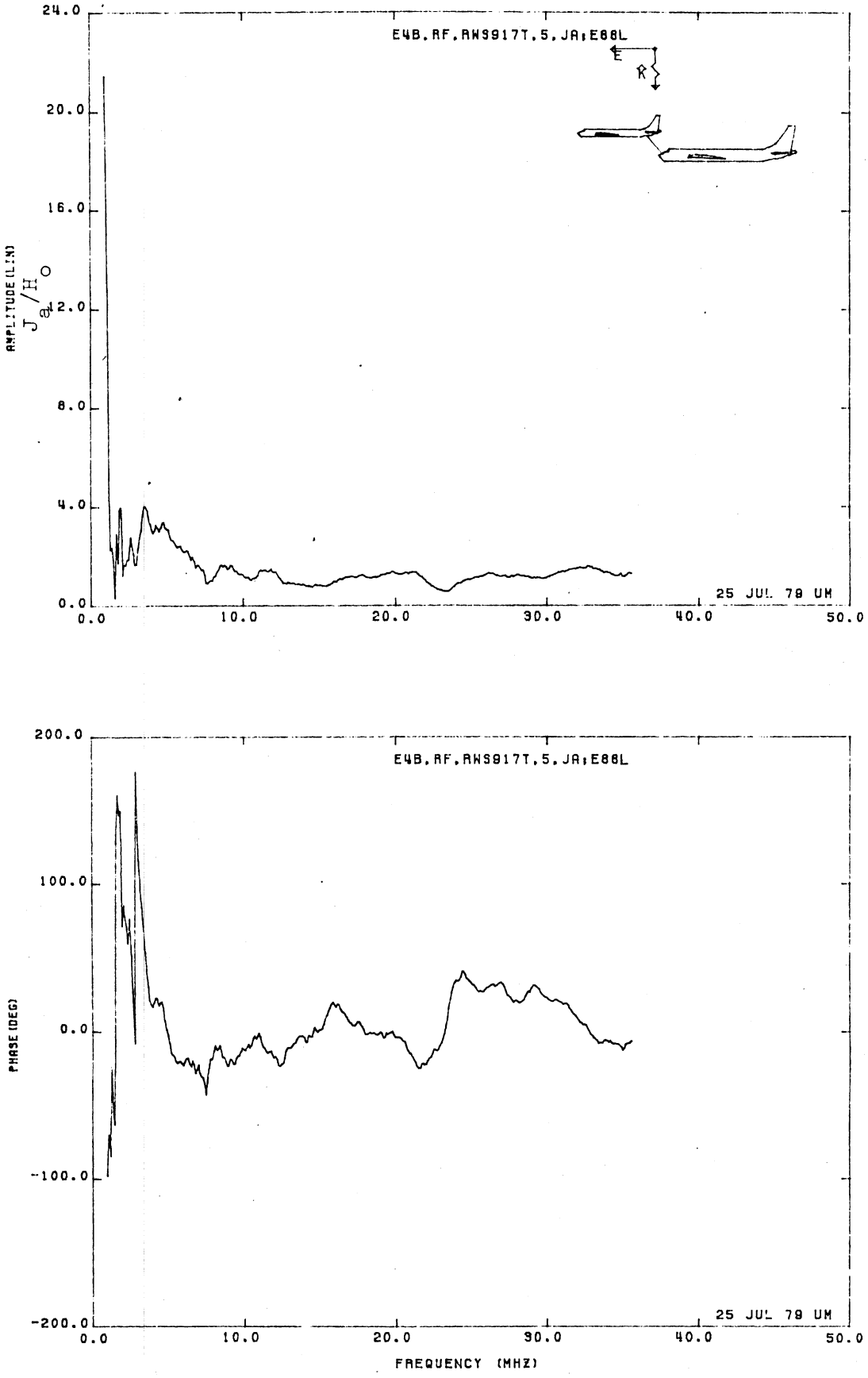

Figure 88L. Axial Current at STA:RWS917T, Excitation 5, 1/125 Model. (Refueling Mode)

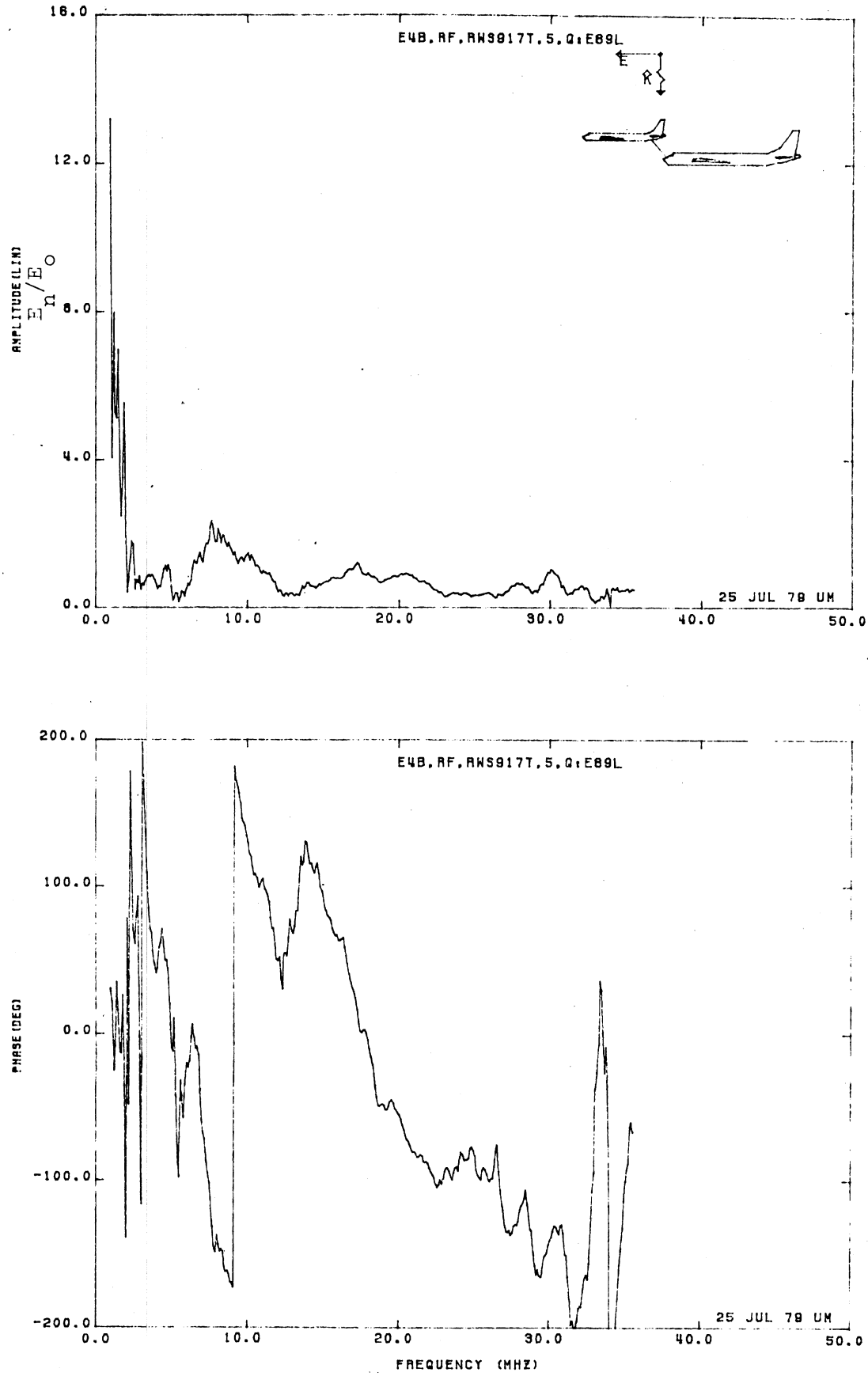

Figure 89L. Normal Electric Field at STA:RWS917T, Excitation 5 1/125 Model. (Refueling Mode)

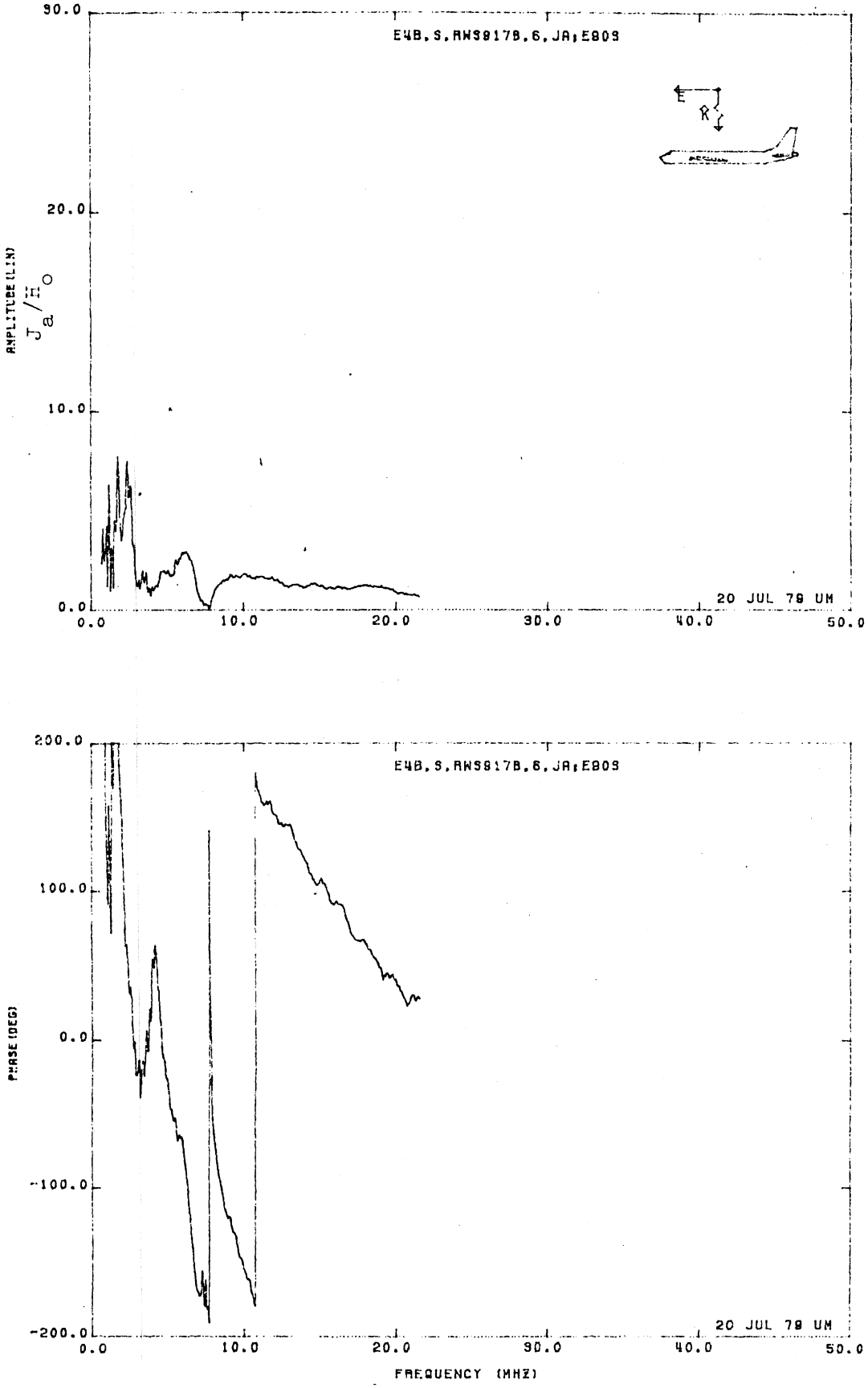

Figure 90S. Axial Current at STA:RWS917B, Excitation 6, 1/200 Model.

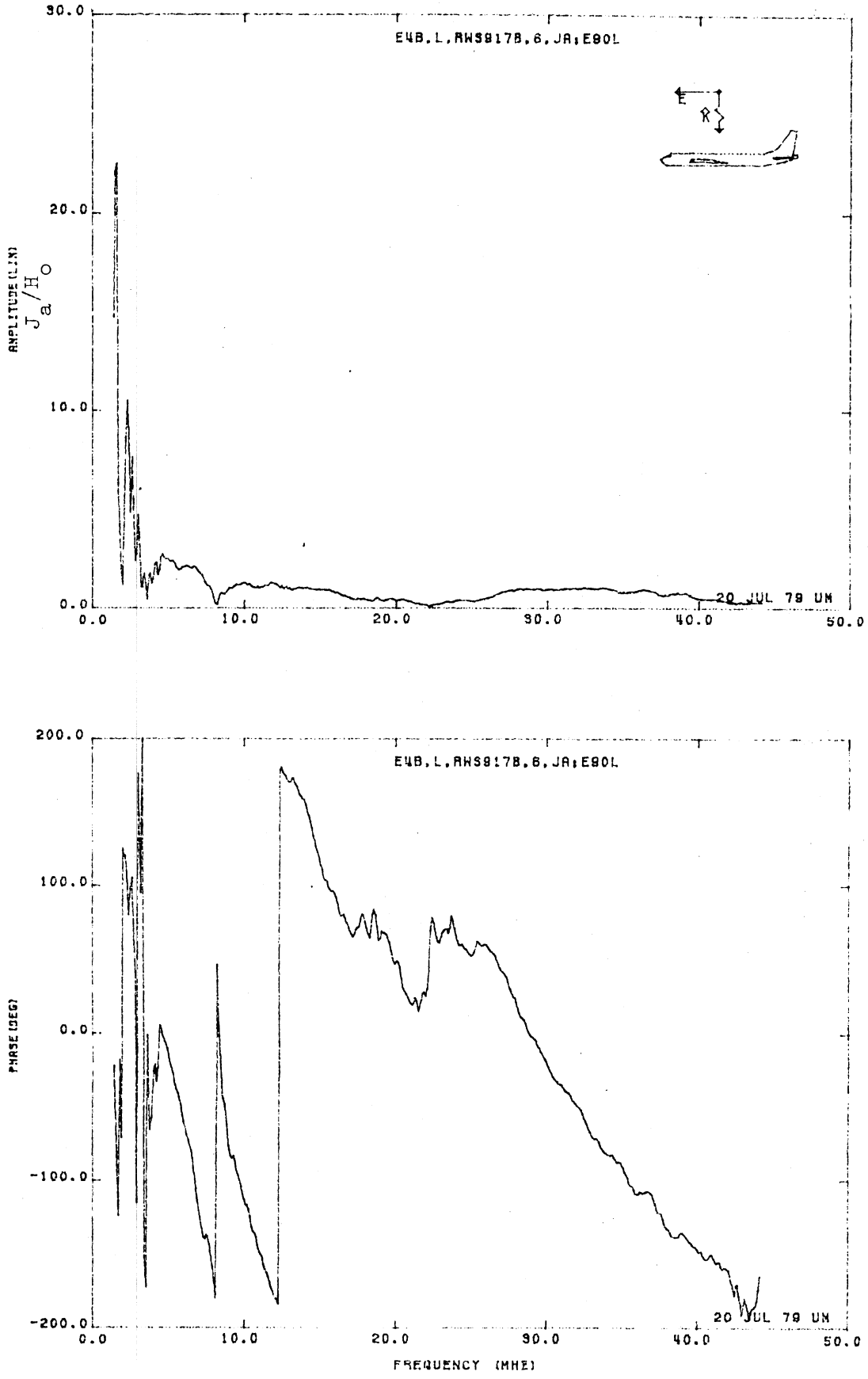

Figure 90L. Axial Current at STA:RWS917B, Excitation 6, 1/100 Model.

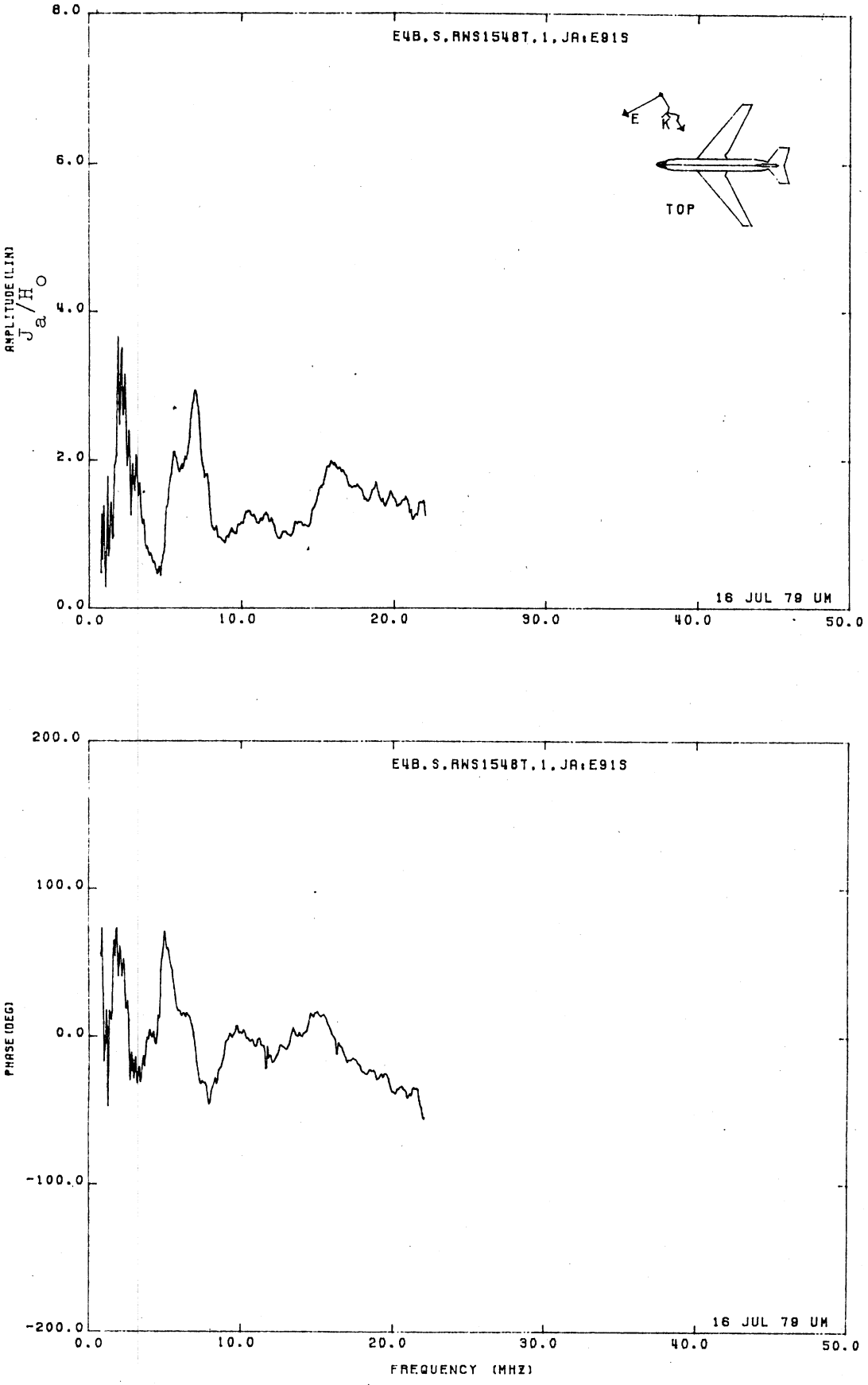

Figure 91S. Axial Current at STA:RWS1548T, Excitation 1, 1/200 Model.

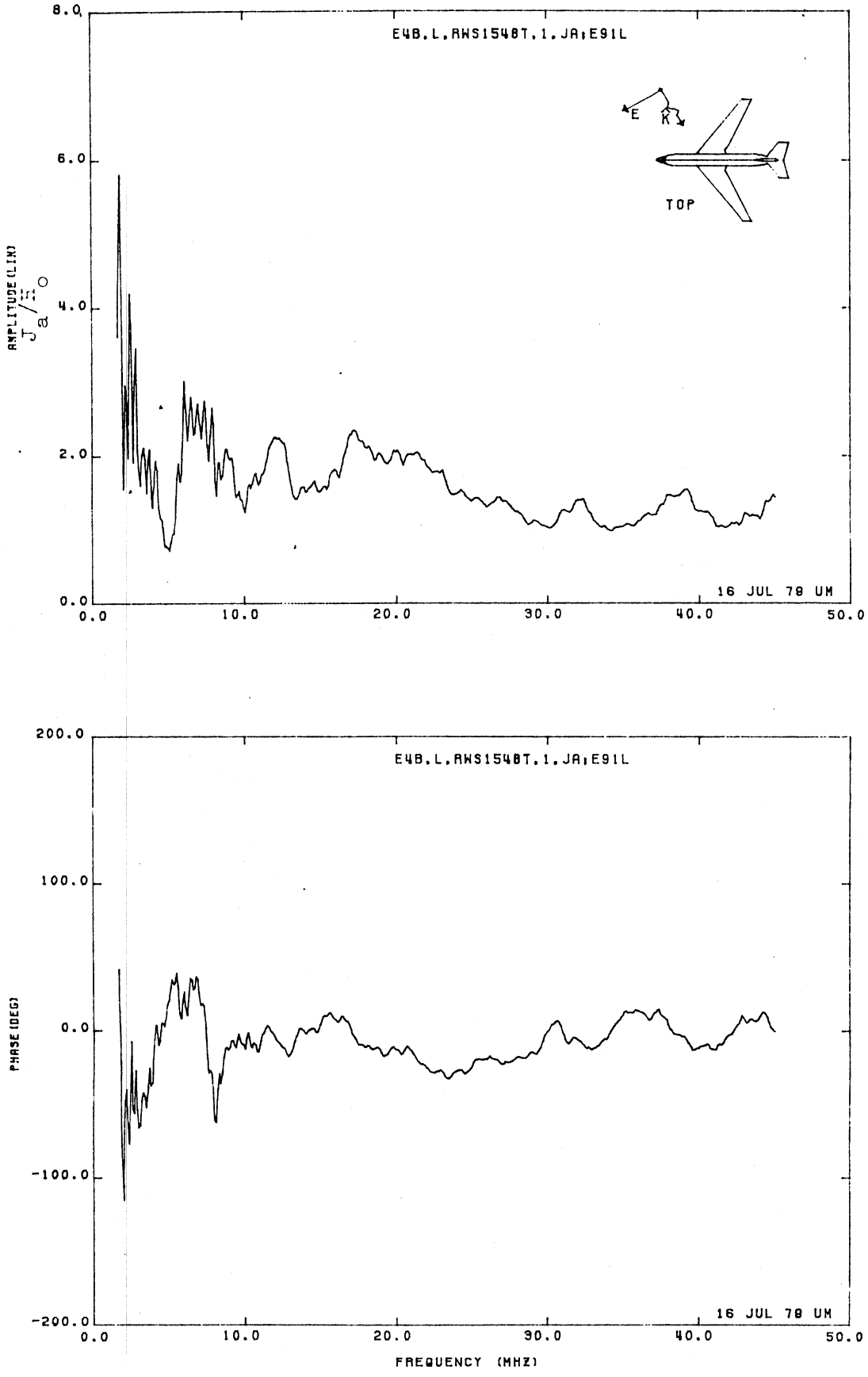

Figure 91L. Axial Current at STA:RWS1548T, Excitation 1, 1/100 Model.

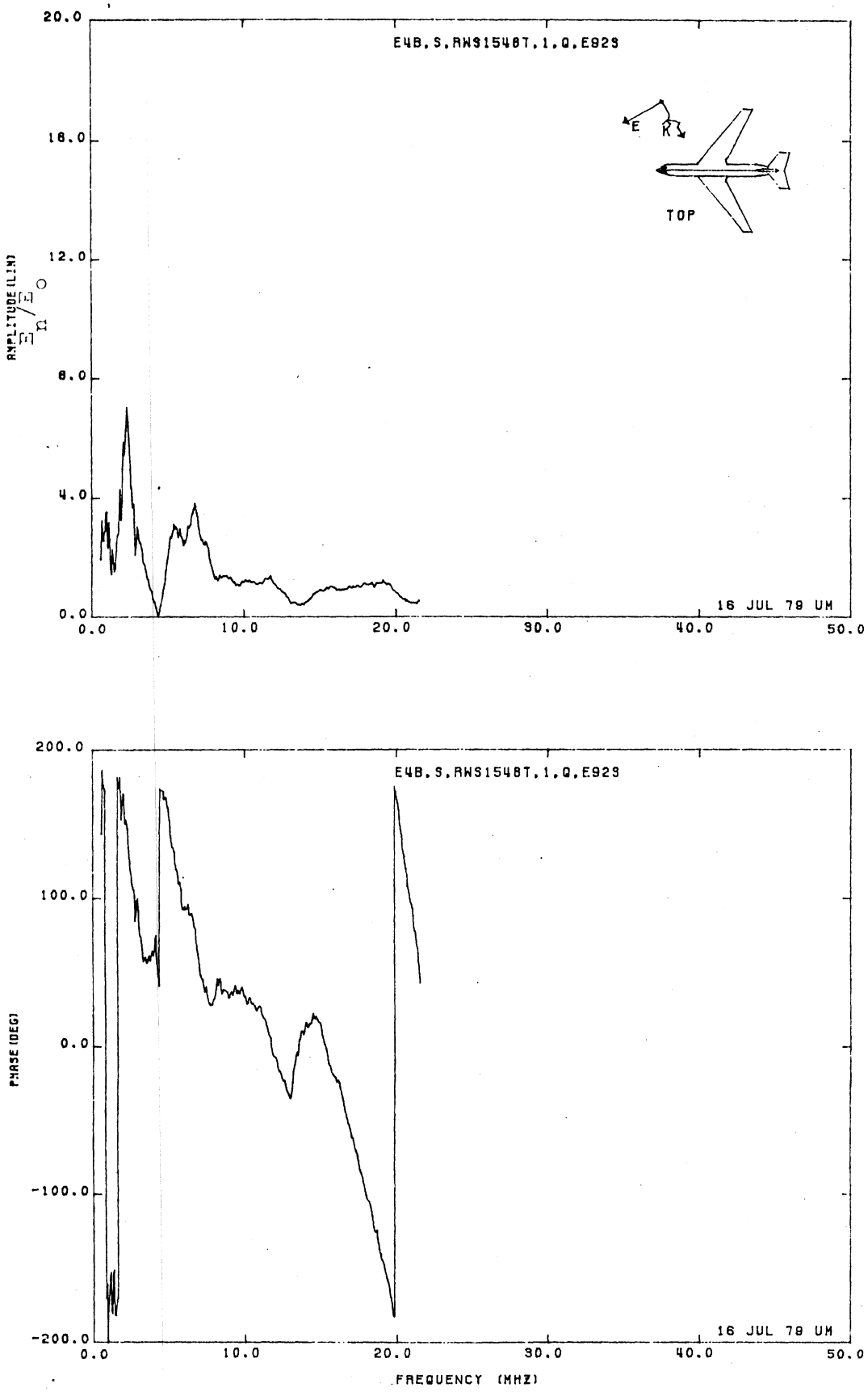

Figure 92S. Normal Electric Field at STA:RWS1548T, Excitation 1, 1/200 Model.

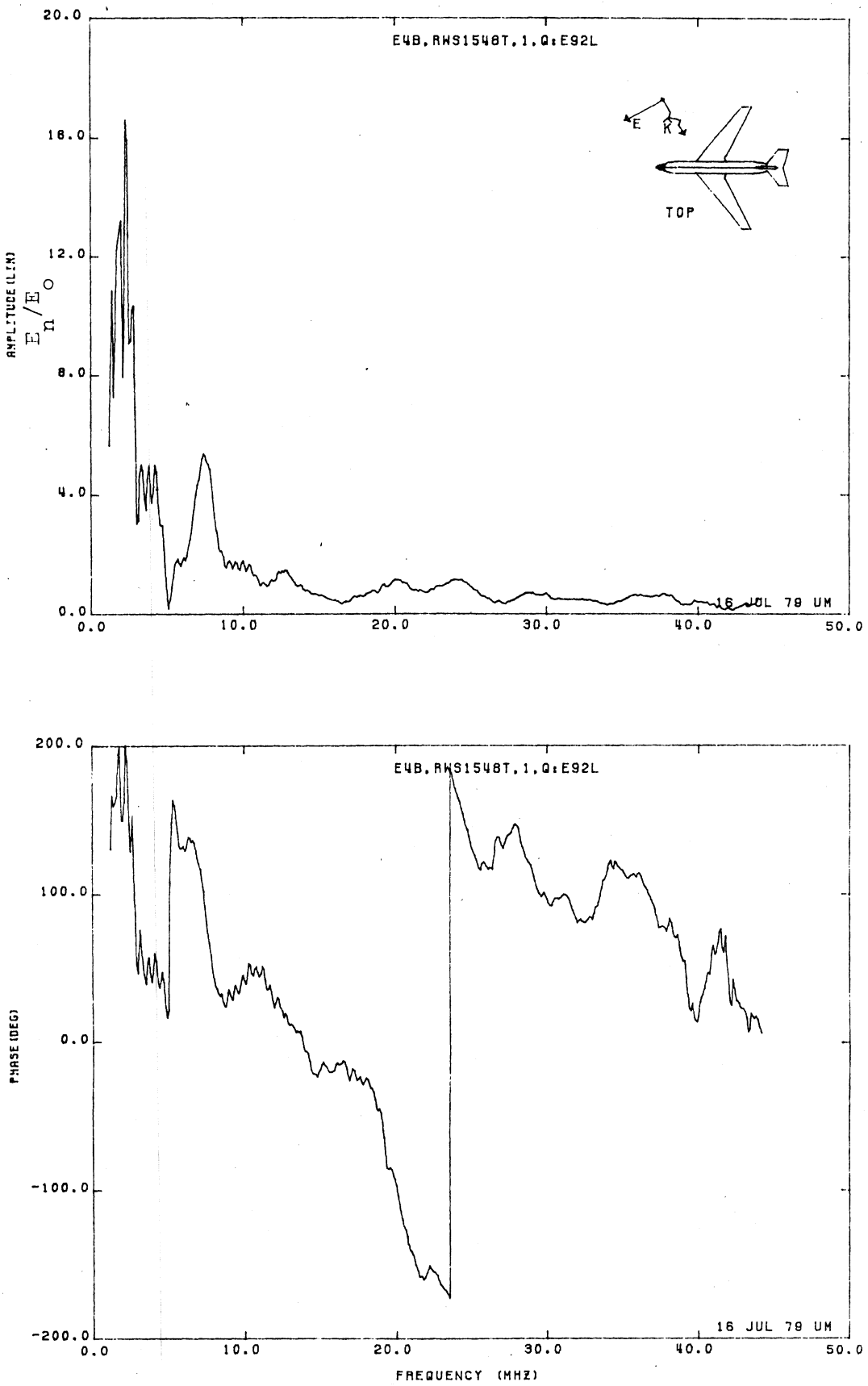

Figure 92L. Normal Electric Field at STA:RWS1548T, Excitation 1, 1/100 Model.

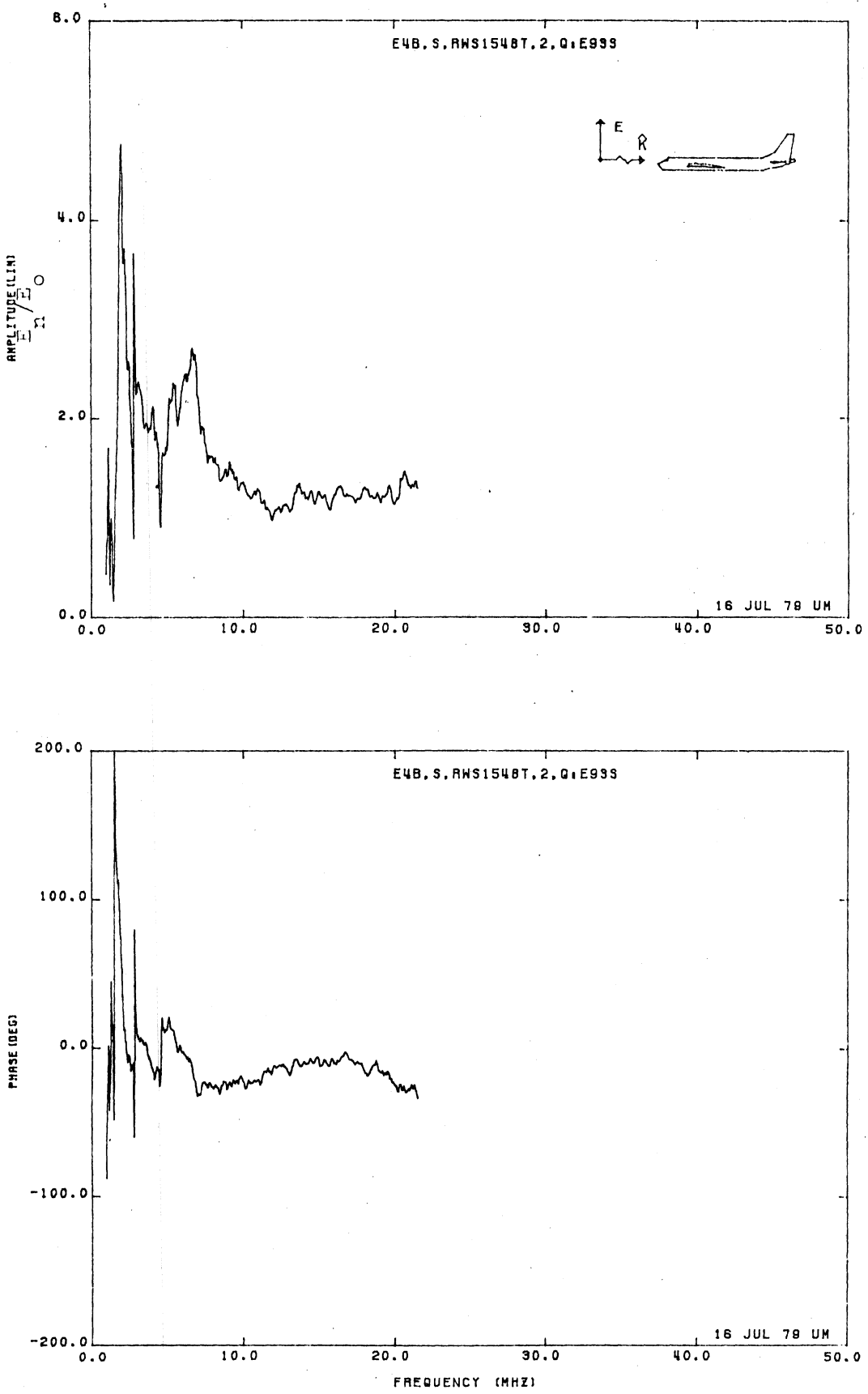

Figure 93S. Normal Electric Field at STA:RWS1548T, Excitation 2, 1/200 Model.

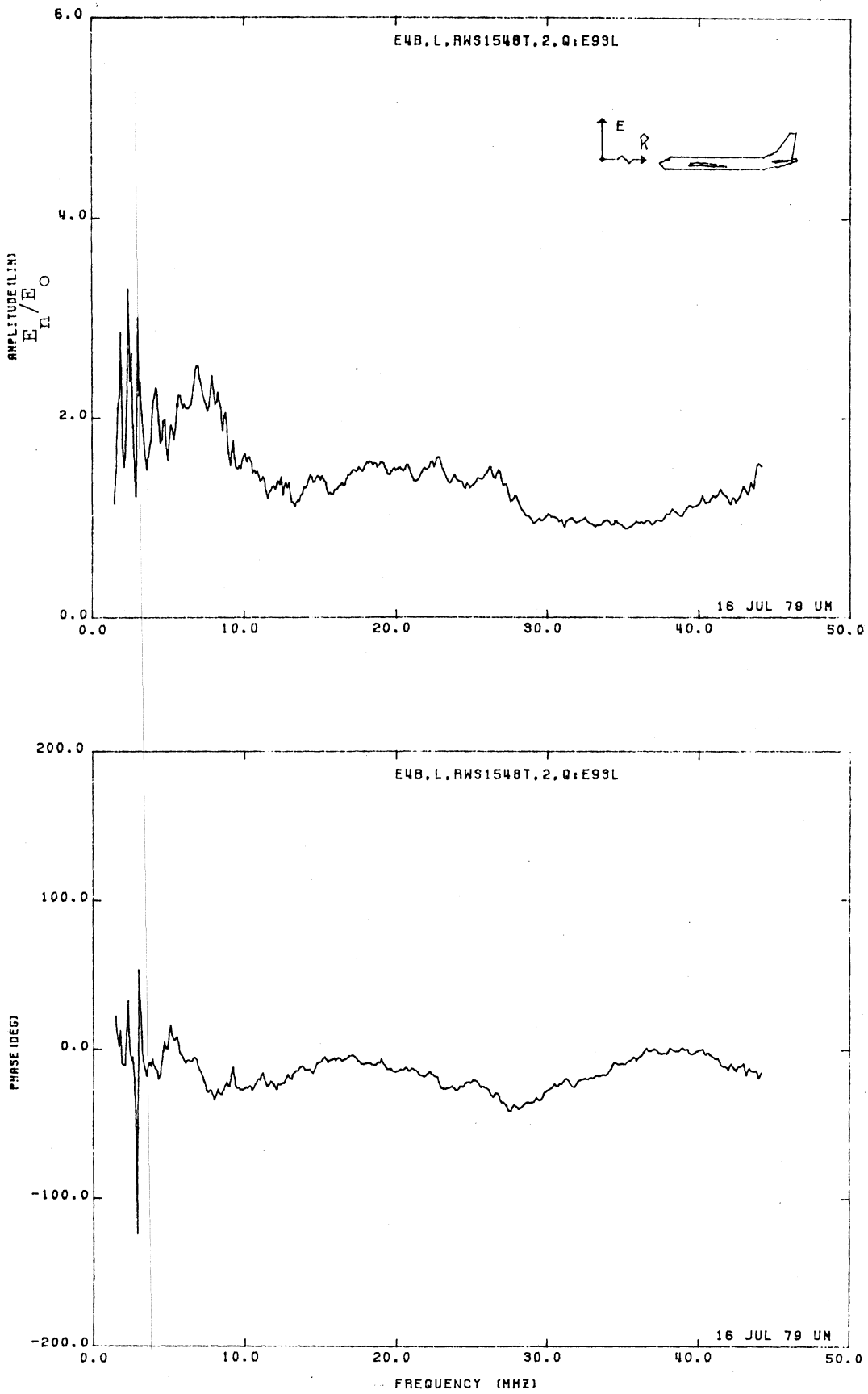

Figure 93L. Normal Electric Field at STA:RWS1548T, Excitation 2, 1/100 Model.

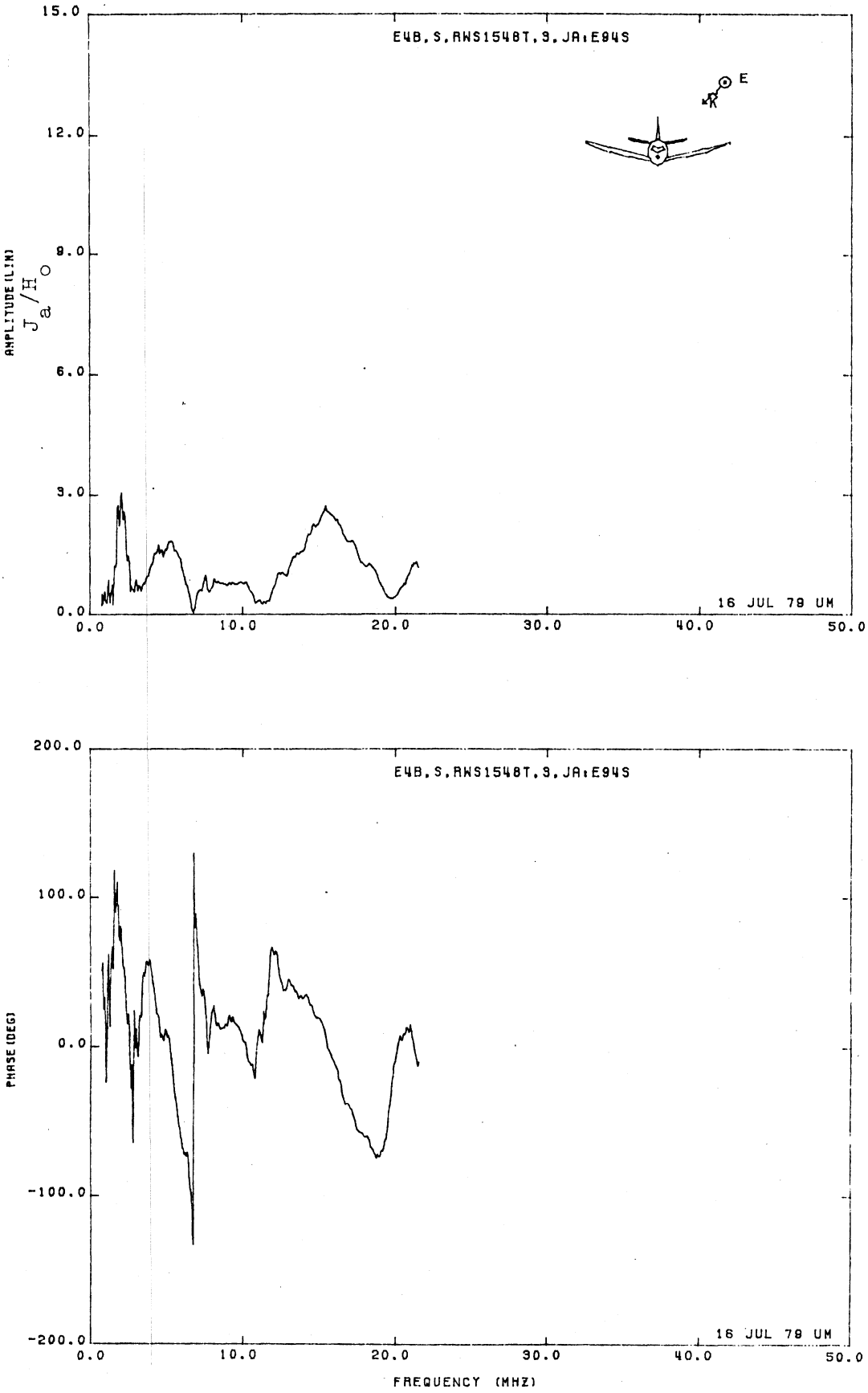

Figure 94S. Axial Current at STA:RWS1548T, Excitation 3, 1/200 Model.

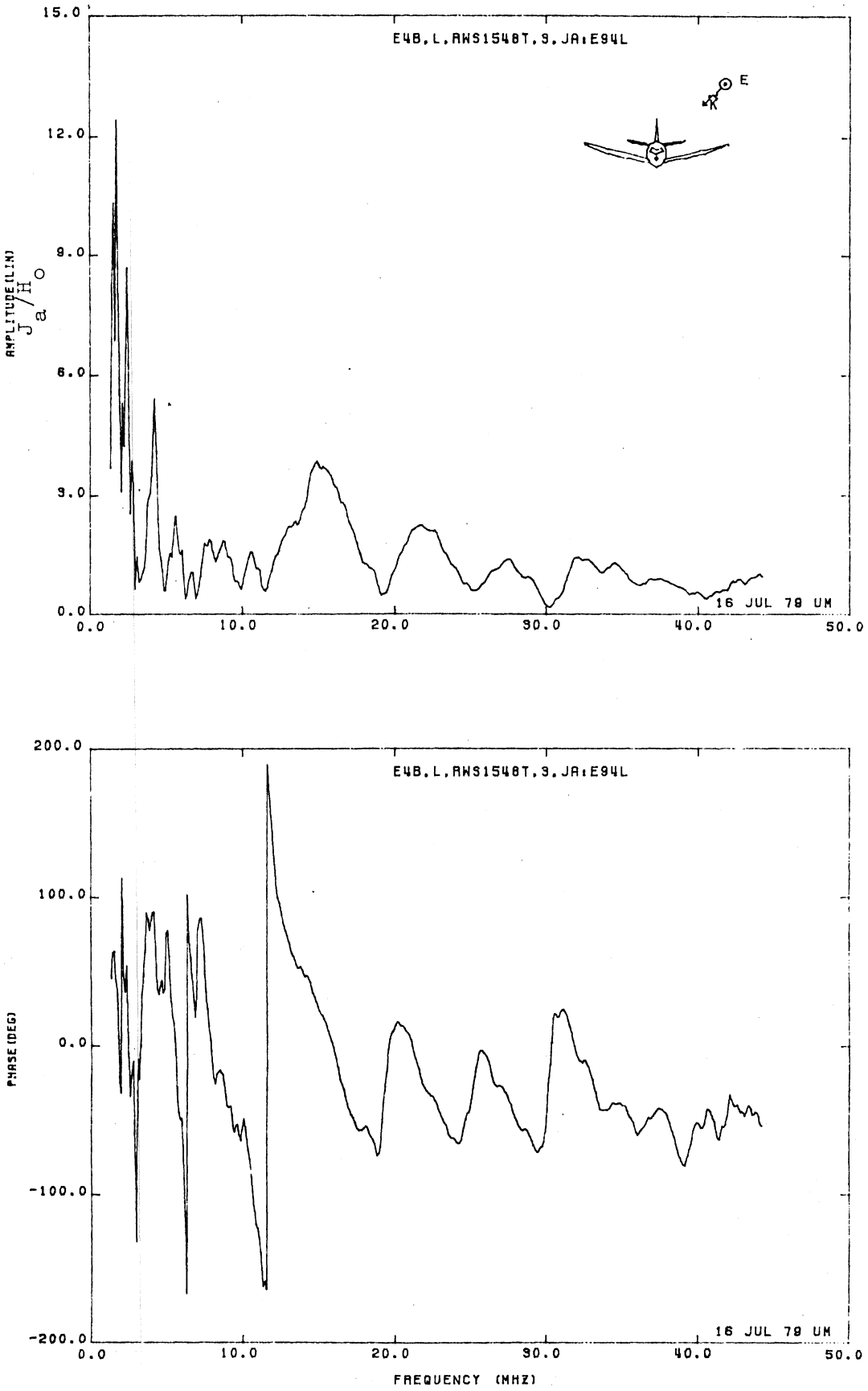

Figure 94L. Axial Current at STA:RWS1548T, Excitation 3, 1/100 Model.

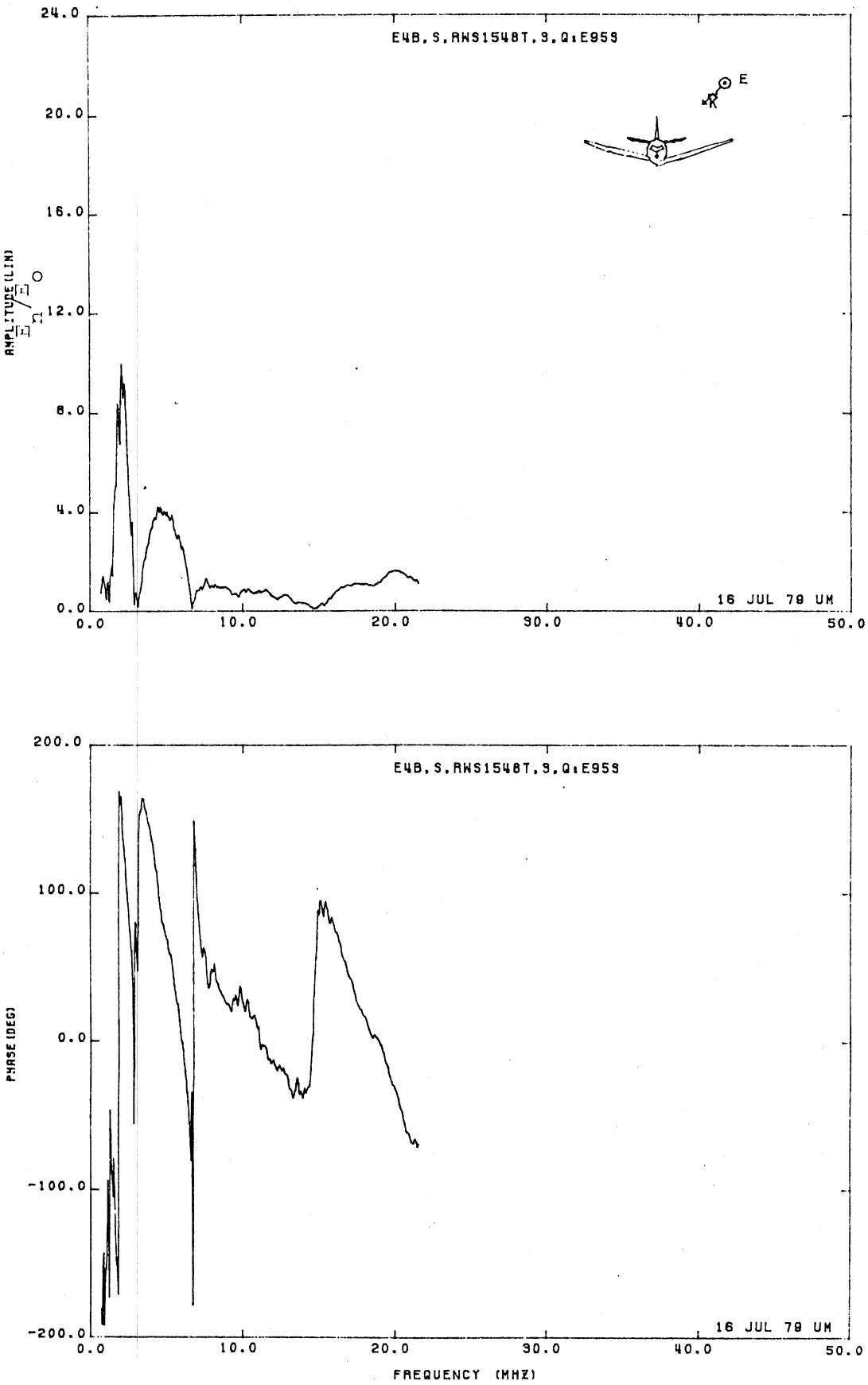

Figure 95S. Normal Electric Field at STA:RWS1548T, Excitation 3, 1/200 Model.

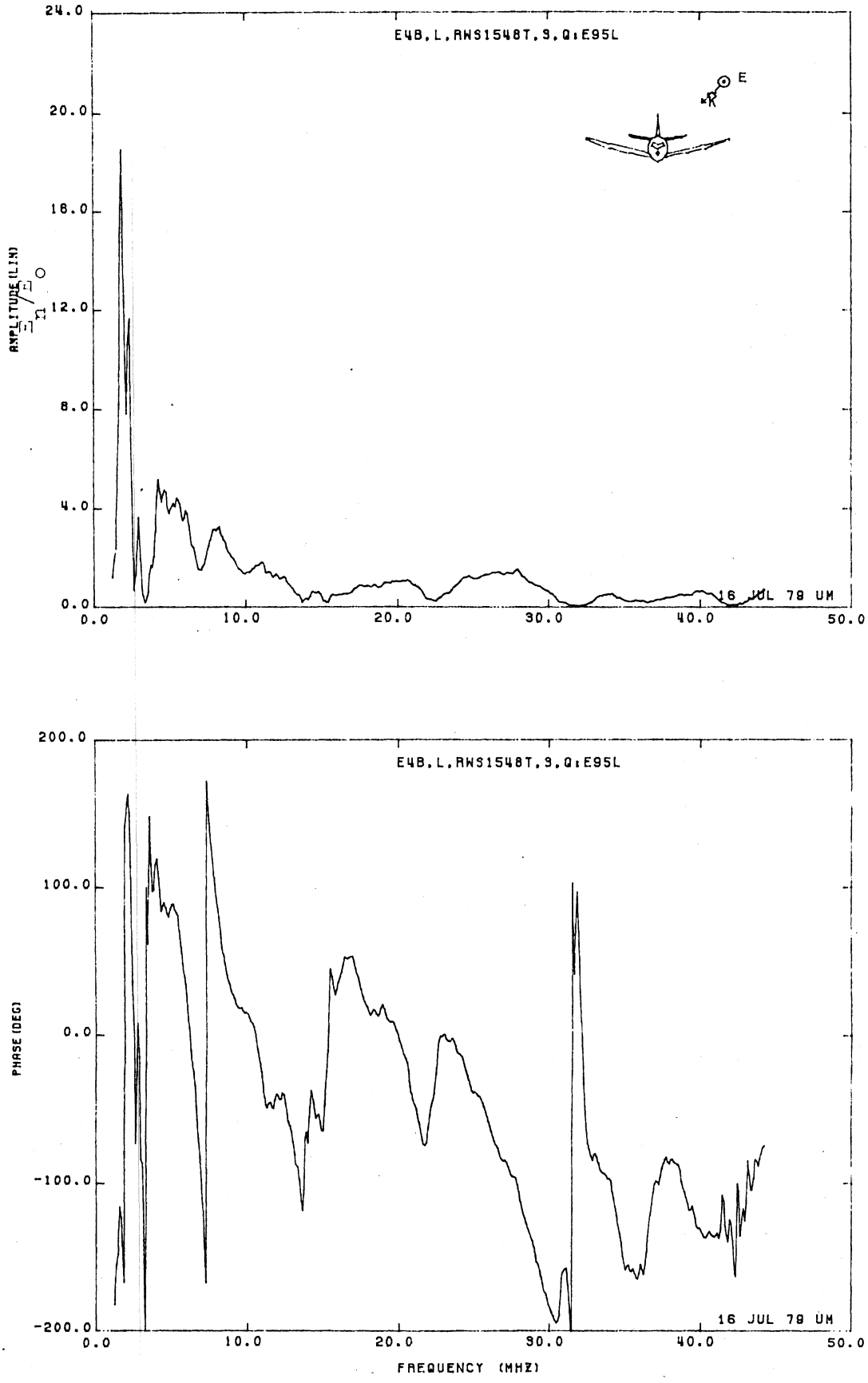

Figure 95L. Normal Electric Field at STA:RWS1548T, Excitation 3, 1/100 Model.

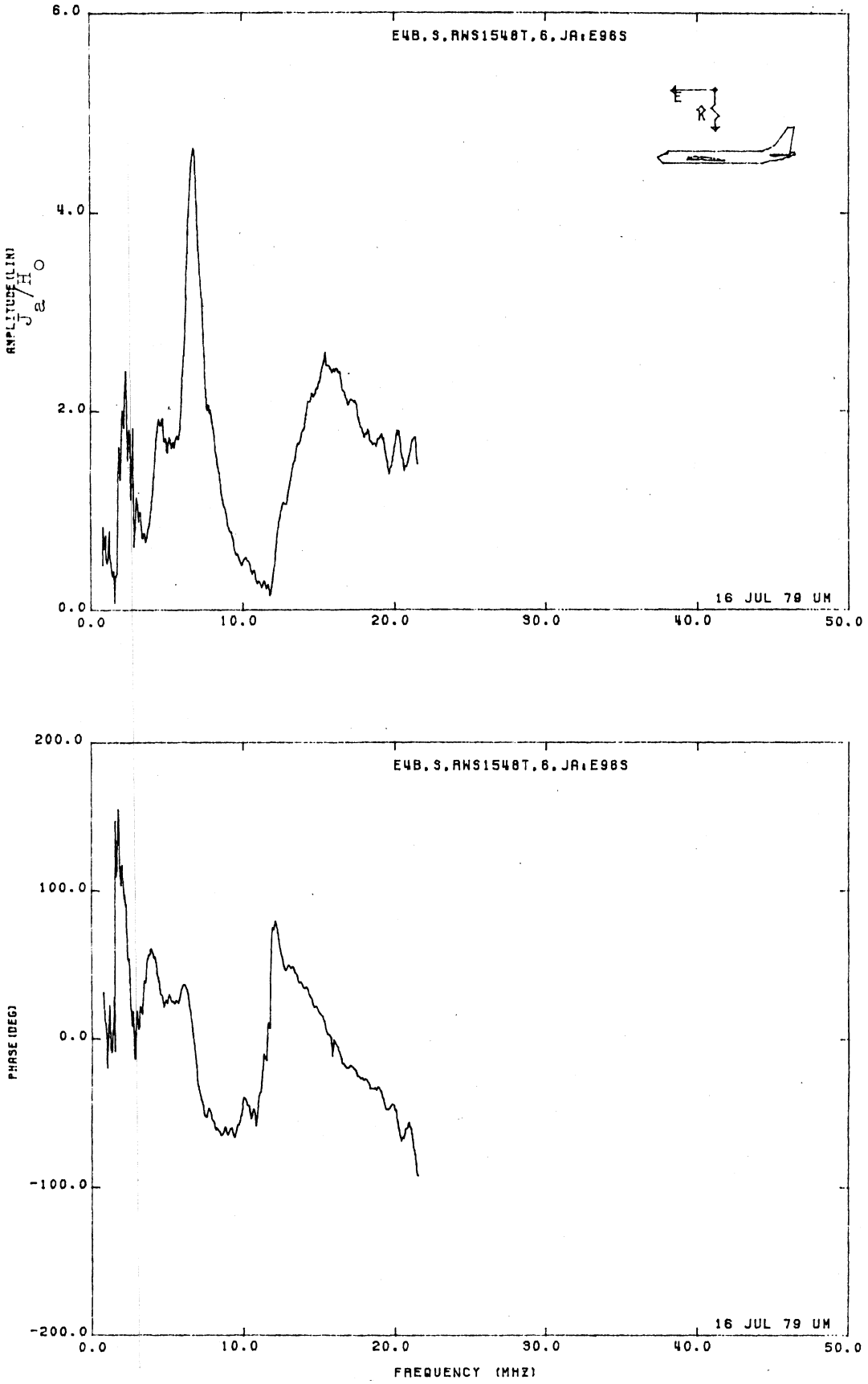

Figure 96S. Axial Current at STA:RSW1548T, Excitation 6, 1/200 Model.

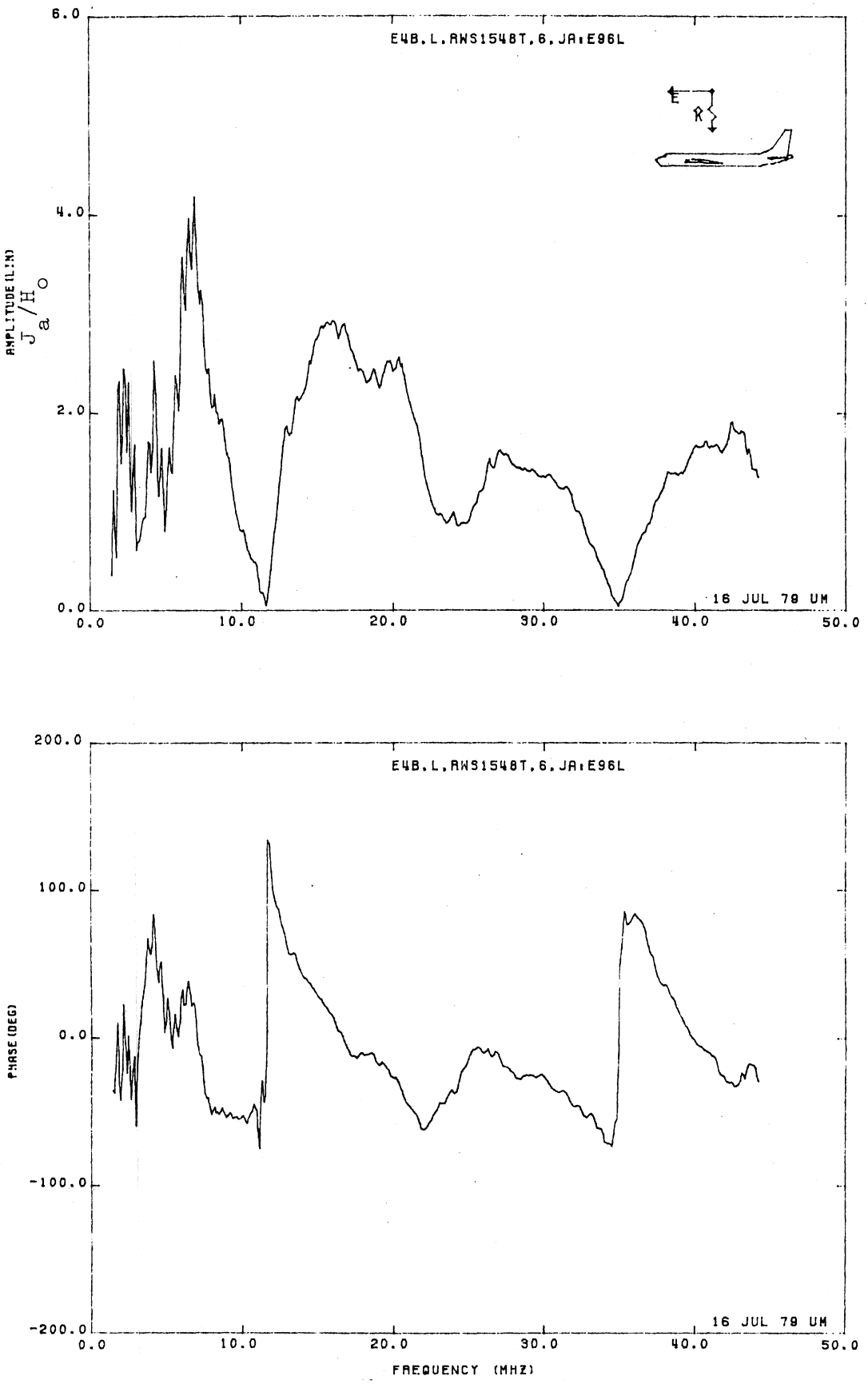

Figure 96L. Axial Current at STA:RWS1458T, Excitation 6, 1/100 Model.

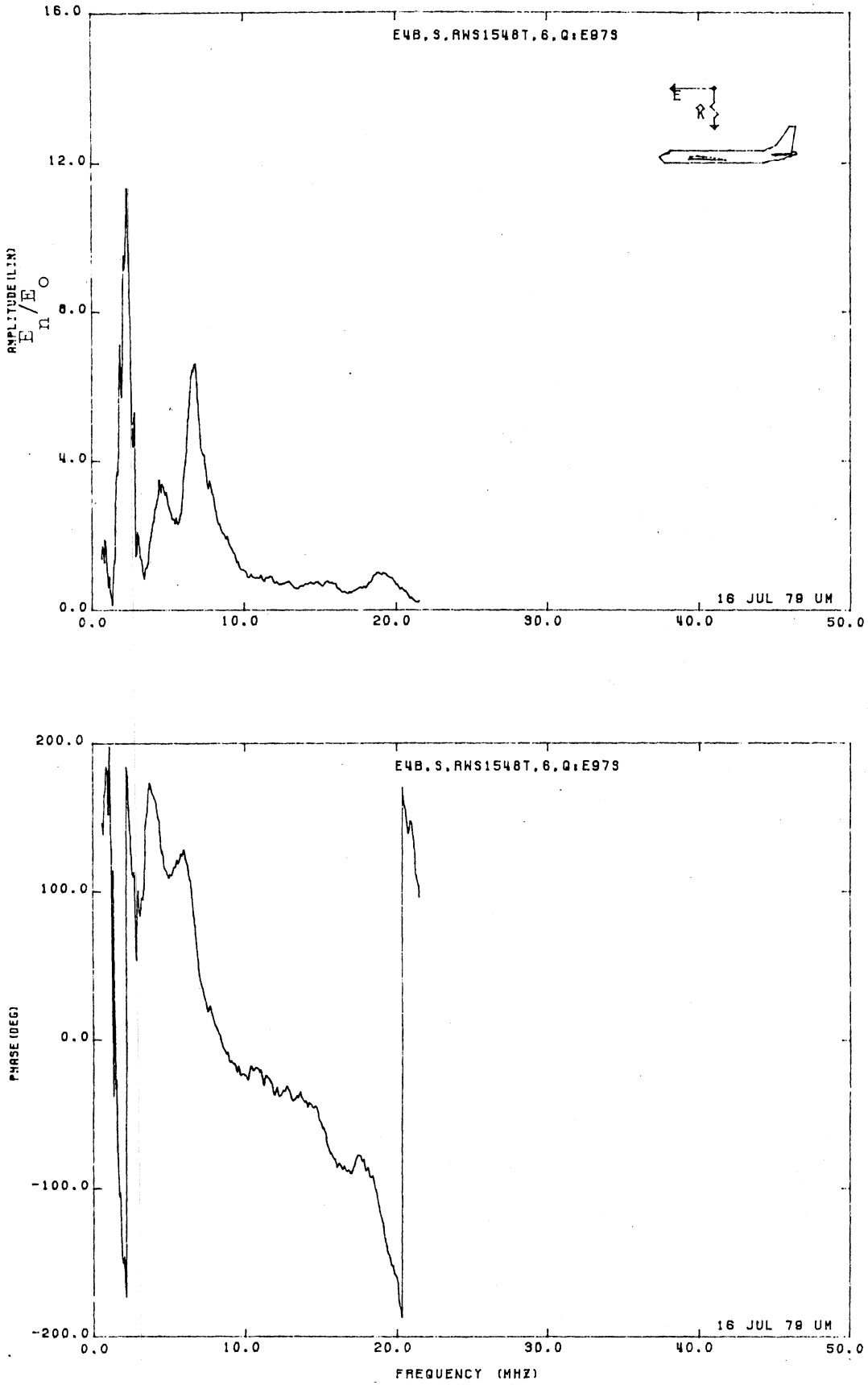

Figure 97S. Normal Electric Field at STA:RWS1548T, Excitation 6, 1/200 Model.

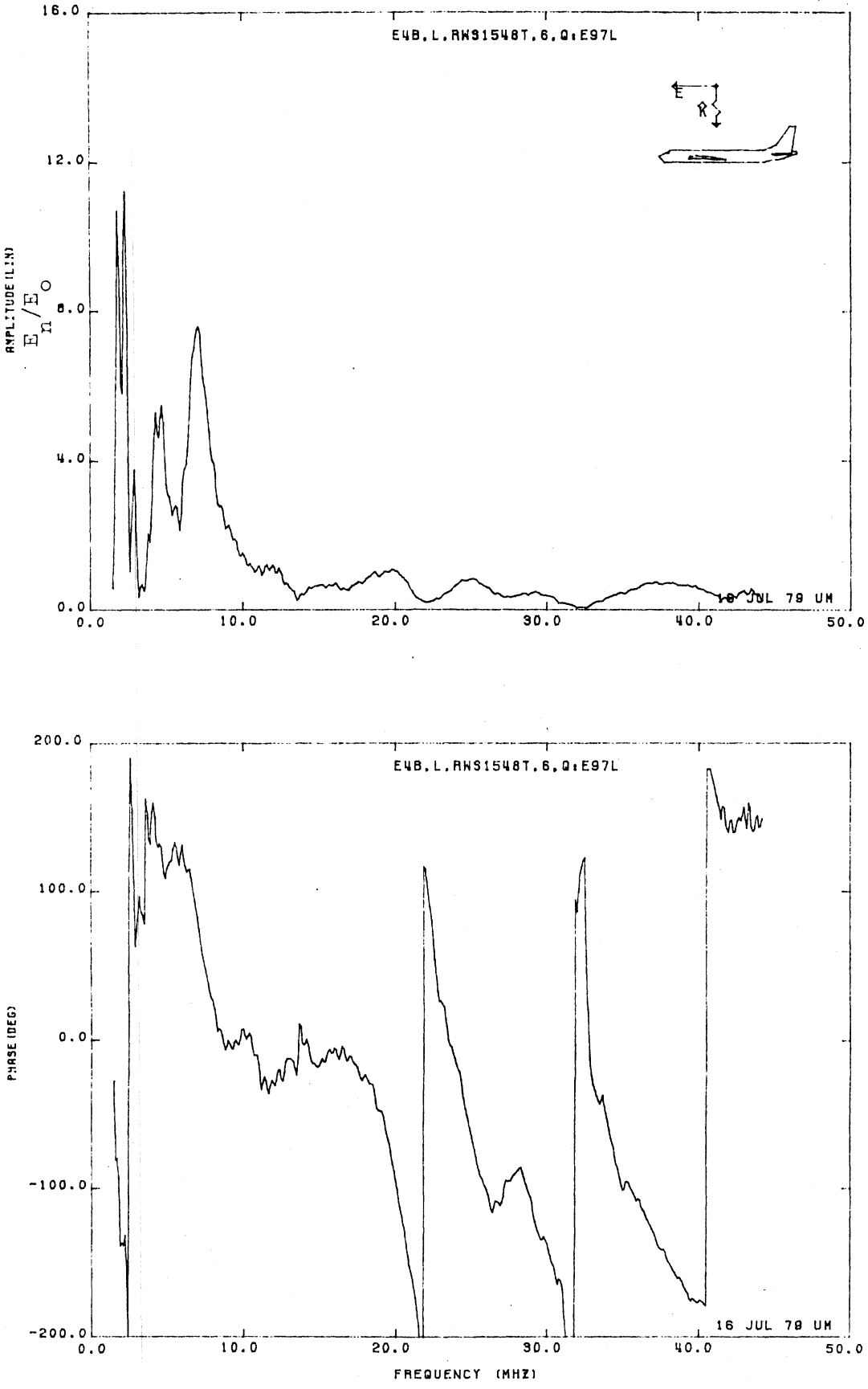

Figure 97L. Normal Electric Field at STA:RWS1548T, Excitation 6, 1/100 Model.

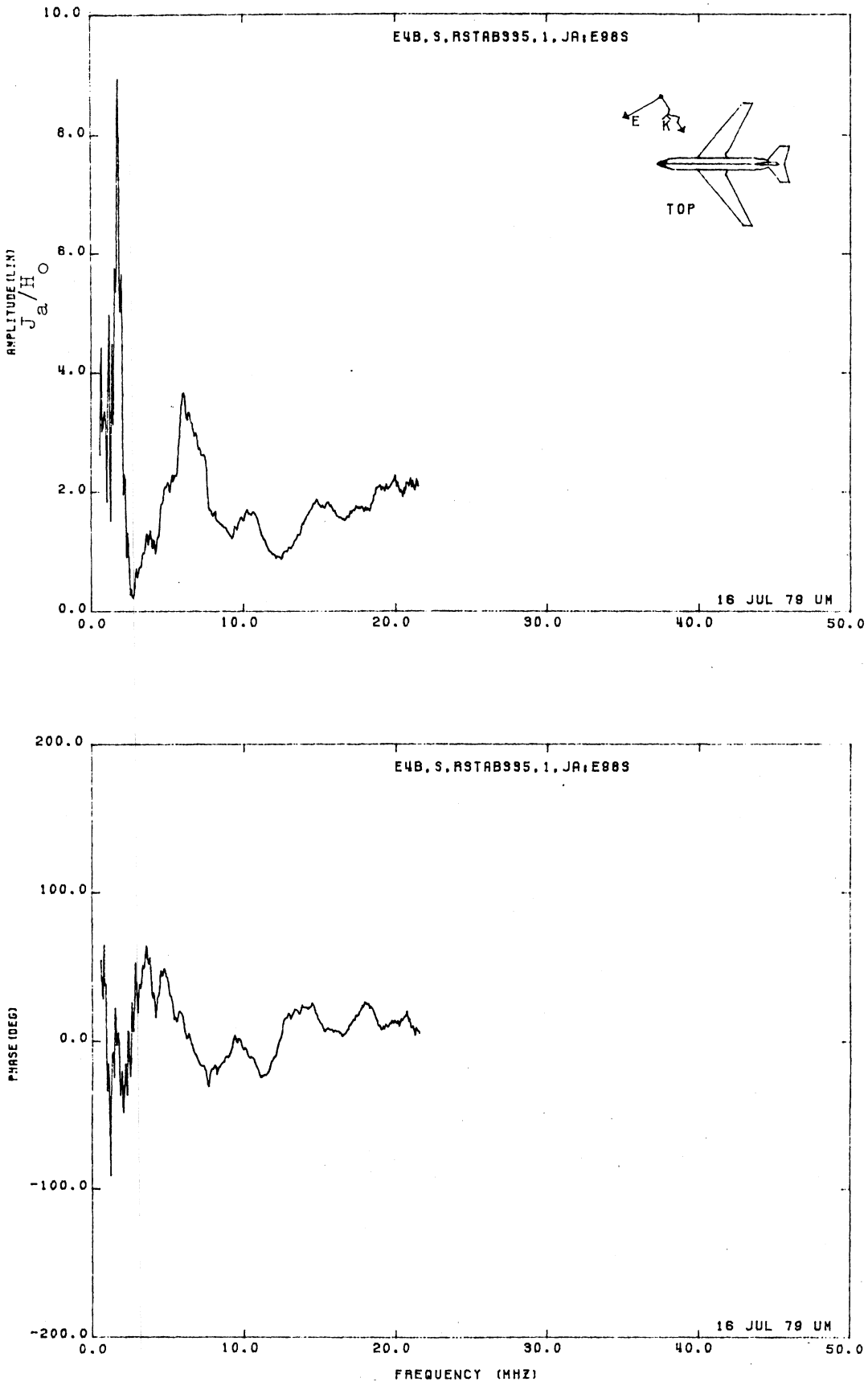

Figure 98S. Axial Current at STA:RSTAB335, Excitation 1, 1/200 Model.

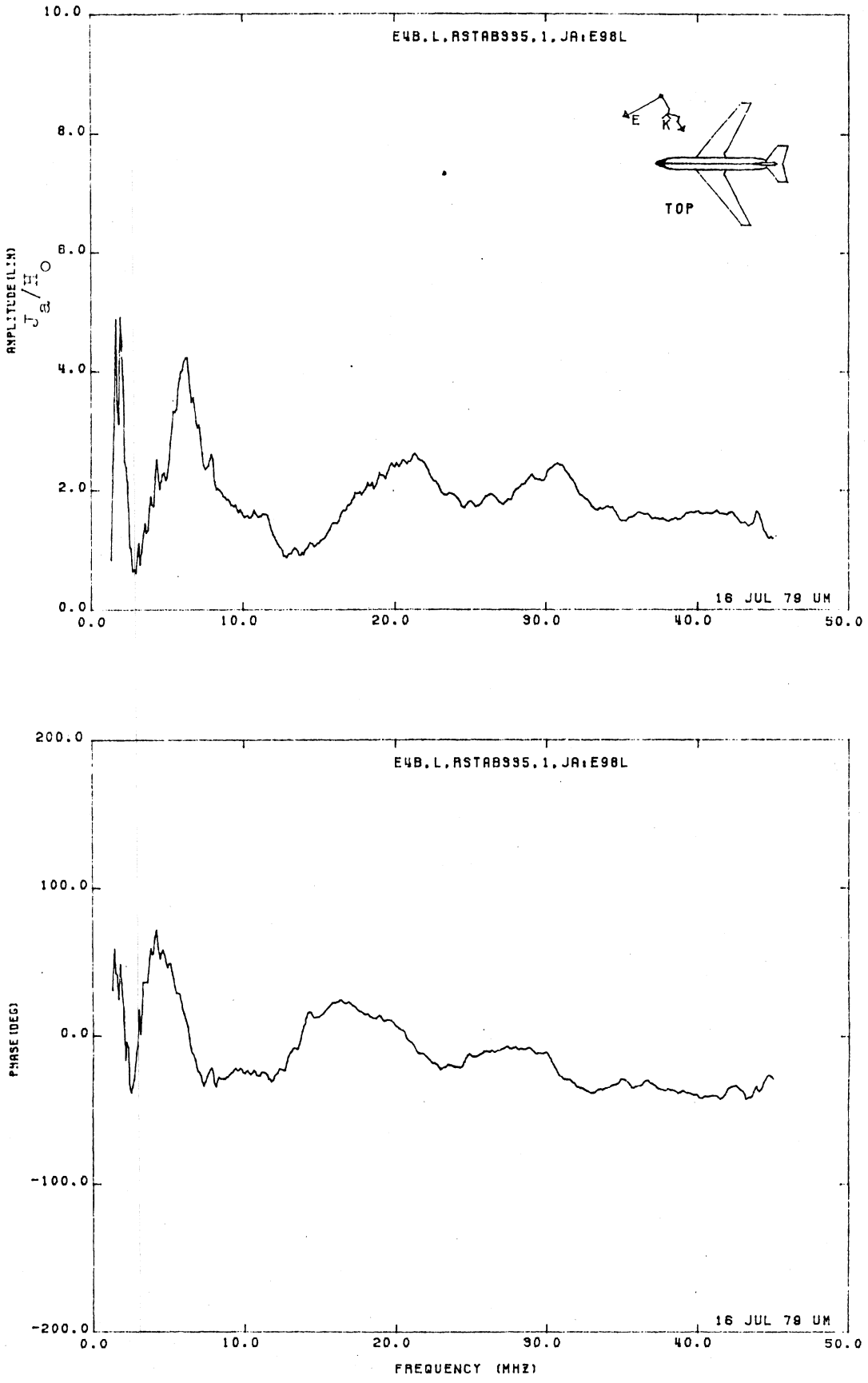

Figure 98L. Axial Current at STA:RSTAB335, Excitation 1, 1/100 Model.

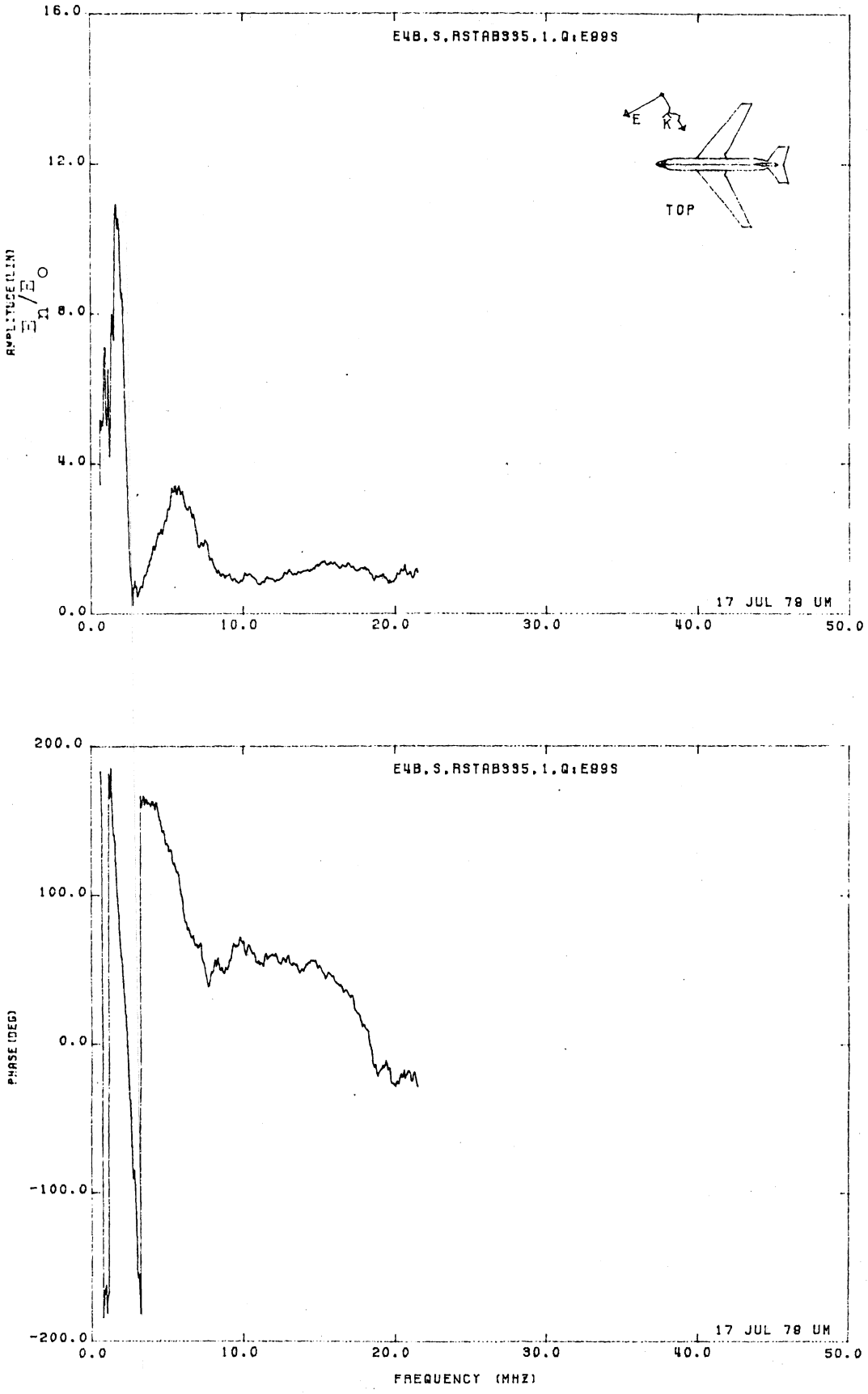

Figure 99S. Normal Electric Field at STA:RSTAB335, Excitation 1, 1/200 Model.

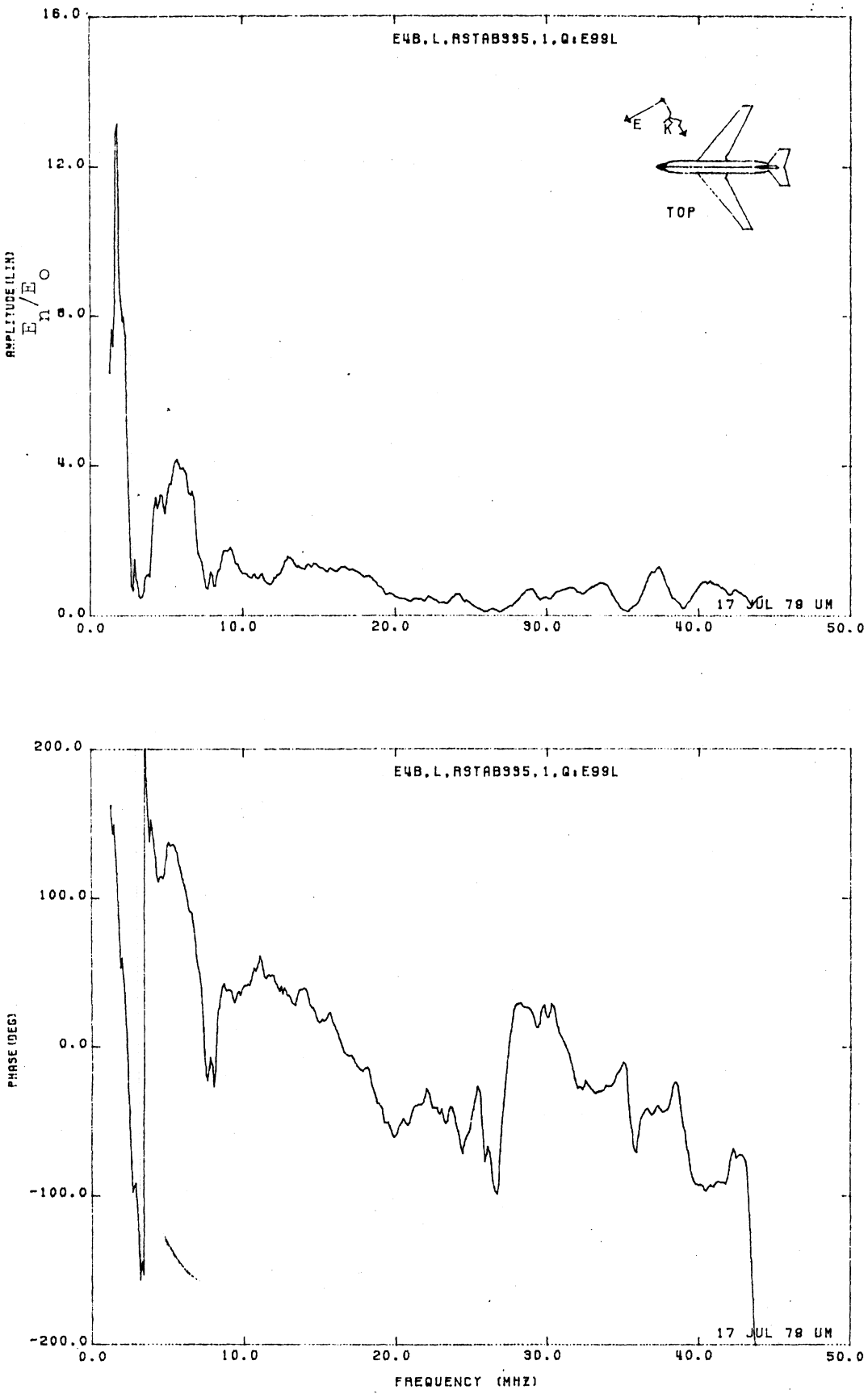

Figure 99L. Normal Electric Field at STA:RSTAB 335, Excitation 1, 1/100 Model.

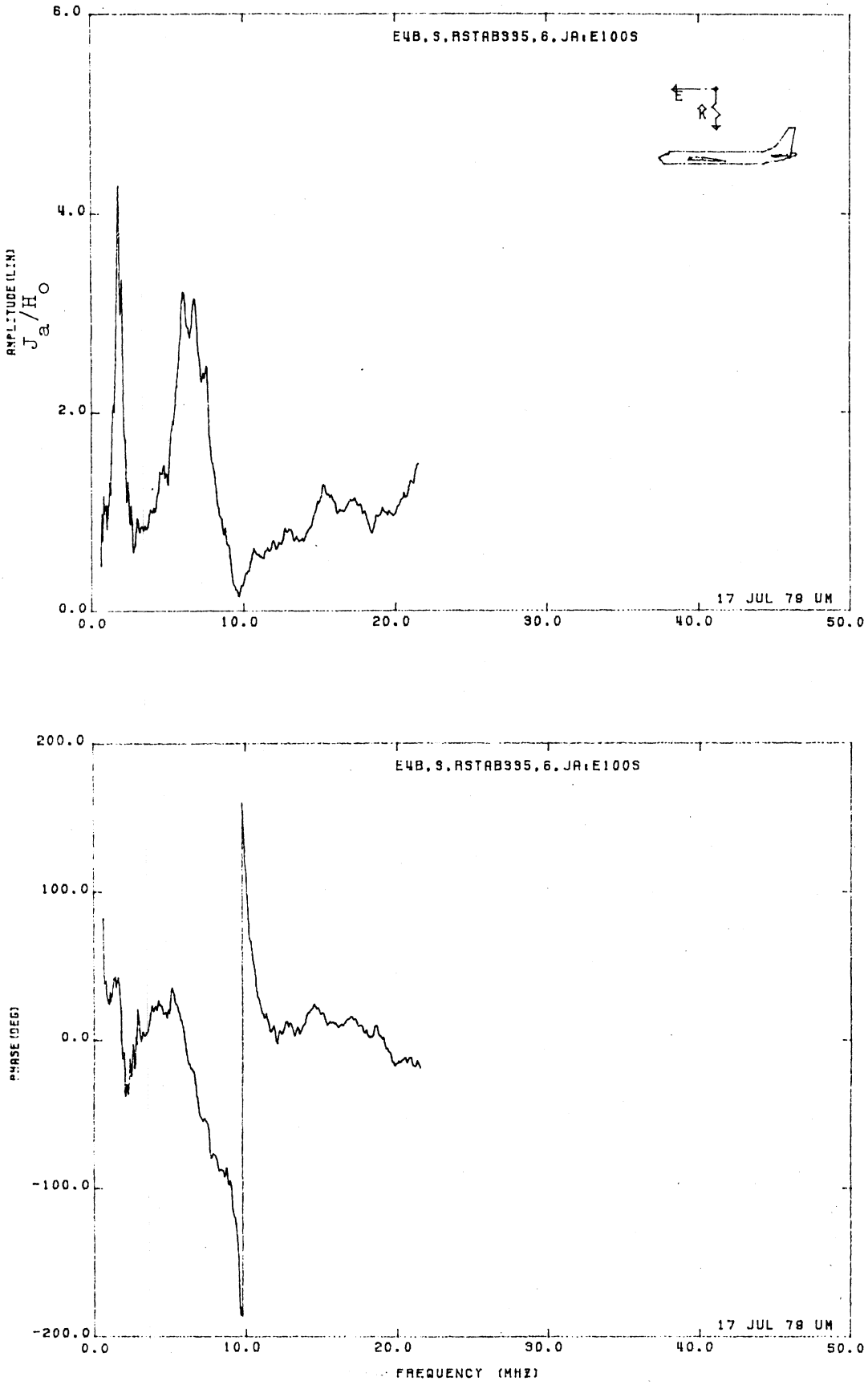

Figure 100S. Axial Current at STA:RSTAB335, Excitation 6, 1/200 Model.

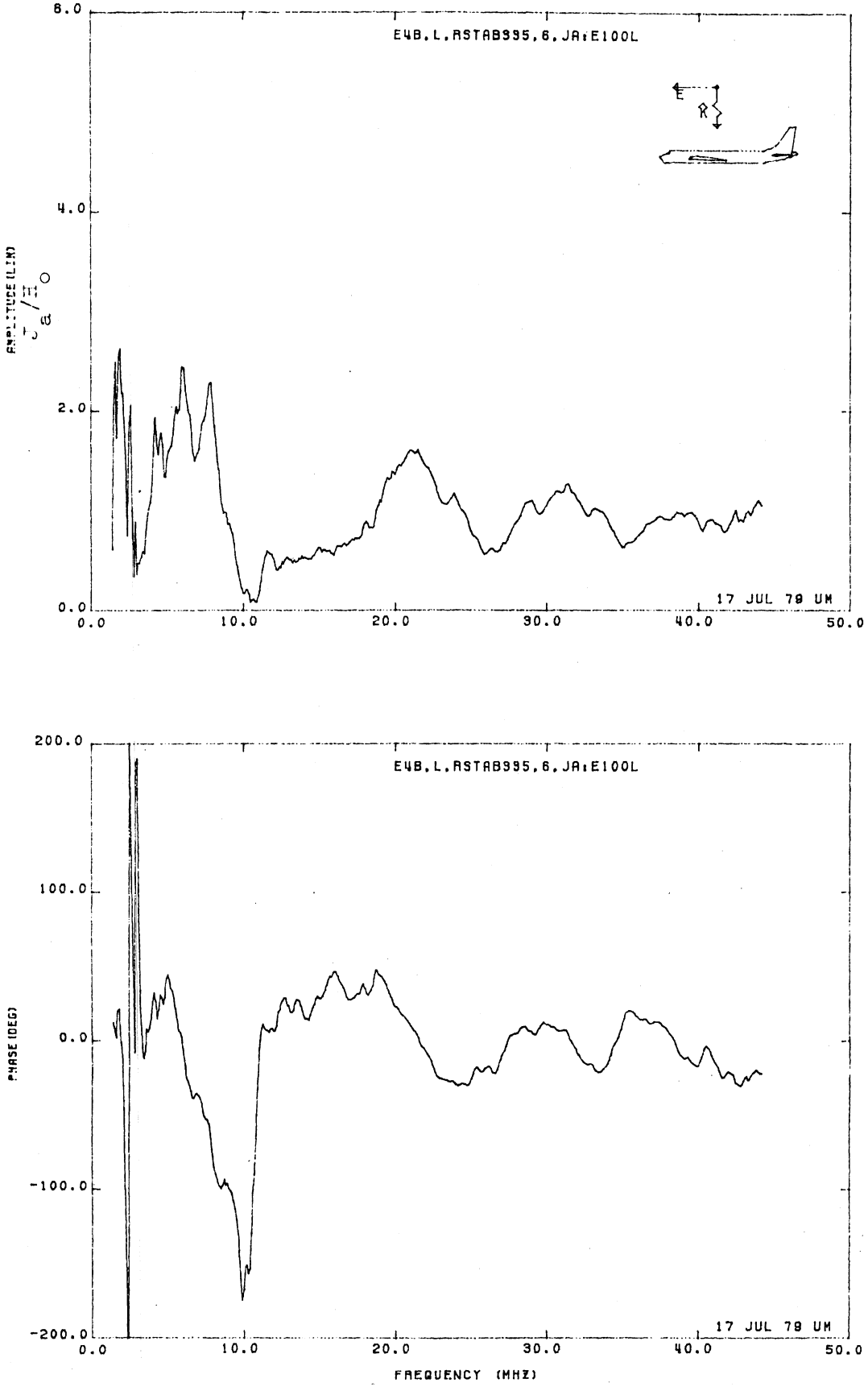

Figure 100L. Axial Current at STA:RSTAB335, Excitation 6, 1/100 Model.

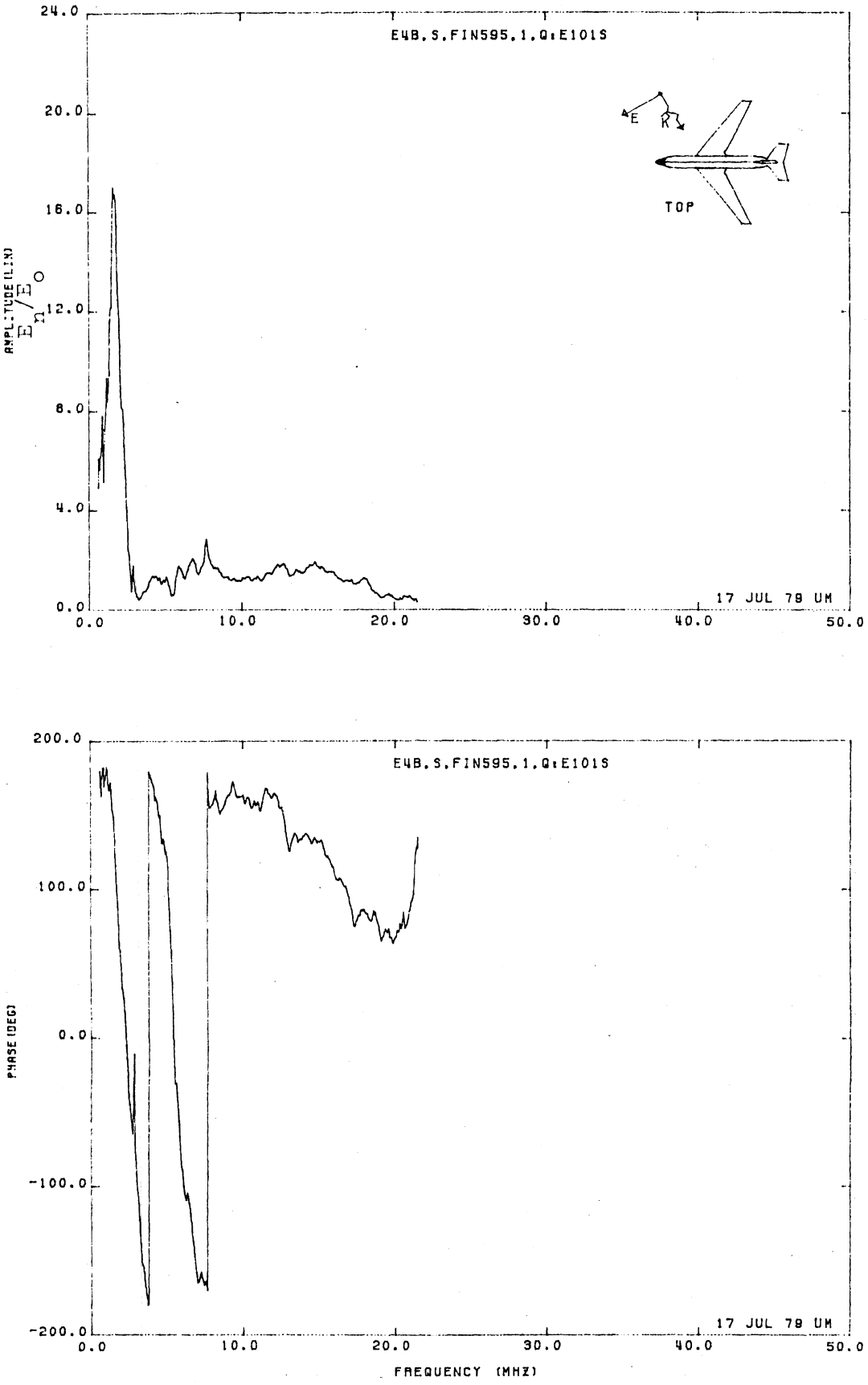

Figure 101S. Normal Electric Field at STA:FIN595, Excitation 1, 1/200 Model.

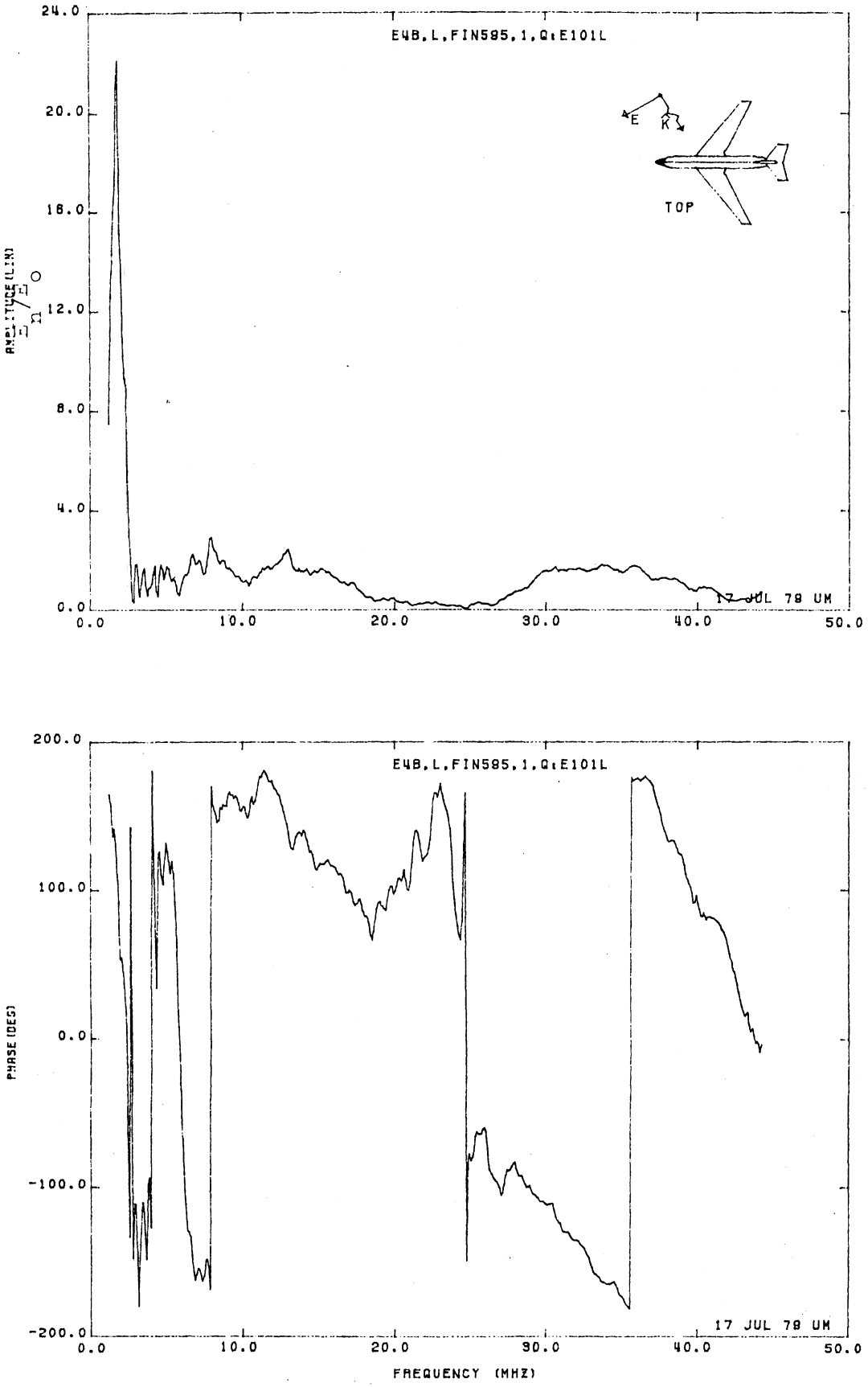

Figure 101L. Normal Electric Field at STA:FIN595, Excitation 1, 1/100 Model.

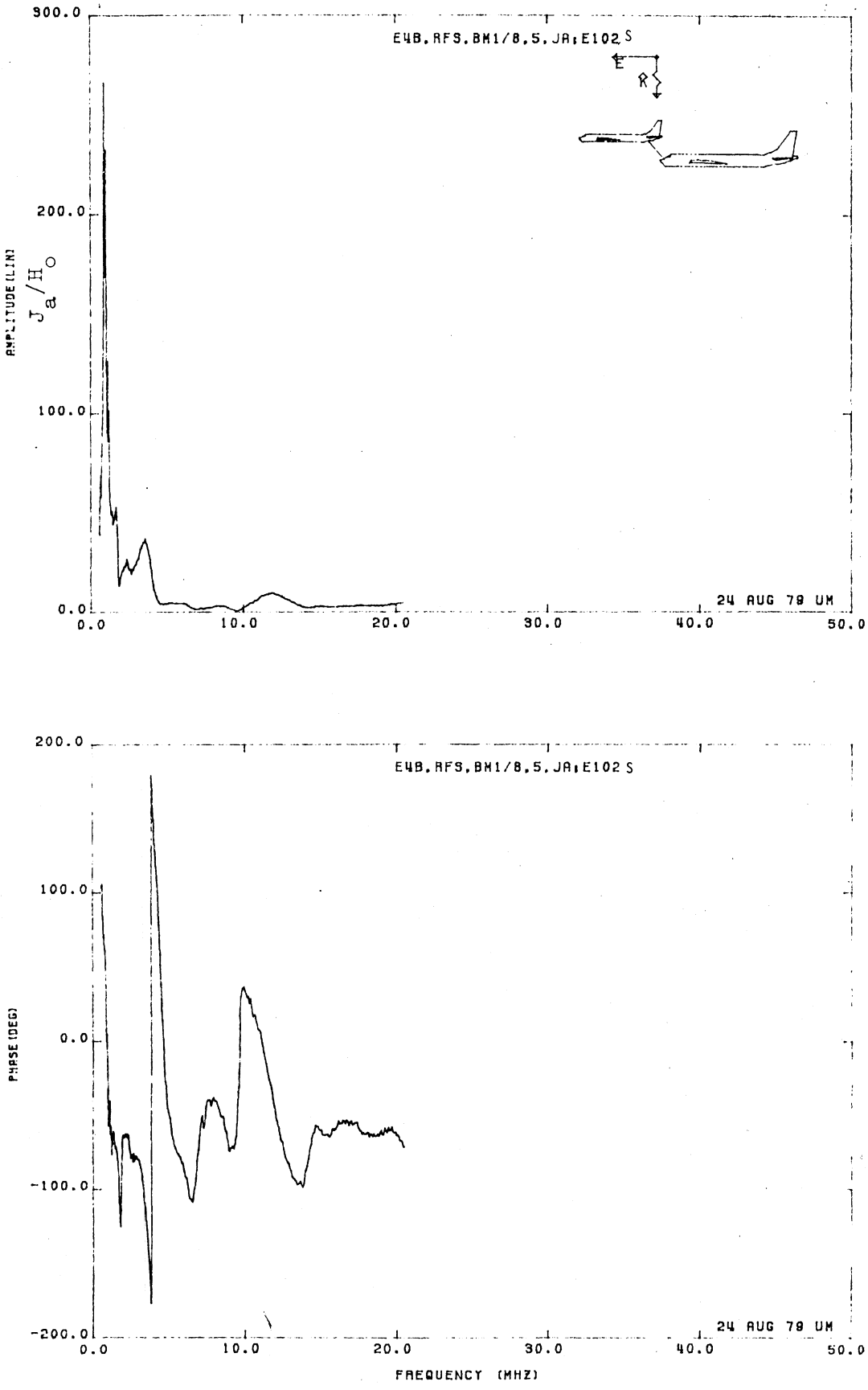

Figure 102S. Axial Boom Current at STA:BM1/8, Excitation 5, 1/215 Model. Uncorrected data.

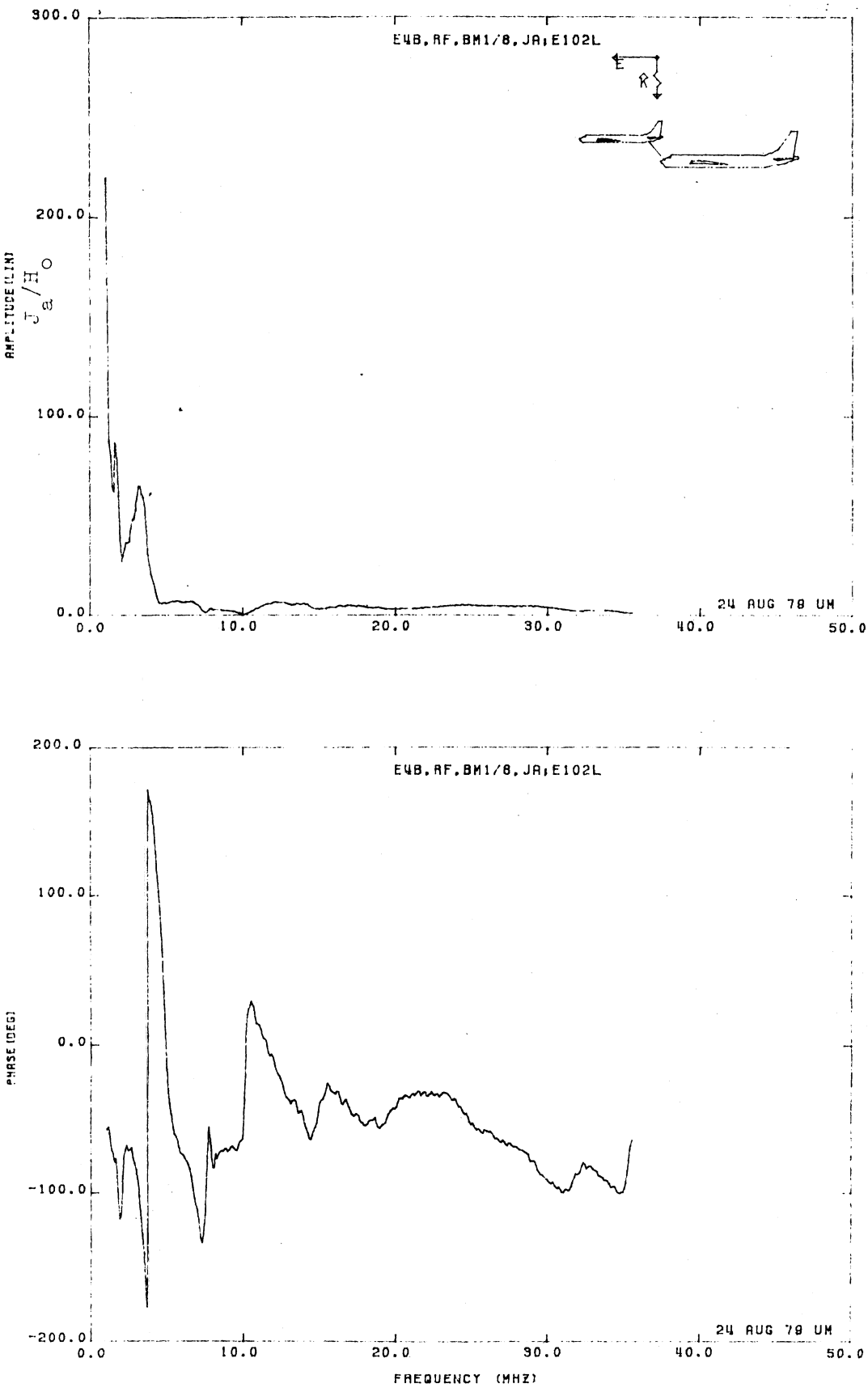

Figure 102L. Axial Boom Current at STA:BM1/8, Excitation 5, 1/125 Model. Uncorrected Data.

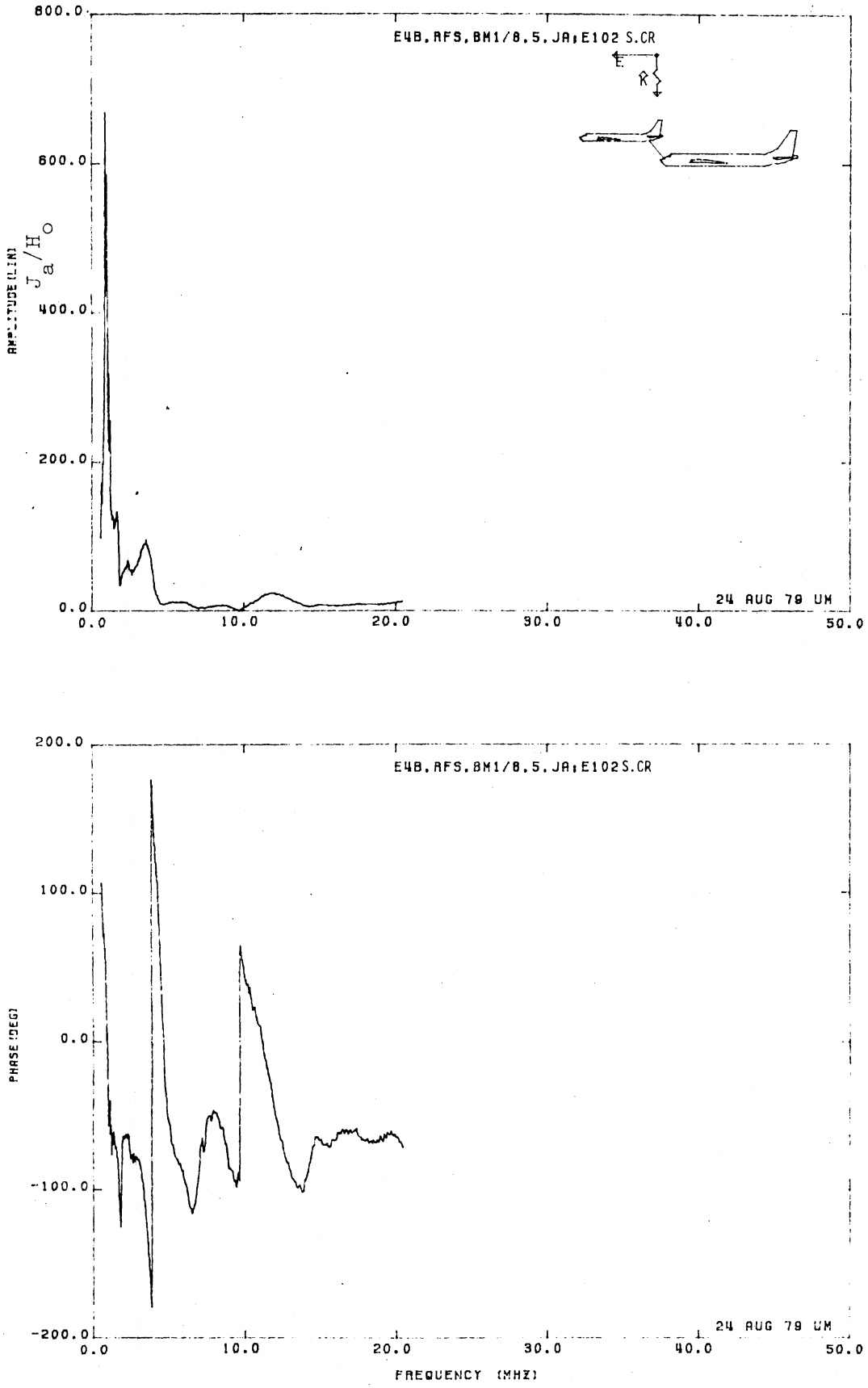

Figure 102S.CR. Axial Boom Current at STA:BM1/8, Excitation 5, 1/215 Model. Corrected Data.

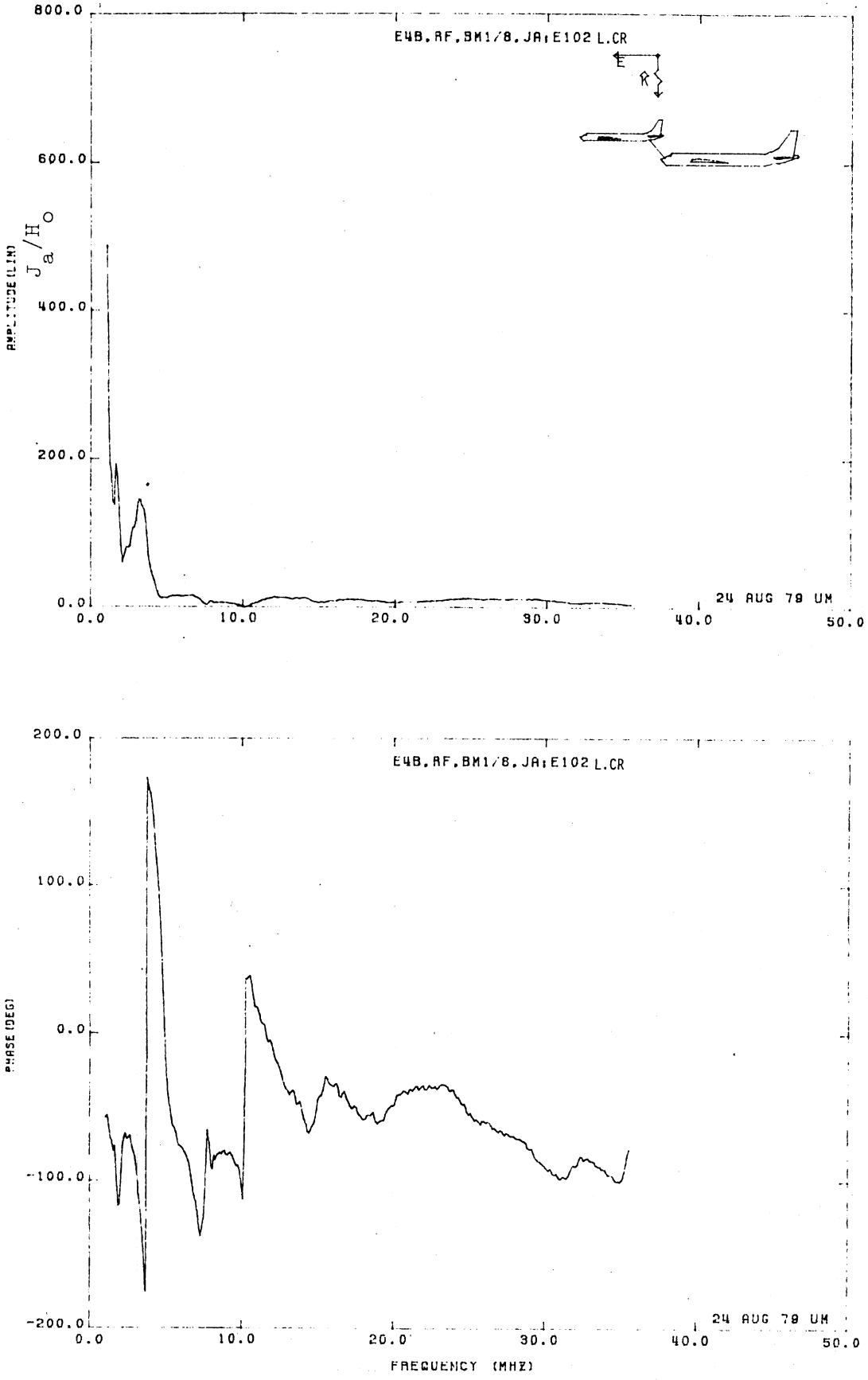

Figure 102L.CR. Axial Boom Current at STA:BM1/8, Excitation 5, 1/125 Model. Corrected Data.

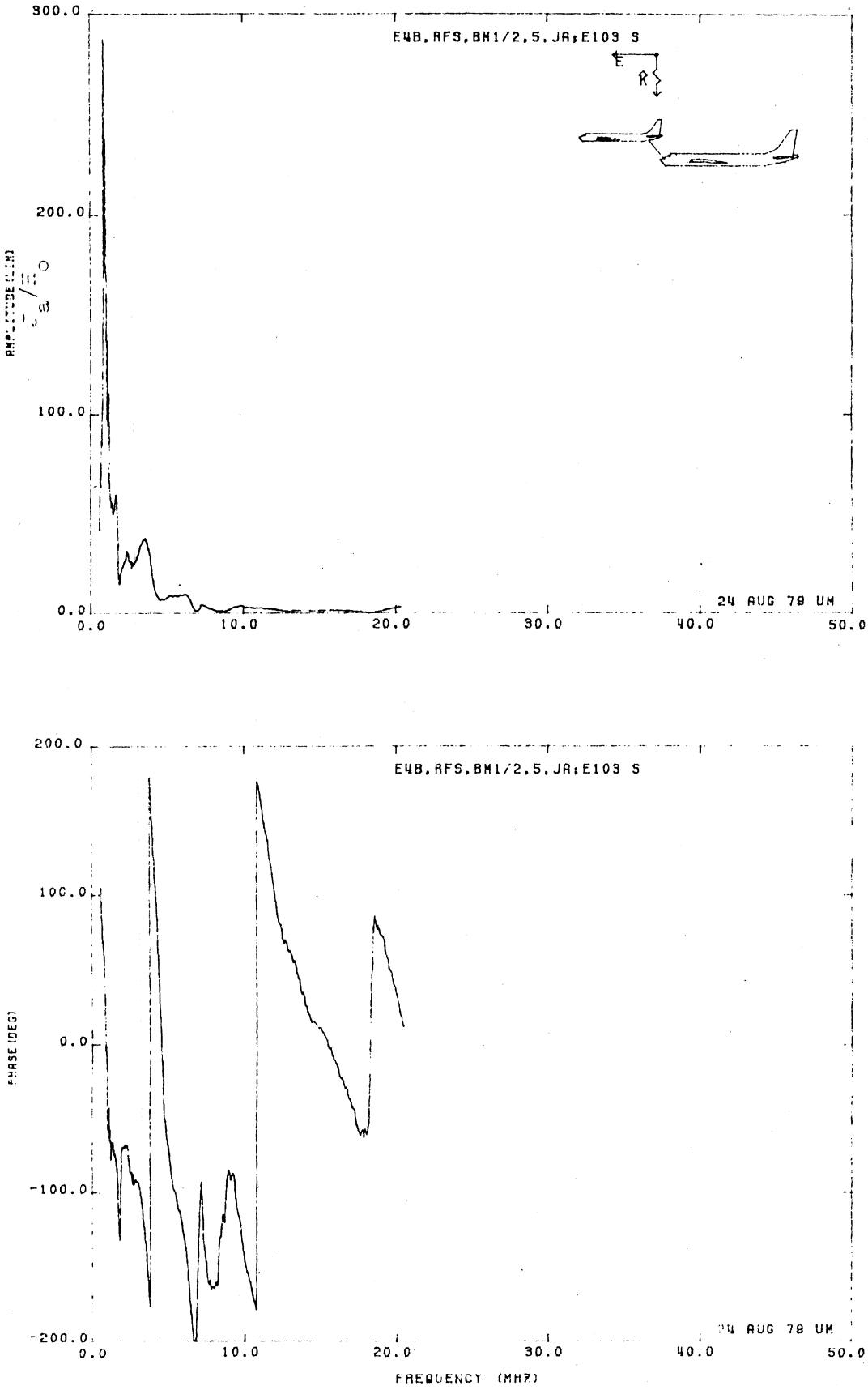

Figure 103S. Axial Boom Current at STA:BM1/2, Excitation 5, 1/215 Model. Uncorrected Data.

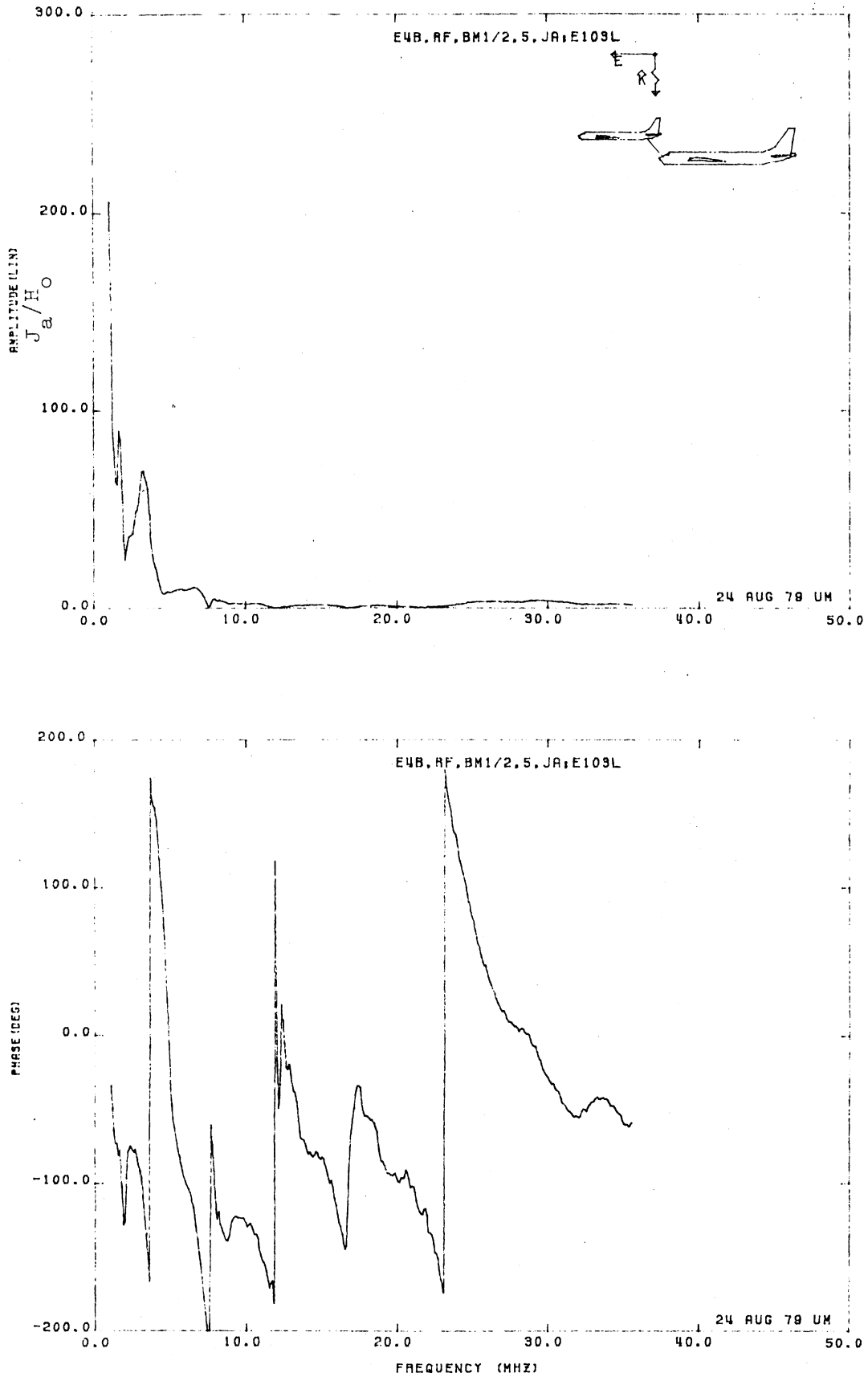

Figure 103L Axial Boom Current at STA:BM1/2, Excitation 5, 1/125 Model. Uncorrected Data.

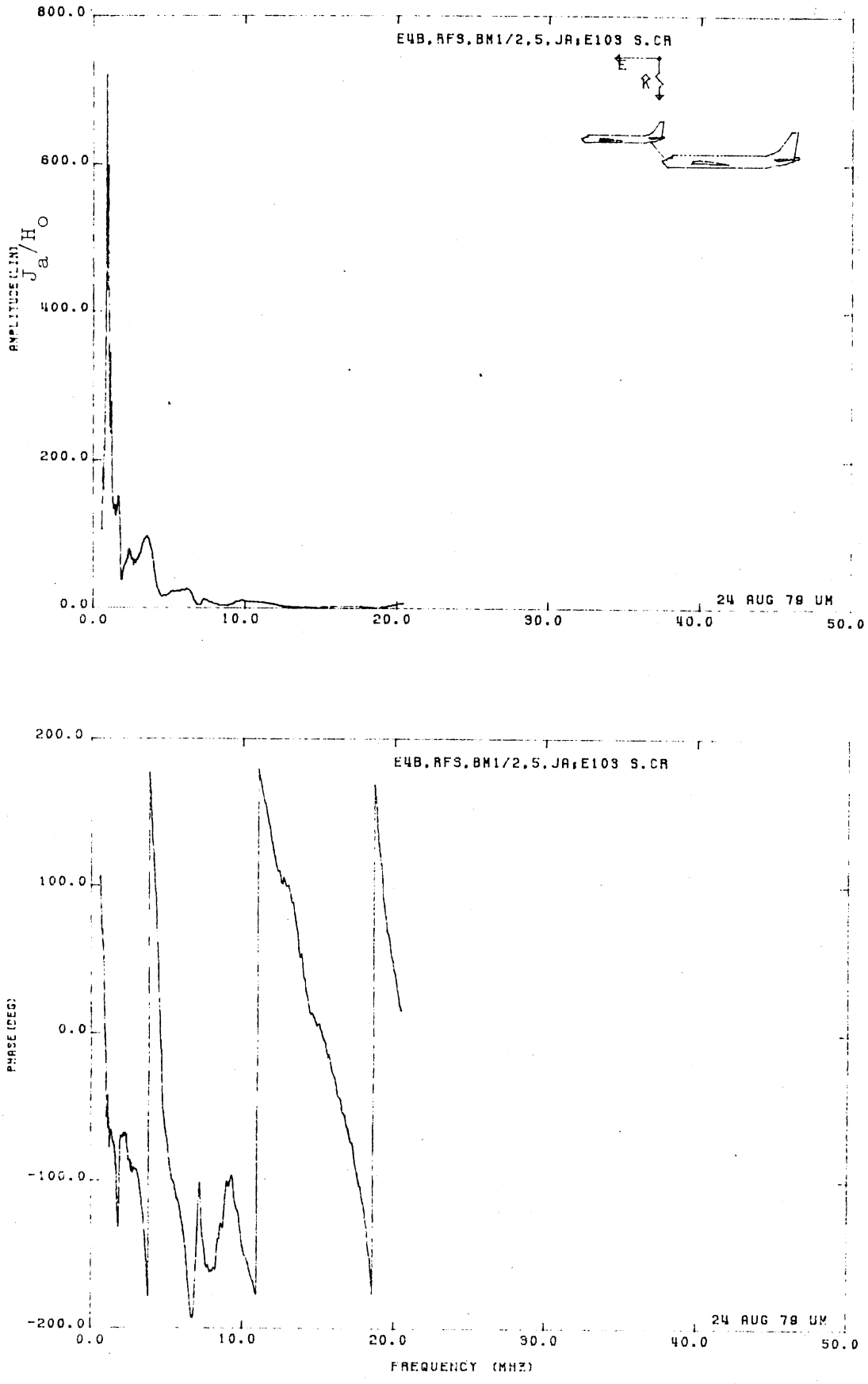

Figure 103S.CR. Axial Boom Current at STA:BM1/2, Excitation 5, 1/215 Model. Corrected Data.

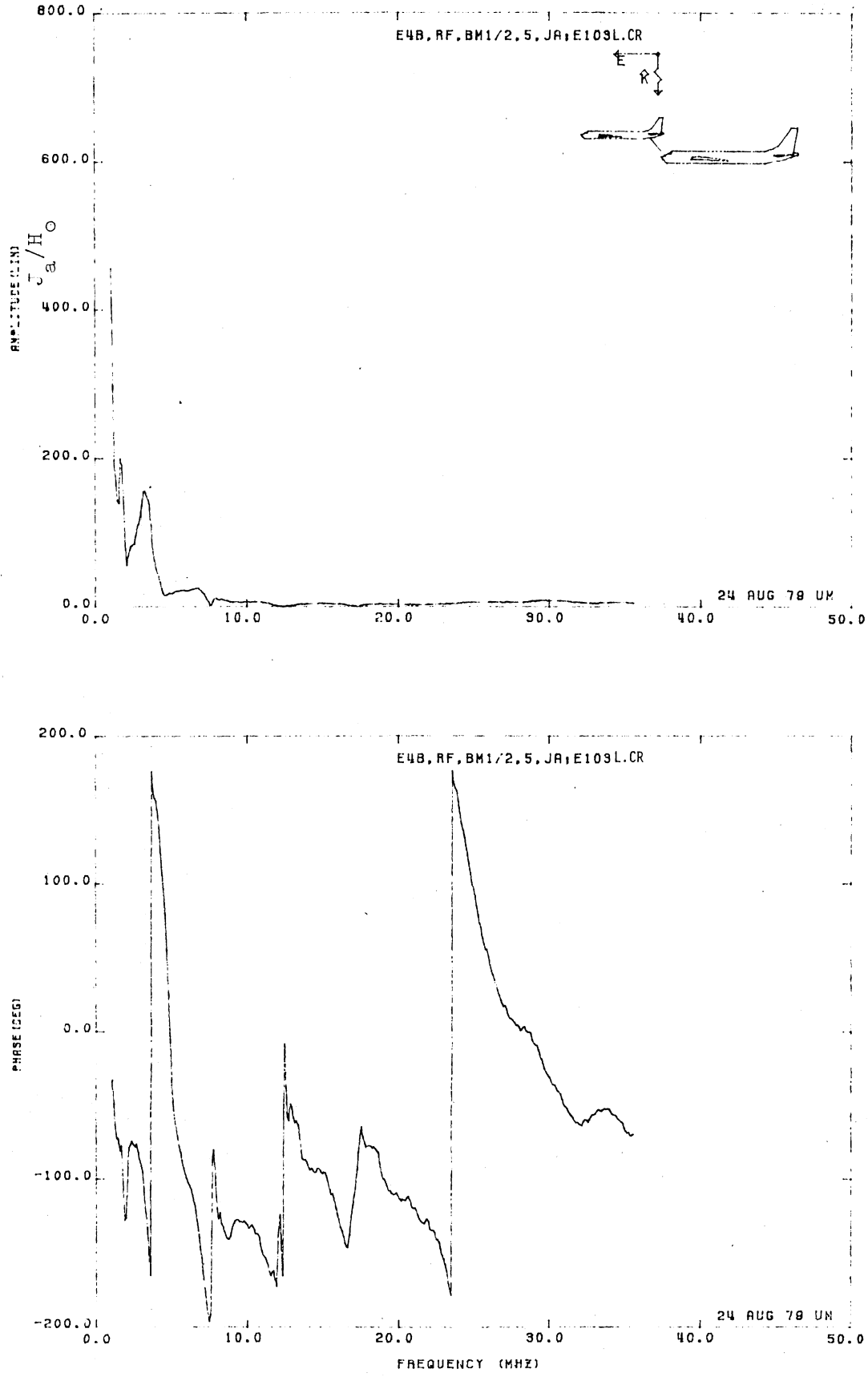

Figure 103L.CR. Axial Boom Current at STA:BM1/2, Excitation 5, 1/125 Model. Corrected Data.